Inorganic porous microspheres for drug delivery

Tye, Ching Kim

Award date:
2002

Awarding institution:
University of Bath

INORGANIC POROUS MICROSPHERES FOR DRUG DELIVERY

Submitted by
Ching Kim Tye B.Pharm.
for the degree of Doctor of Philosophy
of the University of Bath
2002

Ching Kim Tye

ProQuest LLC
789 East Eisenhower Parkway
P.O. Box 1346
Ann Arbor, MI 48106-1346

Acknowledgements

Firstly, I would like to express my thanks to my research supervisors, Prof. Ron Stevens and Dr. Mike Tobyn, for their continuous advice, support and encouragement throughout the period of my PhD and for their perpetual faith in my ability.

I felt very fortunate to have had access to the excellent facilities in the Department of Pharmacy & Pharmacology and the Dept of Engineering and Applied Sciences at the University of Bath. I am also very grateful for the opportunities given to me to present my work at conferences.

Thanks are given to all the postgraduates, postdoctoral staff and technicians of the Pharmaceutical Technology Group and the Dept of Engineering and Applied Sciences for their help and assistance during my three years in Bath. They have also given me a great social life in Bath. I would like especially to thank Dr. Rob Price for his encouragement, and Ursula Potter from Electron Optics for her technical help with the scanning electron microscopy.

The Department of Pharmacy and Pharmacology and the Overseas Research Students Awards are gratefully acknowledged for their financial support that enabled me to undertake this work.

I would like to thank all my friends and colleagues for their friendship, which gave me the strength and dedication to complete this task.

Last but not least, I thank my parents and my family for all their unconditional love and support during the course of my studies.

Abstract

Novel inorganic porous microspheres for drug delivery have been developed. Two types of inert bioceramic microspheres, dibasic calcium phosphate and tricalcium phosphate microspheres, were produced and tested.

The microspheres were produced by spray-drying suspensions of the ceramic powders. Initially, the feasible spray-drying conditions were explored, and then, the effects of the slurry compositions and the key parameters in the spray-dryer operating conditions were studied for their effect on the spray-dried products. It was demonstrated that ceramic microspheres having a range of properties (size; porosity; and morphology) could be produced by systematically varying the slurry composition (solids content; binder type and binder concentration; dispersant concentration; ceramic powder type; and powder particle size) and spray-dryer operational conditions (temperature; jet size).

The spray-dried microspheres were then sintered at temperatures in the range of 900 °C – 1300 °C. It was found that under controlled sintering conditions, microspheres with controlled porosity, pore size, and surface area were produced. The physical and chemical characteristics of these microspheres were studied using SEM, XRD, DSC, mercury intrusion porosimetry, surface area analysis, and density measurements, in order to optimise the combination of properties.

Subsequently, model drugs – benzamide, propranolol hydrochloride and paracetamol – were incorporated into the microsphere systems using three methods, by direct co-spray-drying with the ceramic powder, by vacuum loading into the sintered microspheres and by cultivating drug crystals in the sintered microspheres. The *in vitro* drug release profiles of drugs from these systems were then studied by dissolution tests.

The optimised microspheres systems which have been developed are considered to have favourable characteristics to be used in bone implant, transdermal needle-free powder injection and oral delivery.

Table of Contents

List of Abbreviations

β-TCP	Beta Tri-Calcium Phosphate
DCP	Dibasic Calcium Phosphate
DCPA	Dibasic Calcium Phosphate Anhydrous, $CaHPO_4$
DSC	Differential Scanning Calorimetry
EDX	Energy Dispersive X-ray
HA	Hydroxyapatite
HCl	Hydrochloric Acid
HPMC	Hydroxypropyl Methylcellulose
LTSEM	Low-Temperature Scanning Electron Microscopy
LVC	Large-Volume Circulating Cell
MS	Mass Spectroscopy
NaCMC	Sodium Carboxymethylcellulose
NaOH	Sodium Hydroxide
NMR	Nuclear Magnetic Resonance
PEG	Polyethylene Glycol
pph	parts per hundred by weight
Propranolol.HCl	Propranolol hydrochloride
SDC	Spray-drying Conditions
SEM	Scanning Electron Microscopy or Scanning Electron Microscope
SLS	Sodium Lauryl Sulphate
SVC	Small-Volume Stirred Cell
UV	Ultra Violet
XRD	X-ray Diffraction

1 Introduction

1.1 Drug Delivery Systems

The average development time of a New Chemical Entity is ~ 10-15 years, and costs ~ $150-350 million[1]; while the development of new methods of delivery for existing drugs is generally less time consuming and costs considerably less[1]. New delivery methods may present the drugs with improved efficacy and bioavailability, and/or reduced dosing frequency to improve side effect profiles and enhance patient compliance. For example, Vectura Maxsol™ and Elan Nanocrystal® technologies improve the dissolution characteristics and bioavailability of poorly soluble drugs; Shire Microtol™ and Yamanouchi Pharma Technologies OCAS™ are controlled release systems which allow reduced drug dosing frequency. New drug delivery systems may also open up new avenues for chemical entities that were not previously available for use because of their toxicity or poor bioavailability. For example, delivery of antineoplastic agents directly to tumour cells can greatly reduce toxic systemic side effects[2].

Today, due to cost and competition, pharmaceutical companies are under pressure to maximise the full potential of a drug candidate at an early stage in its life cycle[1,2]. This aim can be achieved by incorporating the drug into various drug delivery systems. This exercise can also add economic value to drugs by providing product patent life extension, higher level of product differentiation and convenient dosage forms. Furthermore, companies can also make use of the regulatory exclusivities of the US Federal Food, Drug, and Cosmetic Act (FDCA) to effectively extend product franchises through the use of new delivery systems even where patent protections have expired[3].

The future of gene therapy will also largely depend on innovative drug delivery techniques to deliver genes directly and precisely to their targets[2,4], *e.g.* the cell nuclei. In addition, in the last twenty years, there has been a growing demand for more patient-compliant dosage forms, such as, dosage forms with controlled release properties to reduce dosage frequency, and dosage forms with improved organoleptic properties.[1]

As a result, there has been a boom in drug delivery corporations and medical device companies. The value of the drug delivery market is expected to increase 5 fold from $2.4 billion to nearly $12 billion in just 5 years[3], and the demand for innovative drug delivery technologies is expected to grow continuously[1].

1.2 The Concept of Controlled Release and Drug Carriers

The ideal drug delivery system is one that releases the drug into the appropriate part of the body when and where it is required, at the minimum dose level needed for the desired therapeutic effects. Such a system should have a programmable concentration-time release profile or environmentally sensitive controls to enable it to achieve the optimum therapeutic results. However, such ideal systems are not always available. Nevertheless, scientists have moved closer to this goal by developing controlled release drug delivery systems. Controlled release describes a predictable and reproducible drug release kinetics[5], *i.e.*, a controlled drug concentration in the targeted tissue.

As the name implies, controlled-release drug delivery systems serve two functions. Firstly, 'drug delivery' indicates it involves the transport of the drug to a particular part of the body. This may be accomplished in a number of ways including intravenously, transdermally or orally. Secondly, 'controlled release' describes the rate at which the drug is made available to the body once it has been delivered.

Controlled release systems are particularly useful for drugs with narrow therapeutic windows where minimum fluctuation of blood concentration is desirable. Figure 1.1 shows how the plasma drug concentration profile of a conventional oral delivery system, which requires multiple dose administration in a day, compares to the plasma drug concentration achieved using a controlled release system. For conventional therapy, the concentration of drug available to the body immediately peaks and then declines rapidly. At times, the drug concentration is very high, contributing to adverse side effects and compromised drug safety[6]. At other times, the concentration is too low to provide therapeutic benefit. Controlled release systems can provide sustained blood concentration, reduce side effects caused by the peak and trough effect, and reduce dosing frequency, therefore improve patient compliance.

The basic controlled release formulation consists of an active drug and a carrier, arranged to allow the drug to be released at the target over a period of time and at a controlled rate. The carrier, typically an organic polymer, serves as a barrier against drug release in order to achieve gradual drug release and/or to protect the drug from chemical or biological degradation. The drug particles are normally dispersed or encapsulated as solid solution or crystalline material in the carrier.

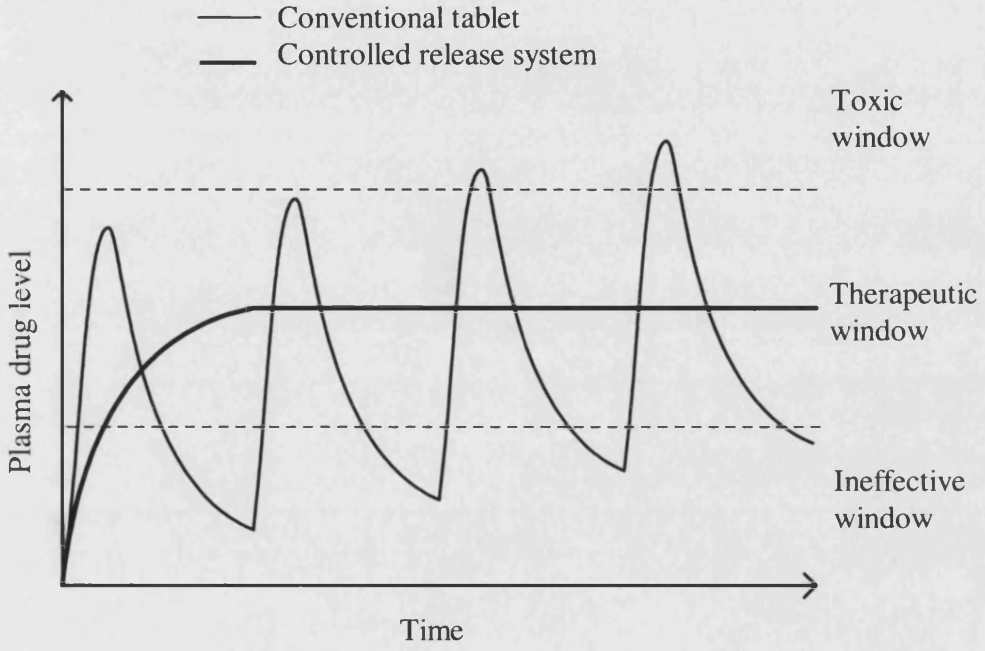

Figure 1.1. Plasma drug level of a drug versus time profile when administered orally as a conventional tablet compared to a controlled release drug delivery.

Controlled release systems can be classified based on their controlling mechanism of drug release as chemically controlled systems or diffusional controlled systems[7].

In chemically controlled systems, the drug is contained within a polymer membrane or matrix. The polymer is designed to degrade and release the drug at a specific location in the body. As the polymer degrades by hydrolysis or enzymatic cleavage, the drug is freed and made available to the body[7].

In diffusional systems, the drug is either encapsulated in a polymer membrane (membrane-reservoir systems) or suspended within a polymer matrix (matrix system). Typically the course of events is as follows: water diffuses into the membrane or matrix, the drug dissolves, and finally the dissolved drug diffuses out of the polymer. In a membrane system, the rate-determining step is the diffusion of a drug through the polymer. The rate of release is constant and proportional to the concentration of drug initially present. For these systems, before the establishment of a steady release rate, it is common that the initial release rate is much higher. This so called "burst effect" is due to the initial drug saturation of the membrane. In a matrix system, due to the increasing diffusional resistance and the decreasing area at the penetrating diffusion front as matrix diffusion proceeds, the rate of release depends upon the amount of drug present at a particular time, thus the rate of release is time dependent[8,9].

There is also a sub-group of diffusion-controlled systems that depends on osmotic pumping mechanism. The drug is surrounded by a semi-permeable membrane that regulates the osmotic permeation of water. The membrane contains a small, laser-drilled hole. Within the membrane there is a high concentration of an osmotic agent, either the drug itself or a salt, which causes water to enter through the membrane. The drug is then forced out through the hole because of the increased pressure[9]. For a fixed reservoir, the device delivers a volume of drug solution equal to the volume of osmotic water uptake in a given time interval. The rate of drug release from these systems is generally regulated by the osmotic pressure of the drug core formulation and by the water permeablility of the semipermeable membrane[7].

1.3 Microsphere Drug Delivery Systems

The term 'microsphere' or 'microparticle' is a general name used to describe spherical particles with a diameter between 1 μm - 1000 μm[10]. Microsphere/microparticulate delivery systems developed from organic polymeric materials have been widely investigated for controlled and targeted delivery of biologically active substances. The production technology mainly uses either the emulsion solvent evaporation/solvent extraction process[11,12] or spray-drying[13,14,15].

1.3.1 Organic Microspheres

Almost all microsphere drug delivery systems studied until today are made from organic materials. These are biodegradable and biocompatible polymers, which include lactic and glycolic acid derivatives[11], polyanhydrides[16], cellulose derivatives[10,14], chitosan[13,17], liposome[18,19], gelatin[20], acrylic polymers[21] and silk[22]. They are mainly membrane-reservoir systems. The drug is surrounded by a rate-controlling membrane. A saturated reservoir maintains a constant rate of drug release. The kinetics of drug release depends on the diffusion of drugs across the membrane.

Pharmaceutical scientists welcome the concept of 'microsphere drug carrier' because by encapsulating drugs in microspheres, each particle is a delivery system itself. Therefore, the chance of dose dumping due to failure of one system is reduced. Furthermore, microspheres can be filled into containers of any size or shape and be formulated into various dosage forms.

Microsphere drug carriers also have the flexibility to be adopted for various delivery modes. Microspheres have been shown as promising drug delivery systems for oral[23,17], vitreoretinal[24], parenteral[23], transdermal[25,26], pulmonary[14], nasal[17] and implants[13] delivery. For example, poly-DL-lactic-poly(ethylene glycol) microspheres were studied as hepatitis B antigen carriers for oral and subcutaneous administration, and they were shown to induce a better immune response than conventional alum-absorbed antigens[23]; mucoadhesive hydroxypropylcellulose microspheres were prepared as powder for inhalation and were shown to enhance pulmonary drug absorption[14]; chitosan microspheres were studied as drug carrier for long acting injectable implants[13] and were shown to be effective influenza vaccine carrier also via nasal delivery[27]; drug-loaded polylactic acid and poly(lactic-co-glycolic) microspheres have been used to treat diverse vitreoretinal diseases via intravitreous injection[24]; hollow microspheres were used as floating drug delivery systems to increase gastric retention of the drugs for oral delivery[28]; and acrylate/vinyl ester microspheres have been patented for use in adhesive transdermal delivery systems[25].

As explained earlier, the main advantages of using organic polymers microspheres are that they are biocompatible and bioerodible. However, there are limitations to these organic microspheres:

1. Toxicity – Preparation of organic microspheres mostly involve the use of organic solvents, *e.g.* chloroform and glutaraldehyde, which are toxic. Therefore, there is a possibility of toxic contamination in the end products.
2. Stability problems – Some organic microspheres are not stable. For example, liposomes are unstable unless the lipid bilayers are specifically stabilised. As a result, they have a very short shelf life. The exposure of protein drugs to organic solvent may have adverse effects on the stability of the proteins[11].
3. Dependent on erosion kinetics – For bioerodible organic microspheres, the incorporated drugs are released when the polymer erodes by hydrolysis or enzymatic cleavage. Therefore the release profile of the drug is dependent on the erosion kinetics of the matrix and in turn, the erosion kinetics is dependent on the environment.
4. Low drug loading – The organic microspheres are usually non-porous and the carrier matrix makes up most of the content. Hence the drug loading capacity is correspondingly reduced.

1.3.2 Inorganic Microspheres

There are very few published reports about the use of inorganic microspheres as drug carriers. Kortesuo *et al.*[29] studied the uses of spray-dried silica gel microspheres for controlled drug delivery. Silica xerogel had previously been studied in the form of monoliths or crushed particles and was found to show controlled release characterisitics[30]. The spray-dried silica gel microspheres produced had a smooth surface without pores on the external surface and were found to release toremifine citrate and dexmedetomidine HCl in a period of 7 to 50 days. Compared to the production of monoliths, the production of spray-dried silica gel microspheres was simpler and less time consuming. Also, spray-dried silica gel microspheres were found to accommodate lower drug loading and degrade more slowly (~10 % degradation in 30 days) than silica xerogel monoliths. This was probably due to the condensed structure of the silica gel microspheres compared to the monoliths.

In this study, the potential of inorganic calcium phosphate microspheres, as drug delivery carriers was investigated. It is proposed that these calcium phosphate microspheres systems will have the following advantages over organic systems:

1. Non-toxic – Preparation of microspheres does not require the use of toxic organic solvents.
2. Stability and strength – Calcium phosphates are ceramic materials that provide the structural stability of a largely immutable solid. They can be used to protect and stabilise drugs that are embedded in their matrix. They can also be used as a skeleton for more complex systems. For example, as the basis for bone implants.
3. Controlled porosity – The microspheres are porous and the drug release will be controlled by the porosity and pore-size of the microspheres. The drug release is not erosion kinetics-dependent; therefore, its drug release is not environment dependent.
4. Bone delivery – Calcium phosphates are biocompatible with our bones. They can be absorbed by the bone to form the precursor of new bone[31]. Therefore, they are potentially suitable to be used as bone implants.
5. High drug loading – The microspheres are porous and can accommodate high amounts of drug.

1.4 Calcium Phosphates for Drug Delivery

Calcium phosphates are inorganic materials found in most animals, often in appreciable quantities[32]. They are the main constituent of teeth and bone in human bodies, and calcium phosphate spherical particles have been found inside and outside bone cells[32].

In this study, calcium phosphates were investigated because their biocompatible nature means that they may be applicable in various administration routes, including oral, bone implantation and transdermal delivery. Furthermore, they are well-studied pharmaceutical excipients.

Calcium phosphates are everyday ingredients in the pharmaceutical industry. The common forms are dibasic calcium phosphate (DCP), $CaHPO_4$, in dihydrate or anhydrous form, beta-tricalcium phosphate (β-TCP), $Ca_3(PO_4)_2$, and hydroxyapatite

(HA), $Ca_{10}(PO_4)_6(OH)_2$. The physicochemical properties of calcium phosphates are described in a recent monograph by de Groot *et al.*[35]

DCP is one of the most widely used excipients for direct tableting, because it is cheap, has low hygroscopicity, a high bulk-density, and its aqueous dispersions[33] are neutral in pH. β-TCP is widely used as a diluent in tablets and capsules, a calcium source in health supplement preparations, and an anticaking agent in food applications[33]. Tablets prepared with DCP or β-TCP do not disintegrate readily, therefore, a disintegrant is always necessary[33]. DCP itself has been shown to retard drug release in controlled release tablets[34].

HA is the most stable form of calcium phosphate at pH > 4.2[35]. Its crystallography and chemical composition closely resemble those of bone and tooth mineral. Natural bone contains approximately 70% of HA by weight[36]. HA is a bioceramic that is now commercially used for bone repair, bone substitution, hard tissue implantation or as a coating on implants[37].

Bioceramics are ceramic materials that are used for the repair and reconstruction of diseased, damaged or 'worn out' parts of the body. Calcium phosphate-based bioceramics, especially HA and β-TCP, have had a distinct place in the biomaterials research field for the last 30 years[35]. This is because they are biocompatible, non-toxic, non-immunogenic towards living tissue[37], and most importantly, they exhibit bioactive behaviour.

Bioactive behaviour means that calcium phosphate bioceramics are integrated into bone tissue by the same ongoing processes active in remodelling healthy bone, through resorption and deposition of bone mineral. This leads to osseointegration - an intimate physicochemical bond between calcium phosphate implants and bone[31]. Calcium phosphates are also known to support osteoblast adhesion and proliferation. Porous HA implants have been found to promote the growth of soft connective tissues[37], and bone and bone marrow cells were found inside HA implants pore structure[38,39]. β-TCP implants have also been found to be biocompatible and have connective tissue grown in

their pore structure[37]. β-TCP implants are classified as resorbable[35], and are designed to degrade gradually with time, whilst being replaced with tissue.

Calcium phosphates have also found increasing usage as drug delivery devices. Lasserre *et al.*[40] recently published a comprehensive review on ceramic controlled drug delivery devices that include porous block ceramics, matrices, inserts, ceramic reservoirs and cements, mainly used as implants. The article discusses advantages and disadvantages of conventional drug delivery systems and different approaches used to deliver chemical and biological agents, by means of ceramic devices.

HA and β-TCP bioceramics have been investigated as drug delivery system for antibiotics, anticancers and analgesics. Itokazu *et al.*[41] reported that antibiotics impregnated in porous HA cubic blocks, continue to release antibiotics and maintain their concentration levels above the minimum inhibitory concentration after 42 days. Seven patients with osteomyelitis have been treated using this system and no complications were observed during the follow up period of 8 - 36 months. Shinto *et al.*[38] demonstrated that the release of antibiotics from HA blocks, both *in vitro* and *in vivo*, was sustained and still effective at week 12. Martins *et al.*[42] showed that a HA anionic collagen composite supports sustained released of ciprofloxacin and shows good biocompatibility associated with bone tissue growth.

Uchida *et al.*[39] and Itokazu *et al.*[43] studied the release of anticancer agents (cis-platinum and methotrexate, respectively) from HA blocks. It was reported that drug release was maintained at high enough concentrations, up to as much as 12 weeks.

Otsuka *et al.*[44,45,46,47,48] investigated the *in vitro* and *in vivo* release characteristics of analgesics, indomethacin and aspirin, from self setting calcium phosphate cements and found that sustained release of drugs was achieved.

The apparent disadvantage of using calcium phosphates as drug carriers for bone delivery is the invasion treatment necessary to insert the materials into the body. Other disadvantages of using calcium phosphates may be associated with specific applications.

1.5 Spray-drying

Spray-drying is the transformation of feedstock from a fluid state into a dried product by spraying the feedstock into a hot drying medium, usually a gas[49]. The feedstock can be a solution, emulsion or suspension.

Spray-drying has long been an important processing step in the food, pharmaceutical and ceramics industries. It is a useful quick drying method, which results in weight and volume reduction. Some examples of spray-dried products are instant coffee, baby foods, powdered milk, fertilisers, plastics and structural ceramics.

In the pharmaceutical industry, spray-drying is widely used in the production of excipients, antibiotics, enzymes, and as an alternative to wet granulation for tablet formulations that cannot be directly compressed[50]. The advantages of spray-drying include:

1. It can produce powders with controlled flowability, bulk-density, moisture content, and particle size of narrow distribution.
2. It is applicable to both heat sensitive and heat resistant materials because the fast moisture evaporation keeps the particles cool.
3. It can be run continuously, adaptable to full automatic control and suitable for mass production.

There are four key steps in the spray-drying process:

1. Atomisation of feedstock into fine droplets

   This is achieved by using a pneumatic/nozzle or rotating wheel atomiser. In pneumatic atomisation, a high-pressure air jet disintegrates a stream of feedstock that is pumped in at low-pressure. In rotary wheel atomisation, the feedstock flows onto a rapidly rotating wheel and is converted to a fine mist. Pneumatic atomisers are more suitable for producing very fine sprays (droplet size < 50 μm) but are more energy consuming.
2. Spray-air contact

   The cloud of sprayed droplets meets a stream of hot drying air.
3. Moisture evaporation and particle shape formation

When the droplets come into contact with the hot air, the liquid, usually water, evaporates leaving the dry solid behind.

4. Separation of dried product from the air

   The dried product is passed into the cyclone where it is separated from the air stream. The resulting product is then collected in a collection bottle.

There are three types of airflow designs for spray-dryers[51] as illustrated in Figure 1.2:

a) Co-current flow – The feedstock is sprayed in the same direction as the flow of the hot air. The sprayed droplets meet the hottest part of the air when they are most moist.

b) Counter current flow – The feedstock is sprayed in the opposite direction of the flow of the hot air. The sprayed droplets meet with increasingly hotter air in the chamber.

c) Mixed flow – The feedstock is sprayed upwards, briefly encounters the hot drying air coming from the top. Then, due to gravity, the product falls downwards and travels through the cooler part of the chamber.

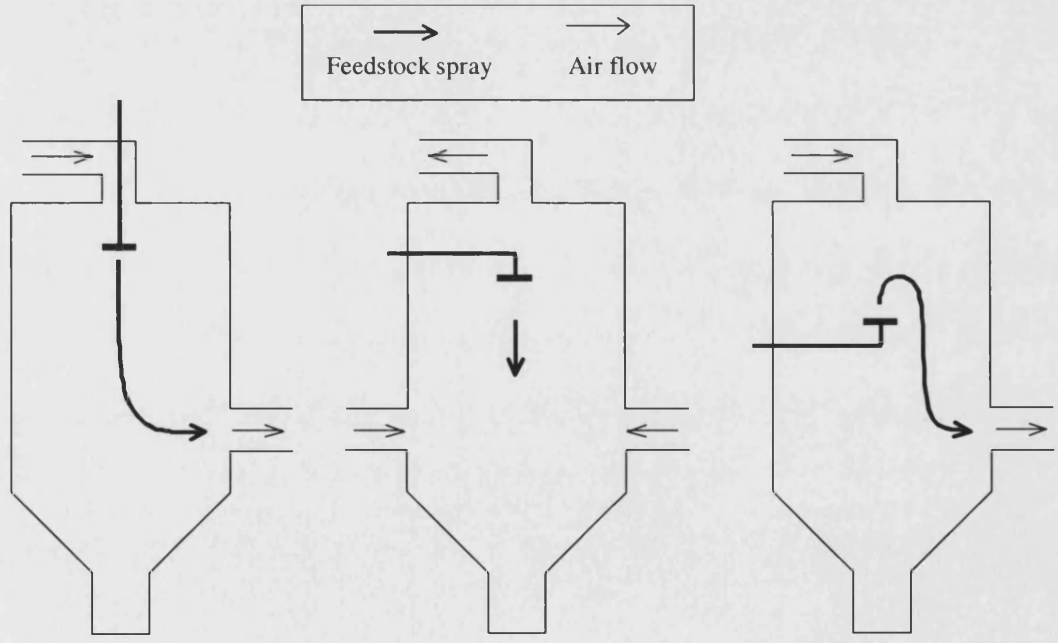

(a) Co-current flow (b) Counter current flow (c) Mixed flow

Figure 1.2 Various air-flow designs for spray-dryer.

Co-current flow design is more suitable for thermally sensitive products because the droplets come into contact with the hot drying air when they are most moist. The moisture evaporation keeps the droplets temperature down. Product temperature on discharge from the dryer is lower than the exhaust air temperature. The counter current design is suitable only for thermally stable products which require a degree of heat treatment during drying. The temperature of the powder leaving the dryer is usually higher than the exhaust air temperature. Therefore, the products contain less residual moisture in the case of counter current design than in the co-current design. The mixed flow design has the advantages of both co-current and counter current spraying methods. Due to the fact that the product is only in the hot zone for a short time, it is also suitable for both thermal sensitive and thermal stable products.

1.5.1 Drying of a Single Droplet

In the atomised liquid, each droplet consists of many tiny solid particles with solvent holding them together. When the droplet first comes into contact with the hot drying medium, evaporation of the solvent is immediate and rapid. Soluble materials, such as binders, are left behind forming a skin or film on the surface of the droplet (Figure 1.3). Due to the rapid evaporation process, the droplets are maintained at a relatively cool temperature even during the period they are exposed to the hot air.

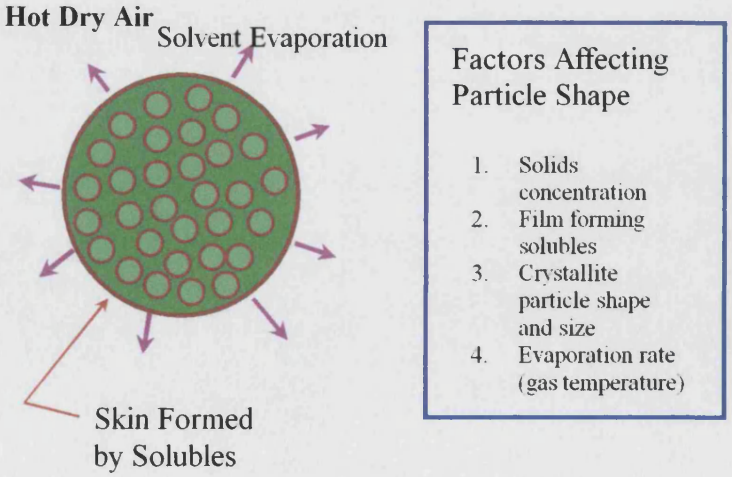

Figure 1.3 The drying of a spray-dried droplet (adapted from Shaw[52]).

The second stage of evaporation occurs at a slower rate[52]. The drying state proceeds at a constant rate as long as the surface remains saturated with liquid. The drying rate decreases as the liquid-vapour interface recedes into the porous material, until almost all liquid is evaporated.

Spray-drying produces particles of a variety of shapes, including hollow spheres, doughnut shaped particles and solid spheres.

The suggested mechanisms for the formation of hollow spheres are[52,53,54]:

(1) During solvent evaporation, the suspended solids are drawn to the droplet surface when the liquid at the interior of the droplet slowly diffuses to the surface to evaporate. As evaporation progresses, the skin grows inwards resulting in a hollow sphere. Internal pressure is built up in the droplet during this stage. If the shell is porous, this pressure could be released and a hollow sphere would be formed. If the shell is non-porous, a hollow sphere might erupt under the high internal pressure, and collapse (Figure 1.4).

(2) A low-permeability elastic film forms around the droplet. The internal pressure builds up during evaporation and causes 'ballooning'.

(3) The presence of entrapped air in the slurry persists as voids.

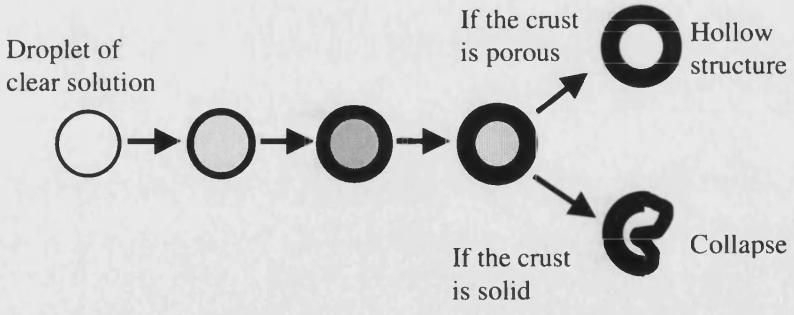

Figure 1.4 Illustration of hollow sphere formation (adapted from Luo *et al.*[53]).

The mechanisms suggested for the formation of doughnut shaped particles are[52,53]:

(1) In diluted slurries, the mobility of insoluble particles within droplets is high. These particles tend to travel to the bottom due to gravity, and elongated shape droplets are formed. This increases the surface area, which in turn increases the

total surface energy of the droplet. When the droplet is detached from the stream, the strong effect of surface spring-back occurs to minimise the surface-to-volume ratio. This spring-back action results in the inward collapse of the opposite faces of the drop and a doughnut shaped particle is formed (Figure 1.5).

(2) Since droplets do not rotate as they travel through the drying air, one side of the droplet always meets the hotter gas. Therefore, evaporation is quicker on this side and the shell grows thicker more readily. The trailing side will have only a thin shell and the interior on this side will tend to stay wet and fluid. While the liquid and solids migrate to the hot side, the thin side is drawn inward, resulting in a hollow sphere with a dimple - the doughnut shaped particles.

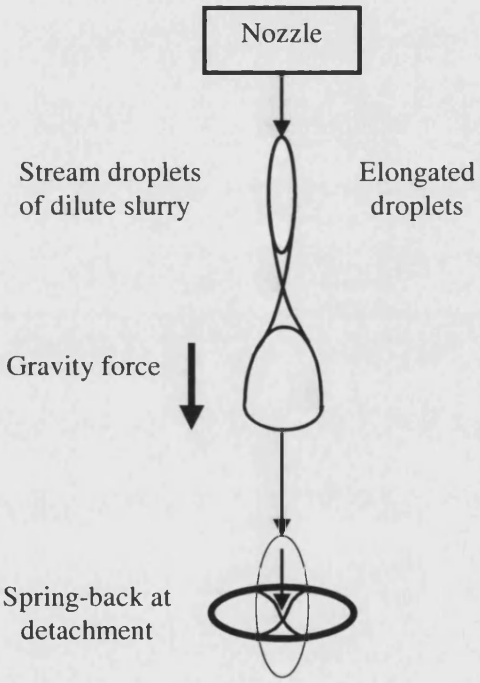

Figure 1.5 Illustration of the mechanism of doughnut shaped particle formation (adapted from Luo *et al.*[53]).

Solid spheres are formed during the spray-drying of high solid content slurries. In these cases, the surface temperature of the spray droplet exceeds the boiling point of water during drying. Moisture rapidly flows to the droplet surface by capillary action. A thick shell of insoluble precipitation rapidly forms and hence heat transfer into the interior of the droplet becomes difficult and the temperature at the interior can never reach the boiling point. The drying process is thereby controlled by the outward

diffusion process of water. The result is the formation of solid spheres[53]. The denser the starting slurry, the denser the solid spheres.

The properties of spray-drying products, such as appearance, particle size, particle density and porosity, can be altered by changing the spray-drying parameters, such as atomisation, spraying temperature, airflow, and the slurry composition, including concentration, rheology, additives and the dispersion state of the slurry[55]. Since the effects of each change on the final product are difficult to predict, development normally proceeds on a trial and error approach[56].

1.5.2 Spray-drying of Ceramics (Inorganic Materials)

The spray-drying of inorganic materials is widely practised in the ceramic industry. The basic ceramics manufacturing techniques are: mill, dry, press, and fire. Spray-drying is a versatile process for producing the dry and free-flowing powders directly from milled ceramic slurries. It also incorporates a particle formation process. The process can control the powder characteristics produced in terms of particle size, flowability, bulk-density and moisture content. In the ceramic industry, the ability to control these powder characteristics during the drying stage is very important because the quality of the finished piece depends on them.

Spray-drying is used in the manufacture of powder for whitewares (tiles, dinnerware), structural ceramics (biomedical parts, wear parts), and more importantly in the advanced ceramic industry, electronic ceramics (semi-conductors, capacitors)[57].

When making ceramic powders, the feed material is usually a water-based suspension, often called a slurry. To spray dry a slurry, the slurry must be pumpable. The homogeneity of the slurry and the solids content are critical for optimum atomisation. The air dispersing conditions are controlled to achieve reproducible powder quality.

Sometimes, additives are mixed in. In spray-drying for dry pressing, binders, dispersants and lubricants are often added to improve the subsequent pressing operation. Binders are added to increase particle strength. Dispersants are added to achieve higher total solid content for the control of powder density. Lubricants are

added so that the dried product on pressing requires less applied pressure and also aids the release of the pressed item from the die.

All additives are soluble, hence spray-dried products consist of soluble additives and insoluble ceramics. During spray-drying, the soluble materials form an even coat around each ceramic particle, holding the submicron primary particles together. The additives are normally organic and are used in very small quantities, typically 1% - 2% by weight. Only small amounts of additives are needed because the homogenous coating of these materials on all particle surfaces is effective with spray-drying. By applying laser microscopy and immersion liquid technique, Zhang *et al.*[58] reported that a binder was observed to effectively distribute itself onto the surfaces of spray-dried ceramic particles. Additives may have a negative effect on the properties of the final product. This is why organic additives, which are easily burned out in the subsequent firing process, are mainly used.

For most ceramic systems, spray-dried granules should ideally be uniform solid spheres. Solid spheres form the best compacts, which sinter well to form finished products with the least number of defects.

The spray-drying of hydroxyapatite was studied by Luo *et al.*[53]. It was reported that agglomerated spherical hydroxyapatite granules with controlled particle sizes and structures were produced. It was observed that by adjusting the spray-drying conditions, such as the volume fraction of feed slurry and the atomisation pressure, the granules produced were doughnut shapes, solid spheres or hollow spheres and of various sizes. The mechanisms of formation of these structures proposed by the authors are included in the discussion earlier in section 1.5.1.

Takami *et al.*[59] produced granulated DCPA for direct tabletting by a restricted crystal growing synthesis of DCPA, followed by spray-drying of its aqueous dispersion. It was reported that the technique produced spherical DCPA with remarkably improved compressibility and flowability, higher specific surface area (~ 33 m^2/g) and lower crystallinity, compared to conventional DCPA. Tablets prepared with spray-dried DCPA were also found to have a relatively higher tensile strength. It was proposed that the free-flowing properties of the spray-dried DCPA were due to a significant reduction

in interparticle friction because of their spherical shape, and the higher tensile strength was due to an increase in interparticle bonding in the tablet as a results of plastic deformation of the spray-dried DCPA particles which were porous and had low crystallinity.

1.6 Sintering

A ceramic green body is a molded shape made from a multitude of ceramic particles. The assembly of these ceramic powder particles usually has pores filled with atmospheric gas. When the temperature increases, material flows from various sources within the green body to fill the pores between particles. This process is termed *sintering* and the new deformed particles are referred to as grains.

Sintering is a standard technique used in ceramic industry for strengthening the ceramic green body. During sintering, the ceramic is heated to very high temperatures that are close to its melting point. The results of sintering include:

a) Changes in *grain*-size and shape;
b) Changes in *pore*-size and shape.

In brief, sintering is a process where particles coalesce under heat without liquefaction. A schematic representation of sintering is illustrated in Figure 1.6. During sintering, particles coalesce, small pores disappear and shrinkage takes place (shrinkage is illustrated by ΔL). This leads to increase in density of the materials[60,61].

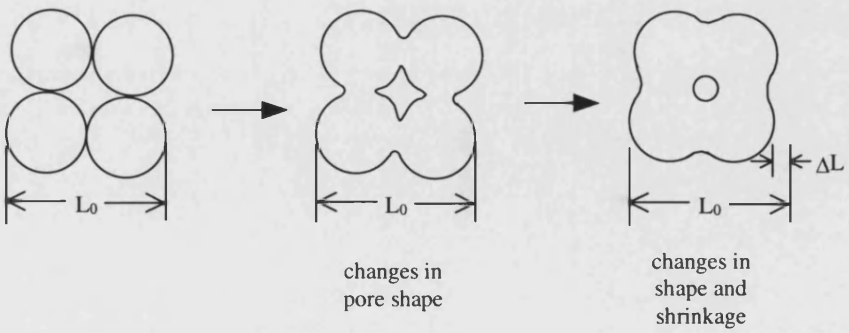

Figure 1.6. Process of sintering (adapted from de Groot *et al.*[35]).

The driving force for sintering is the reduction of total surface area[62], where the high surface energy solid-air interfaces of a powder are replaced by the lower energy solid-solid interfaces in the form of grain boundaries. The surface of a solid material usually consists of high energy chemical bonds, which are comparable to stretched springs. In nature, low energy state bonds are preferred. When particles touch each other, spontaneous joining does not occur because there is an energy barrier, the activation energy (Figure 1.7). During sintering, the activation energy is provided and this barrier is overcome[62]. Hence, the stretched springs relax, energy is released as heat, the surfaces merge, and the stretched bonds on the surface move into the lattice vacancies of nearby material becoming ordinary internal chemical bonds[63]. Since the newly formed grain boundary also represents an area of high energy in the system, there is also a driving force for grain growth, which will result in the elimination of the grain boundary.

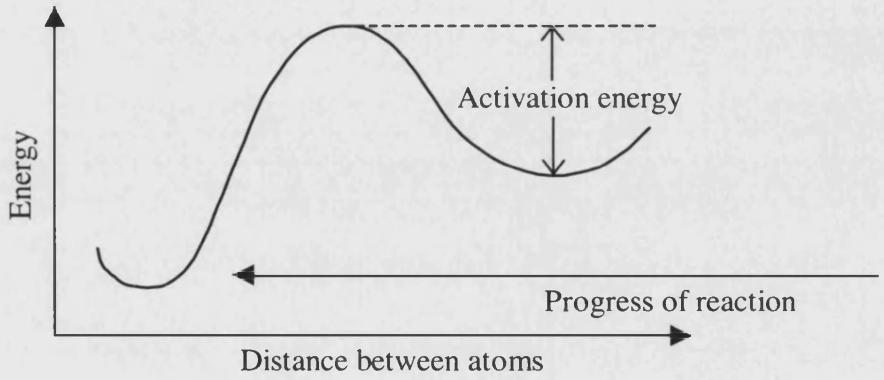

Figure 1.7 Activation energy (taken from Shanefield[62]).

Solid state sintering takes place in three stages as described in Table 1.1[60]. During sintering, materials migrate mainly due to surface curvature and vapour pressure[36]. In the initial stage, also referred to as neck growth, the system tries to minimise its surface free energy by migrating high energy bonds into existing lattice vacancies, as described in the previous paragraph. If there is a difference in the concentration of lattice vacancies, materials will move from areas of low concentration to areas of high concentration. Due to the surface curvature, the lattice vacancies near the neck are greater; as a result, during sintering materials migrate towards the neck area. This leads to increased particle contact, neck growth, and the grain centres moving closer together, resulting in interparticle shrinkage and an increase in density. Since the vapour

pressure also changes with respect to the curvature, it also promotes material transfer[64]. The first grain growth represents the termination of the initial sintering stage and the beginning of the intermediate stage. At this point, pores are continuous, interconnected and intersected by grain boundaries. During the intermediate stage, the cylindrical pores shrink and break up into a string of spherical, closed pores (Figure 1.8)[60] and the grain size grows slowly. In the final stage, these isolated pores shrink continuously until they disappear, and the sintering process is considered complete. An alternative final stage of sintering occurs when the discontinuous grain growth occurs before all the porosity is removed. Further heating results in the elimination of pores at the grain boundaries, but the pores situated within the grains still remain. Generally, small pores that are a fraction of the powder particle size will disappear during sintering, but larger pores cannot be sintered out[62].

Table 1.1 Stages of microstructural characteristics during solid state sintering of powder compacts[60].

Stage	**Observations**
Initial	Surface smoothing of particles
	Grain boundaries form, neck growth
	Rounding of interconnected, open pores
	Porosity decreases <12%
Intermediate	Shrinkage of open pores intersecting grain boundaries
	Mean porosity decreases markedly
	Slow grain growth
Final (1)	Closed pores containing kiln gas form when density is ~ 92%
	(>85% in heterogeneous material)
	Closed pores intersect grain boundaries
	Pores shrink to a limited size or disappear
	Pores larger than grains shrink relatively slowly
Final (2)	Grains of much larger size appear rapidly
	Pores within larger grains shrink relatively slowly

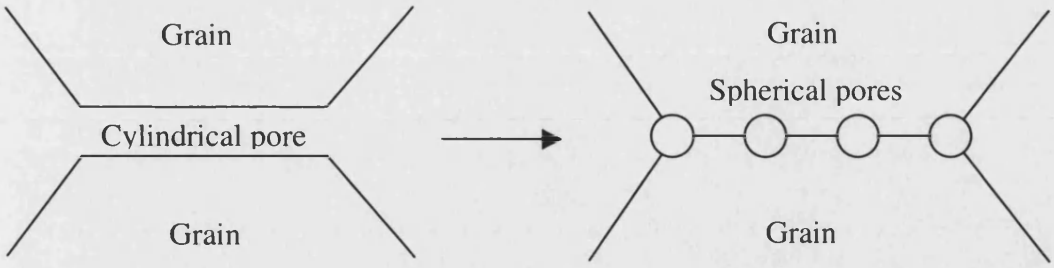

Figure 1.8 Break up of a cylindrical pore into a string of spherical pores (adapted from Ring[60]).

The higher the surface area per gram of powder, the more surface energy is available as a driving force for sintering. Hence, the specific surface area of the starting powder can be a good indicator of how well a powder will sinter under favourable conditions[62]. Different sintering conditions such as temperature, duration and atmosphere of sintering will cause the primary particles to 'coalesce' to different degrees[36]. Therefore, by modifying the starting powder and the sintering conditions, it is possible to tailor make ceramics with desired porosity and pore-size.

Sintering adds mechanical strength to a material but generally does not change the chemical nature of a material. Sintered calcium phosphates are biocompatible and sintered hydroxyapatite is commonly used as a bone substitute.

1.7 Project Background

As discussed earlier (section 1.5), under the right conditions spray-drying can produce inorganic free-flowing hollow centred agglomerates or microspheres (Figure 1.9). These microspheres are held together by a binder, which is mainly distributed on the surface of the microspheres. It is envisaged that these microspheres can be used as drug carriers. Their hollow centres can be used as drug reservoirs while their shells and the binder layer can act as a barrier to avoid the instant release of drugs.

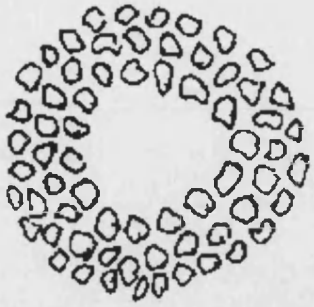

Figure 1.9 Schematic of a microsphere.

It is proposed that microspheres of different sizes would release incorporated drug at various rates. Therefore, if a drug carrier system contains microspheres of two particle sizes, it is reasonable to expect that the drug might be released at two different rates. An extended or a biphasic drug release profile may be achieved. This concept is illustrated in Figure 1.10.

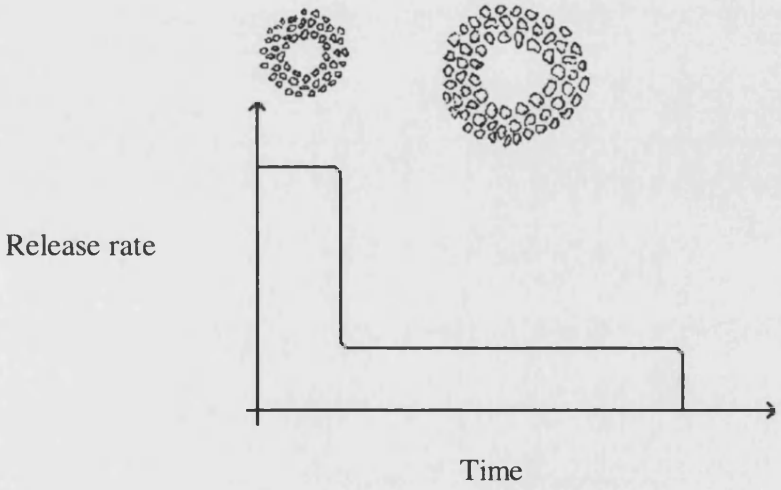

Figure 1.10. Microspheres of two different particle sizes may produce two different drug release rates. An extended release profile can be achieved.

If a drug carrier system contains two or more types of microspheres, and these microspheres are made from materials which have different dissolution rates (Figure 1.11), two or more different release rates can be achieved (illustrated in Figure 1.12).

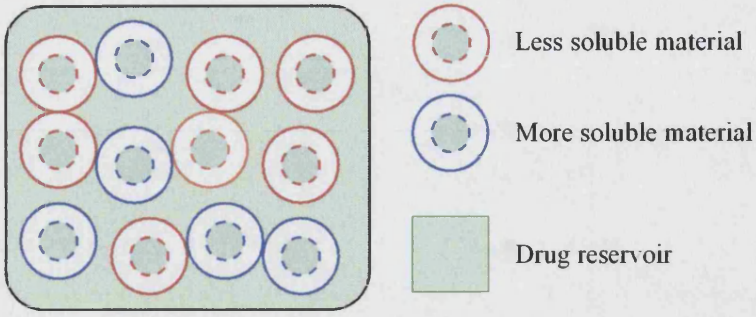

Figure 1.11 A system with microspheres of different solubilities.

Furthermore, by using binders of different solubilities, or by adding external coatings to the microspheres, the release of drugs may be further delayed and targeted at different absorption sites of the gastrointestinal tract depending on the properties and solubility of the coatings.

The porosity and pore-size of these inorganic microspheres can be further modified by sintering. Different sintering conditions can produce microspheres with different pore-sizes, which may deliver drugs at different rates. Controlled pore-size may lead to controlled drug release. In short, different combinations of the microspheres may be used to achieve desired patterns of delivery.

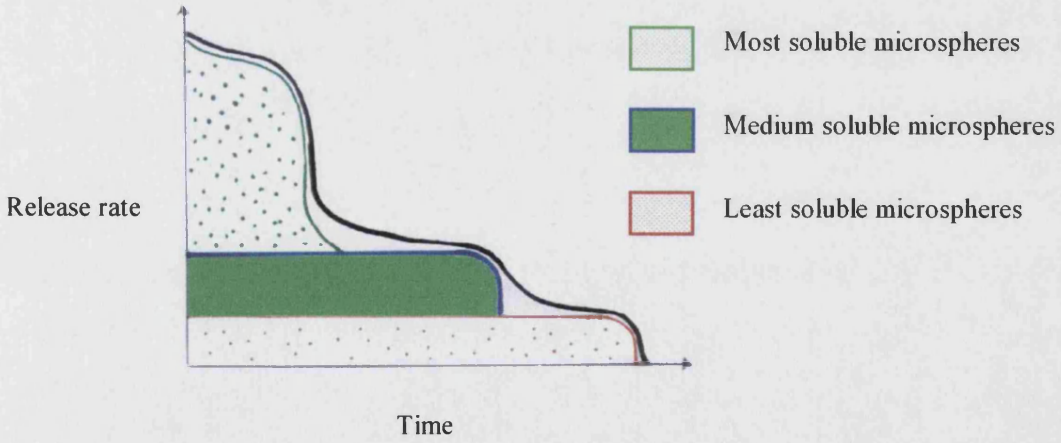

Figure 1.12 Carrier materials with different dissolution rates could produce a multiphase drug release system.

There are several probable methods of loading a drug into the microspheres:

1. A drug is mixed with the slurry, and the drug-containing slurry is then spray-dried.
2. Microspheres are placed in a vacuum, and a drug, either as powder or solution, is then vacuum forced into the microspheres.
3. Drug crystals are cultivated within the microspheres by soaking the microspheres in supersaturated drug solution.
4. A drug is bound to a polymer and then the drug-containing polymer is loaded into the microspheres.

In summary, it is proposed that ceramic microspheres can be developed into a novel drug delivery system. The system is flexible and allows customised multiphase drug release profiles. It is envisaged that flexibility of the system to delivery drugs at various rates can be achieved by:

1. Using microspheres of various sizes;
2. Using microspheres made from materials of different dissolution properties;
3. Controlling the pore-size of the microspheres by sintering;
4. Further coating the microspheres with polymers (for example, acid resistant polymer for target release in the intestine).

Apart from being highly flexible, it is expected that the new system will also be attractive from the manufacturers' viewpoint because:

1. The ingredients involved are low cost pharmaceutical materials;
2. No toxic solvents are needed in the process;
3. The process is suitable for automatic mass production;
4. Ceramic systems are stable, heat resistance, have long shelf life, and can be easily sterilised by either heat or gamma radiation.

1.8 Potential Usage of Calcium Phosphate Microspheres

1.8.1 Bone Delivery

Osteomyelitis is the infection of bone, usually of bacterial origin. Infections are chronic, painful and require urgent treatment. The success of the treatment depends on

the delivery of bactericidal concentration of antibiotics to the infected bone. Currently, osteomyelitis is treated with antibiotic-impregnated polymethylmethacrylate (PMMA) beads/cement as implants in the infection site, and systemic antibiotics[65].

Bone implants are effective in delivering high concentration of antibiotics. However, the main disadvantage of the PMMA systems is that they have to be changed at regular intervals, and they must also be removed before sound bone can re-grow in the defect. The reopening of the wound for changing is a very costly and painful process. Other disadvantages of PMMA systems include:

- During polymerisation of PMMA cement, antibiotics such as penicillin and its derivatives could be deactivated[40];
- PMMA does not bond to living bones;
- PMMA toxicity poses a practical clinical problem. It has been reported that even at low concentrations, the polymer can seriously suppress the phagocytic and bactericidal activity of human leukocytes[66].

As discussed earlier (section 1.4), calcium phosphates are biocompatible, resorbable, and can act as bone precursors. As a result, calcium phosphate microspheres would be ideal implant drug carriers for the treatment of osteomyelitis and other bone disorders. The main advantage of these systems is that they do not have to be surgically removed after the delivery of drug. They can either dissolve in the body or become part of the bone tissue by a natural growth process. In other words, after the delivery of antibiotic, the carrier forms the basis of a bone graft.

By using calcium phosphates of a range of solubilities, these drug carrier systems can be engineered to resorb at a known rate, part of the structure dissolving at a predetermined rate and part of the structure remaining insoluble to be integrated to the new bone structure. These microspheres can be antibiotic reservoirs, which release antibiotics directly at the site over a sustained period of time. By controlling the morphology and pore-size of these microspheres, precise control of drug delivery rates may also be achieved. Should very low rates of delivery be required, the drug might be incorporated into a polymer host and then be held in the ceramic host superstructure.

1.8.2 Oral Delivery

Since calcium phosphates are usual excipients in tabletting, calcium phosphate microspheres can be taken orally. Potentially, the microspheres could be used in the pharmaceutical and food industries. For example, due to their robust nature, they could be used as a protective carrier to stabilise food substances or drugs in the digestive tract, or during the storage period. They could also be used as carriers to mask the bitter tastes or strong smells of drugs or health foods. This masking method could be advantageous over traditional methods of packing materials in capsules or using tablet coatings, as some capsules and coated tablets are difficult to swallow due to their size.

These microspheres could be coated with biopolymers of different properties, *i.e.*, gelatin, chitosan, carrageenan or eudragits, to further delay the release of the drugs from the microspheres and to achieve controlled release, or to improve the taste masking property of the microspheres.

Spray-dried calcium phosphate microspheres are highly porous and therefore have the potential to accommodate high drug loading. High drug loading carriers could reduce the size of dosage forms, making them more acceptable to patients. Also, some drugs that are currently only feasible to be formulated as tablets could be formulated as capsules if they are to be incorporated into these microspheres.

By modifying the pore-size and structure of the microspheres, the release of drugs from them could be modified and controlled. Therefore, the microspheres themselves could be the basis of an oral controlled release system.

Sintered microspheres are not expected to dissolve in the intestine and therefore not be absorbed by the body through the gastro intestinal tract, but will leave the body as ghosts. Since these microspheres are in the micron size range (mainly < 30 μm in diameter), they should not be noticeable in the faeces.

1.8.3 Transdermal Delivery – Needle-Free Injection

When the oral route is inappropriate, for example when the first pass mechanism needs to be avoided or the patient cannot ingest orally, alternative drug delivery routes are

explored. Parenteral needle injections can be an effective alternative, however, such parenteral administration have the following disadvantages[67]:

1. Complexity of dose preparation and administration, therefore, professional skills are required for their application.
2. Due to stability issues after reconstitution, they have a limited shelf life.
3. Compromised patient compliance. Fear of injections can seriously affect patient compliance and needle phobia is common. Pain upon injection is also a factor for certain drugs and injection sites.
4. Health workers are at risk of injuries by patients' needles, which may expose them to serious health hazards that include AIDS and hepatitis B.

To overcome the above issues, needle-free injections were invented. Needle-free injections eliminate 'needle phobia' and reduce patient anxiety. They also eliminate the risk of bloodborn pathogen transmission through accidental needlestick injuries. Hence the safety for health workers is much improved. The injection occurs in a fraction of a second and therefore is very time effective to immunise large numbers of people quickly and economically[68].

Needle-free liquid jet injections have been used for many years[69]. However, needle-free powder injections have only recently been used. Professor Bellhouse at the University of Oxford discovered the possibility of using compressed gas to blast fine particles of a drug through the surface of the skin in 1992, and a patent was submitted for the use of the needle-free syringe using supersonic gas flow for particle delivery in 1994[70].

Needle-free powder injection is also known as 'high velocity powder injection'. It works by accelerating particles to a sufficiently high velocity such that they penetrate the outer layers of the target tissue and deposit the particles close to the site of action for uptake. The technology is based on the principle of supersonic gas dynamics. The driving force is compressed gas, helium, which is accelerated to high velocities through a specially designed convergent-divergent nozzle[70]. The drug particles are entrained within this gas flow and acceleration is generated by drag, a function of relative slip velocity between the particle and gas[67]. The particle acceleration and exit velocity

depends on several factors related to the device, *e.g.*, gas pressure, nozzle geometry, and the drug particles themselves, *e.g.*, the density and size.

The skin is considered the largest organ of the human body. It is mainly classified into three layers: epidermis, dermis and hypodermis. The epidermis is the outermost layer and it can be subdivided into many layers including the stratum corneum. The stratum corneum, which is 10 – 25 μm thick[75], is the principle diffusional barrier to percutaneous drug absorption. Powder injection typically delivers the particles into the skin to a depth not more than 100 μm. The particles cross the stratum corneum, but still stay predominantly in the epidermis. The drug molecules contained in the particles then dissolve to act locally or diffuse into the rich capillary beds of the nearby dermis to enter the systemic circulation.

Powder injection technology has been developed for the administration of a range of medicines, including local anaesthetics (*e.g.* lignocaine[67]), proteins and peptides (*e.g.* calcitonin, alprostadil[71]), and DNA vaccines (*e.g.* hepatitis B and influenza vaccines[72]).

The optimum particle characteristics required for powder injection are different from the conventional dosage forms. In addition to standard compatibility and stability parameters, particle quality and size distribution are also important. There is a strict requirement for physical stability in addition to chemical stability. The powder must retain its size distribution during transport and storage, and particles must also survive the unique action of the gas jet within the device and the impact with the skin at high velocity. Furthermore, the powder should also have dissolution characteristics appropriate for the given application.

The relatively small-volume of the target epidermis imposes a limitation on the mass of powder that can be delivered per unit area of skin. Current powder injection systems capable of delivering the drug payload over an area of up to 2 cm^2 are generally restricted to doses in the low milligram range.

In the case of DNA delivery, the ultimate aim is to deliver the DNA into the cell nucleus. DNA has been precipitated onto dense gold particles (1 μm - 3 μm) and

delivered via a powder injection system by PowderJect Pharmaceutical plc. The results showed that a much lower dose of vaccines, ~ 1000 fold less, was needed to produce a balanced immune response compared to direct syringe and needle injection[73]. This is because the system delivered the DNA vaccine directly to the intracellular compartment[74]. The use of smaller does of DNA vaccines means that the treatment cost can be dramatically reduced.

The depth of particle penetration depends on momentum, *i.e.* it is related to the particle size, mass and velocity (Equation 1.1)[67]. Ideally, optimum momentum conditions will be achieved with large, dense particles. However, there is only a practical range of particles that can be used. Basic clinical experiments showed that organic particles of less than 20 μm have insufficient momentum to penetrate target tissues; particles of 20 μm - 100 μm penetrated the skin[75]; particles of excessive size can cause minor subdermal haemorrhages and are not suitable for cosmetic reasons.

$$P = k\left(\frac{m}{A}\right)\log\left(1+\frac{(v_0 - v_t)^2}{\Phi}\right) \qquad \text{Equation 1.1}$$

P = depth of particle penetration (m)

k = Petry constant[67], related to the biomechanical properties of the target tissue

m = mass of particle (g)

A = plan area of particle (m^2)

v_0 = impact particle velocity (m/s)

v_t = threshold particle velocity for penetration (m/s)

Φ = penetration coefficient (m/s)

Depending on the particle and density, formulations for intracellular or extracellular can be achieved via powder injection. To achieve intracellular delivery, DNA vaccines were precipitated onto high-density carriers, microscopic gold particles that are only 1 μm - 3 μm in diameter[76]. These particles achieve the momentum needed to deliver the vaccine directly into cells. The average diameter of target epidermal cells is 20 μm, therefore the delivered particle does not interfere with cell viability. Once inside the cells, the DNA elutes off the gold and becomes transcriptionally active, producing the encoded protein to trigger an immune response[77].

For extracellular delivery, pharmaceutically acceptable sugars and polymers were used as excipients to aqueous vaccines to impart stability, density and hardness to the vaccine particles[78]. Particles in the 20 μm - 70 μm size range were used because particles smaller than these were stopped by the skin barrier, and these particles are too large to enter individual cells, resulting in extracellular delivery[77].

Sintered calcium phosphate microspheres are potentially a better drug carrier than the currently used organic carriers (sugars, polymers) or gold for powder injection technology because:

1. Calcium phosphates bioceramics are much denser than most organic materials. They have a high density of ~ 3 g/cm^3 and therefore have the capability of achieving high momentum to penetrate the skin.
2. Calcium phosphates bioceramics are much stronger mechanically than most organic materials. They can provide the physical strength and stability required for this technology.
3. Calcium phosphate microspheres can be manufactured to have high porosity to accommodate high drug loading. This is particularly beneficial because the small-volume of the viable target epidermis is a limiting factor for the amount of particles that can be delivered by powder injection. The high packing density of drugs inside the microspheres may also serve as a reservoir for drugs to achieve a sustained release profile of drug delivery.
4. Calcium phosphates are non-toxic, biocompatible and bioerodible. Calcium phosphate particles are commonly found in all vertebrates[32] and they can be resorbed by the human body after drug delivery. This is a significant advantage over gold, which has been shown to cause severe side effects, especially when used in long-term disease management, *e.g.* in rheumatic arthritis.
5. For achieving intracellular delivery, calcium phosphates are much cheaper than gold.

It is possible that the injected sub-dermal calcium phosphate particulates may be encapsulated by fibrous tissue and formed a cyst under skin. However, it is more likely that the calcium phosphate particulates will be dissolved by the body tissue and any non-dissolved parts will be removed from the body together with dead skin cells in our natural skin shedding process.

1.9 Aims of Study

The aim of the project is to develop novel inorganic microsphere drug delivery systems using calcium phosphates. The project can be divided into three sections:

1) To produce inorganic porous microspheres using spray-drying
2) To control the porosity and pore-size of the microspheres by sintering
3) To investigate the delivery profiles of drugs via the microspheres

Firstly, the feasibility and limitations of producing calcium phosphate microspheres by spray-drying were investigated. The effects of the composition of the slurries and the influence of key parameters in the spray-drying process were studied.

Secondly, the porosity and pore-size of the microspheres were modified and controlled by sintering. The effects of sintering conditions on the microspheres were investigated. The physical and chemical changes of microspheres after sintering were characterised by various analytical techniques.

Thirdly, methods of loading model drugs into these microspheres were studied, followed by the investigation of *in vitro* drugs release profile from these microspheres to evaluate the drug delivery potential of the systems.

2 Materials, Equipment and Methods

2.1 Materials

Material	Batch/Lot no.	Supplier
Calcium phosphate dibasic	38H0675	Sigma-Aldrich Chemical Co., Dorset, UK
Capsules, hard gelatin (natural transparent)	size 0: 200820699 size 2: 30013721 size 3: 200247099	Davcaps Ltd., Gloucester, UK
Deionised water (purified by reverse osmosis)	Freshly purified	Millipore, Watford, UK
Dispex A40	00054742	Allied Colloids Ltd., Bradford, UK
Ethanol (99.7-100% v/v)	L121307	BDH Laboratory Supplies, Poole, UK
Eudragit L100	03-80047	Röhm Pharma, Weiterstadt, Germany
Hydrochloric acid	k28090152 031	BDH Laboratory Supplies, Poole, UK
Paracetamol	77H1805	Sigma-Aldrich Chemical Co., Dorset, UK
Polyethylene glycol 1000	17H0551	Sigma-Aldrich Chemical Co., Dorset, UK
Polyethylene glycol 6000	23265351	FSA Laboratory Supplies, Loughborough, UK
Polyethylene glycol 10000	02920EY	Sigma-Aldrich Chemical Co., Dorset, UK
Polyethylene glycol 20000	2172A 8908869	BDH Chemicals Ltd., Poole, UK
Potassium dihydrogen orthophosphate	A224724 033	BDH Laboratory Supplies, Poole, UK
Propranolol hydrochloride	12896031	Cosma S.P.A. Ciserano (BG), Italy
Sodium carboxymethylcellulose	60804	Honeywill & Stein Limited, Surrey, UK
Sodium hydroxide pellet	B255950 828	BDH Laboratory Supplies, Poole, UK
Sodium lauryl sulphate	36724 225	Fisons Scientific Equipment, Loughborough, UK

Tragacanth, powdered (BP)	94RH/L2756/1	Thornton and Ross, Huddersfield, UK
Tri-calcium phosphate	K21547743	E Merck, Damstadt, Frankfurter Strasse, Germany

2.2 Equipment

Equipment	Model	Supplier
Accelerated surface area and porosimetry analyser	ASAP 2010	Micromeritics Instruments Co., Georgia, USA
Dilatometer	214 1 392	Netzsch Thermal Analysis, Bavaria, Germany
Dissolution bath	Type PTWS3C	Pharma Test Apparatebau GmbH, Hainburg, Germany
Dissolution software	WinDiss Version 4.106	Pharma Test Apparatebau GmbH, Hainburg, Germany
Furnace for sintering	CWF 13/13	Carbolite, Sheffield, UK
Filter, sintered glass	porosity 4	BDH Laboratory Supplies, Poole, UK
Magnetic Stirrer	H1 190M	Hanna Instruments Ltd, Bedfordshire, UK
Mastersizer	Mastersizer X, Mastersizer 2000	Malvern Instruments Ltd., Malvern, UK
Oven	OV-440	Gallenkamp, Loughborough, UK
pH meter	Jenway pH meter 3305	Spectronic Analytical Instruments, Garforth, Leeds, UK
pH papers, (pH 8-10 and pH 4-7)	Fisherbrand	Fisher Scientific UK Ltd, Leicestershire, UK
Pump (for dissolution)	C8-midi	Watson-Marlow AliteaAB, Stockholm, Sweden
Scanning electron microscope	Jeol T330 and Jeol T6310	Japanese Electron Optics Ltd., Tokyo, Japan
Spray-dryer	SD-05	LabPlant Ltd., West Yorkshire, UK

Sputter coater, carbon	Pirani Penning, Model 4	Edwards High Vacuum Ltd., Sussex, UK
Sputter coater, gold	Model S150B	Edwards High Vacuum Ltd., Sussex, UK
Surface area analyser	Gemini 2360	Micromeritics Instruments Co., Georgia, USA
Tapped density tester	-	J. Engelmann AG, Ludwigshafen a. Rh, Germany
Ultramicrotome	OM U3	C. Reichert AG, Vienna, Austria
Ultrasound bath	Fb200b	Decon Laboratories Ltd. Hove, East Sussex, UK
UV/VIS spectrophotometer	Unicam 8625 and Helios α	ThermoSpectronic, Cambridge, UK
Vacuum pump	A-C motor, 5KC48PN0202X	GE Motors, Halifax, UK
Water bath (Refrigerated Circulator)	DC5-K20	Thermo Haake, Karlsruhe, Germany.
X-ray diffractometer	Philips PW 1710	Philips Analytical, Cambridge, UK

2.3 Particle-Size Analysis

Particle-size distributions were determined using either a Mastersizer X or a Mastersizer 2000 (Malvern Instruments Ltd., Malvern, UK). Mastersizer instruments measure the Low Angle Laser Light Scattering (LALLS) pattern of particles as they come into contact with a laser beam. Assuming that particles are spherical in shape, Mastersizer's calculations are based on the Mie theory that solves the equations for interaction of light with matter. The fundamental measurement produced by Mastersizer instruments is a size/volume distribution.

On passing through the beam, samples scatter the laser beam at a low angle in a forward direction[79]. The angle at which the light is scattered by a particle is inversely proportional to the size of the particle. Small particles will give rise to large angles of scatter, and large particles will give rise to small angels of scatter[80]. A Fourier lens then

focuses the scattered light onto a detector. The response is averaged and numerically inverted to produce the size distribution results. The instrument can be used to characterise particles in both liquid and gas suspending media.

The particle-size distribution results were expressed as volume mean diameter, as follows:
d(v, 0.1) = particle diameter, such that 10% of the total particle volume is composed of particles of smaller diameter.
d(v, 0.5) = particle diameter, such that 50% of the total particle volume is composed of particles of smaller diameter. This is the volume median diameter.
d(v, 0.9) = particle diameter, such that 90% of the total particle volume is composed of particles of smaller diameter.

2.3.1 Mastersizer X

The Mastersizer X uses a low power helium-neon laser beam (λ = 0.63 μm). It has three separate lenses: 45 mm, 100 mm, and 300 mm, which are capable of measuring particle-sizes in the range of 0.1 μm - 80 μm, 0.5 μm - 180 μm, and 1.2 μm - 600 μm respectively.

Obscuration is the amount of light being scattered. The concentration of the sample is best when the obscuration is within 10% - 30%. If too little sample is used, the sample signals are not clearly distinguished from the background noise; conversely, if too much sample is used, secondary scattering or multiple diffraction occurs and the conditions on which the sample analysis are based do not apply.

Particle-size distributions measured by Mastersizer X were obtained either by suspending the particles in a small-volume (15 ml) stirred cell (SVC), a large-volume (1 litre) circulating cell (LVC), or via a dry powder feeder (DPF). In this study, enough of a sample was added until an obscuration of 15% - 25% was obtained. It was assumed that solid and opaque particles of the calcium phosphate sample have a refractive index of 1.53.

2.3.1.1 Small-Volume Stirred Cell (SVC)

Most measurements in this study were obtained using the SVC, in conjunction with the 100 mm lens. The advantage of the SVC is that it only requires a small amount of sample and suspending medium. Firstly, the SVC was filled with ~ 15 ml of deionised water, the optics were then aligned. The diffracted light with no sample present was measured to establish a background reading. A 20 ml vial was filled with ~ 5 ml deionised water and ~ 1 mg of sample was added into the vial, followed by a small amount of the dispersant, tetrasodium pyrophosphate. The vial was manually shaken to facilitate wetting of the sample, and then sonicated for the required period of time. The suspensions were then pipetted into the SVC. All samples were prepared and analysed in triplicate.

2.3.1.2 Large-Volume Circulating Cell (LVC)

The LVC was used when particle-size distributions below 0.5 μm were to be determined, as the 45 mm lens was designed to be used in conjunction with the LVC. The LVC allows for automated sample dispersion, with variable pump, stir and ultrasonication rates available. The LVC was first filled with deionised water and a small amount of the tetrasodium pyrophosphate dispersant was then added. The sample pump, stir and ultrasonication rates were all set to the LVC scale of 5. The sample was then added to the cell by a pipette. All samples were prepared and analysed in triplicate.

2.3.1.3 Dry Powder Feeder (DPF)

DPF allows dry powders to be measured directly. The powder is sucked through the laser beam by means of a vacuum cleaner (Electrolux Powder system 1500W, Bedfordshire, UK) to prevent dust being sprayed into the environment. DPF may result in poorer dispersion than using a liquid dispersing medium. However, in conjunction with a suspension analysis it can be valuable in determining the amount of agglomerated material in the dry state.

2.3.2 Mastersizer 2000

Compared to the Mastersizer X, the Mastersizer 2000 is a more advanced model. It has two lasers: a red helium neon laser and a blue solid state laser. It can measure particle-sizes in the range of 0.02 μm - 2000 μm with a single lens. The particle refractive index of the calcium phosphate sample was determined using the Mastersizer 2000 and was found to be 1.30. This value was used for all calculations.

Samples (~ 1 mg) were suspended in cyclohexane using 0.1% lecithin, as suspending agent, in a 25 ml glass vial. This was stirred for 5 min, followed by sonication for 5 min. The pre-dispersion was then added using a plastic pipette to the dispersant (pure cyclohexane) in a small-volume sample dispersion unit in the Mastersizer, until the obscuration was in the range 5% - 15%. All samples were prepared and analysed in triplicate.

2.4 Density Measurements

2.4.1 Tap Density

Tap density was measured using a tap density tester (J. Engelsmann AG, Ludwigshafen a. Rh, Germany). Approximately 10 ml of sample powder (3 g - 7 g) were poured into a 10 ml graduated cylinder. The accurate weight and volume of the samples were recorded and the bulk-density calculated. The graduated cylinder was tapped in a cycle of 500 taps. The volume of the sample was recorded after each cycle, and the cycle was repeated until no further decrease in volume was observed. A total of 6 cycles was performed for every sample (total tapping = 3000). The tap density was calculated from the final tapped volume recorded. Each sample was analysed in triplicate.

2.4.2 True Density

The true density was determined using a helium pycnometer (AccuPyc 1330, V2.01, Micromeritics Instruments Co., Georgia, USA). Approximately 2.5 g - 2.9 g of each sample was accurately weighed into the pycnometer sample cell on a 4-point balance. The sample was put in an oven (Size 2 incubator, model 1H150, Gallenkamp, Loughborough, UK) at 60 °C for two days to eliminate moisture. The sample was then

placed into the pycnometer, and was purged with helium. Ten sequential density measurements were then collected and the mean density value was determined. The mean value of 3 experimental runs, using different powder samples, was calculated. Samples were oven treated before density measurements were carried out because preliminary experiments showed that oven treated samples were 3% - 4% less dense than untreated samples.

2.5 Surface Area Analysis

The surface area characteristics of powders are important because they greatly influence the behaviour and the processing methods that can be used.

2.5.1 Surface Area Analyser

The specific surface area of samples was determined using a 5-point BET N_2 adsorption apparatus (Gemini 2360 Analyser, Micromeritics Instruments Co., Georgia, USA). Nitrogen was used as the pressure gas or adsorbate; an empty balance tube of identical dimensions to the sample holder was used to measure the generated pressure differential.

An accurately weighed sample was loaded into a glass tube (12 cm^3), and degassed (FlowPrep 060 Degasser, Micromeritics Instruments Co., Georgia, USA) at 105 °C for 24 h to remove surface moisture and pre-adsorbed gases. This temperature (105 °C) was used to decrease the degassing time. After degassing, the sample was re-weighed, and the value obtained was used for the surface area determinations. The sample was cooled to the boiling point of the adsorbate gas (–196 °C) by immersing it in a Dewar flask filled with liquid nitrogen. The sample was then exposed to partial pressures of the adsorbate gas until the surface was covered by the gas. The liquid nitrogen Dewar was removed from the sample cell. The amount of the previously adsorbed gas was measured by a detector as the sample warmed to room temperature. Using the BET equation, the surface area was derived from the volume of gas adsorbed. This calculation was performed by the Gemini analyser. Five replicates were obtained for each sample.

2.5.2 Accelerated Surface Area and Porosimetry Analyser

An Accelerated Surface Area and Porosimetry Analyser (ASAP) 2010 (Micromeritics Instruments Co., Georgia, USA) was used to determine the surface area of samples. This equipment can also provide information about pores in the nanometer range (pore diameter of 0.35 nm - 300 nm).

The basics of the analytical technique is that a sample contained in an evacuated sample tube is cooled to cryogenic temperature, then is exposed to analysis gas at a series of precisely controlled pressures. With each incremental pressure increase, the number of gas molecules adsorbed on the surface increases. The pressure at which adsorption equilibrium occurs is measured and the universal gas law is applied to determine the quantity of gas adsorbed. As adsorption proceeds, the thickness of the adsorbed film increases. Firstly, the micropores in the surface are quickly filled, then the free surface becomes completely covered, and finally larger pores are filled. The process may continue to the point of bulk condensation of the analysis gas. The desorption process may then begin in which pressure is systematically reduced allowing for the liberation of the adsorbed molecules. As with the adsorption process, the changing quantity of gas on the solid surface is measured. The two sets of data obtained describe the adsorption and desorption isotherms, respectively. Analysis of the isotherms yields information about the surface characteristics of the material.

An accurately weighed sample was placed in a standard glass sample tube (25 cm^2). The higher total surface area available for measurement, the more reliable the analysis becomes. Therefore, a larger amount of sample was used for samples with predicted low surface area and vice-versa. Preliminary studies indicated that non-sintered samples have high surface areas, so ~ 1 g of powder was used in each experiment, whilst sintered samples have smaller surface area and ~ 9 g of powder was used.

Firstly, a sample was placed in a degas port of the analyser and degassed by vacuum pumping down to 1 mmHg with the heating jacket at 200 °C, overnight. The sample tube was then backfilled with nitrogen gas to atmospheric pressure, before it was transferred to an analysis port. This was to reduce the risk of mixing with atmospheric gases during the transfer. At the analysis port, the sample was cooled down to the

boiling temperature of nitrogen (–196 °C) by immersing the sample holder in the Dewar filled with liquid nitrogen. The sample was then exposed to increasing partial pressures of nitrogen. The volume of gas adsorbed was measured at each partial pressure. A series of pressure/volume measurements were made over a sequence of ascending relative pressures from 0.00001 to 0.97000. The procedure was then reversed by reducing the relative pressure over a sequence of descending relative pressures, back to 0.00001.

2.6 Mercury Intrusion Porosimetry

To investigate the pore-size and the porosity of the microspheres, a Micromeritics Autopore II Porosimeter (Type 9220 V3.03, Micromeritics Instruments Co., Georgia, USA) was used. The Autopore measures the volume distribution of pores in materials by mercury intrusion or extrusion. It operates in the pressure range of 3.4 kPa – 413685 kPa that corresponds to pore analysis in the range of 360 μm- 0.003 μm, assuming 130° is the mercury wetting angle. Mercury has a high surface tension and is non-wetting to most materials; hence, pressure must be applied to introduce mercury into pores of solid materials. Mercury porosimetry is based on the capillary law that governs liquid penetration into small pores.

The Autopore has two pressure chambers: a low-pressure chamber, operating from 3.4 kPa - 207 kPa; and a high-pressure chamber operating from 207 kPa - 413685 kPa. The filling pressure, *i.e.* the pressure at which mercury is introduced in the penetrometer, can be controlled between 3 kPa - 69 kPa. The pressure was generated by a hydraulic pump and the amount of mercury entering the head of the penetrometer from the penetrometer stem was tracked using a conductance detector. All aspects of the pressure analysis, data collection and data deduction were processed by a computer control module.

Samples ~ 0.2 g - 0.5 g were weighed into a 5 ml powder penetrometer that has a stem volume of 0.392 ml. They were then evacuated at a pressure of 50 μmHg for 5 min to remove any absorbed gases and moisture. The fill pressure was set to 68 kPa. After degassing, the penetrometer was filled with mercury and was transferred manually to a

high-pressure port. The penetrometer, fill pressure and sample size were carefully selected so that the penetrometer stem volume used was between 25% and 90% to ensure reliable results. Measurements were carried out at room temperature using an equilibration time of 5 s. The surface tension, contact angle, and density of the mercury were taken to be 0.485 N/m, 130 °C and 13.5438 g/ml respectively.

2.7 Scanning Electron Microscopy (SEM)

In SEM, a finely focused electron beam is scanned across the sample's surface. The diameter of the electron beam, at its point of impact on the sample, influences the microscope's performance because this diameter is the finest resolvable detail in the image. To minimize the interaction of the electron beam with air, the SEM column and the sample chamber are evacuated to a pressure of ~ 1 x 10^{-5} Pa. Magnification of up to × 100 000 can be obtained. Due to enhanced contrast and large depth of field, surfaces can be sharply focused, even when relatively large height variations are present. SEM is a versatile technique for observation of surface and microstructure of a wide range of materials, including pharmaceutical drug crystals and drug delivery systems[81].

The scanning electron microscopes used were the Jeol T330 (Japanese Electron Optics Ltd., Tokyo, Japan); and the Jeol T6310 (Japanese Electron Optics Ltd., Tokyo, Japan). The latter model allows for electronic collection and storage of images.

2.7.1 Topographic Imaging and Backscattered Electron Imaging

When a surface is bombarded with a high energy electron beam, secondary low energy electrons and backscattered high energy electrons are released from the surface. Both types of emergent electrons can be collected by detectors to construct an image.

During topographical imaging, secondary electrons are collected. The number of secondary electrons detected is affected by the geometrical orientation of the specimen's surface. Therefore, topographical information can be obtained from these signals.

During backscattered electron imaging, backscattered electrons are collected. The signals of backscattered electron increase with the mean atomic number of the sample. Therefore, areas with high atomic number elements are emphasised and displayed as bright regions in the image.

2.7.2 X-Ray Analysis

When an electron beam interacts with an element, characteristic secondary X-rays are emitted. If these X-rays are collected, a fingerprint spectrum can be produced. Therefore, X-ray analysis can identify the presence of specific elements, provided that their localised concentration exceeds ~ 0.1%. The relative intensities of the spectral peaks can be used as a rough guide of the relative concentration of each element in the specimen. To perform X-ray analysis, an energy dispersive spectrometer is fitted as an attachment to the SEM. The spectra produced by the energy dispersive X-ray spectrometer are plots of X-ray counts versus X-ray energy. The qualitative analysis may also be presented in a graphic format, called a *dot map*. In this technique, the brightness of the SEM beam at each point on the display is modulated by the X-ray output from the element of interest.

SEM combined with Energy Dispersive X-Ray Analysis (EDX) was used in this study. The set-up used was a Jeol T6310 (Japanese Electron Optics Ltd., Tokyo, Japan) fitted with Oxford Inst, AN 10 000 X-Ray Analyser (Gatan, UK). All images were taken at a voltage of 10 kV or 15 kV.

2.7.3 Conductive Coating

Ideally SEM requires specimens that are dry, mechanically stable, non-volatile and electrically conducting[82]. However, most pharmaceutical powders do not have these characteristics. Non-conducting or poorly conducting samples accumulate electrons during electron irradiation and cause local electrical charges. These charges on the samples result in distortion of the beam, over brightness, and poor focus of the image. To avoid the charging effects, samples are usually sputter coated with a fine conductive layer of gold for topographic imaging. The coating becomes the main source of secondary electrons, and also protects the specimen against heat generated on exposure

to the electron beam. One disadvantage of gold coating is that it absorbs X-rays. Also, Large gold peaks on the spectra may overlap with specimen's peaks. Therefore, specimens for X-ray analysis are usually coated with carbon, which is lighter and less absorbent of the X-rays. Backscattered imaging specimens are also normally coated with carbon because gold, being a high atomic number element, produces high backscattered electrons that may interfere with the specimen's signals.

In this study, samples for topographical imaging were coated with gold using a sputter coater (Model S150B, Edwards High Vacuum Ltd., Sussex, UK) while samples for backscattered electron imaging were coated with carbon (Edwards coating unit, Pirani Penning, Model 4, Edwards High Vacuum Ltd., Sussex, UK).

2.7.4 Sample Preparation for the Investigation of Surface Morphology of Microspheres

Microsphere samples were sprinkled onto adhesive carbon pads and then placed in an oven at 60 °C overnight. The sample surfaces were then gold coated with a sputter coater for 10 min at a voltage of 1.4 kV.

2.7.5 Sample Preparation for the Investigation of Internal Morphology of Microspheres (Resin-Embedded Technique)

Preliminary experiments indicated that the calcium phosphate microspheres could be sectioned by firstly embedding them in an epoxy resin (Hard Grade, Taab Resin, Taab, Reading, UK). This resin provided a strong support for sectioning of the hard sintered calcium phosphate. The microsphere samples were mounted in the resin by the following procedure. About 2 ml of resin was added to a small amount of microspheres. The resin/microspheres mixture was put under vacuum to eliminate trapped gas and facilitate the penetration of resin into the microspheres. They were then placed on a rotatory mixer rotating slowly for ~ 3 h to further allow the resin to penetrate into the samples. The resulting mixtures were poured into plastic moulds. The samples were placed in an oven at 60 °C overnight for the resin to set. The samples were then allowed to cool and the moulds were removed. The resin-embedded samples were then manually trimmed on an ultramicrotome (Om U3, C. Reichert AG,

Vienna, Austria) using a razor blade, followed by a glass knife (freshly prepared), and a diamond knife, when necessary, to obtain a flat and smooth surface that exposed the internal structure of the samples. The resin blocks were then coated with colloidal graphite (Agar Scientific, Stansted, UK) to ensure good electron conductivity, leaving only the freshly trimmed surface free of carbon. For topographical imaging, the samples were then sputter coated with gold for 3 min; for backscattered electron imaging, the samples were coated with carbon for 3 min.

2.8 Low-Temperature Scanning Electron Microscopy (LTSEM)

In this study, LTSEM was employed for imaging samples containing drug crystals to overcome image distortion associated with conventional SEM. A schematic of a low-temperature scanning electron microscope is shown in Figure 2.1. The equipment consists of a cold-stage (C) fitted inside the microscope's specimen chamber. The cold-stage is cooled with nitrogen gas that circulates within a Dewar flask (D1). The cryopreparation chamber, attached to the side of the microscope and evacuated by a vacuum pump, has a second cold-stage (P) which is thermally cooled down by liquid nitrogen from a second Dewar flask (D2). A sputter head for gold coating (S) is placed above the sample. The two chambers are separated by a gate valve (G). The microscope used was a Jeol T6310 (Japanese Electron Optics Ltd., Tokyo, Japan).

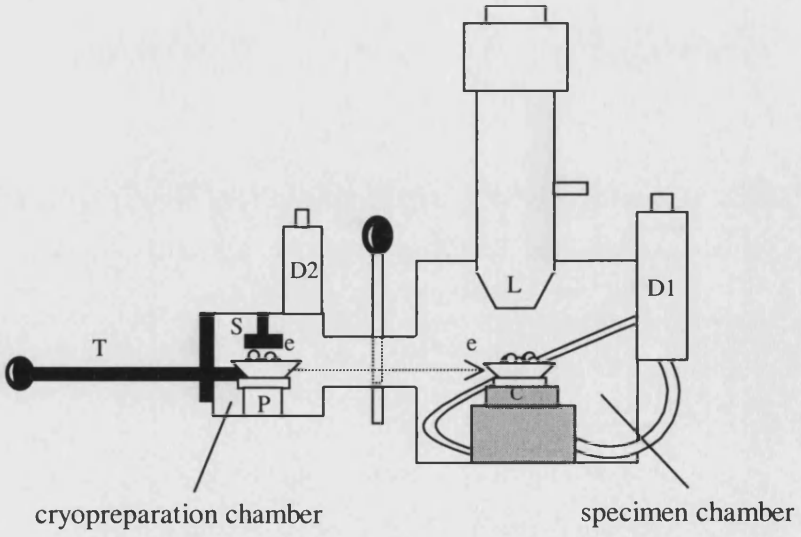

Figure 2.1 Low-temperature SEM (adapted from Potter *et al.*[83]).

2.8.1 Sample Preparation for LTSEM

Each sample was sprinkled onto an adhesive carbon pad that was then attached to a metal stub on the end of a transfer rod (T). The sample was transferred to cold stage (P) in the cryopreparation chamber and allowed to cool down to ~ −180 °C for 10 min to freeze water molecules contained in the sample. The sample was then transferred into the specimen chamber for 5 min for sublimation of contaminating surface frost at ~ −180 °C. The process of surface frost sublimation/disappearance could be observed under the microscope at this stage. The sample (e) was then placed back in the cryopreparation chamber to be sputter coated, with gold, for 3 min in a low-pressure atmosphere of argon at ~ −180 °C. The sample was then placed back into the specimen chamber and the final examination of the sample was performed at ~ −170 °C.

2.9 Thermal Analysis - Differential Scanning Calorimetry

Differential Scanning Calorimetry (DSC) is a thermal analysis technique that is widely used in pharmaceutical applications for the investigation of the purity, crystallinity and polymorphism of materials. In DSC, the sample and reference are maintained at the same temperature as heat is supplied to the system. The heat flow required to keep the equity in temperature is measured. Therefore, the heat exchange as physical and chemical changes occur during a heating process is recorded. The energy input per unit time is recorded as a function of temperature. Hence, DSC plots are obtained as the differential rate of heating against temperature. The area under a DSC peak is directly proportional to the heat absorbed or evolved by the thermal event.

A differential scanning calorimeter (DSC 2910, TA Instruments Ltd., Leatherhead, UK) with a liquid nitrogen cooler attached was used to investigate the change of crystallinity of model drugs before and after drug loading experiments. The calorimeter was first calibrated using indium (mp = 156.6 °C) as a standard reference material. A sample of ~ 5 mg - 8 mg was accurately weighed in an aluminium pan that was then hermetically sealed. An empty sealed aluminium pan was used as a reference. The heat flow rate was recorded from 30 °C - 250 °C at a rate of 10 °C/min. The samples were purged with nitrogen at a feeding rate of 25 ml/min. The collected data were then analysed using the Universal V1.8M software (TA Instruments Ltd., Leatherhead, UK).

2.10 X-ray Diffraction (XRD) Studies

X-ray powder diffraction studies are widely used for the identification of solid phases. The X-ray powder pattern of every crystalline form of a compound is unique, making this technique particularly suited for the identification of different polymorphic forms of a compound. When a material is irradiated with a parallel beam of monochromatic X-rays, the atomic lattice of the material acts as a 3-dimensional diffraction grating, causing the X-ray beam to be diffracted to specific angles, related to the inter-atomic spacing. By measuring the angles of diffraction, the inter-atomic spacing of the material can be determined and used to identify the crystallographic structures of the material[84].

The phase changes of calcium phosphate after sintering and the possible change of model drugs after drug loading experiments were investigated by X-ray diffraction studies. The XRD patterns were obtained on a Philips powder diffractometer, using monochromatic Cu-Kα, Ni-filtered radiation, at 2θ, and a scanning speed of approximately 1°/min. Powder samples were placed in an aluminium sample holder, and pressurised to ascertain that the sample surface was flat and level with the surface of the holder. The crystalline phases were then compared to the standard reference pattern from the International Centre for Diffraction Data.

The equipment used was Philips PW1730/00 4kW X-ray generator; Philips PW2273/20 long fine focus 2kW copper target X-ray tube, operated at 40 kV & 25 mA; Philips PW1820/00 computer controlled vertical diffractometer goniometer; Philips PW1711/00 xenon proportional counter with PW1752/00 graphite monochromator & PW1368/55 automatic divergence slit assembly; Philips PW1710/00 microprocessor diffractometer control; and Philips PW1877 PC-APD, version 3.5b, diffraction software.

2.11 Dissolution Studies

To investigate the *in vitro* release of drugs from the microspheres, the dissolution tests that comply with BP 1998 standard - apparatus II (paddle) method, were carried out.

Experiments were performed in a Pharmatest dissolution bath (Type PTW S3C, Pharmatest Ltd., Frankfurt, Germany) at 37 °C ± 0.5 °C. Paddles were positioned at 25 mm from the inside bottom of the vessel, and their rotating speed was set to 50 rpm. The dissolution medium was 900 ml of BP phosphate buffer, pH = 6.8. Samples to be studied were placed in gelatin capsules, which in turn were individually placed in a sinker to allow the capsules to sink to the bottom of the vessels. Sinkers were hand-coiled tin-plated copper wire. The capsule size chosen in each experiment was the smallest size which could hold the required amount of sample. The percentage of drug release from the dissolution test was calculated using the equation below:

$$\%\ drug\ release\ at\ time\ t = \left(\frac{amount\ of\ drug\ release\ at\ time\ t}{mean\ total\ drug\ loading} \right) \times 100\ \% \quad \text{Equation 2.1}$$

2.12 Determination of Drug Contents

The loading efficiency of model drugs was determined as follows: 100 mg or 150 mg of accurately weighed drug-loaded microsphere sample were placed in a 250 ml volumetric flask containing around 200 ml of freshly prepared 0.1 M HCl. These were then sonicated for ~ 5 min, or until full dissolution was achieved as verified by visual examination. This was then made up to the designated volume. Each sample was tested in triplicate. The UV absorbance of drug in the final acid solution was determined by spectrophotometry (Unicam Helios α, Cambridge, UK), and compared to the drug absorbance and concentration calibration plot. Dilutions were performed if the measurements were outside the calibration plot. The calibration plots for model drugs can be found in Appendix IV. DCPA and β-TCP dissolved in 0.1 M HCl were found not to interfere with the drug identification peaks for all model drugs chosen.

The percentage drug loading was calculated using the equation below:

$$\%\ Drug\ Loading = \left(\frac{weight\ of\ drug}{weight\ of\ drug - loaded\ microspheres} \right) \times 100\% \quad \text{Equation 2.2}$$

3 Manufacture of Novel Drug Carrier Systems by Spray-drying

3.1 Introduction

The overall aim of this study was to obtain porous inorganic microspheres to be used as drug carriers. To produce the microspheres, the spray drying method was investigated.

Spray-drying has a wide range of applications within the pharmaceutical, food, and ceramic industries[57,49]. The spray-drying process usually produces free-flowing spherical powders in a short time. By modifying the spray-drying conditions, it is possible to alter and control the properties of spray-dried powders, such as morphology, bulk-density, porosity, moisture content, flowability, stability, friability, particle-size and size distribution[50,85,86].

This chapter describes the development process of establishing feasible spray-drying conditions to produce bioceramic microspheres using pharmaceutical grade calcium phosphates. The desirable characteristics of the microspheres include being highly porous, free-flowing, and well-formed spherical particles with narrow size distribution. Two types of calcium phosphates, dibasic calcium phosphate anhydrous (DCPA) and beta-tricalcium phosphate (β-TCP) were studied. These were chosen mainly because they are orally acceptable pharmaceutical excipients, and they are cheap.

In the preparation of ceramic slurries for spray-drying, a few points should be considered[54]:

1) Binder addition

   Binders are used in ceramic processing to provide enough strength to the ceramic green body (see section 1.6) to maintain its shape until it is sintered. The desirable characteristics of binders are[63]:

   - Ease of thermal removal;
   - Strong adhesion and cohesive strength;
   - Solubility in fluidising liquid;
   - Low cost.

Organic binders, such as polyvinyl alcohol (PVA), polyethylene glycol (PEG), and polyethylene oxide (PEO), are commonly used[63] (Figure 3.1). The method of adding binder to the slurry is important. Adding binder as a prepared solution is desirable so that the required solids content is consistent. This also allows for preliminary screening of undissolved or undispersed binder materials. The presence of organic agglomerates exposes defects to the final product[87] which persist during sintering[88]. Typically, powders contain 0.5% - 4.0% (weight) binder, based on the dry weight of the ceramic powder[54].

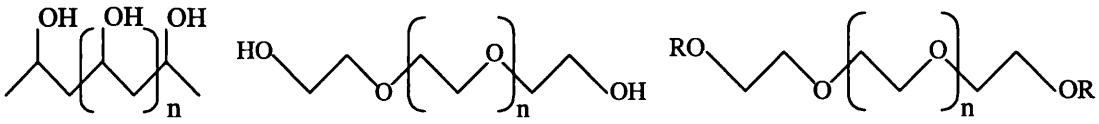

PVA PEG PEO

Figure 3.1 Molecular structures of PVA, PEG and PEO. RO specifically depends upon initiator/terminator. PEO is typically more monodisperse than PEG.

2) Powder dispersion

To produce good spray-dried products, the powders must be homogeneously dispersed. Since most powders to be spray-dried are several micron in diameter, the slurry can be considered a colloidal system. The DLVO theory regarding colloidal stability suggests that the stability of colloidal system depends on the particle surface charge, and stable systems are deflocculated[54]. Dispersants are commonly used in the preparation of ceramic slurries to produce deflocculated systems. The dispersants such, as organic polymers, adjust the surface charges of the ceramic particles by being adsorbed on the surface of the particles by van der Waals forces or hydrogen bonding[54].

3) Solids content

A high solids content slurry is desired for economic and technical reasons. Since dryer capacities are specified by the quantity of water that can be evaporated per hour, a higher solids content slurry means an increased powder output. When formulating a slurry for spray-drying, it is valuable to estimate the approximate maximum solids content achievable. A reduction in the mean particle-size of the

powder will decrease the maximum solids content that can be achieved. This is because the distance between particles decreases with decreasing particle-size, and agglomeration and flocculation can happen readily when the particles are close together[54]. The viscosity of the slurry increases, and operation difficulties arise. The maximum concentration of solids that can be achieved for micron-sized ceramic powders is normally 40% - 50%. However, for the slurries to be fluid enough to be sprayed, the maximum concentration of solids is 30% - 40% even in the presence of dispersants. This is due to the viscosity becoming too high.

Initially, the spray-drying of DCPA was studied. The suitability of various excipients, slurry compositions and spray-drying conditions in producing DCPA microspheres were investigated.

The excipients investigated were:

a) Binders - PEG 1000; PEG 6000; PEG 10000; PEG 20000; Plasdone K-90; Polyplasdone XL-10; Eudragit L100; and Maltodextrin;
b) Surfactant – Sodium Lauryl Sulphate (SLS);
c) Suspending agent – Tragacanth;
d) Dispersant – Dispex A40.

The slurry composition variables investigated were:

a) Solids content;
b) Solid particle-size;
c) Binder concentration;
d) Dispersant concentration.

The spray-drying conditions investigated were:

a) Temperature;
b) Jet size;
c) Pump speed.

The spray-drying of β-TCP was then investigated, followed by a search of the optimal conditions to obtain free-flowing β-TCP microspheres.

Due to time constraints, the full range of variables was not studied, and replicates were limited to a small number of conditions. The sets of experiments chosen were based on the best knowledge derived from the experience acquired with preliminary tests.

3.2 Spray-dryer

A bench-top SD-05 Laboratory Scale Spray-dryer (LabPlant Limited, West Yorkshire, UK) (Figure 3.2) was used in this study.

The SD-05 spray-dryer has co-current airflow, *i.e.*, the liquid is sprayed in the same direction as the flow of the air (section 1.5). The liquid is sprayed into the drying chamber (500 mm × 215 mm) through a two-fluid nozzle. Two-fluid nozzles are nozzles in which atomisation is achieved using high-velocity air, gas or steam[89]. The stainless steel jet spray assembly of the SD-05 spray-dryer consists of an inner tube for the liquid sample leading to a close tolerance internal diameter jet. The outer tube directs the supply of compressed air to the nozzle, and the close tolerance gap between the nozzle and the jet ensures that the liquid jet is produced as a fine vaporised spray.

Various jet sizes, from 0.5 mm to 2.0 mm internal diameter are available. For two-fluid atomisers, the jet size (the diameter of the final discharge orifice) is an important dimension for atomisation because theory predicts that mean drop size is roughly proportional to the square root of the jet diameter[89].

The jet spray assembly of the spray-dryer has an automatic plunger de-blocking device to remove blockages. The de-blocking device is a spring-restrained needle activated by an integral compressor. De-blocking is important especially when spraying high solids content slurry. In this study, the de-blocking frequency was set to maximum at all times because the calcium phosphate slurries were found to block the jet frequently.

Figure 3.2 The SD-05 Laboratory Scale Spray-dryer

3.3 Spray-drying Parameters

The spray-drying conditions determine the characteristics of the powder produced. The important spray-drying parameters are:

a) Inlet temperature

The inlet temperature is the temperature of the heated drying air. The air used in the drying process is drawn in over a heater by the aspirator motor. The heated air temperature is measured prior to flowing into the drying chamber.

b) Outlet temperature

The outlet temperature is the temperature of the air with the solid particles before entering the cyclone. Unlike the inlet temperature, it cannot be set with a temperature regulator. The outlet temperature depends on the inlet temperature, the air-flow rate, the peristaltic pump setting and the concentration of the material being sprayed. Outlet temperature is an important parameter as it generally represents product quality, *i.e.* the bulk-density, colour, flavour, activity and moisture content[90].

c) Air-flow

The air-flow measures the amount of air flowing through the chamber. Because the amount of energy available for solvent evaporation depends on the amount of drying air present, air-flow has an important effect on the performance of a spray-dryer. The vaporisation performance is also influenced by other factors such as the concentration of the spray solution and the moisture content of the drying air.

d) Pump speed

The peristaltic pump delivers the feedstock to the nozzle. Increasing pump speed means more feedstock passes through the nozzle at any one time, *i.e.* increasing rate of sample feed. Keeping the inlet temperature constant, an increase in the pump speed will reduce the outlet temperature. This is because a higher amount of feedstock was fed into the system at any one time and this means more heat is removed in the vaporisation process. Therefore, the moisture content of the product normally increases.

e) Compressor air pressure

This is the pressure needed to convert the spray into fine mist. The higher the compressor air pressure, the smaller the size of the particles in the final product.

The parameters described above are interdependent. Adjusting one parameter may lead to alteration of others. The characteristics of the spray-drying products not only depend on the spray-drying conditions, but also depend on the type and the physical dimension of the drying chamber. Therefore, the investigation of the spray-drying processing conditions relies mainly on trial and error.

In this study, before the start of each spray-drying experiment, the spray-dryer was allowed to warm up to the target temperature, followed by spraying of deionised water for ~ 5 min. This is to ensure that all the glassware reach the required temperature and the system is in equilibrium under the experimental conditions.

3.4 Expression of Concentrations

In this document, all the solids content (ceramic powders) of the slurries are expressed in weight percentage of the dry solids to the final slurry weight (%w/w); while all the concentrations of excipients (binders, surfactant and dispersant) are expressed in parts per hundred by *weight* (pph), based on the dry weight of the ceramic powder. The density of the ceramic powder used is ~ 3 g/cm^3, therefore, readers should note that the values of the concentrations of excipients would be ~ 3 times higher if they were expressed in part per hundred by *volume.*

3.5 Preliminary Studies – Slurry Preparation

Preliminary studies were performed using DCPA. Excipients that can be used for producing free-flowing calcium phosphate microspheres were investigated. The products of spray-drying experiments were examined under the SEM. The details of the SEM techniques used are detailed in section 2.7.

3.5.1 Water

Using deionised water as feedstock, complete water evaporation was observed in the SD-05 spray-dryer at the operating conditions below:

Spray-drying Conditions (SDC) Set 1

Jet size	0.5 mm
Inlet temperature	200 °C
Pump Speed	350 ml/h (dryer scale = 10)
Drying air flow rate	62-64 m^3/h (dryer scale = 41-44) (maximum setting)
Compressor air pressure	150 kPa (maximum setting)

Preliminary results indicated that by keeping other parameters in SDC Set 1 constant, lower inlet temperatures, lower air-flows, lower compressor air pressures, or higher pump speeds always resulted in incomplete water evaporation in the chamber.

3.5.2 Dibasic Calcium Phosphate Anhydrous (DCPA)

A slurry of 5% w/w DCPA (200 ml) in deionised water was prepared, and magnetically stirred to prevent the sedimentation of the solids. Spray-drying was carried out under SDC Set 1. The experiment produced a moderate yield and the product obtained was a free-flowing powder. Under the SEM, the spray-dried powder looked similar to the DCPA powder as-received. No microspheres were obtained.

3.5.3 Binders

To promote the agglomeration of DCPA particles and produce microspheres, a binder was added to the spray-drying slurry.

Polyethylene glycols (PEGs), a type of water-soluble organic binder, were initially chosen in this study because they are commonly used in the ceramic industry as binders[91]. PEGs are also widely used as excipients in a variety of pharmaceutical formulations including parenteral, topical, ophthalmic, oral, and rectal preparations. PEGs are easily removed during firing; therefore, they do not interfere with the subsequent sintering process.

3.5.3.1 Polyethylene Glycol (PEG) 1000

A 200 g slurry containing 5% w/w (10 g) of DCPA and 40 pph (4 g) of PEG 1000 was prepared by first dissolving the PEG in water, then adding the DCPA powder, and

finally adding more water to make up to the final weight. The resultant slurry was spray-dried at inlet temperatures of 150 °C, 200 °C, 220 °C and 245 °C. All other adjustable parameters of the spray-dryer were kept unchanged as in SDC Set 1 (see section 3.5.1). Very low yield obtained for all four experiments, and each 200 g slurry took ~ 30 min to spray dry.

3.5.3.1.1 Results and Discussion

During the experiments, two problems were encountered:

(a) The DCPA was poorly suspended. Sedimentation of DCPA occurred very readily, *i.e.* homogenous powder dispersion was not achieved.

(b) The spray-dried products were not free-flowing, but were wet and sticky instead. These products tended to deposit on the walls of the main chamber and the cyclone.

The practical highest inlet temperature that can be operated on the SD-05 spray-dryer is 245 °C. Even spraying at this temperature the results showed that the products were sticky and free-flowing products were not obtained.

3.5.3.2 Other Binders

The use of other pharmaceutical excipients as binder, including PEGs of higher molecular weight (PEG 6000, PEG 10000, PEG 20000), and Plasdone K-90, Polyplasdone XL-10, Eudragit L100, and Maltodextrin were investigated. Slurries of 5% w/w DCPA and 1 pph binder were spray-dried under SDC Set 1 (section 3.5.1).

3.5.3.2.1 Results and Discussion

None of the spray dried products were free-flowing. Slurries with PEGs produced products that were wet and had a clear gum texture. Slurries with Plasdone K-90, Polyplasdone XL-10, Eudragit L100 or Maltodextrin produced products which looked relatively drier than slurries with PEGs, judging by the powder flowed pattern in the cyclone. It was decided to define *dry products* as being white, free-flowing powders that flowed into the collection bottle, and *wet products* as being sticky gums which stuck to the walls of the main chamber and the cyclone wall. The yields for all

experiments were low. Among all the binders, it was observed that Eudragit L100 produced the best flow products, which are assumed to contain the least water content, but the water content was not determined. One particle of the products was selected and examined under the SEM. It was found that this was a doughnut-shape particle with a smooth surface (Figure 3.3).

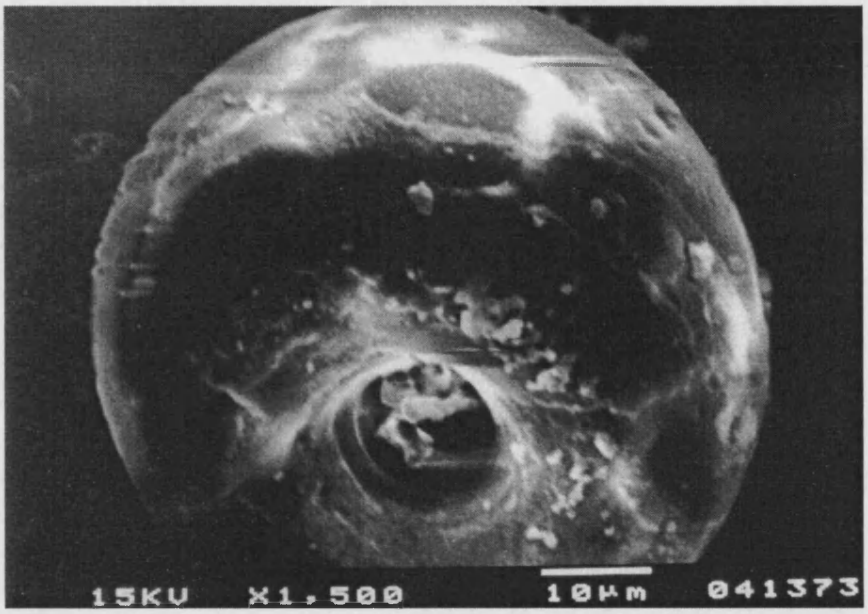

Figure 3.3 SEM micrograph of spray-dried product obtained from the slurry of 5% w/w DCPA and 1 pph Eudragit L100.

3.5.4 Surfactant

Surfactants could improve the wetting of PEGs, therefore may assist the dispersion of the polymer. Aiming to produce free-flowing spray-dried products, *i.e.*, the addition of a surfactant, sodium lauryl sulphate (SLS), to the spray-drying slurry was investigated.

SLS (20 pph; 60 pph; 80 pph) was added to slurries of 5% w/w DCPA and 40 pph PEG 1000. (That is of 1, 3 or 4 g of SLS was added to 5 g of DCPA, 2 g of PEG 1000 and water to produce a 100 g slurry,). The slurries were spray-dried under the SCD Set 1 (section 3.5.1).

The effect of SLS on other slurries containing different binders to PEG 1000 was also investigated. The experiments above were repeated replacing PEG 1000 with 20 pph of PEG 6000, PEG 10000, PEG 20000 and Maltodextrin.

3.5.4.1 Results and Discussion

Results showed that with the addition of SLS, powders with better flow characteristics were produced. This is probably because SLS assisted the wetting and spread of the PEGs, therefore local aggregation of PEGs was reduced and a more uniform dispersion of PEGs was achieved. For the slurries containing PEG 1000, it was also noted that with increasing concentration of SLS, the spray-dried products became less sticky and flowed better in the spray-dryer. However, products were mainly accumulated in the cyclone and did not reach the collection bottle.

The results for slurries containing other binders, namely, PEG 6000, PEG 10000, PEG 20000 and Maltodextrin, followed a similar trend: spray-dried products from slurries containing SLS had improved flow properties compared to their counterparts which did not contain SLS. The appearance of products was that of a white powder instead of a clear gum. Under the SEM (Figure 3.4), all SLS containing products were irregular shaped agglomerates, small 'bubble' structures.

These experiments showed that the inclusion of SLS improved the flow characteristics of the spray-dried products. However, in the present of SLS, the desirable spherical shaped agglomerates were not produced (Figure 3.4), therefore the use of SLS was discontinued.

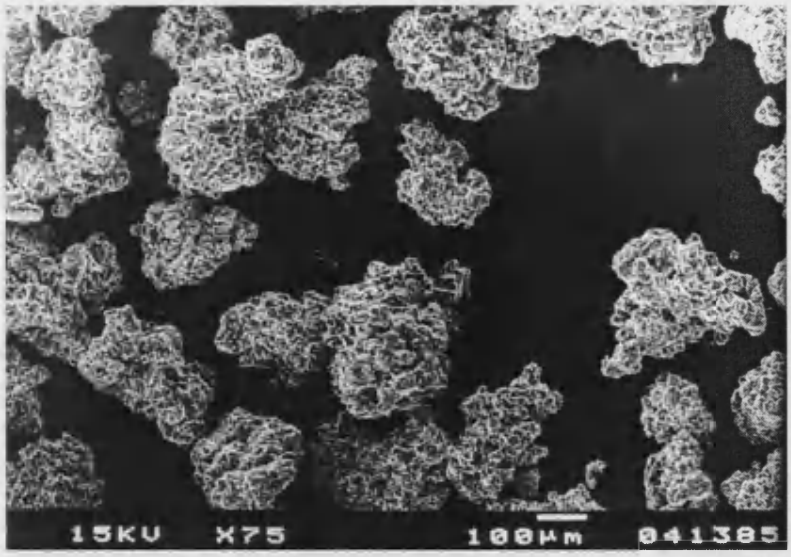

(a)

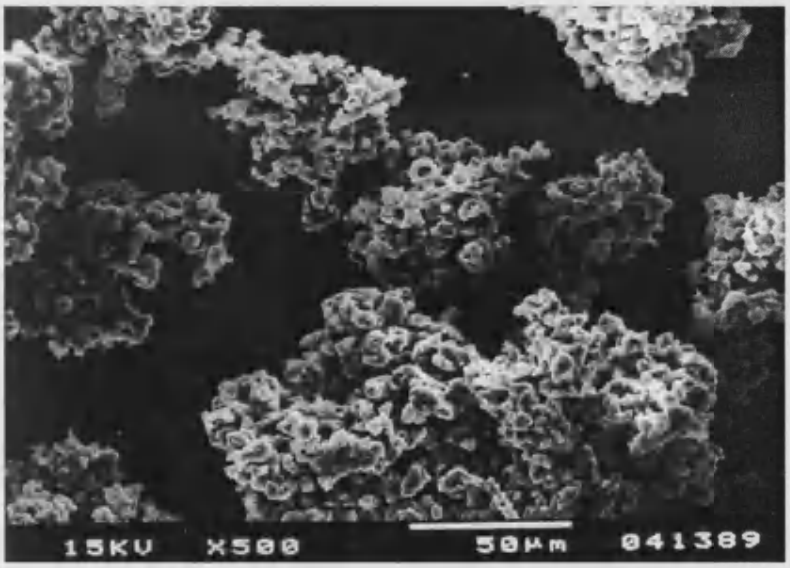

(b)

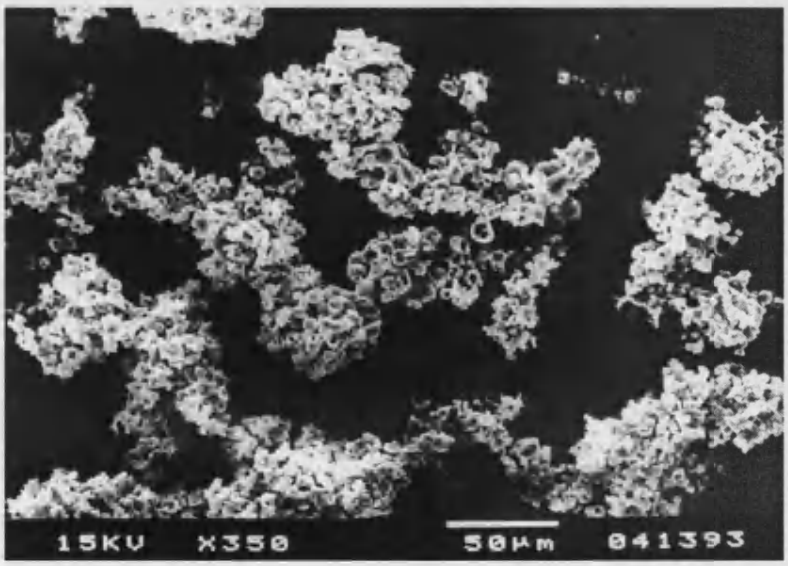

(c)

Figure 3.4 SEM micrographs of spray-dried products obtained from slurries of 5% w/w DCPA, 40 pph of PEG 1000, and a) 20 pph; b) 60 pph; c) 80 pph of SLS.

3.5.5 Suspending Agent

The DCPA powder was poorly suspended in water, and sedimentation occurred readily. To produce a stable suspension, the use of a suspending agent was investigated.

Tragacanth is a traditional pharmaceutical suspending agent. A slurry containing 5% w/w DCPA, 40 pph PEG 1000 and 20 pph tragacanth was prepared and spray-dried under SDC Set1 (section 3.5.1).

3.5.5.1 Results and Discussion

Tragacanth produced a thick, foamed DCPA suspension. However, the spray-dried products were of a waxy gum-like consistency that deposited on the top part of the cyclone. The use of the suspending agent was then discontinued.

3.5.6 Particle-Size Reduction

The possibility of using powders with smaller particle-size to produce more stable suspensions was then investigated. To reduce the particle-size of the DCPA powder, two ball-milling methods, wet-milling and dry-milling, were investigated:

a) Dry-milling: 200 mg of DCPA powder were placed in a 500 ml plastic container (7.5 cm × 11.5 cm) with 80 zirconia beads (1 cm × 1 cm zirconia cylinders, Corning Inc., New York, USA) and ball-milled for 10 h at an optimum speed to obtain cascading of the grinding media;
b) Wet-milling: 200 ml of 30% w/w of DCPA powder in deionised water was prepared, placed in a 500 ml plastic container (7.5 cm × 11.5 cm) with 80 zirconia beads (1 cm × 1 cm zirconia cylinders, Corning Inc., New York, USA) and was ball-milled for either 10 h and 40 h at an optimum speed to obtain cascading of the grinding media. The experiment was repeated using 40% w/w and 50% w/w slurries.

The particle-size distribution of DCPA powders before and after milling, were determined using Mastersizer X. Details of particle sizing methods are described in section 2.3. Three measurements were performed for each sample.

3.5.6.1 Results and Discussion

Before milling, the DCPA powder and water mixture was a highly unstable suspension, sedimentation of the DCPA particles happened readily. After subjecting the mixture to ball-milling, the mixture became a relatively thick, viscous and stable slurry. SEM micrographs of DCPA powder as-received and after dry-milling for 10 h are shown in Figure 3.5. It can be seen that the size of agglomerates and primary particles had both decreased after ball-milling and the ball-milled powder looked more flat and flaky.

The results of particle-size analysis of DCPA powders as-received and after ball-milling, are shown in Table 3.1. The as-received powder was found to have a volume mean diameter, d(v, 0.5), of 4.56 μm. After 10 h dry-milling, no marked reduction in d(v, 0.5) was detected. For slurry with 50% w/w solids content, 10 h of wet-milling reduced the powder d(v, 0.5) to 2.01 μm; and 40 h of wet-milling further reduced the powder d(v, 0.5) to 1.45 μm. These results show that wet-milling was more effective than dry-milling in particle-size reduction of the DCPA powder, and a longer session of milling produced finer particles. Wet-milling is more effective because the lubrication of water prevents the fine particles from sticking together again after they break up. The water also neutralises the electronic charges on the newly formed particle surfaces.

The mean d(v, 0.5) for the 30%, 40% and 50% w/w solids content slurries after 10 h wet-milling was found to be 2.15 μm, 1.71 μm and 2.01 μm, respectively. No trend can be concluded from these results, indicating that the solids contents at these concentrations do not markedly affect the particle reduction in wet-milling.

Representative particle-size distributions of wet-milled (40% w/w solids) and dry-milled products are compared in Figure 3.6. The graph shows that wet-milling produces a single model particle-size distribution and almost all particles are below 10 μm; while dry-milling produces a bimodal particle-size distribution and about half of the particles are above 10 μm. Since wet-milling produces single model particle-size distribution, and is more effective in particle-size reduction, it was the method chosen for the reduction of DCPA particle-size.

The dry-milled powder was measured while suspending in liquid (using large-volume cell, dispersion medium = water) and in gas (using dry powder feeder, dispersant medium = air). The results showed that both methods produce similar results, the d(v, 0.5) obtained being 4.77 μm and 4.89 μm respectively.

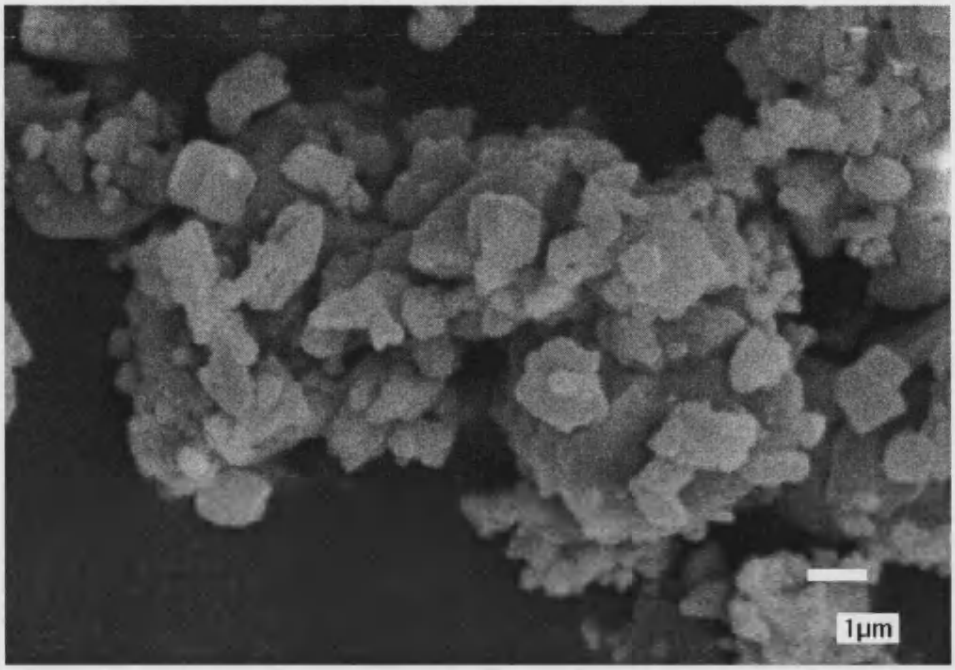

(a)

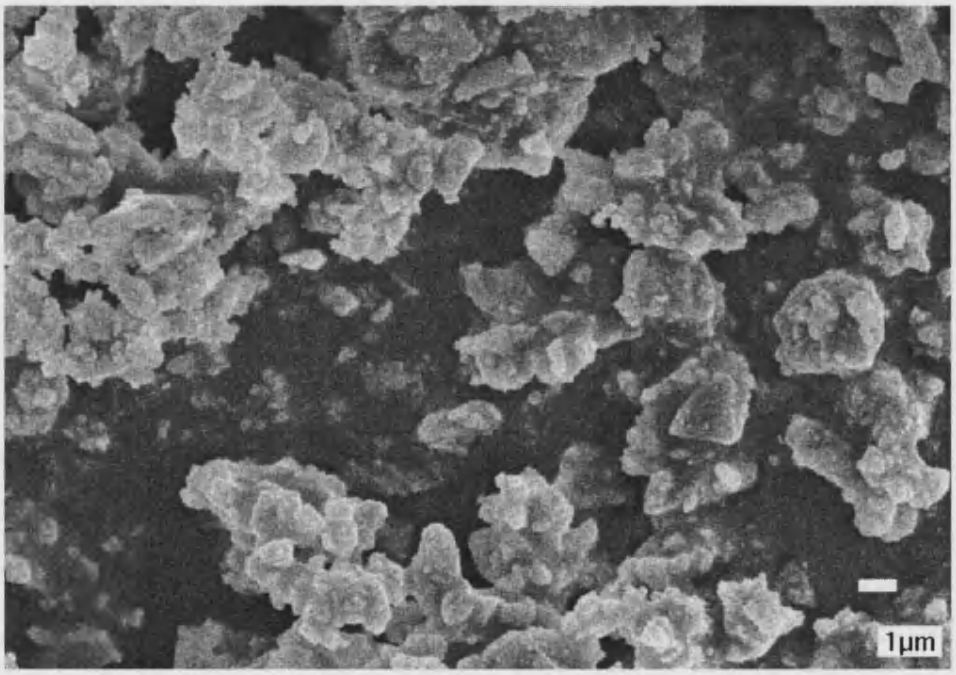

(b)

Figure 3.5 DCPA powders (a) as-received, (b) after dry ball-milling.

Table 3.1 The results of particle-size analysis for DCPA samples.

DCPA samples	Cell	Focus lens	d(v, 0.1)/μm 10% volume diameter			d(v, 0.5)/μm volume median diameter				d(v, 0.9)/μm 90% volume diameter		
			Run 1	Run 2	Run 3	Run 1	Run 2	Run 3	mean	Run 1	Run 2	Run 3
Powder as-received	SVC	100 mm	0.74	0.74	0.74	4.59	4.25	4.84	4.56	21.16	17.30	19.74
50% solids wet-milling (10 h)	SVC	100 mm	0.68	0.66	0.67	2.21	1.79	2.03	2.01	7.21	5.23	7.76
50% solids wet-milling (40 h)	SVC	100 mm	0.63	0.62	0.63	1.42	1.41	1.51	1.45	4.15	4.27	5.02
40% solids wet-milling (10 h)	SVC	100 mm	0.64	0.65	0.65	1.66	1.71	1.76	1.71	5.66	6.48	7.09
	LVC	45 mm	0.46	0.48	0.46	1.58	2.13	1.60	1.77	5.06	5.45	5.20
30% solids wet-milling (10 h)	SVC	100 mm	0.65	0.65	0.66	2.19	2.12	2.15	2.15	10.89	9.49	8.88
Dry-milling (10 h)	LVC	45 mm	0.60	0.61	0.60	4.72	4.76	4.84	4.77	27.32	27.01	27.55
	DPF	45 mm	0.60	0.61	0.62	4.84	4.97	4.86	4.89	27.55	27.80	27.43

Note: SVC = small-volume cell (samples were sonicated for 5 min before analysis)

LVC = Large-volume cell

DPF = Dry powder feeder

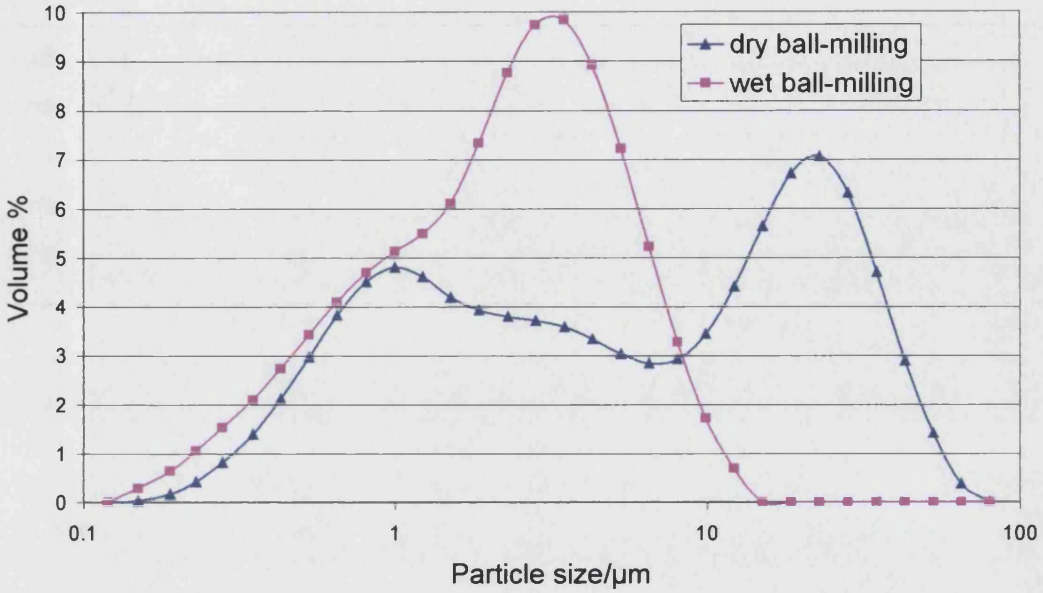

Figure 3.6 Particle-size distribution of dry ball-milled and wet ball-milled DCPA samples.

3.5.7 Solids Content

One of the reasons for lack of success in producing free-flowing product was thought to be due the slurrie's high water content or, in other words, their low solids content (5% w/w). Masters[57] illustrated that, for a given production rate, increase in feed solids content from 10% to 25%, will result in a 66.6% reduction in heat input, even increasing solid content from 25% to 50% will result in a similar heat input reduction. Heat input is reduced because as the solid content increases, the water content is reduced. Hence, the amount of moisture evaporation needed to produce a unit weight of dry powder is reduced; the major factor being that the heat of evaporation of water (~ 2300 J/g or ~ 540 cal/g at 100 °C) is so much larger than the specific heat of ceramic particles, for example, oxides or phosphates. A high solids content also has the advantage of stabilising the ceramic powder mixture, so that sedimentation does not occur readily.

3.5.7.1 Results and Discussion

DCPA slurries with a higher solids content were investigated. Slurries of ceramic powder with high solid contents (> 50% w/w) were found to be highly viscous, and it is not spray-drying feasible because:

1) The slurry was too viscous to be pumped through the tube to the nozzle;
2) When the slurries reached the nozzle, they blocked the nozzle instantly.

To reduce the viscosity so that the slurries could be processed using a spray-dryer, a dispersant was considered to be necessary.

3.5.8 Dispersant

Dispersants, sometimes called 'deflocculants', are commonly added to ceramic slurries for two main reasons[63]:

1) To lower the viscosity of the slurry;
2) To prevent particle agglomeration.

The most commonly used ceramic dispersants are polyacrylates[63]. These are powerful dispersants which can provide a low viscosity ceramic slurries even when only small amounts of solvent are present. In the ceramic industry, the concentration of dispersants used is typically ~ 0.2 - 2.0 pph of ceramic powder by weight. The viscosity of the ceramic slurry is normally found to be at a minimum when there is a monolayer of dispersant adsorbed onto the powder surface[92].

In this study, the polyacrylate dispersant chosen in DCPA slurries is Dispex A40. Dispex A40 is anionic and performs best as deflocculating agent at pH 8 - 9 (for more information on dispersant refer to section 3.8).

A 200 g slurry of DCPA was prepared by ball-milling 50% w/w DCPA in water overnight. 2 pph PEG 1000 and 1 pph Dispex A40 were then added, followed by the addition of aqueous ammonia (2.7 M, ~ 2 ml) to adjust the pH to ~ 8. The slurry was then further ball-milled for 30 min before it was spray-dried under SDC Set 1 (section 3.5.1).

3.5.8.1 Results and Discussion

The initial mixture of 50% w/w DCPA powder in water was highly viscous. The addition of Dispex was found to markedly decrease the viscosity. The mixture was further ball-milled after the addition of the binder and the dispersant to ensure thoroughly mixing in of the excipients, and the elimination of any agglomerates formed. This high solids content slurry was pumpable, and was successfully spray-dried.

3.6 Spray-drying of Dibasic Calcium Phosphate Anhydrous (DCPA)

Following the success of ceramic slurry production for spray-drying in the preliminary studies, the optimum spray-drying conditions required to produce DCPA microspheres were further investigated.

Spray-drying slurries of DCPA for all experiments were prepared as follows:

1) DCPA powder, deionised water and zirconia beads were placed in a plastic container, and ball-milled for 10 h (as described in section 3.5.6);
2) A binder (either PEG 1000 or Eudragit L100) was added;
3) A dispersant, Dispex A40, was added;
4) Sufficient quantities of aqueous ammonia (2.7 M), typically ~ 2 ml for 200 g slurry, were added to adjust the slurry pH to 8 - 9. The increase of pH was monitored using pH paper (Fisherbrand, range pH 8.0 - 10.0, Fisher Scientific UK Ltd., Leicestershire, UK);
5) The slurry was then ball-milled for another 30 min before spray-drying.

During the spray-drying process, the DCPA slurries were continuously stirred with a magnetic stirrer. Air-flow and compressor air pressure were set to the maximum value in all experiments at 62 - 64 m^3/h and 170 kPa, respectively.

3.6.1 Effect of Temperature

To investigate the effect of spraying temperature on spray-dried DCPA products, slurries containing 40% w/w and 50% w/w DCPA were spray-dried at 240 °C – 100 °C and 240 °C – 70 °C, respectively.

3.6.1.1 40% w/w Solids Content Slurries

Slurry containing 40% w/w DCPA, 2 pph PEG 1000; and 1 pph Dispex A40 were prepared and spray-dried at inlet temperatures 240 °C - 100 °C, with decrements of 20 °C. 200 ml of slurry was spray-dryed at each temperature. The other spray-dryer conditions were kept constant as in SDC Set 1 (section 3.5.1).

3.6.1.1.1 Results and Discussion

As the inlet temperature dropped below 160 °C, wet products started to accumulate at the base of the main chamber. When the inlet temperature dropped further to below 100 °C, water condensation was also observed in the cyclone and in the collection bottle. These temperatures were not suitable for spray-drying as the products were not dried properly. There were no obvious changes observed in the flow characteristics of the product in the spray-dryer in the range of inlet temperature investigated. Most products accumulated in the cyclone and did not flow into the collection bottle. However, it was interesting to note that with decreasing inlet temperature, relatively more product reached the collection bottle.

Products collected in the collection bottle were studied under the SEM (Figure 3.7). They consisted of spherical agglomerates, *i.e.* microspheres. On visual inspection, the products obtained at the spraying temperatures of 220 °C - 160 °C were found to be of better spherical shape, and therefore more desirable. The reason for this observation could be complicated and might be related to a number of factors including viscosity, and mass of the particles of the DCPA powder, water, and binder which were sprayed. If the water inside the particle "boiled", the sphere would first become hollow and then burst. Both the air flow rate and temperature affect the shape of the particle formed.

Inlet temperature = 240 °C

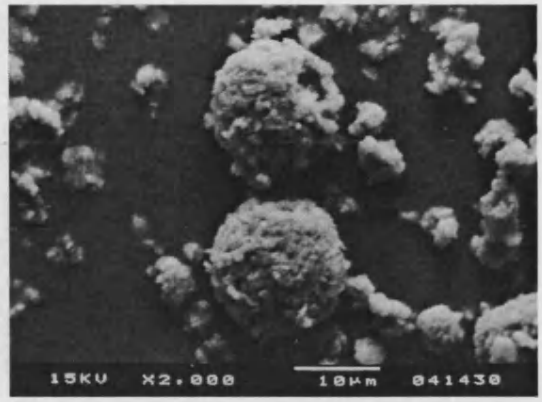

Inlet temperature = 220 °C

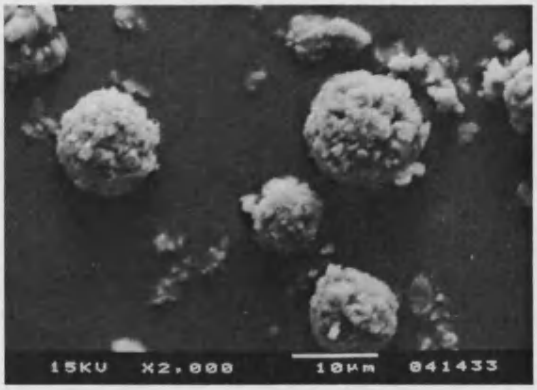

Inlet temperature = 160 °C

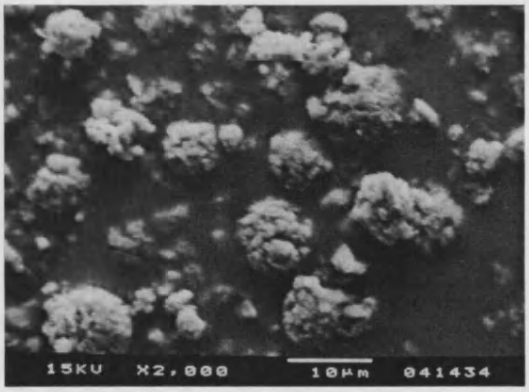

Inlet temperature = 120 °C

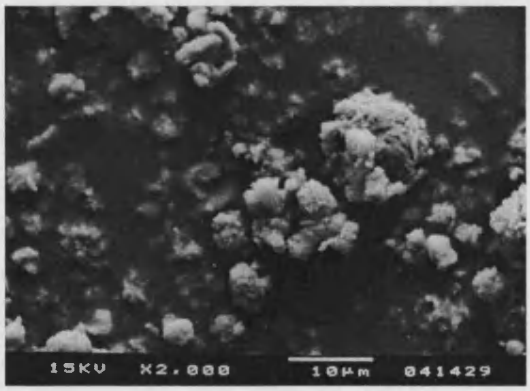

Inlet temperature = 100 °C

Figure 3.7 SEM micrographs of spray-dried products of 40% w/w DCPA produced at various inlet temperatures.

3.6.1.2 50% w/w Solids Content Slurries

Slurries of 50% w/w DCPA, 2 pph PEG 1000; and 1 pph Dispex A40 were prepared and spray-dried at inlet temperatures of 240 °C - 70 °C, with interval decrements of 20 °C.

All other spray-dryer conditions were kept constant as in SDC Set 1 (section 3.5.1), except for experiments with inlet temperatures > 100 °C, where the pump rate was increased from ~350 ml/h to ~500 ml/h (dryer scale = from 10 to 15). This was done because it was found that high solids content slurries readily caused nozzle blockage. A higher feeding rate helped preventing the blockage. All spray-dried products were examined under the SEM.

For SEM examination, initially the microsphere samples were sputter coated with gold for 3 min, 5 min or 8 min. However, these samples were found to have marked charging effects under the microscope. This was because the round shape of the microspheres only allows one point of contact with the support disc and the conduction of electrons was limited. The effect was exacerbated by the convoluted surface morphology of the microspheres, where breaks in the conducting coating were inevitable. Subsequently all the microsphere samples for SEM were gold coated for 10 min.

3.6.1.2.1 Results and Discussion

As the inlet temperature dropped below 90 °C, water condensation was observed in both the cyclone and the collection bottle, at 70 °C, it was almost impossible to produce a proper spray. At these temperatures there was insufficient energy available for moisture evaporation to produce 'dry looking' products.

In all experiments, apart from deposited in the collection bottle, products were also found to accumulated heavily on the cyclone wall. Products collected in the cyclone and collection in the collection tube from same batch of products were examined under the SEM. The results showed that the microspheres collected in the cyclone were generally smaller in size than those collected in the collection bottle.

SEM micrographs of the spray-dried products are shown in Figure 3.8. By comparing the SEM micrographs of the microspheres obtained from the 50% w/w solids content slurries and the 40% w/w solids content slurries, it was found that higher solids contents slurries generally produced bigger microspheres.

3.6.2 Slurry Solids Content

To further investigate the effect of solids content of the DCPA slurry on the resultant spray-dried products, slurries with solid contents of 20%, 30% and 60% w/w DCPA, 2 pph PEG 1000 and 1 pph Dispex A40 were spray-dried as before, SDC Set 1, section 3.5.1 (exception: pump speed of 60% w/w slurry were set to ~ 500 ml/h, dryer scale = 15, to prevent nozzle blockage). The spray-drying processes were observed and the products were compared under the SEM.

3.6.2.1 Results and Discussion

Slurries with 20% w/w solids content could not be spray-dried successfully. The products were 'wet' and sticky due to the high water content. It was noticed that the lower the solids content, the more products deposited in the cyclone and the fewer products reached the collection bottle. The higher the solids content, the better the spray-dried product flowed in the spray-dryer. Slurries with 60% w/w solids content produced free flowing powder that flowed smoothly into the collection bottle.

SEM micrographs of spray-dried products obtained from various slurries with various solid contents (20% - 60% w/w) are shown in Figure 3.9. The products of low solids content, 20% and 30% w/w, have high moisture content. They appeared to be relatively smaller sized microspheres and they clustered together. The higher the solids content, the bigger the microspheres obtained. 60% w/w slurry produced well-formed microspheres. A SEM micrograph of one of these microspheres is shown in Figure 3.10.

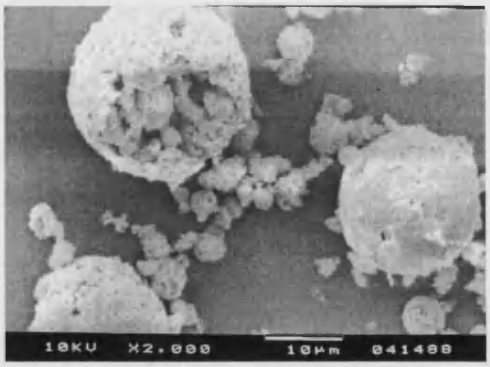

Inlet temperature = 240 °C

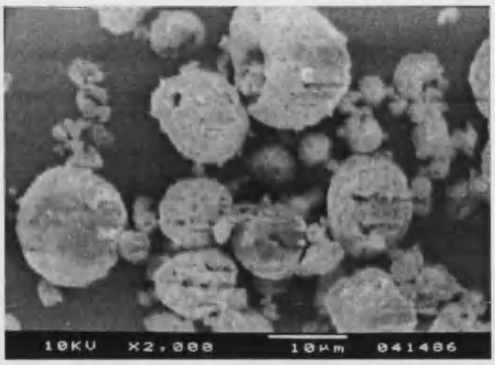

Inlet temperature = 220 °C

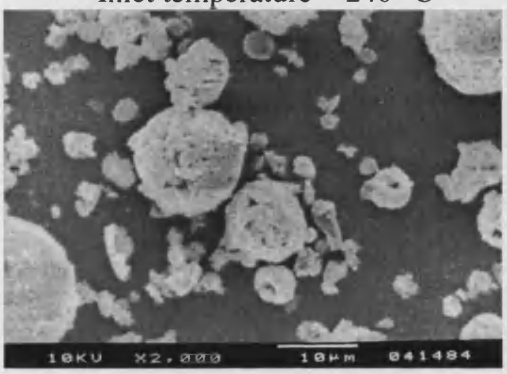

Inlet temperature = 200 °C

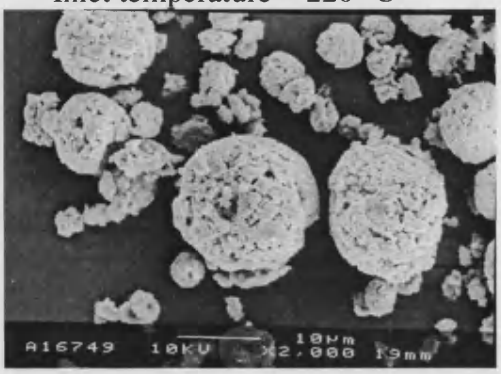

Inlet temperature = 180 °C

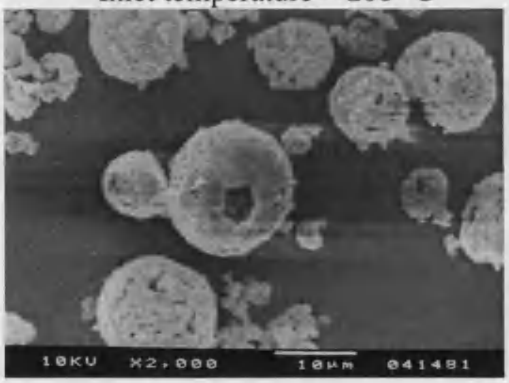

Inlet temperature = 120 °C

Inlet temperature = 100 °C

Inlet temperature = 90 °C

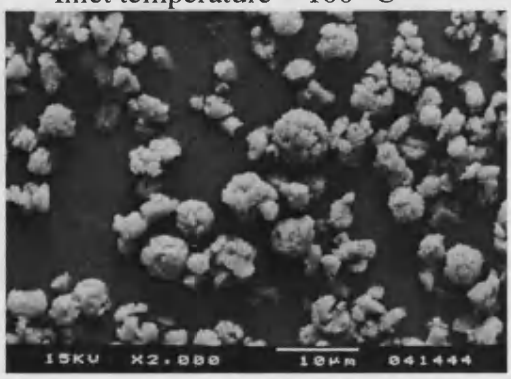

Inlet temperature = 70 °C

Figure 3.8 SEM micrographs of spray-dried products of 50% w/w DCPA produced at various inlet temperatures.

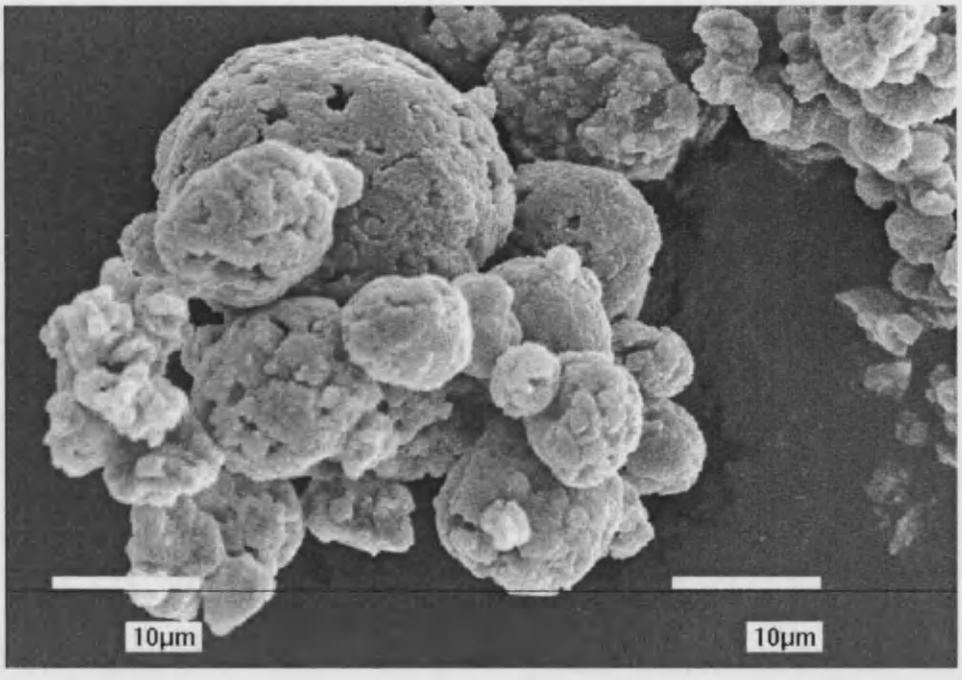

(a) Solids content = 20% w/w

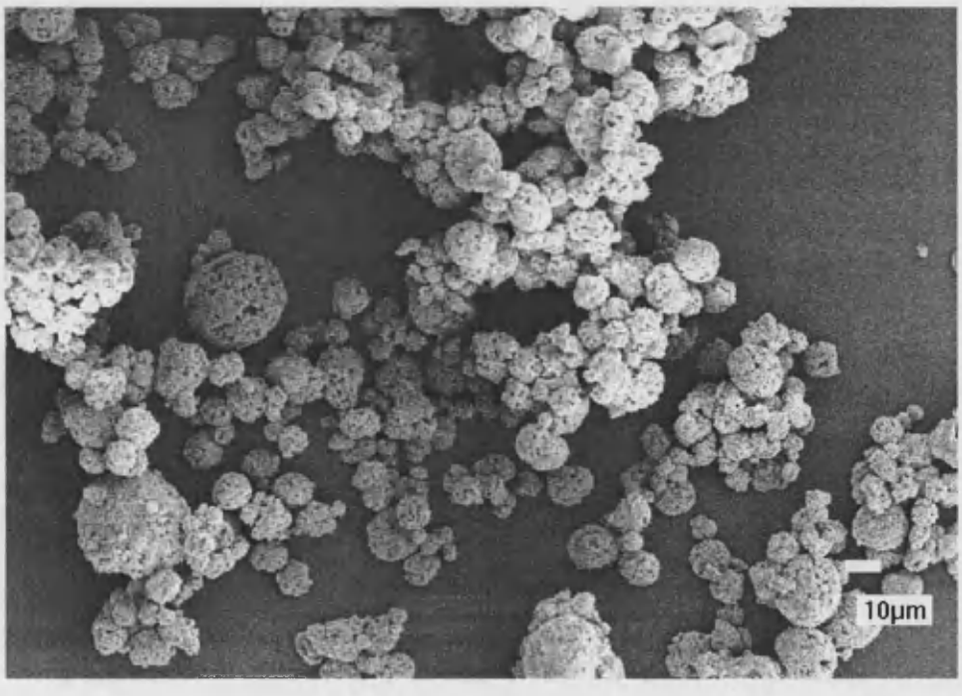

(b) Solids content = 30% w/w

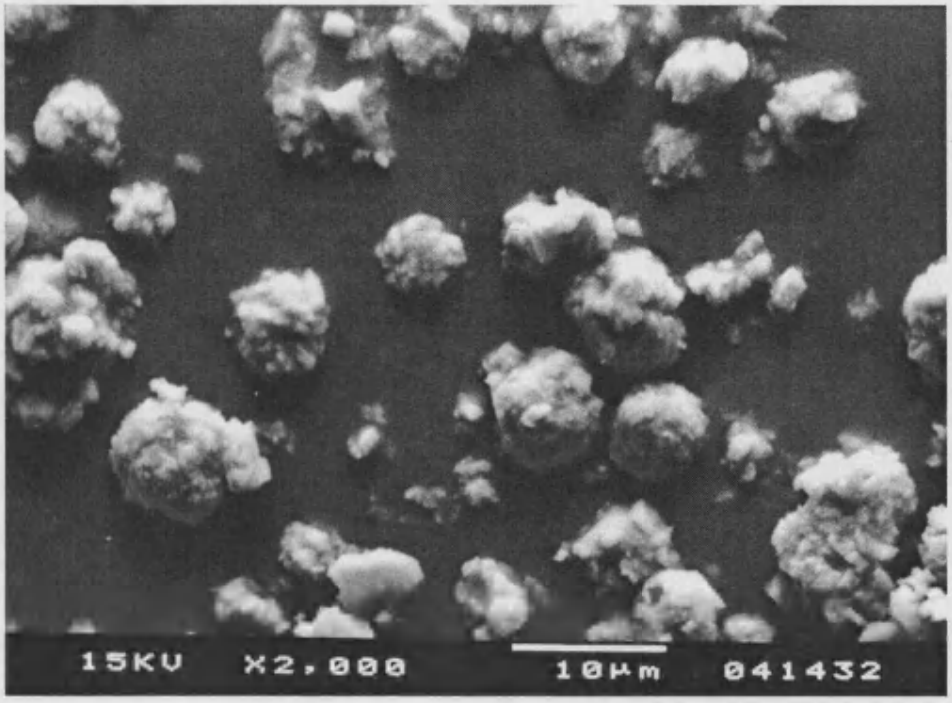

(c) Solids content = 40% w/w

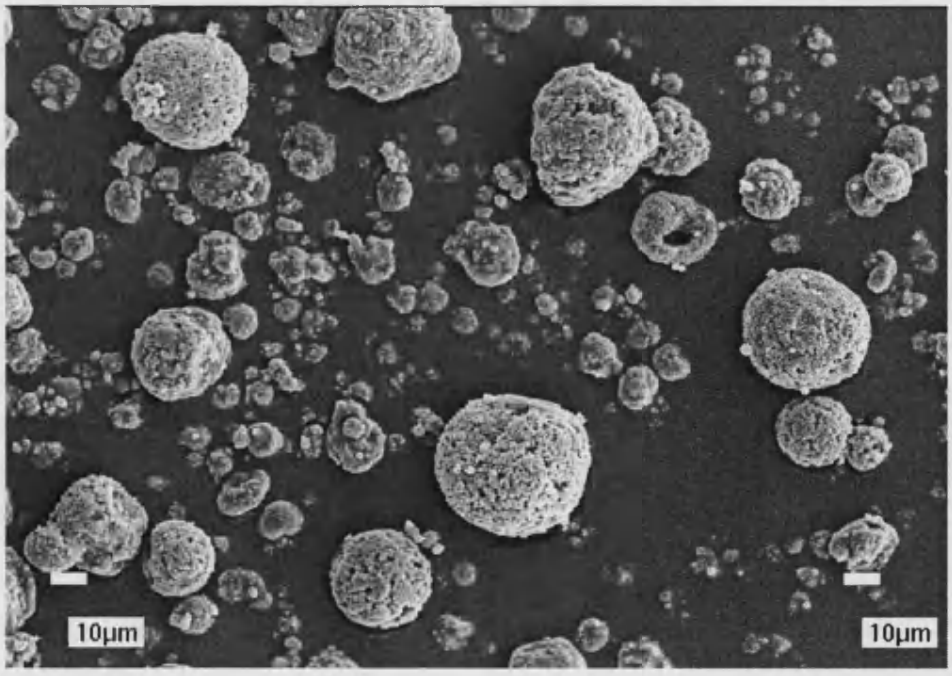

(d) Solids content = 50% w/w

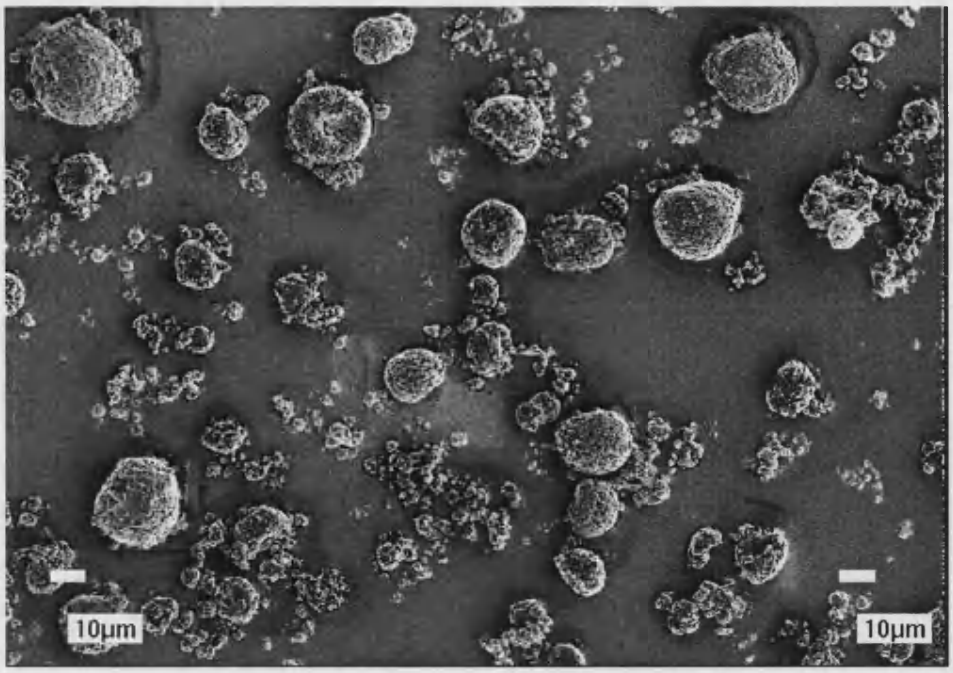

(e) Solids content = 60% w/w

Figure 3.9 SEM micrographs of spray-dried products obtained from slurries of various solids content of DCPA, (a) 20% (b) 30%, (c)40%, (d) 50% and (e) 60%.

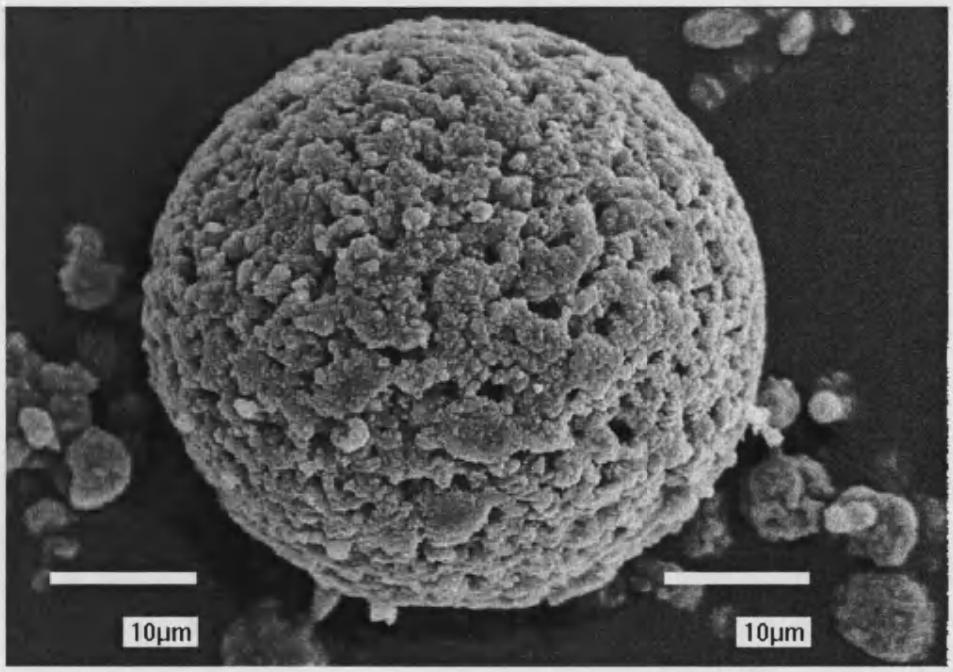

Figure 3.10 SEM micrograph of a spray-dried microspheres obtained from 60% w/w DCPA slurry.

3.6.3 Dispersant Concentration

To investigate the effect of the dispersant concentration on the spray-dried products, 200 g slurries of 30% w/w DCPA and 2 pph PEG 1000 were prepared with various amounts (1 pph, 2 pph or 3 pph) of Dispex A40 and sufficient quantity of aqueous ammonia to adjust the slurry pH to 8 – 9. These spray-dried under SDC Set 1 (section 3.5.1). The experiments produced low yields. The spray-dried products were examined under the SEM.

3.6.3.1 Results and Discussion

SEM examination results (Figure 3.11) showed that at higher concentration of dispersant, microspheres of smaller size were produced. The decrease in microsphere size may be explained by the reduction of slurry viscosity due to the addition of dispersant. It is known that viscosity is one of the factors that influences the mean drop size of a spray, but the viscosity was not measured in the experiments. The results obtained are in agreement with the finding that an increase in feedstock viscosity results in an increase in mean drop size of the sprays, and therefore producing particles of bigger size[50,93].

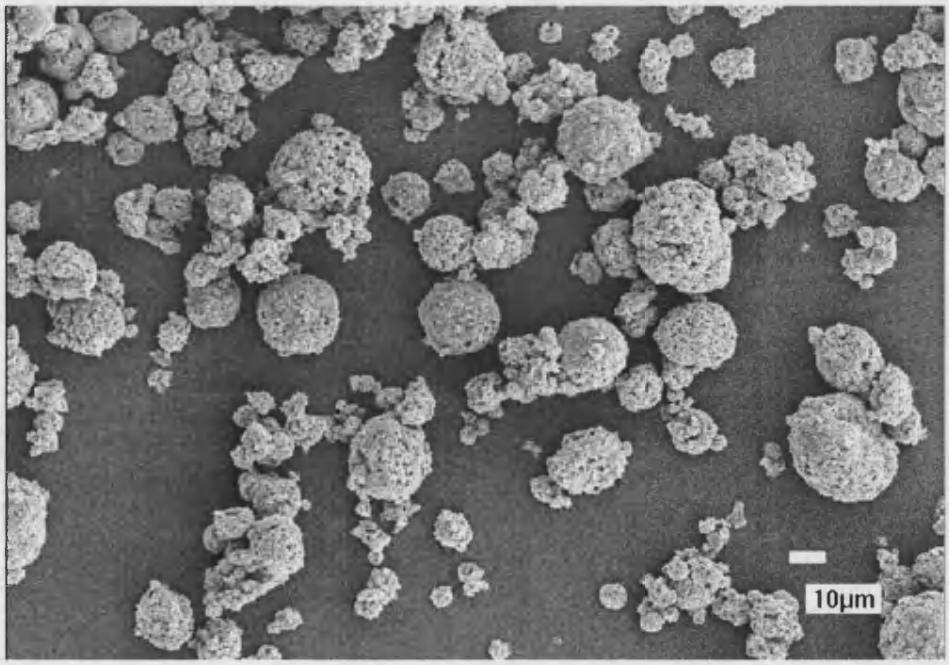

(a) Dispex concentration = 1 pph

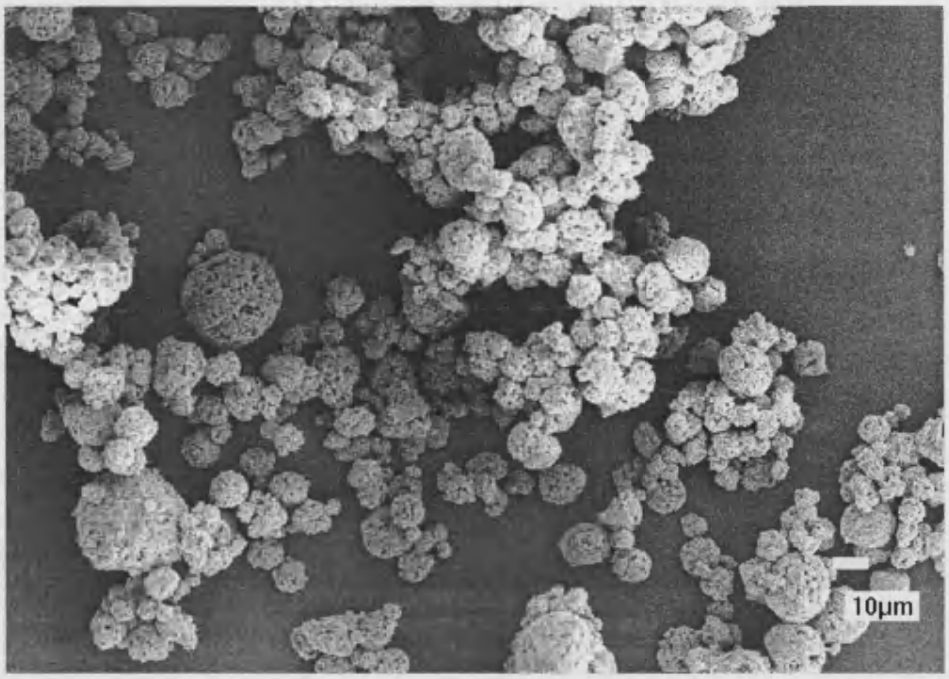

(b) Dispex concentration = 2 pph

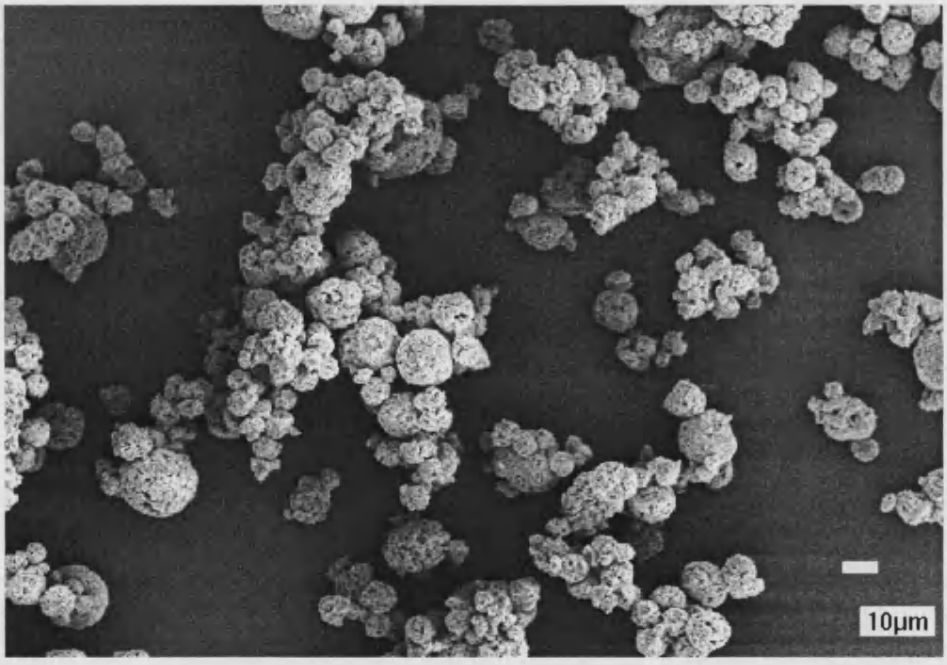

(c) Dispex concentration = 3 pph

Figure 3.11 Spray-dried products from slurries containing (a) 1 pph, (b) 2 pph, and c) 3 pph of Dispex A40. (Magnification × 500)

3.6.4 Binder Concentration

To investigate the effect of binder concentration, slurries (200 g) with 30% w/w DCPA and 2 pph of Dispex A40 were added with 2 pph or 3 pph of PEG 1000. The slurries were then spray-dried under SDC Set 1 (section 3.5.1) and the experiments produced a low yield. The spray-dried products were examined under the SEM.

3.6.4.1 Results and Discussion

The SEM results (Figure 3.12) showed that the morphology of the microspheres changed when the concentration of binder increased from 2 pph to 3 pph. 3 pph PEG 1000 produced microspheres with smoother surfaces. This can be due to higher amount of binder accumulating on the surface of the microspheres. Zhang *et al.*[58] have reported that a surface layer with a large amount of binder was formed in the ceramic spray-dried granule, and the binder segregation was influenced by initial binder concentration.

It was also noted that slurry with the higher concentration of PEG 1000 produced spray-dried products which flowed less well. The products accumulated mainly in the cyclone. The presence of PEG 1000 may have helped to retain moisture. Therefore, the products were dried less efficiently. It is concluded that the lesser the PEG the better the product flow; 2 pph PEG is more suitable concentration.

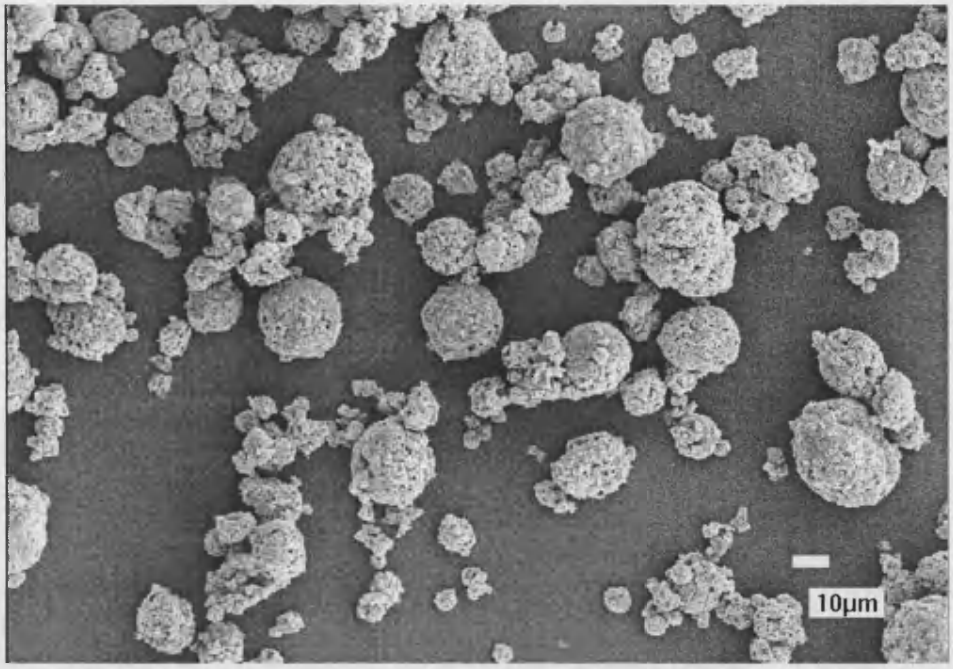

(a) binder concentration = 2 pph

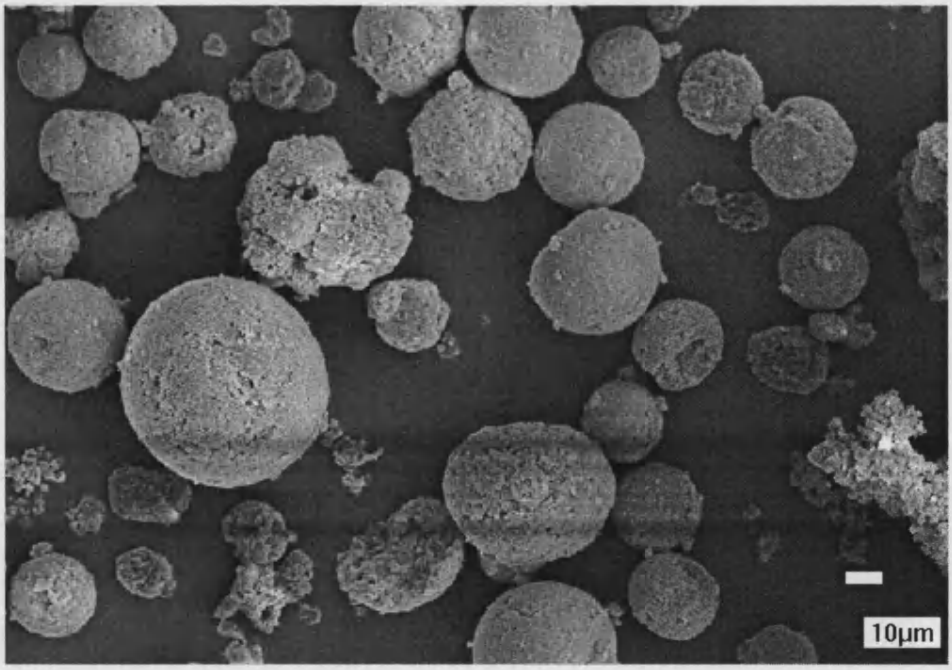

(c) binder concentration = 3 pph

Figure 3.12 Spray-dried product of 30% w/w DCPA, 2 pph Dispex A40 and PEG 1000 (binder) concentrations of (a) 2 pph, and (b) 3 pph. (Magnification × 500)

3.6.5 Jet Size

The effect of atomiser jet size was also investigated. The size of the spray droplets is closely linked to the jet size. Theory predicts that the mean drop size is roughly proportional to the square root of the liquid jet diameter[89]. With the aim of producing a larger spray-dried product, the use of a bigger jet size, 1.5 mm (vs. 0.5 mm used previously) was investigated.

A suspension (200 g) of 30% w/w DCPA, 2 pph PEG 1000 and 2 pph Dispex A40 was sprayed under these following conditions:

Spray-drying Conditions (SDC) Set 2

Jet size	1.5 mm
Inlet temperature	200 °C
Pump speed	350 and 500 ml/h (dryer scale = 10 or 15)
Drying air flow rate	62-64 m^3/h (dryer scale = 41-44)(maximum setting)
Compressor air pressure	80 kPa (maximum setting)

Experiments were performed at two different pump speeds, 350 ml/h and 500 ml/h. The compressor air pressure was set to maximum as in SDC Set 1 (section 3.5.1), and the reduction in its values was due to the change of jet size. Both experiments produced a very low yield.

3.6.5.1 Results and Discussion

A jet with a bigger diameter decreases the velocity of the feed sprayed through the nozzle at any one time if the pump speed remains constant. At a pump speed of 350 ml/h, the sprayed droplets landed mostly on the base of the main chamber because the sprayed products were wet, the moisture evaporation being far from complete. At an increased pump speed of 600 ml/h, slurry droplets were dribbling from the nozzle, because there was not enough energy to convert the slurry into a fine mist. It was therefore concluded that the 1.5 mm jet nozzle was not suitable for these studies.

3.6.6 Change of binder to Eudragit L100

As mentioned in the preliminary studies (section 3.5.3.2), Eudragit L100 was found to produce microspheres with smooth surfaces that flowed relatively well in the spray-dryer, compared to other binders tested. It was then decided to further investigate the use of Eudragit L100 as a binder, replacing PEG 1000, in the DCPA spray-drying slurry.

Eudragits are a variety of acrylic resins that are based on poly(ethylacrylate-methymethacrylate) esters[33], and are widely used in the pharmaceutical industry as a coating material for oral dosage forms to prepare film-coated, enteric coated or sustained-release granules or tablets[21]. Films with different solubility characteristics can be obtained using different types of eudragits. For example, Eudragit E is used as a plain or insulating film coating because it is soluble in gastric fluid below pH 5. In contrast, Eudragit L and S types are used as enteric coating agents since they are resistant to acidic pH in the stomach, *e.g.*, Eudragit L 100 is soluble at pH > 6.

Eudragits are also used in both aqueous and organic wet-granulation processes as binders. Larger quantities (5% - 20%) are used to control the release of active drugs[33]. Solid Eudragits may also be used in direct compression to produce controlled release tablets[94].

Six slurries, containing Eudragit L100, with compositions listed in Table 3.2, were prepared and spray-dried at the inlet temperature given in the table. All other spray-drying conditions are as in SDC Set 1 (section 3.5.1).

Table 3.2 Slurry compositions and spray-drying conditions for formulation A - F.

	Formulation					
	A	B	C	D	E	F
DCPA/%w/w	50	30	60	60	60	60
Eudragit L100/pph	2	2	2	3	3	3
Dispex A40/pph	1	1	1	1	1	1
Inlet temperature/°C	120	200	200	200	180	160

3.6.6.1 Results and Discussion

It was observed that compared to slurries with PEG 1000, slurries with Eudragit L100 generally produced spray-dried products with better flow characteristics. All formulations (A-F) produced highly satisfactory spray-dried products. Products flowed smoothly from the main chamber, through the cyclone into the collection bottle. This flow pattern was different from the flow pattern of PEG containing products, which tended to stay in the cyclone.

Formulation A was a 50% w/w DCPA slurry spray-dried at inlet temperature of 120 °C and the product was a free flowing powder. This experiment shows that slurries with Eudragit L100 can be successfully spray-dried at temperatures as low as 120 °C, as the products obtained are still relatively dry. This was not the case for slurries with PEG 1000. Under the same spray-drying conditions, the moisture evaporation for slurries with Eudragit L100 appears to be more complete than for slurries with PEG. This is probably due to the different properties of Eudragit L100 and PEG.

SEM micrographs of the spray-dried product of Formulation A at three different magnifications are shown in Figure 3.13. These micrographs show hollow microspheres. The shell of the some of the hollow spheres erupted under the high internal pressure created during moisture evaporation and the shell collapsed as explained in section 1.5.1. Hence, some microspheres had dimples, holes or were doughnut-shaped. At ×10,000 magnification, it was clear that these microspheres were made up from DCPA particles of different sizes, a consequence of the ball-milling process (see Table 3.1 in section 3.5.6 for particle sizing results).

SEM micrographs of spray-dried products from Formulation B, C, D, E and F are shown in Figure 3.14. The difference between Formulation B and Formulation C is the solids content (30% and 60% w/w DCPA respectively). 60% w/w slurry produced bigger microspheres. This is observation is consistent with the results obtained from slurries using PEG 1000 as a binder (section 3.6.2).

Formulation C and Formulation D have Eudragit L100 concentration of 2 pph and 3 pph respectively. SEM results show that the slurry with a higher concentration of binder (Formulation D) produced bigger and rounder microspheres. These microspheres also appeared to have bigger hollow centres and thinner shells.

Formulation D, E and F have the same composition, but were spray-dried at different inlet temperatures (200 °C, 180 °C and 160 °C respectively). These formulations produced microspheres with thin shells and big holes on the surface. Products from Formulation D and E were found to be similar, while Formulation F (lowest inlet temperature) contained some of the biggest microspheres.

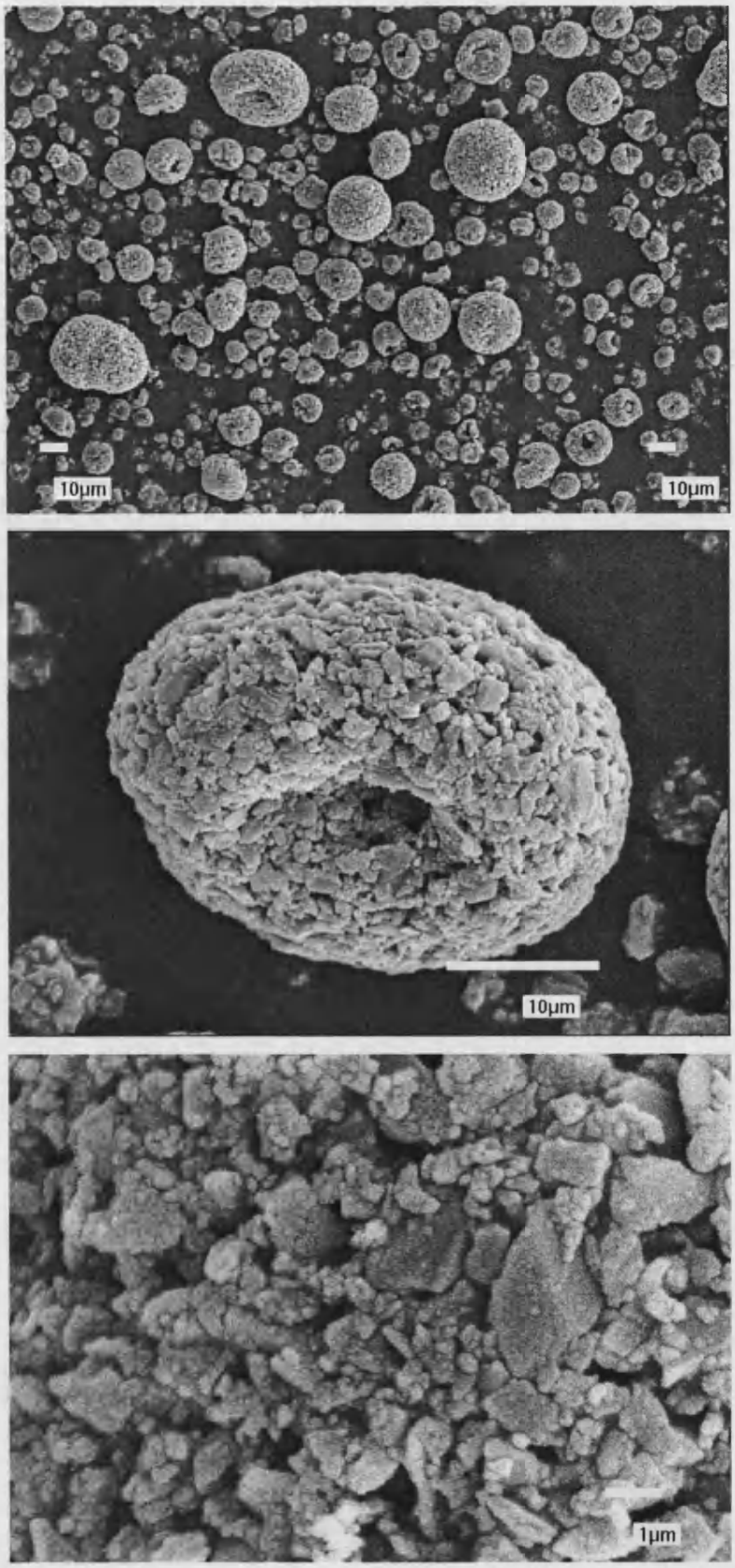

(a)

(b)

(c)

Figure 3.13 SEM micrographs of spray-dried products obtained from Formulation A at magnification of a) ×500, b) ×2700 and c) ×10,000.

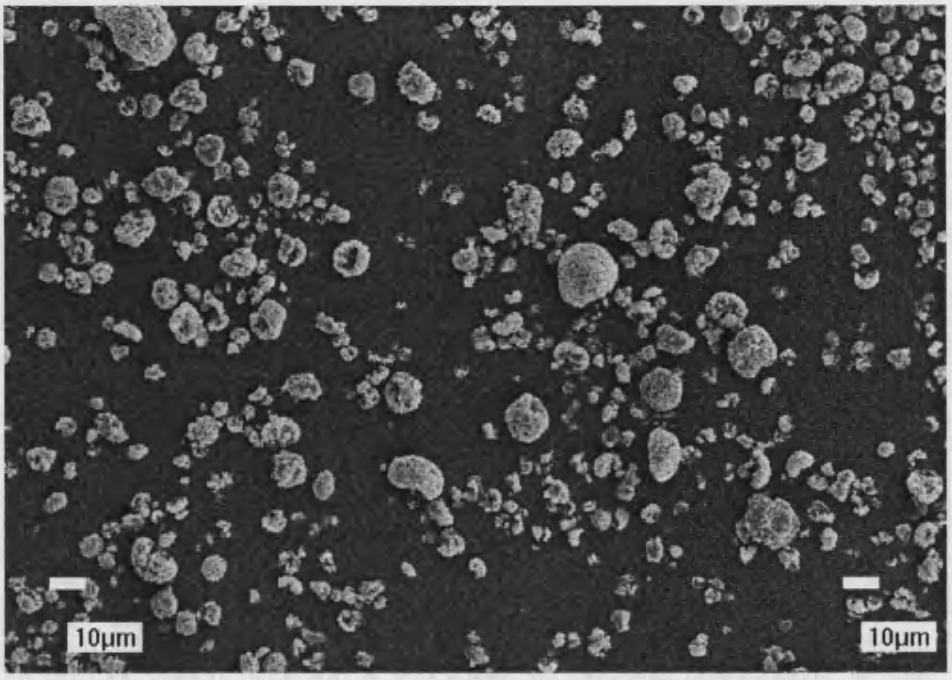

(a) Formulation B

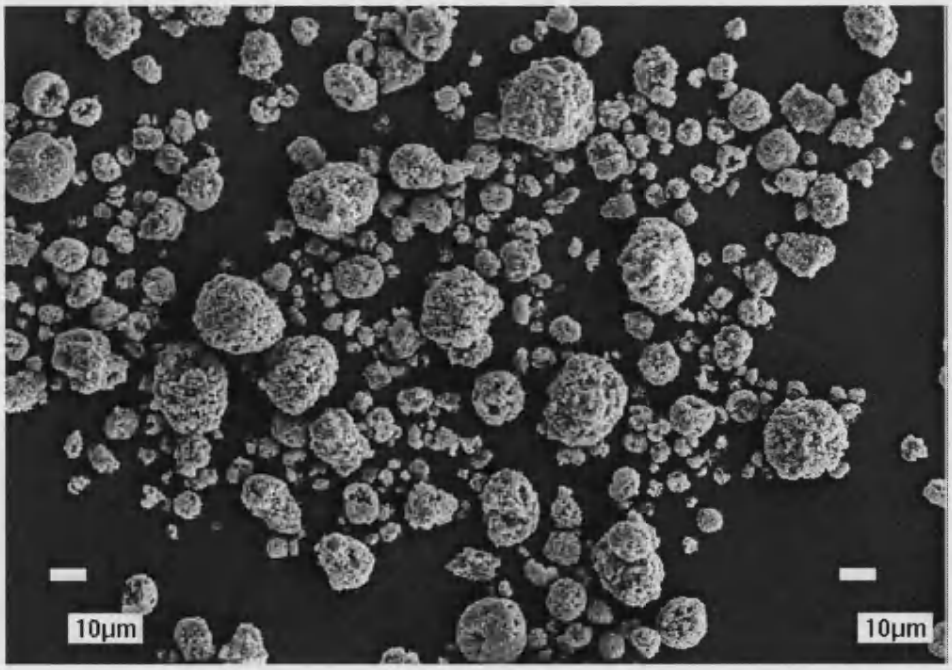

(b) Formulation C

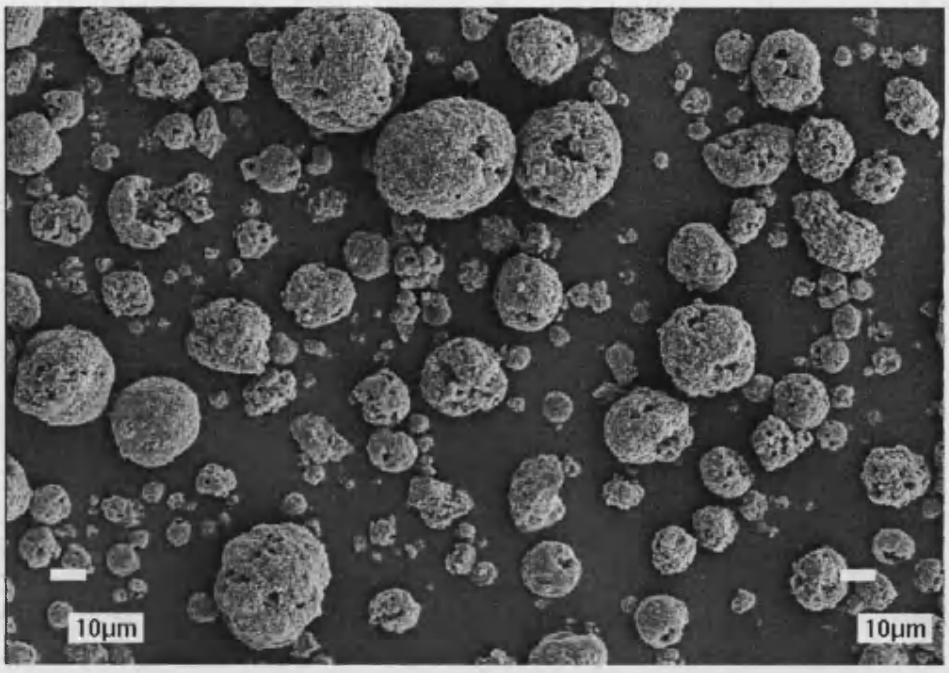

(c) Formulation D

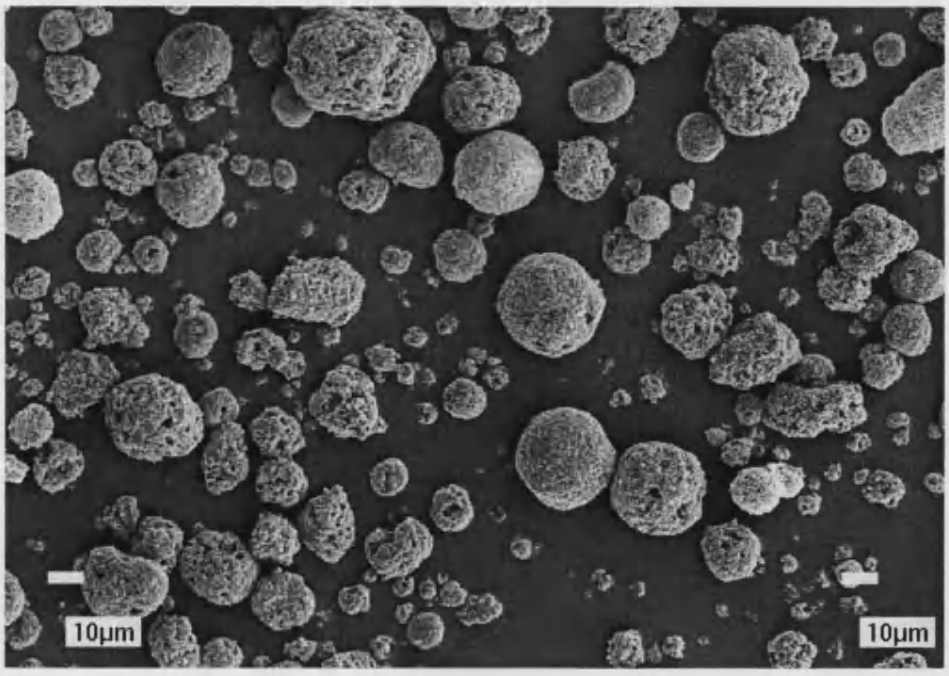

(d) Formulation E

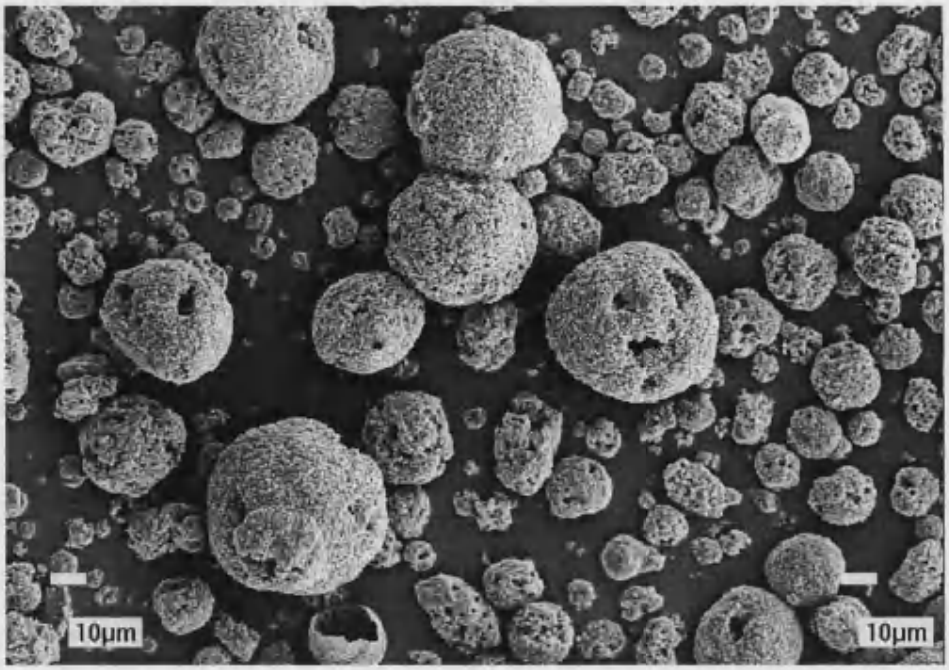

(e) Formulation F

Figure 3.14 SEM micrographs of spray-dried products obtained from Formulation B to Formulation F (constant magnification of ×500).

3.6.7 Internal Morphology Studies

To investigate the internal morphology of microsphere samples under the SEM, the microspheres need to be sectioned. The microspheres are too fragile and too small to be hand manipulated; therefore, for the sectioning procedure to be carried out, the microspheres need a good support in the form of a resin matrix. There are hydrophobic (epoxy) and hydrophilic (acrylic) resins available for embedding samples.

In this study, an epoxy resin was used. Microsphere samples were first mixed with a liquid resin, and the resin was allowed to penetrate into the pores. When the resin was polymerised and hardened, it provided a good platform for the samples to be sectioned or polished. For details of the resin embedding technique and SEM examination procedure please refer to section 2.7.5.

3.6.7.1 Results and Discussion

Samples of epoxy resin-embedded microspheres were found to have good contrast for SEM examination. SEM micrographs of sectioned microspheres obtained from Formulation F are shown in Figure 3.15. The results showed that hollow-centred microspheres had been produced. It was expected that these big hollow centres were created during the moisture evaporation when the droplets were sprayed into the main chamber, as explained in section 1.5.1. The suspended solids were drawn to the droplets' surfaces and the liquid at the interior of the droplets diffuses to the surfaces to be evaporated. Hence, the centres of the droplets are empty and the solids form the shells.

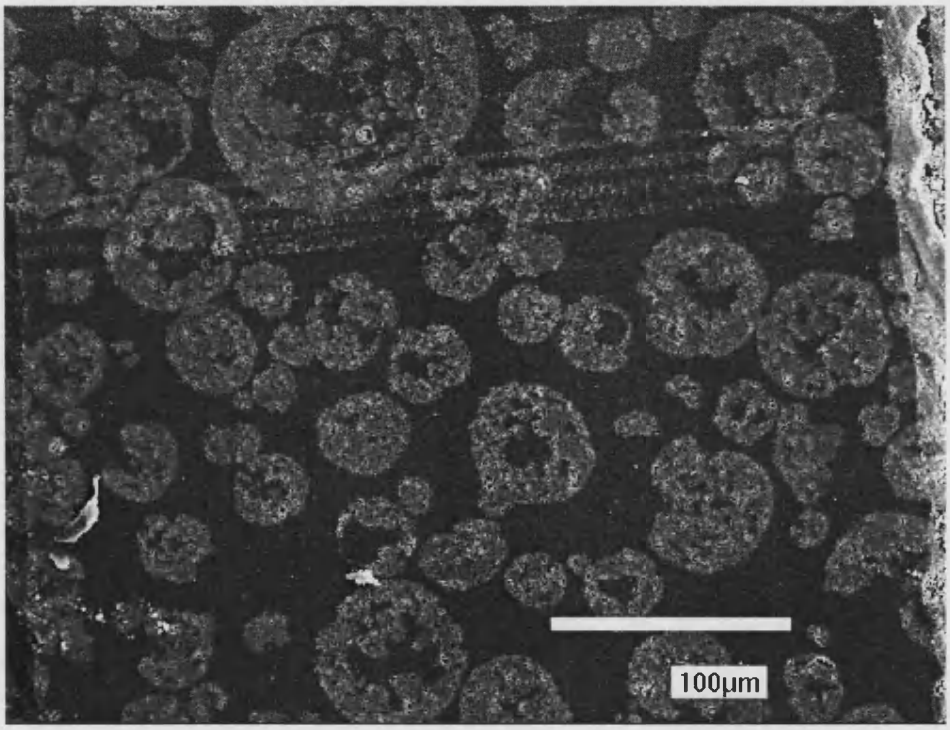

Figure 3.14(a) SEM micrographs of sectioned microspheres obtained from Formulation F at ×300 magnification

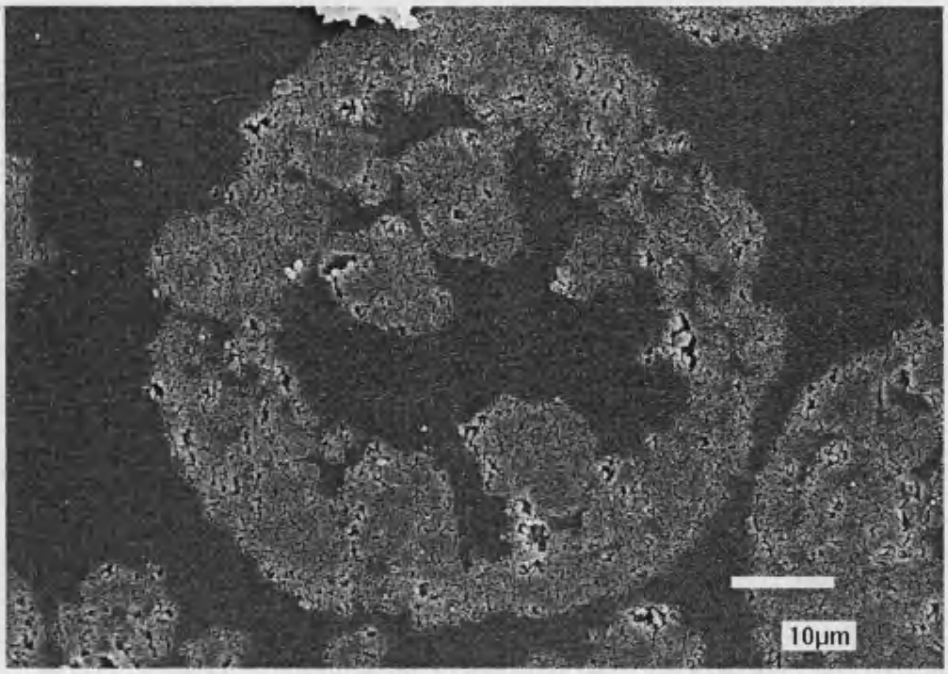

Figure 3.15(b) SEM micrographs of sectioned microspheres obtained from Formulation F at ×1400 magnification.

3.7 Spray-drying of Beta-Tricalcium Phosphate (β-TCP)

3.7.1 Characterisation of Powder As-Received

The spray-drying of beta tri-calcium phosphate (β-TCP), $Ca_3(PO_4)_2$, was also studied. Visually, β-TCP powder has a more 'fluffy' appearance compared to DCPA powder. The β-TCP as-received was imaged under the SEM (Figure 3.16) and its particle-size distribution was analysed using a Mastersizer X (section 3.7.5). These results were then compared to the DCPA powder as-received.

3.7.1.1 Results and Discussion

The SEM micrographs of β-TCP as-received powder are shown in Figure 3.16. Compared to DCPA as-received [Figure 3.5 (a)], in terms of shape, β-TCP particles are more 'flaky' while DCPA particles are more 'cubic'.

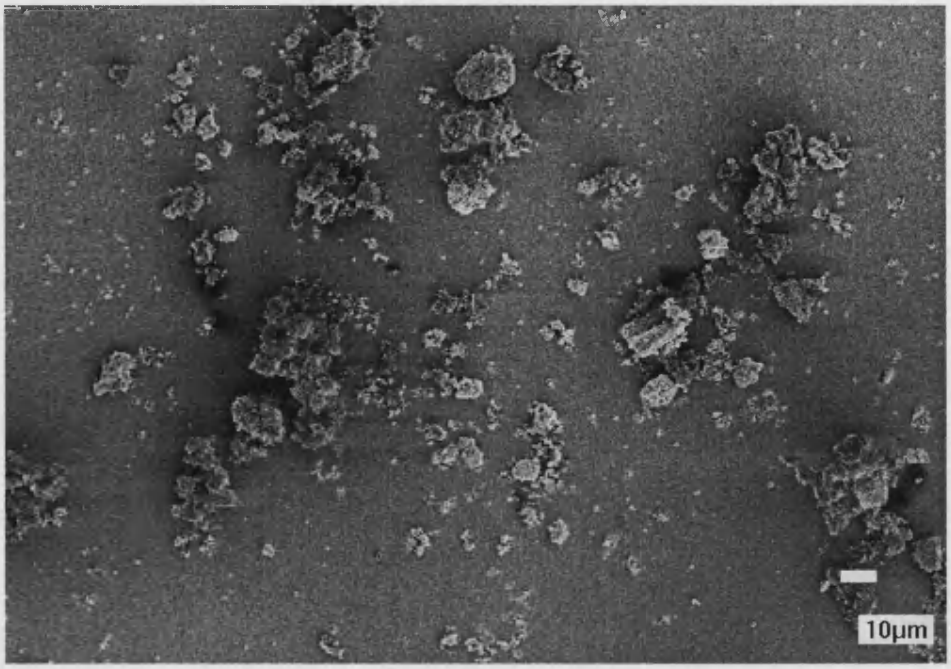

(a) Magnification = ×500

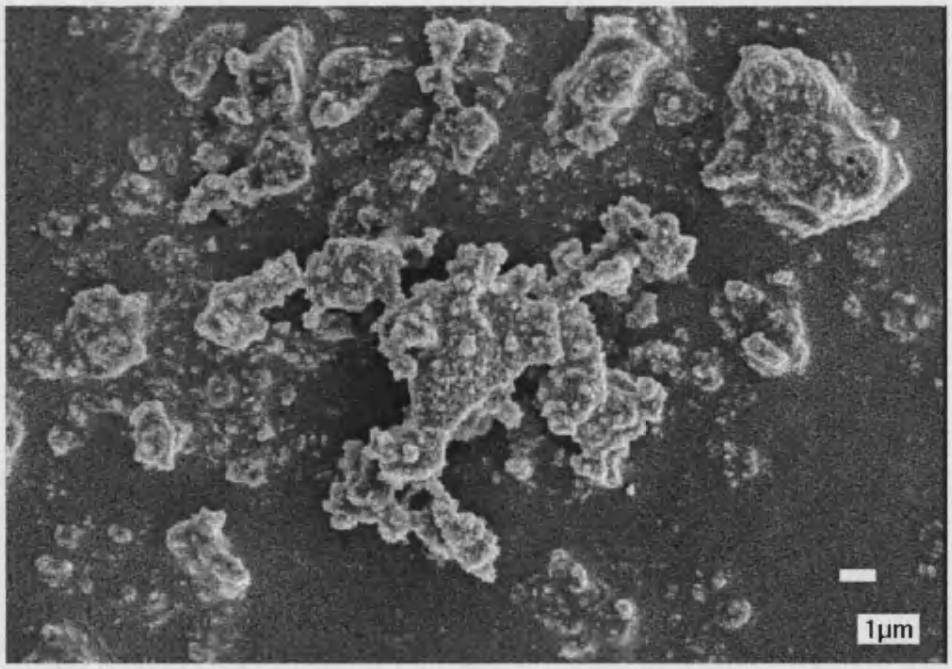

(b) Magnification = ×5000

Figure 3.16 SEM micrographs of β-TCP powder as-received at magnification of a) ×500, b) ×5000

The results of particle-size analysis are summarised in Table 3.3. Comparing the two powders, the results indicated that β-TCP powder has a smaller volume mean diameter (DCPA: 4.56 μm; β-TCP: 3.41 μm) and has a narrower particle-size distribution (80% confidence interval, DCPA: 0.74 μm - 19.4 μm; β-TCP: 1.01 μm - 9.58 μm).

Table 3.3 Results of particle-size analysis of DCPA and β-TCP powder as-received.

	Particle-size/μm, n = 3		
Sample	d(v, 0.1)	d(v, 0.5)	d(v, 0.9)
DCPA as-received	0.74 ± 0.00	4.56 ± 0.30	19.4 ± 1.95
β-TCP as-received	1.01 ± 0.01	3.41 ± 0.03	9.58 ± 0.35

Note: Measurements were made in the small-volume cell (SVC) and the samples were subjected to 5 min sonication before analysis.

3.7.2 Stage 1 Study for β-TCP

As described earlier (section 3.5.6.1), 30% w/w solids content DCPA in water was a liquid suspension. However, 30% w/w β-TCP in water was found to be a viscous paste, which could not be pumped into the spray-dryer. It is interesting to note that with an addition of 2 pph Dispex A40 to the β-TCP paste, the viscosity of the paste reduced markedly, and it became a pumpable liquid slurry. By visual observation, it was noticed that this slurry was a good suspension, since it was thick enough to suspend all the particles with no sedimentation, the pre-treatment of ball-milling carried out for DCPA was therefore unnecessary for β-TCP.

Four β-TCP formulations (T1, T2, T3 and T4) were prepared and spray-dried. Their compositions and spray-drying conditions are listed in Table 3.4. Two binders were investigated: T1 and T2 contained PEG 1000, while T3 and T4 contained Eudragit L100. T1 has a higher pump speed (500 ml/h) compared to T2; and T3 was sprayed at a higher temperature (245 °C) compared to T4 (200 °C).

Table 3.4 β-TCP slurry compositions and spray-drying conditions for Stage 1 Study.

			Formulation			
			T1	T2	T3	T4
Compositions	β-TCP/%w/w		30	30	30	30
	Binder /pph	PEG 1000	2	2	-	-
		Eudragit L100	-	-	2	2
	Dispex A40/pph		2	2	2	2
Conditions	Inlet temperature/°C		200	200	245	200
	Pump speed/dryer scale (ml/h)		15 (500)	10 (350)	10 (350)	10 (350)
	Jet Size/mm		0.5	0.5	0.5	0.5

Note: Air-flow and compressor air pressure were set to the maximum values, 62 m^3/h - 64 m^3/h and 180 kPa respectively, in all experiments.

Slurries with PEG 1000 were prepared as follows:

1) PEG 1000 was weighed out and dissolved in deionised water in a vial.
2) Dispex A40 was weighed out and dissolved in deionised water in a vial.
3) β-TCP powder was weighed out in a beaker.
4) The solutions of binder and dispersant obtained in 1) and 2) were added into the beaker containing β-TCP.
5) Sufficient quantity of aqueous ammonia (2.7 M) to adjust the pH to 8.4-8.7 was added by pipette. The increase of pH was monitored by pH paper.
6) Deionised water was added to make up to the final weight.

A typical formula is illustrated as below:

DCPA	60.0 g	(30% w/w)
Eudragit L100	1.2 g	(2 pph)
Dispex A40	1.2 g	(2 pph)
Aqueous ammonia (2.7M)	~ 2 ml	(to adjust pH to 8.4-8.7)
Purified water to	200.0 g	

To ensure complete dissolution of Eudragit L100, 1) of the above preparation procedure was modified for the preparation of slurries containing Eudragit L100.

Eudragit L100 was first weighed out and dissolved in water with aqueous ammonia. The mixture was then sonicated until all solids dissolved. This precautionary step was carried out because Eudragit L100 does not dissolve well in acidic conditions[33] and β-TCP suspension is slightly acidic, pH ~ 5. All other steps in the procedure above were then followed.

The slurries were magnetically stirred throughout the spray-drying process. The surface morphology and the internal morphology of the spray-dried products were examined under the SEM (sample preparations and resin-embedded techniques are detailed in sections 2.7.4 and 2.7.5).

3.7.2.1 Results and Discussion

With the addition of dispersant, Dispex A40, β-TCP powder was found to readily form a good suspension by visual observation, therefore, the particle reduction process – ball-milling was found to be not necessary. This may be because β-TCP particles are smaller and 'flaky' in shape. This finding was welcome because it reduces the ball-milling steps which may introduce one more possible variation to the final products, and is time consuming.

The spray-dried products of all four formulations obtained were free flowing powders. Their SEM micrographs are shown in Figure 3.17. As can be seen from the micrographs, the products consisted of microspheres with a range of sizes.

SEM results showed that there was no distinctive difference between the products of T1 and T2, *i.e.*, the higher feeding rate (pump speed) of T1 (500 ml/h) has not made a marked difference. T4 (Eudragit L100 as binder, inlet temperature = 200 °C) was found to contain some larger microspheres compared to all other formulations; this could be the result of change in viscosity due to the binder. Viscosity is one of the main factors that influence the droplet size.

It was found that the binder type also influenced the surface morphology of the microspheres produced (Figure 3.18). Eudragit L100 was found to produce microspheres with a smoother surface than PEG 1000.

The SEM micrographs of sectioned microspheres from T3 and T4 (Figure 3.19) showed that T4 consisted of microspheres with hollow regions while T3, even at a higher magnification observation (as shown in Figure 3.19), consisted of more solid centred microspheres. The results indicate that at higher spraying temperature (245 °C) solid microspheres were produced, whilst at lower spraying temperature (200 °C) porous microspheres were produced.

In conclusion, during Stage 1 Study free-flowing spray-dried β-TCP microspheres were successfully produced. β-TCP was found to be easier to spray dry than DCPA because:

1) A homogeneous suspension of β-TCP powder can be readily prepared without the additional step of ball-milling.
2) β-TCP slurries produced spray-dried products which flowed distinctively better in the spray-dryer.

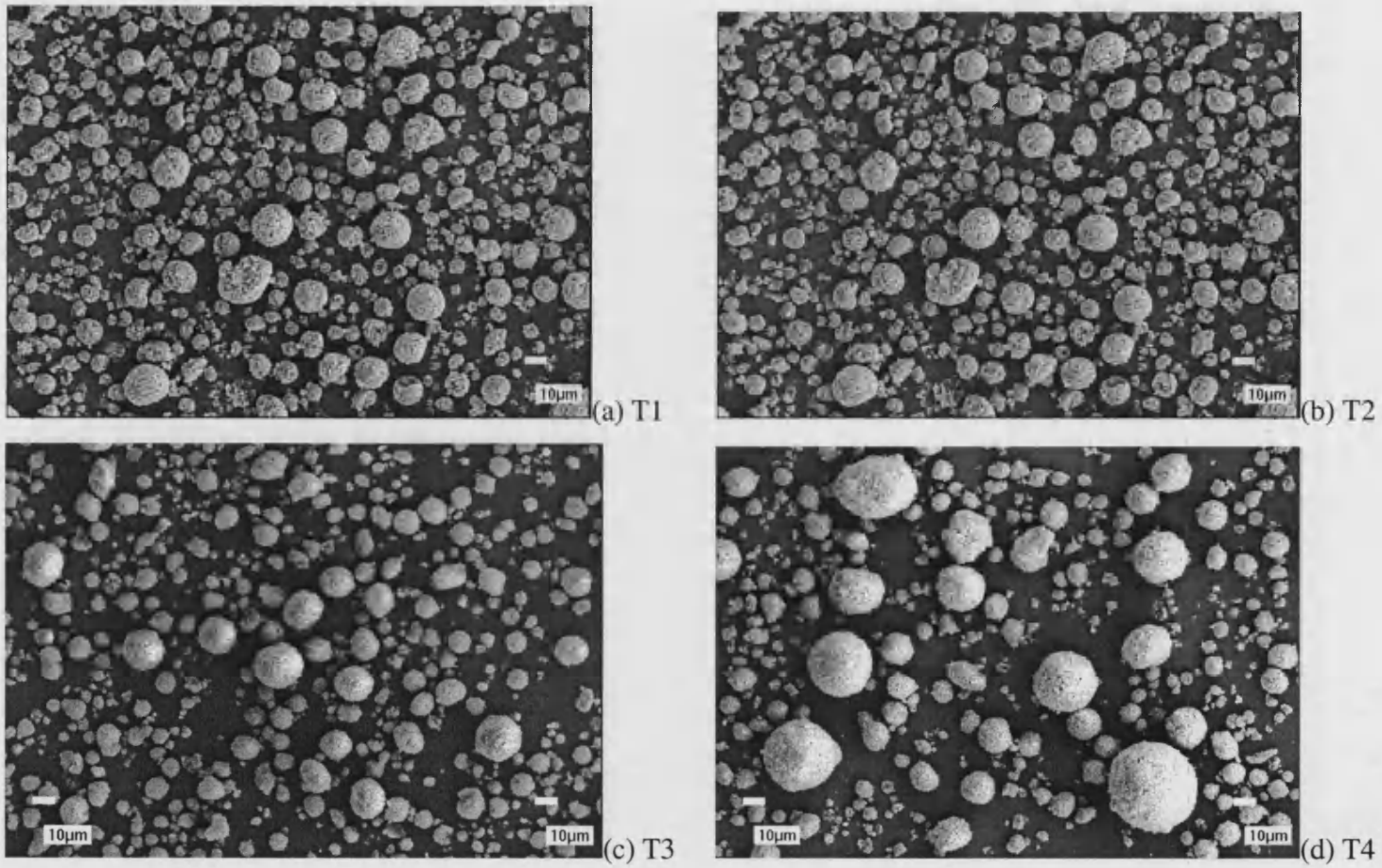

Figure 3.17 Spray-dried products obtained from formulation (a) T1, (b) T2, (c) T3, and (d) T4. (Constant magnification)

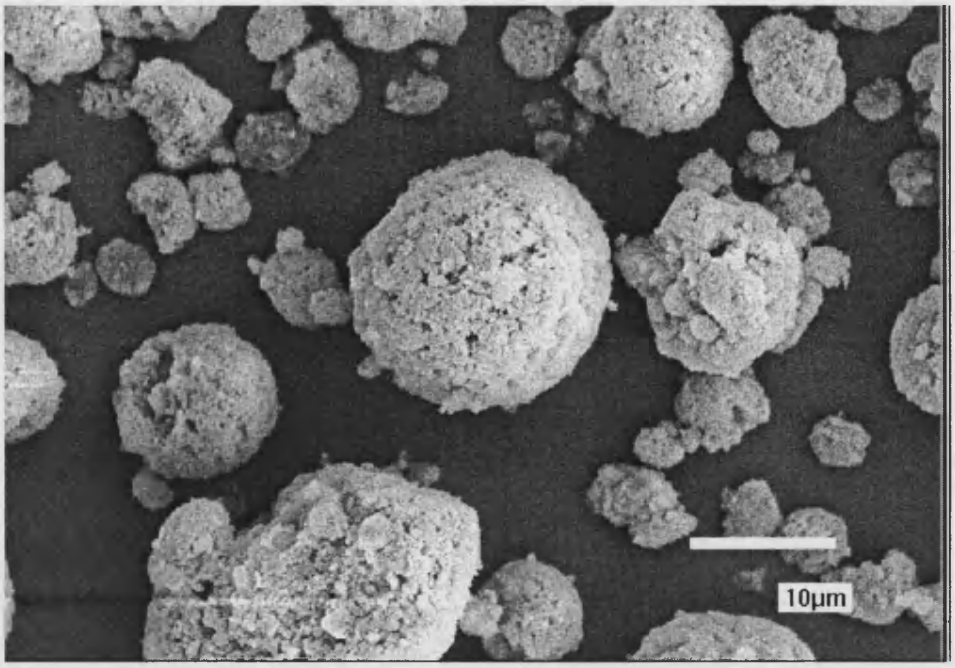

(a) Microspheres containing PEG 1000

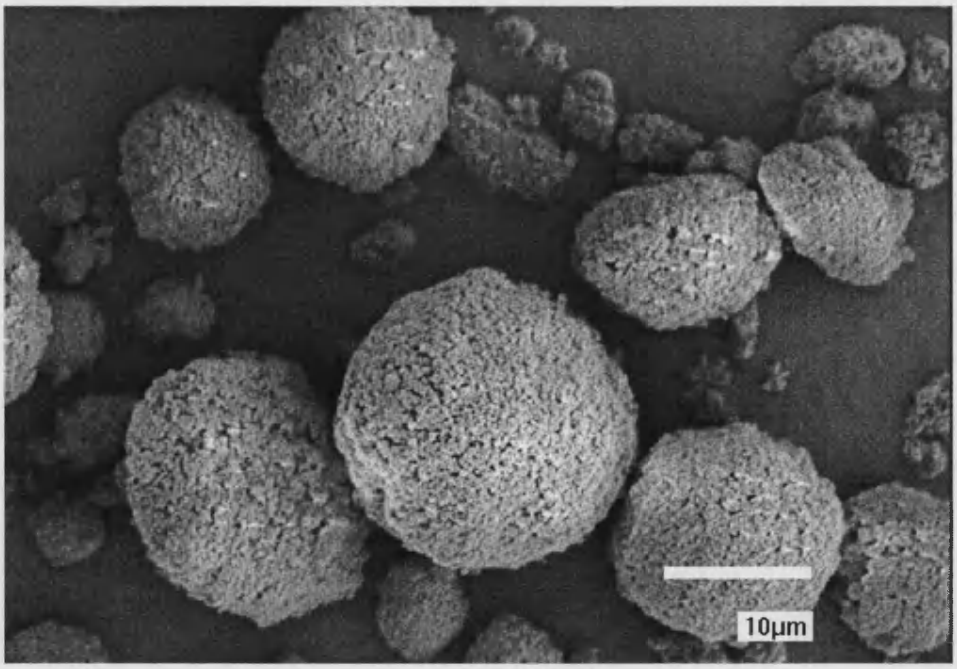

(b) Microspheres containing Eudragit L100.

Figure 3.18 SEM micrographs of β-TCP microspheres using (a) PEG 1000, (b) Eudragit L100, as binder.

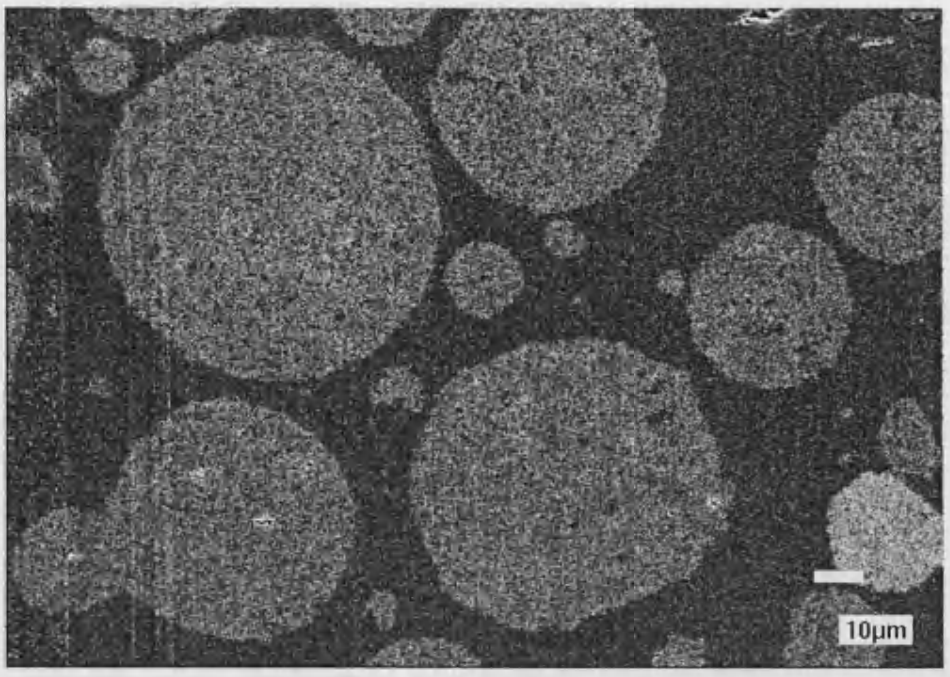

(a) Inlet temperature = 245 °C, T3

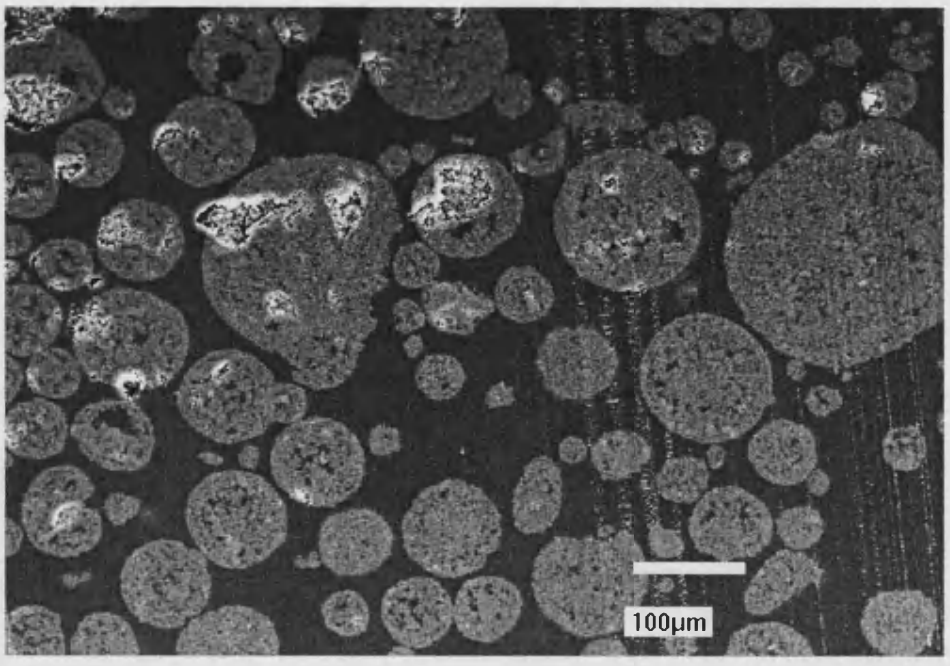

(b) Inlet temperature = 200 °C, T4

Figure 3.19 SEM micrographs of sectioned microspheres obtained from spray-drying at inlet temperature of (a) 245 °C, T3, and (b) 200 °C, T4.

3.7.3 Stage 2 Study for β-TCP

Stage 2 study aimed to refine the slurry compositions and spray-drying conditions to produce microspheres with the following desired characteristics: highly porous, diameter as large as possible and well-formed spherical shape. These characteristics are favourable because the project aims to produce drug carriers which have a high porosity to serve as reservoir, a large diameter for increasing the drug diffusional pathway, therefore delaying the drug release, and a uniform geometry for uniform drug release.

The range of slurry compositions and the spray-drying conditions chosen for Stage 2 Study were based on the results obtained from Stage 1 Study and previous experience as presented below:

I) Inlet temperature

The inlet temperatures of 180 °C and 200 °C were chosen because:

a) Temperatures ≤ 160 °C are unlikely to supply enough energy for moisture evaporation to produce free flowing products (section 3.6.1);
b) The higher temperature tested (245 °C) was found to produce relatively less porous microspheres (section 3.7.2);
c) The frequency of nozzle blockage was found to increase with increasing inlet temperature, for a given pump speed;
d) Pharmaceutical products should preferably to be spray-dried at the lowest possible temperature to reduce the risk of heat damage.

II) Solids content

To investigate the effect of solids concentration on the spray-dried products, β-TCP slurries with solids content of 10% w/w to 50% w/w, at an increment of 10%, were chosen. A high solids content is desirable in the spray-drying of ceramics, as discussed in section 3.1. Solids concentration as high as 50% w/w were tried to estimate the approximate maximum solids contents that is achievable.

III) Dispersant

The Dispex A40 concentration of 2 pph was used because it was found to produce a well-dispersed suspension in Stage 1 Study (section 3.7.2). The spray-drying of slurry without Dispex A40 was also investigated. The effect of Dispex A40 as a dispersant for the systems was further studied by measuring the height of sediments as detailed in section 3.8.

IV) Binder

Eudragit L100 was chosen over PEG 1000 to be used as the binder. This is because in the Stage 1 Study (section 3.7.2), it was found that the spray-drying of Eudragit containing slurries produced microspheres which:

a) flowed better in the spray-dryer, as observed visually;
b) had the largest diameter (Figure 3.17);
c) had uniform spherical shape and smooth surface (Figure 3.18).

IV) Jet size

The mean drop size is roughly proportional to the square root of the liquid jet diameter[89]. A higher drop size will theoretically produce particles with larger diameter. A jet with internal diameter of 0.5 mm was used in Stage 1 Study. Aiming to produce microspheres with larger diameter, the use of jets with internal diameter of 1.0 mm and 1.5 mm was investigated. Bigger jet sizes also have the added advantage of having less nozzle blockages.

Fourteen formulations with compositions listed in Table 3.5 were prepared and spray-dried at the conditions given in the table. Note that the sequence of formulation listed in the table does not represent the chronology sequence of the experiments. Slurries were magnetically stirred throughout the spray-drying process. All spray-dried products were then examined under the SEM. The internal morphology of these products was studied by examining the sectioned open resin-embedded samples (technique see section 2.7.5) under the SEM.

Table 3.5 β-TCP slurry compositions and spray-drying conditions for Stage 2 Study.

		Formulation													
		T5	T6	T7	T8	T9	T10	T11	T12	T13	T14	T15	T16	T17	T18
Composition	β-TCP/%w/w	30	30	30	20	20	10	10	10	30	15	30	10	30	40
	Eudragit L100/pph	4	2	2	2	2	2	2	2	2	2	2	2	2	2
	Dispex A40/pph	2	2	2	0	2	2	2	2	2	2	2	2	2	2
Condition	Inlet temperature/°C	180	180	180	180	180	180	200	200	200	200	180	200	160	180
	Pump speed /dryer scale*	10	10	10	15	15	15	15	25	10	15	10	15	10	15
	Jet size/mm	0.5	0.5	1.5	0.5	0.5	0.5	0.5	0.5	1.5	0.5	1.0	1.0	0.5	0.5

*Dryer scale: 10 = 350 ml/h, 20 = 600 ml/h, and 30 = 1000 ml/h according to the spray-dryer operational manual (LabPlant Ltd., UK).

Air-flow and compressor air pressure were set to the maximum value, ~ (62 - 64) m^3/h and ~ (150 –180) kPa respectively, at all time.

3.7.3.1 Results and Discussion

I) Inlet Temperature

30% w/w β-TCP slurries were spray-dried at inlet temperature of 180 °C (T6). Slurries with the same composition have also been spray-dried at 200 °C (T4) and 245 °C (T3) in Stage 1 Study while other conditions remained constant. The products of these formulations were examined and compared under the SEM (Figure 3.20). A temperature of 245°C was found to produce microspheres of smaller diameter and cause frequent nozzle blockages. Also, whilst temperatures of 180 °C and 200 °C were found to produce highly porous microspheres, a temperature of 245 °C was found to produce solid centred microspheres (as discussed earlier in section 3.7.2.1. and shown in Figure 3.19)

II) Solids content

Slurries with solids content of 10% w/w - 40% w/w β-TCP were successfully spray-dried. Slurries with solids content > 40% could not be prepared because there was not enough water to wet all the solids. Therefore, only slurries with solids content up to 40% w/w are listed in Table 3.5. T10, T9, T6 and T18 contained solids contents of 10%, 20%, 30% and 40% w/w respectively, and their SEM micrographs are shown in Figure 3.21. Under the SEM, it appears that microspheres with larger diameter were obtained with increasing solids content.

III) Dispersant concentration

Slurries of 20% w/w β-TCP were successfully prepared and spray-dried with, and without Dispex A40 (T8 and T9 respectively). The resultant spray-dried microspheres appear to be similar under the SEM (Figure 3.22). These results suggest that at lower solids content (< 30% w/w), the addition of Dispex A40 is not essential. However, slurries of 30% w/w solids content, are too viscous to be spray-dried and the use of Dispex is essential.

IV) Binder concentration

The only difference between T5 and T6 is the binder concentration, at 4 pph and 2 pph Eudragit L100 respectively. Under the SEM, in terms of surface morphology and

dimensions of the microspheres obtained, no marked difference was observed between the spray-dried products of these formulations (Figure 3.23).

V) Jet Size

Slurries of 30% w/w β-TCP were spray-dried using jet sizes of 0.5 mm, 1.0 mm and 1.5 mm (T6, T15, T7 respectively) while other conditions remained constant. Visual observation under the SEM found that there was no marked increase in spray-dried microsphere diameter with increasing jet size (Figure 3.24). Experiments also revealed that the 1.5 mm jet is not suitable as wet products accumulated in the main chamber; the 0.5 mm jet produced good spray but it got blocked easily; the 1.0 mm jet produced good spray and the best free flowing products without frequent nozzle blockages. Therefore it was concluded that 1.0 mm jet is the most suitable jet size for the 30% w/w β-TCP slurry.

Slurries of 10% w/w β-TCP were also spray-dried using 0.5 mm and 1.0 mm jet (T11 and T16 respectively). The 0.5 mm jet was found to produce good spray but the 1.0 mm jet produced wet products at 10% solids content. This indicates that different jet sizes are suitable for slurries with different solids content.

VI) Internal morphology of microspheres

By examining the sectioned open microspheres, it was found that all microspheres produced were porous. These sectioned open samples were also subject to backscattered electron imaging because backscattered electron images are useful for identifying and confirming pores within the microspheres. The regions containing calcium phosphate are presented as bright areas in the image while the pores and the resin are presented as dark areas. The images obtained have excellent contrast and give a good indication of the hollowness of the microspheres. A typical backscattered electron image is shown in Figure 3.25. This is from a sample obtained from T9.

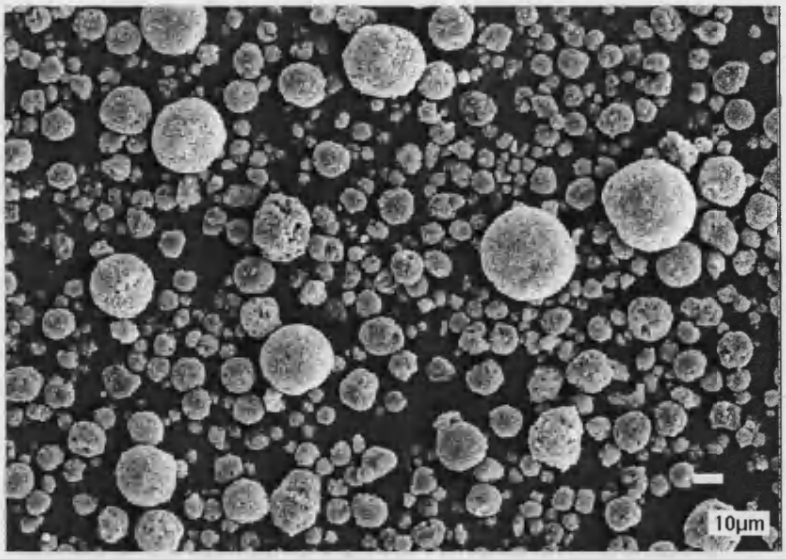

(a) 180°C, T6

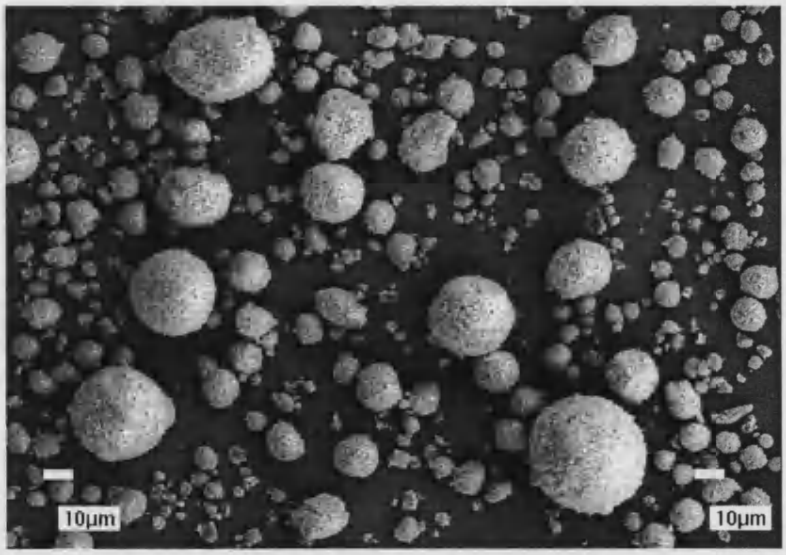

(b) 200°C, T4

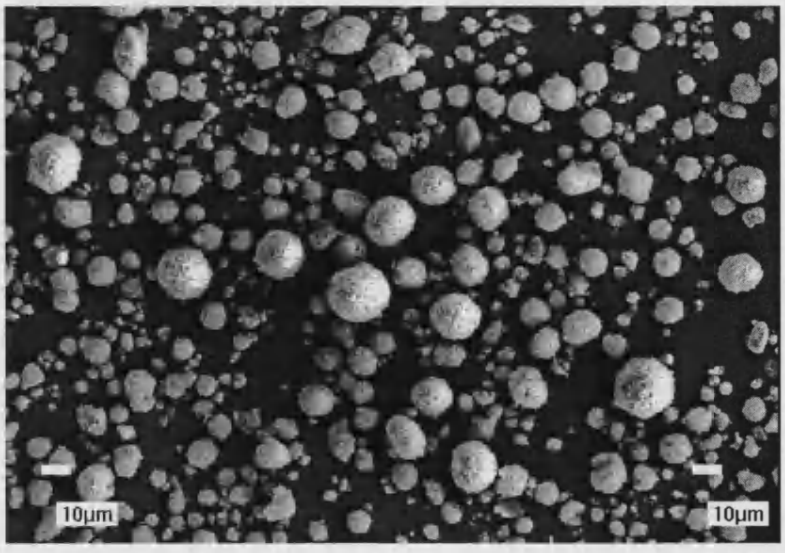

(c) 245°C, T3

Figure 3.20 Spray-dried products from 30% w/w β-TCP slurries spray-dried at (a) 180°C, T6, (b) 200°C, T4, and (c) 245°C, T3.

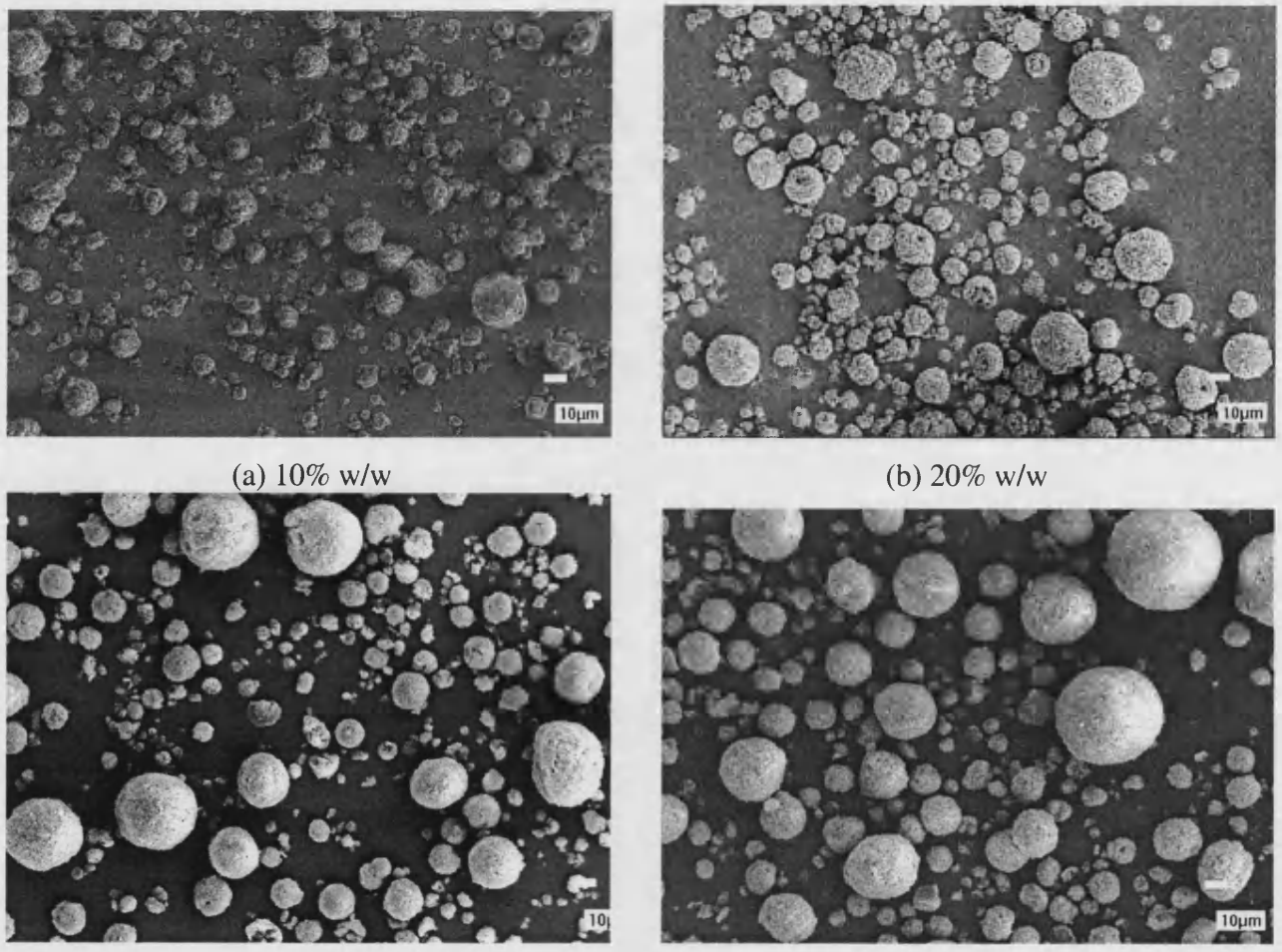

(a) 10% w/w (b) 20% w/w

(c) 30% w/w (d) 40% w/w

Figure 3.21 Spray-dried products obtained from slurries with (a) T10, (b) T9, (c) T6, (d) T18.

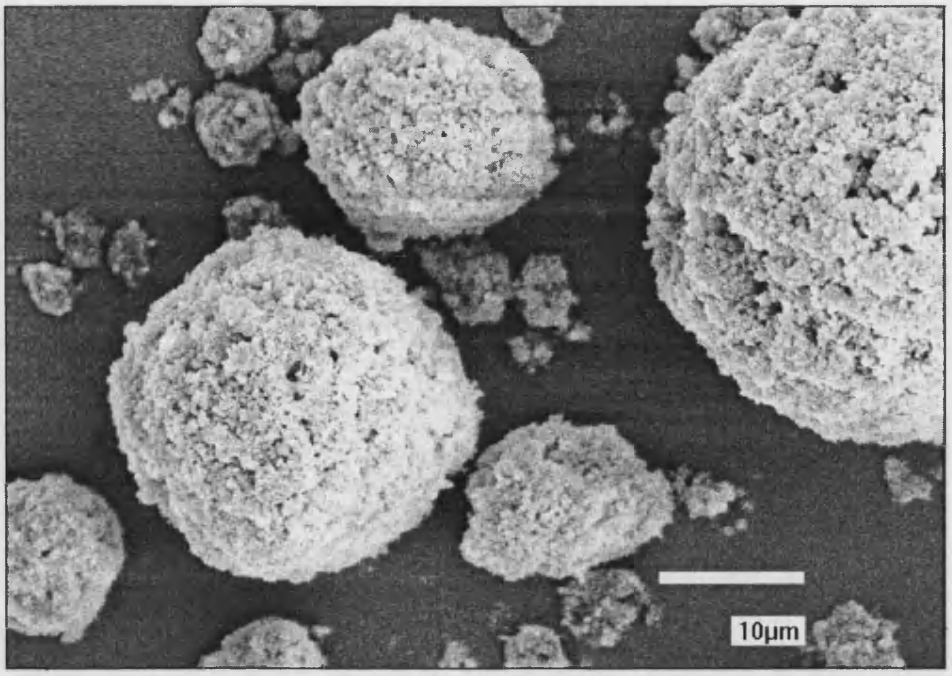

(a) without Dispex A40

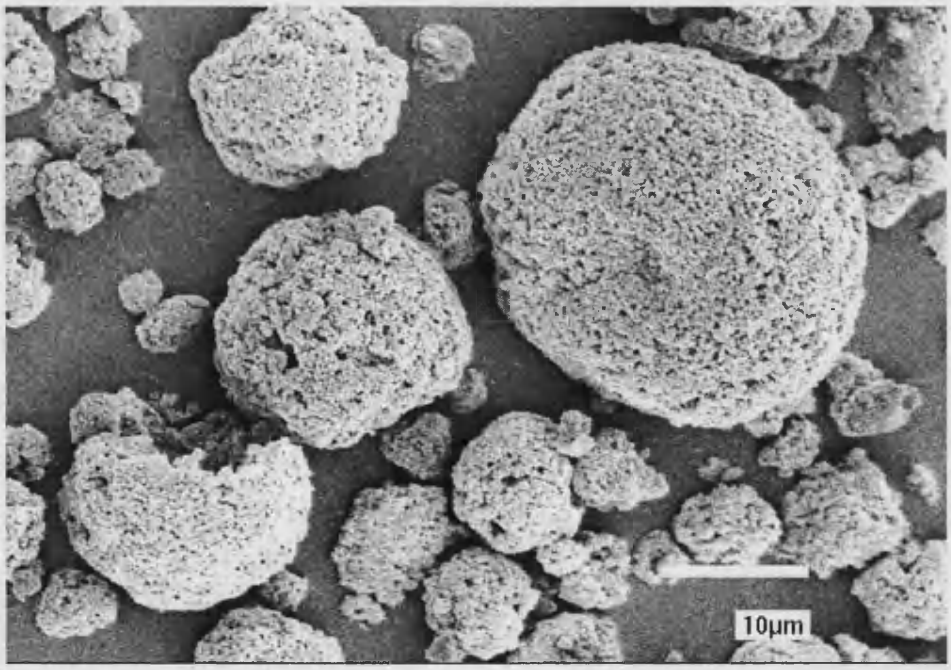

(b) with 2 pph Dispex A40.

Figure 3.22 Spray-dried microspheres obtained from 20% w/w slurry, (a) T8 without Dispex A40, (b) T9 with 2 pph Dispex A40.

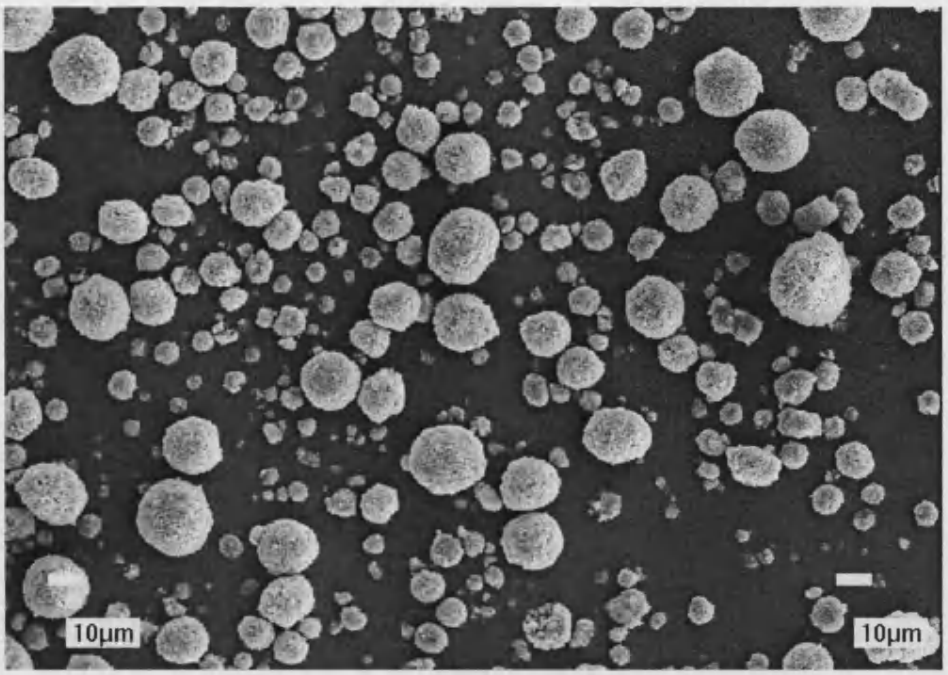

(a) 4 pph binder (T5)

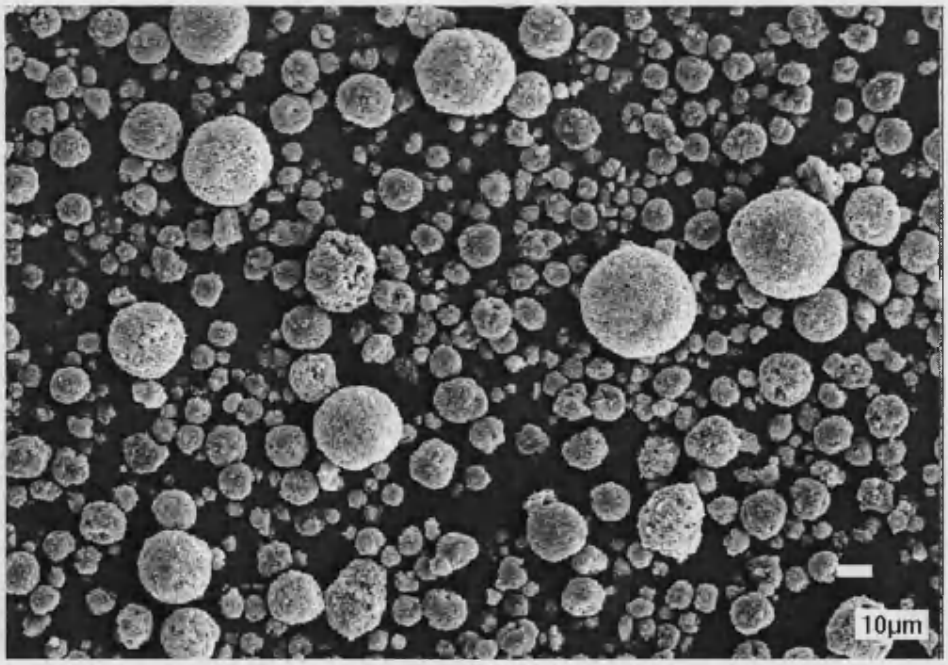

(b) 2 pph binder (T6).

Figure 3.23 SEM micrographs of spray-dried microspheres obtained from slurries with (a) 4 pph, (b) 2 pph binder (Eudragit L100).

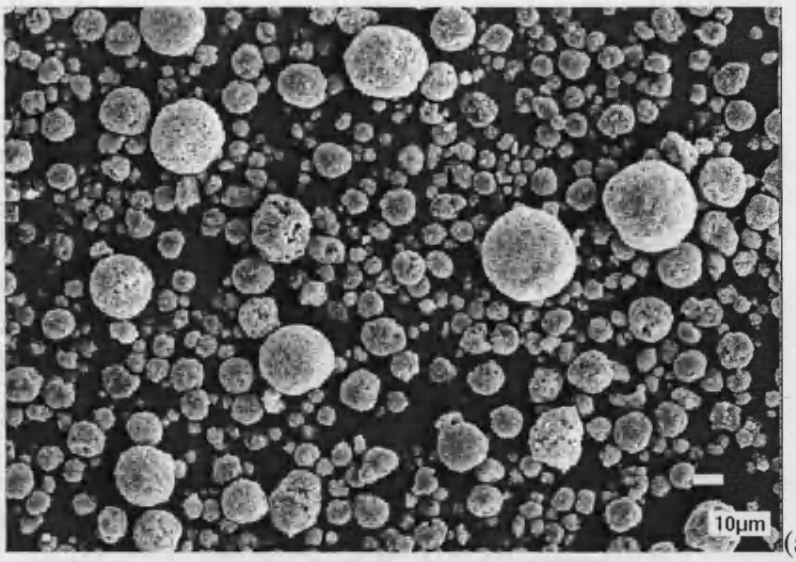

(a) 0.5 mm jet

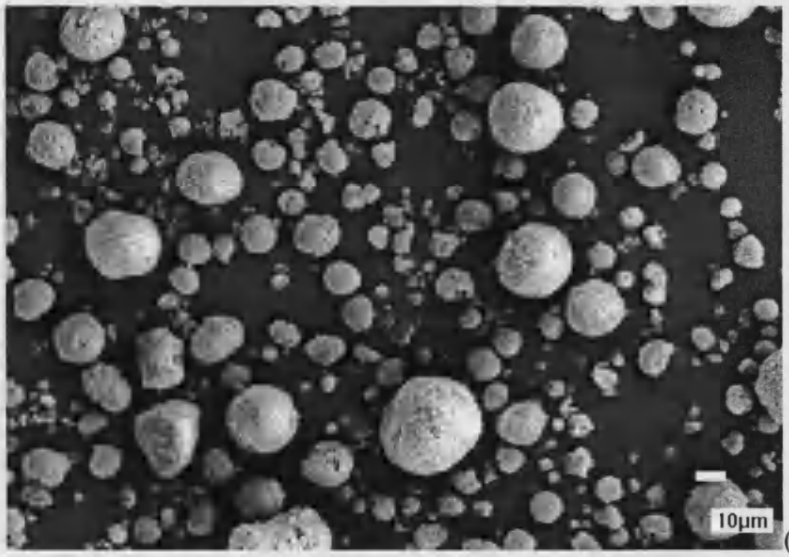

(b) 1.0 mm jet

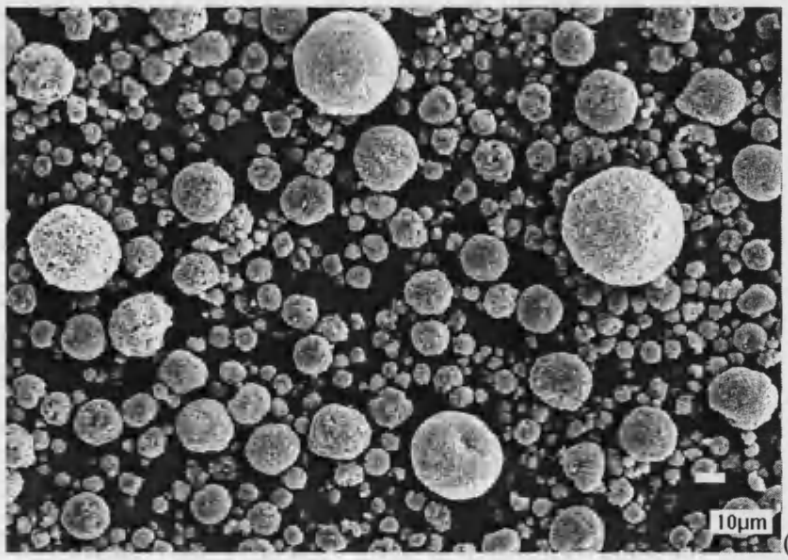

(c) 1.5 mm jet

Figure 3.24 SEM micrographs of spray-dried products from jet of three different sizes (a) 0.5 mm (T6); (b) 1.0 mm (T15); (c) 1.5 mm (T7).

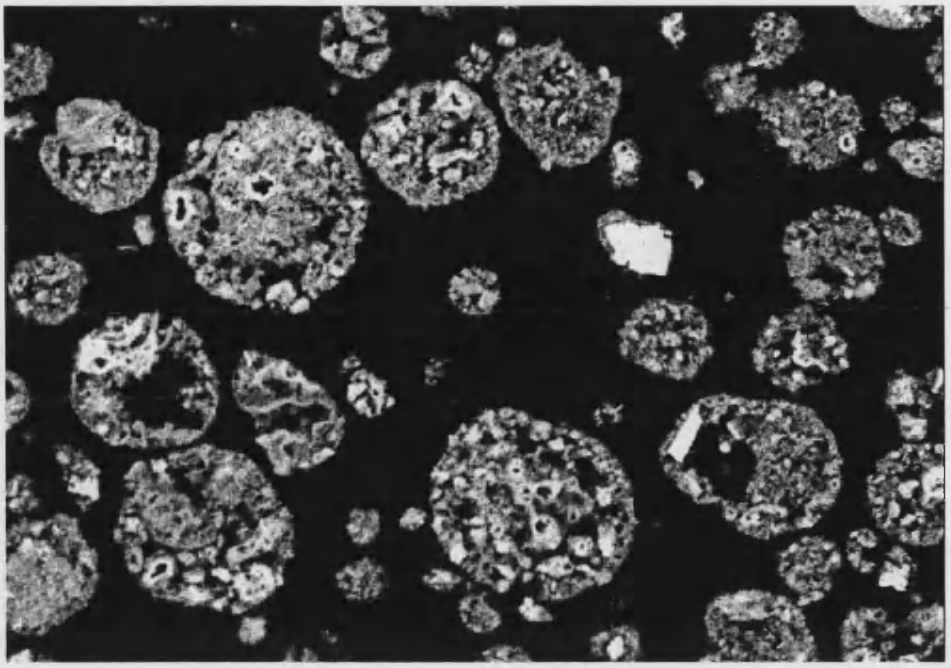

Figure 3.25 Backscattered electron image of sectioned microspheres obtained from T9.

3.7.4 Scale-Up Manufacturing

From Stage 1 and Stage 2 Studies, it was found that Formulation T15 produced the best spray-dried microspheres. Therefore, based on this formula, the production was scaled up to produce larger batches of microspheres (from ~ 200 g to 800 g slurries per batch) to be used in all other following stages of this project.

The composition, method and spray-drying conditions used in the scaling up of microspheres production are described below:

Slurry Composition (T15):

β-TCP	240.0 g	(30% w/w)
Eudragit L100	4.8 g	(2 pph)
Dispex A40	4.8 g	(2 pph)
Aqueous ammonia (2.7M)	~ 28 ml	(to adjust pH to 8.4-8.7)
Purified water to	800.0 g	

Methods:

Eudragit L100 (4.8 g) was first weighed out in a flask. 200ml of deionised water and 10 ml of aqueous ammonia (2.7 M) were then added to the flask. The mixture was sonicated for 6 min with occasional manual stirring until all solids dissolved and the solution was clear. Dispex A40 (4.8 g) was then weighed into a small vial and dissolved in about 5 ml of water before it was transferred to Eudragit L100 solution. β-TCP (240 g) was then weighed into an 800 ml flask and the mixture of Eudragit L100 and Dispex A40 prepared earlier was added to the flask. Water was added to make the weight of the mixture up to about ~775 g. ~ 28 ml of 2.7 M aqueous ammonia were then added to adjust the pH to 8.4-8.7. The pH changes were monitored by pH paper. Finally the slurry was made up to the final weight (800.0 g) with distilled water. The final mixture was sonicated for 8 min.

Spray-drying conditions (SDC) Set 3:

Jet size:	1.0 mm	
Inlet temperature:	180 °C	
Exhaust temperature:	108 - 115 °C	
Pump rate:	350 ml/h	(dryer scale = 10)
Compressor:	150 kPa	(maximum setting)
Air flow:	62 -64 m^3/h	(dryer scale = 41-44, maximum setting)

The connection between main chamber and cyclone was lightly greased before each spraying process to provide a better seal. The SD-05 spray-dryer was allowed to warm up for 5 min followed by spraying of deionised water for 5 min before each turn. Throughout the spray-drying process, the slurry was magnetically stirred. Four batches of microspheres were produced.

3.7.4.1 Percentage Product Yield

To investigate the relationship between percentage product yield and inlet temperature, slurries of T15 were spray-dried at inlet temperatures of 200 °C and 220 °C, with other parameters unchanged. Four batches of product were produced at each temperature.

To investigate the relationship between percentage product yield and solids content, slurries of 10%, 20% and 40% w/w solid content of β-TCP with constant Eudragit L100 and Dispex A40 concentrations were also prepared and spray-dried using SDC Set 3. Two batches of product were obtained for each solids content.

3.7.4.2 Results and Discussion:

All products were free-flowing powders. The percentage product yield of spray-dried products from three inlet temperatures was calculated as follows:

$$\%\ yield = \frac{weight\ of\ product}{weight\ of\ solids\ (TCP + eudragit)\ in\ slurry} * 100 \qquad \text{Equation 3.1}$$

The results of percentage product yield at various inlet temperatures are given in Table 3.6. Less than 100% products were obtained in all cases. The product lost can be explained by particles lost in the exhaust air-flow, and those deposited on the walls of the main chamber and the cyclone. One-way analysis of variance at p = 0.05 level showed that there is no significant difference in the % product yield at the three inlet temperatures investigated [$F(2,9) = 2.99$, $p = 0.101$].

The results of percentage product yield for slurries of various solids content are given in Table 3.7. No statistical analysis was performed for the data because the number of repeat is small (n = 2). The results indicate that among solids content of 10% - 40% w/w, 30% w/w slurry gives the highest yield. The percentage yield increases steadily from 10% to 20%, and to 30% w/w. This is probably because as the solids content increases more complete moisture evaporation is achieved. Therefore less products are lost due to deposition on the walls of the main chamber and the cyclone. The 40% w/w slurry was highly viscous and was difficult to achieve a smooth and uniform spray-drying. Interestingly, the results show that the production yield is markedly lower than the 20 % and 30% w/w slurries.

Table 3.6 Percentage product yield at different inlet temperatures of 180°C, 200 °C and 220 °C.

Solids content = 30% w/w β-TCP, n = 4			
Inlet temperature/°C	180	200	220
Yield ± SD/%	63 ± 4.3	70 ± 4.8	68 ± 2.2

Table 3.7 Percentage product yield for slurries at various solids content.

Inlet temperature = 180 °C, n = 2				
Solid content/% w/w	10	20	30	40
Yield/%	41.6	57.3	66.6	44.2

3.7.5 Particle-Size Analysis

The particle-size of spray-dried β-TCP microspheres was characterised by Mastersizer 2000. The experimental method is described in section 2.3.2.

3.7.5.1 Results and Discussion

The results (Table 3.8) show that slurries with increasing solids content produce microspheres with increasing mean diameter, d(v, 0.5). Slurries of 10%, 20%, 30% and 40% (w/w) produced microspheres with volume mean diameter of 10.0 μm, 10.5 μm, 19.1 μm and 25.5 μm, respectively.

During spray-drying, liquid was dispersed into droplets by pressurised gas. In general, the droplet size D can be expressed by an empirical equation[53] as below:

$$D \propto P^{-n} M^{q} \eta^{r} \sigma^{s} \rho^{t} \qquad \text{Equation 3.2}$$

where P = atomisation pressure

M = Liquid flow rate

η = Viscosity of slurry

σ = Surface tension of slurry

ρ = Concentration of slurry

n, q, r, s and t = constants, values depend upon operating conditions[53,95].

Assuming that the spray-dried microspheres size is proportional to the droplet size (other spray-drying conditions remaining constant), an increase in slurry concentration is predicted to increase the size of the microspheres.

Table 3.8 Particle-size analysis results for microspheres obtained by spray-drying β-TCP slurries of various solids content.

Solids content /% w/w	d(v, 0.1)/μm			d(v, 0.5)/μm				d(v, 0.9)/μm		
	Run 1	Run 2	Run 3	Run 1	Run 2	Run 3	Mean	Run 1	Run 2	Run 3
10	3.26	3.28	3.30	10.03	10.04	10.06	10.05	22.21	22.16	22.18
20	3.30	3.32	3.37	10.45	10.46	10.47	10.46	24.62	24.60	24.54
30	4.38	4.39	4.42	19.21	19.06	19.08	19.12	53.16	52.45	53.01
40	5.56	5.53	5.56	25.59	25.39	25.43	25.47	67.11	65.67	66.09

3.7.6 Sieving

The products of spray-dried calcium phosphate slurries are spherical soft agglomerates with a size distribution as shown in Table 3.8. Spray-dried powders are never of one size because the atomiser cannot form a totally homogeneous spray[95]. The droplets are also subjected to shape distortion depending on their drying characteristics and their travelling mode in the dryer. One of the methods to reduce the size distribution of spray-dried products is sieving.

Attempts were made to discard the fines of the spray-dried products, *i.e.*, only retain the coarse microspheres for the sintering and the drug loading studies. Products obtained from T6 were sieved through stacks of 45 μm and 32 μm stainless steel sieves. A sieve shaker (Endecotts Octagon Digital Test Sieve Shaker, Endecotts Ltd., London, UK) was used and the sieving process was performed at amplitude of 5 for 15 min, followed by amplitude of 6 for 15 min. About 6 g - 8 g of powder was sieved per batch. The particle-size of the microspheres before and after sieving (the fraction retained by the 32 μm sieve) was analysed using the Mastersizer 2000 and examined under the SEM.

3.7.6.1 Results and Discussion

The results of particle-size analysis (Table 3.9) show that the sieved products have a slightly higher mean particle-size, d(v, 0.5), but the particle-size distribution range remains similar. SEM examination confirmed that there were still a lot of fines in the sieved powder.

Table 3.9 Particle-size analysis for β-TCP microspheres before and after sieving.

	d(v, 0.1)/μm			d(v, 0.5)/μm			d(v, 0.9)/μm		
Sieving	Run 1	Run 2	Run 3	Run 1	Run 2	Run 3	Run 1	Run 2	Run 3
Before	4.38	4.39	4.42	19.21	19.06	19.08	53.16	52.45	53.01
After	4.84	4.86	4.88	23.25	23.24	23.19	55.86	56.04	55.80

The reasons that render the sieving process ineffective could be:

1. Too much sample was sieved at once.
2. The sieving time was too short.
3. Most microspheres are < 10 μm. For particles of these sizes, the electrostatic charge can be more dominant than gravity. The electrostatic forces between particle-particle and/or particle-sieve are relatively strong.
4. The microspheres broke up during the sieving process.
5. A combination of the factors above.

Possible ways of improving the sieving process include:

1. Using less powder sample in each sieving session.
2. Perform sieving for a longer period of time.
3. Re-sieving and cleaning the sieving surfaces more frequently.
4. Changing the humidity of the sieving environment. Lowering the humidity may decrease the clinging of the powder to the sieve[96].
5. Include the use a Sonic Sifter device, which can help to push the powder through the mesh.

Sieving of fine particles has been well studied[97]. Getting the right sieving conditions and equipment can be a complicated process. Furthermore, to obtain enough sieved samples to be used in sintering the drug loading studies could be a time consuming

process. Due to time and equipment constraints, the sieving experiments were not investigated further.

3.8 Dispersant

3.8.1 Background

The physical properties of a well-formulated suspension for spray-drying are:

a) The suspension must remain homogeneous for at least the period between the moment it leaves the feed container, and the moment it reaches the atomiser.
b) If sediment is produced on standing, it must be easily resuspended by the use of moderate mixing action, *e.g.* stirring mechanism.
c) The viscosity of the suspension may be increased to reduce the rate of settling of the particles. However, the viscosity must not be so high that the product is not pumpable.

Recent studies have shown that the level of flocculation/dispersion of the precursor ceramic slurries, considerably affects the structure of the spray-dried particles. Walker *et al.*[55] reported that denser alumina spray-dried particles were produced at higher deflocculant levels. Takahashi *et al.*[98] showed that changing the pH of the silicon nitride slurries changed their flocculation state. Using well-dispersed slurries, dense and hard granules with irregular shape were produced, whilst using flocculated slurries, lower density granules with well-formed spherical shape were produced.

Flocculation studies were performed, with the aim of investigating the influence of Dispex A40 and of the pH changes on the suspension stability of DCPA and β-TCP slurries. Changes in pH were considered because the performance of Dispex A40, an anionic dispersant, is pH-dependent[99].

In pharmaceutical suspension formulation, highly flocculated suspensions are generally desirable. This is because flocculated systems form loose sediments which are easily redispersed when shaken (*e.g.* when a patient shakes a syrup bottle). In contrast to this, deflocculated systems are required in ceramic slurry preparations, since deflocculated powders settle down more slowly, and are therefore considered a more stable.

The stability of ceramic suspensions can be explained by considering the DLVO theory of colloid stability[100]. DLVO theory has a quantitative approach towards the stability of colloidal systems. It assumes that the only interactions between two particles involved are electrical repulsion (V_R) and v*an der Waals* attraction (V_A), and that these parameters are additive. As a result, the total potential energy of interaction V_T is given by $V_T = V_A + V_R$ (see schematic in Figure 3.26)

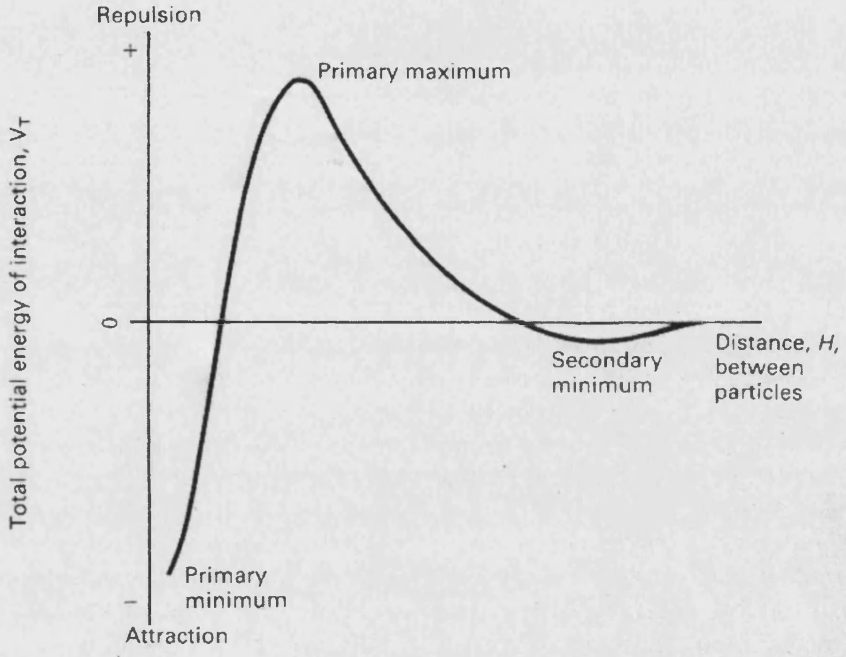

Figure 3.26 Schematic curve of total potential energy of interaction V_T, versus distance of separation, H, for two particles. $V_T = V_R + V_A$ (taken from Aulton[101]).

As two particles approach each other, they initially encounter a weak attractive force, represented by the secondary minimum in the curve. As the two particles move closer to each other, the repulsive electrical force increases exponentially, and the particles strongly repel each other, by means of the electric charges on their surfaces. If the energy supply is enough, and the primary maximum repulsive force is overcome, the two particles collapse into each other.

In a suspension, particles > 1 μm tend to settle due to gravity. The electrical repulsive forces between the particles enable them to slip past one another to form a close packed

arrangement at the bottom of the container, with the small particles filling the voids between the larger ones. Those particles lowermost in the sediment are gradually pressed together by the weight of the ones above. When the repulsive force (represented by primary maximum in Figure 3.26) between the two particles is overcome, the particles move into close contact with each other and physical bonding, leading to 'cake' formation, may then occur. Hence, more energy is required to redisperse the sediment.

In short, when V_T gives a positive potential energy maximum at intermediate particle separation distances, the result is a deflocculated system and when the V_T gives a negative value, the result is a flocculated system. Since V_A is fixed for any given suspension, the shape of the total interaction curve is determined by V_R. The stability of the system is therefore a function of those parameters that control V_R - the particle surface charge and the double-layer thickness.

The surface charge on a particle can be developed through adsorption of charged chemical species (*i.e.*, dispersants) or by adjustment of the solution pH. It is also possible to deflocculate ceramic powders by steric effect, where the spatial arrangement of large adsorbed molecules prevents close particle-particle encounters. Gum arabic, is believed to deflocculate particles by this steric mechanism[102].

The surface charge of a particle also builds up an electric double-layer around itself[100], as shown in Figure 3.27. Consider a solid charged surface in contact with an aqueous solution containing positive and negative ions. The surface charge influences the distribution of ions in the aqueous medium. Counter-ions (ions of the opposite charge) are attracted towards the surface, partially neutralising the charge and co-ions (ions of like charge) are repelled away from the surface. A second layer of co-ions will surround this first layer of counter-ions in a diffuse manner in the aqueous medium. This diffuse layer further neutralise the charges, as the system must be electrically neutral.

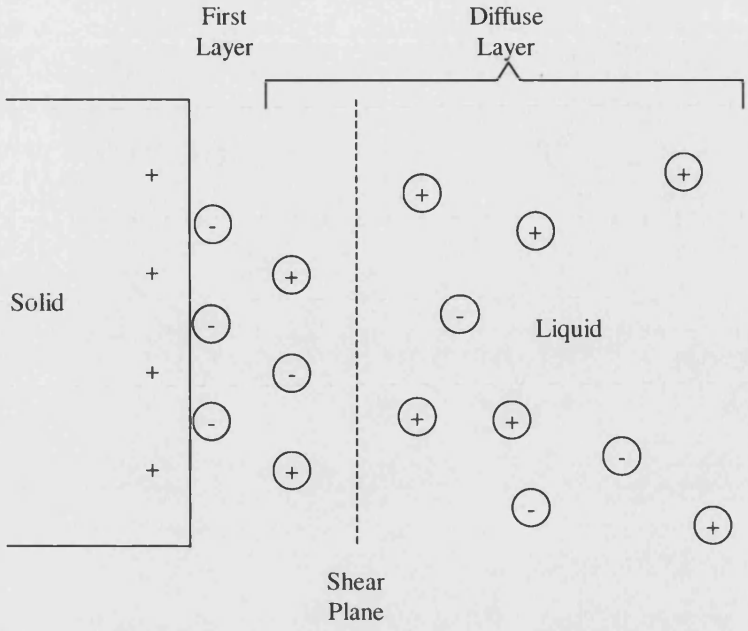

Figure 3.27 The double layer (adapted from Shanefield[100])

3.8.2 Dispex A40

Dispex A40 is a commercial polyelectrolyte that is commonly used in the ceramic industry to produce ceramic suspensions (see also section 3.5.8). Greenwood *et al.*[99] have characterised Dispex A40 and suggest that it is an ammonia-neutralised polyacrylic acid with a molecular weight, M_w, of ~ 10 000 Da and a polydispersity of M_w/M_n, of 1.56. The structure of Dispex A40 is shown in Figure 3.28.

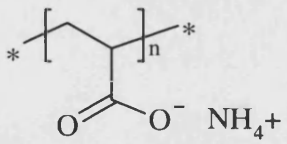

Figure 3.28 Molecular structure of Dispex A40[99].

Polyacrylic acids contain ionisable carboxylic groups, so the degree of ionisation changes with pH and ionic strength. For Dispex A40, the negative charge density increases with increasing pH. The ionisation properties of polyacrylic acids have been studied, and previous work has shown that they are completely ionised at pH > 8[103,99]. Therefore at pH 8 - 9, it is considered that Dispex A40 is fully ionised.

Greenwood and Bergstrom[99] suggest that a fully ionised Dispex A40 will attain a relatively rigid, extended conformation in solution, and usually adsorb flat on a surface with essentially no parts of the polyelectrolyte extending into the solution. This is based on their findings that the plateau value of the adsorption isotherm of Dispex A40 on Ce-ZrO, which corresponds to the area per ionised acrylic acid monomer, was found to be ~ 70 $Å^2$ (0.22 mg Dispex A40 per m^2 powder area). This value corresponds well to the estimations of the cross-sectional area of the acrylic acid monomer, therefore, indicating that Dispex adsorbs in a flat conformation on the powder surface.

The monolayer of ionised Dispex A40 molecules covering the ceramic particles make the particles highly negatively charged (high zeta potential). The double layer electrostatic effect mutually repels the particles, and prevents the particles from flocculating, therefore maintaining a stable colloid and a well dispersed suspension.

3.8.3 Tests for Effectiveness

The effectiveness of the dispersion can be determined by height of sediment and viscosity[92] as explained below:

1) Height of Sediment

If a ceramic powder with a particle-size range of 1 μm - 5 μm is well dispersed in a liquid, *i.e.* a deflocculated system, and then left to settle, after a few hours the particles will form a compact (cake) at the bottom of the container. This is because the liquid lubricates the particles as they fall by gravity, allowing them to pack effectively[63], as explained before (section 3.8.1). The more effective the lubrication is, the better the falling particles arrange themselves to fill in pores close to their sizes, and therefore a better packing results.

In contrast, if a powder is poorly dispersed, *i.e.* a flocculated system, loose sediment with higher volume will be formed. In cases where the powder is highly flocculated and is present in high quantity, the floc can fill the whole container and there might be no visible settling at all[63]. Therefore, the height of the sediment can be used as a quantitative measure of dispersion effectiveness[104;105].

2) Viscosity

Another measure of dispersion effectiveness is the viscosity of the slurry, where the lower the viscosity, the better the dispersion achieved. It is commonly found that the minimum viscosity is achieved when there is approximately a monolayer of dispersant adsorbed on the powder surface[99]. This is often at about 1 g of dispersant in 100 g of ceramic powder[63]. As would be expected, the exact amount of dispersant required to achieve minimum viscosity depends on many variables, including the density of the powder; its specific surface area; and the size of the dispersant's molecule. Typical values found to provide minimum viscosities for 0.5 μm ceramic powders are ~ 0.8% - 1.7% dispersant[106,107].

3.8.4 Experimenting Method

The effect of Dispex A40 with and without pH adjustment, on DCPA and β-TCP slurries was studied. The pH of the ceramic powders before pH adjustment was found to be ~5 - 6 (determined by pH paper). Aqueous ammonia was used to adjust the pH.

Slurries of 30% w/w ceramic powder (DCPA or β-TCP) and Dispex A40 (1, 2, 3 or 5 pph), with or without aqueous ammonia, were prepared as follows: 3 g of ceramic powder were weighed into a 15 ml conical tube (Falcon Blue Max™ Jr. Polypropylene Conical tube, 17 x 120 mm, Becton Dickinson Labware Europe, Meylan Cedex, France). The Dispex A40 (30 mg, 60 mg, 90 mg or 150 mg) was weighed into a vial, dissolved in 7 g of purified water, and this solution was then transferred to the conical tube. In some tubes, aqueous ammonia (using a pipette, ~ 6 drops for DCPA and 27 drops for β-TCP) was then added to adjust the pH to ~ 8.4. The slurries were then vigorously manually shaken and a rough comparison of viscosity was carried out by tipping the tubes upside down to observe the flow of the slurries. The height of the sediments and the redispersability of the systems were examined after allowing the slurries to settle for 2 days. The redispersability was assessed by counting the number of times needed by turning the tubes upside down (manually) for the powder to be resuspended. These results are then transformed into the easiness of redispersability in a scale of 1 to 5. Scale 1 corresponds to the slurry is easily redispersed while scale 5 corresponds to the slurry is difficult to be redispersed.

3.8.5 Results and Discussion

The results obtained for DCPA and β-TCP slurries are shown in Table 3.10 and Table 3.11 respectively. It was observed that the ratio of sediment height to suspension height (S/S_0) for all sediments was reduced by the addition of Dispex A40. This indicates that Dispex is an effective dispersant.

In the case of the DCPA slurries tested, the addition of Dispex produced a reduction in S/S_0 from 0.39 to 0.23 or 0.24. This indicates that better dispersed systems were created with the addition of dispersant. However, increases in the amount of the Dispex A40 added from 0 pph - 5 pph had no obvious effect on the height of sediment. The addition of ammonia also had no marked effect on the height of sediment.

In the case of the β-TCP powder, the effect of Dispex A40 on the S/S_0 is dependent on the amount of Dispex A40 added. The S/S_0 decreases from 0.97 to 0.84 when the Dispex A40 concentration increases from 0 pph to 3 pph; and the S/S_0 then increases to 0.99 when the Dispex A40 concentration increases to 5 pph. Also, the addition of ammonia has a marked effect on the S/S_0. When comparing systems with equal amounts of Dispex A40, the addition of aqueous ammonia further reduces the S/S_0 values. For example, with 2 pph Dispex A40, the S/S_0 values decreases from 0.91 to 0.82 with the addition of aqueous ammonia. This indicates that Dispex works better in the alkaline pH region. It was observed that the viscosity of the slurries was markedly reduced by the addition of Dispex.

The two days sedimentation results indicate that 2 pph to 3 pph Dispex A40 with pH adjustment produce the best dispersed β-TCP slurry. β-TCP systems with 5 pph Dispex A40 were found to increase the S/S_0, which in the first instant may indicate the forming of agglomerates. However, the S/S_0 values for β-TCP systems with 5 pph Dispex A40 were found to decrease to 0.83 and 0.63 (values are not shown in table), for system without and system with ammonia respectively, after allowing them to settle for two months. This indicates that the extra charges contributed by the high concentration of dispersant prevent the collision of the particles and hold the particles in the solution for a longer period of time, thus delaying the settlement of particles.

Table 3.10 The results of dispersant effectiveness tests for 30% w/w DCPA after settling for 2 days

Dispex A40 (pph)	-	1	2	3	5	1	2	3	5
Ammonia (aq)	-	-	-	-	-	Yes	Yes	Yes	Yes
Viscosity	+	++	++	++	++	++	++	++	++
*S/S_0	0.39	0.24	0.23	0.23	0.23	0.24	0.23	0.23	0.23
The number of times turning the tube upside down to redisperse	3	22	34	30	32	31	30	37	39
Redispersability (1= easy,5= hard)	1	3	4	4	4	4	4	4	4

Table 3.11 The results of dispersant effectiveness tests for 30% w/w β-TCP after settling for 2 days

DispexA40 (pph)	-	1	2	3	5	1	2	3	5
Ammonia (aq)	-	-	-	-	-	Yes	Yes	Yes	Yes
Viscosity	+++++	++++	++	+	+	+	+	+	+
*S/S_0	0.97	0.97	0.91	0.84	0.99	0.87	0.82	0.77	0.98
The number of times turning the tube upside down to redisperse	paste, no sediment	3	3	3	61	3	3	3	36
Redispersability (1= easy,5= hard)	-	2	1	1	5	1	1	1	4

*S/S_0 = Sediment height/Suspension height

3.9 General Discussion

The slurry composition and the spray-drying conditions suitable for producing porous microspheres of DCPA and β-TCP was investigated. It was found that under the appropriate conditions, free flowing calcium phosphate microspheres can be produced in batches of ~ 500 mg (60-70 % yield for 800 mg slurry). The average microspheres produced were ~ 10 μm - 20 μm in diameter. These are loosely bound soft agglomerate of calcium phosphates.

This study shows that for producing spray-dried calcium phosphate microspheres, a binder, a dispersant, and high solids content are needed in the slurry.

A binder is necessary for the agglomeration of ceramic powder to form microspheres. Without a binder, there are not adhesive forces to bind the ceramic powder together, and microspheres are not formed. The choice of a binder was found to be crucial as it may make the difference between obtaining free-flowing products or wet and sticky gums. Eudragit L100 was found to be a good binder in this study.

To produce good spray-dried products, the powders must be homogenously dispersed. To produce stable and homogeneous calcium phosphate slurries, it was found that high solids content and dispersant are required. A high solids content is desirable because it increases the viscosity of the slurry, which assists in suspending the powder in the liquid. However, high solids content normally results in highly viscous ceramic pastes not feasible for spray-drying. A dispersant can be used to reduce the slurry viscosity. Dispex A40 was found to be a suitable dispersant for calcium phosphate slurries. Particle-size of the ceramic powder also affects the dispersity of the slurry as large particles encourage rapid sedimentation. Ball-milling was found to effectively reduce the particle-size of DCPA and also help in mixing in all the excipients. β-TCP was found to produce good slurries and no extra step of particle-size reduction was necessary.

DCPA slurries with solids content of 30% - 60% w/w and β-TCP slurries with solids content of 10% - 40% w/w were successfully spray-dried. Higher solids content was found to produce microspheres of bigger size.

The solids content, the binder concentration and the dispersant concentration were all found to affect the spray-dried products. Generally, the results show that smaller microspheres were produced with higher concentration of dispersant.

The influence of spray-drying conditions on the spray-dried products, including the temperature and the jet size, were also investigated. Inlet temperature of ~ 180°C - 220°C was found to be optimum. At these temperatures, hollow centred microspheres were produced. Higher inlet temperature (245°C) was found to produce solid centred microspheres and the frequency of nozzle blockage increased. When the inlet temperature is too low, there is not enough energy for complete moisture evaporation and free-flowing products to be obtained.

Among the jet size of 0.5 mm, 1.0 mm and 1.5 mm, the jet size of 1.0 mm was found to produce the best quality microspheres in this study.

The surface morphology of the microspheres was examined under the SEM. The internal morphology of these microspheres was also studied by examining the sectioned open microspheres. Results showed that highly porous microspheres were obtained.

4 Sintering of Calcium Phosphate Microspheres and Their Characterisation

4.1 Introduction

To modify the porosity and the pore-size of spray-dried calcium phosphates microspheres, the microspheres were subjected to sintering. Sintering is a standard ceramic processing technique. It is a thermal treatment where the ceramic is heated to a high enough temperature, near to its melting point, to bond the particles together by a diffusion controlled mechanism.

Individual researchers have studied the sintering effect of some calcium phosphate compositions, mainly hydroxyapatite. Zakaria[36] studied the microstructural properties changes of porous hydroxyapatite sintered between 1100 °C - 1400 °C and found that the sintering atmosphere (argon or air), temperature and holding time all affect the microstructure (grain size, density, porosity) of the final sintered product. He observed the presence of traces of β-TCP when hydroxyapatite was sintered at temperatures 900 °C and higher, and at > 1300 °C the traces of β-TCP disappeared, but a further decomposition to α-tricalcium phosphate (α-TCP)* and tetracalcium phosphate, $Ca_4P_2O_9$, was found. Tas[108] characterised calcium phosphate compositions (Ca/P ratio = 1.70) heated at 600 °C - 1150 °C in air. It was found that the initial formation of hydroxyapatite happened at 800 °C and 1000 °C, and the powders heated at 1150 °C consisted of single-phase hydroxyapatite.

In this study, dilatometry was used to ascertain the thermal expansion and shrinkage of the DCPA and β-TCP, and their suitable sintering temperatures. Sintering of spray-dried DCPA and β-TCP microspheres was then carried out. The non-sintered and sintered spray-dried DCPA and β-TCP microspheres were characterised and compared. The microstructural changes of the materials as the sintering temperature increases were also studied.

---

* α-TCP is a polymorph of β-TCP.

It is important to include a representative sample in the analysis in powder characterisation. Random sampling and statistical analysis were applied, wherever possible, to improve sampling accuracy in this study.

4.2 Dilatometry

To investigate the thermal expansion and shrinkage of DCPA and β-TCP samples, and to identify the temperature required for sintering, a dilatometer (Netzsch Thermal Analysis, Bavaria, Germany) was used. This apparatus consists of a horizontal tube furnace, a molybdenum coil heating element, a water cooling system, and an alumina rod. It can accurately measure the relative change in sample length during the heating and cooling process, involving temperatures of up to 1550 °C. The apparatus was connected to a computer where the displacement information of the samples was recorded.

A rod of DCPA compact and a rod of β-TCP compact, ~14 mm long × 10 mm wide each, were prepared as follows: Firstly, the powder was fed into a 13 mm hardened steel die and pre-pressed uniaxially with a punch, to a pressure of 1 MPa for 30 s, before it was released. Secondly, the pre-pressed samples were placed inside a colostomy tube and vacuum-sealed, before immersing into the oil of the pressure chamber of a cold isostatic pressing apparatus (ISO-LAB, Stansted Fluid Power Ltd., England). A pressure of 150 MPa for 60 s was applied. The pressurised oil transmitted the pressure uniformly to the samples. The sample diameter was later reduced manually using P320 grit SiC paper (Extec Corp., Enfield, CT, USA) to fit into the alumina holder of the dilatometer (~10 mm). In the dilatometer, the samples were heated up at a rate of 3 °C/min up to 1200 °C and then maintained for 1 h at 1200 °C before cooling down.

4.2.1 Results and Discussion

The linear shrinkage and the rate of shrinkage of DCPA and β-TCP compacts are shown in Figure 4.1 and Figure 4.2 respectively. From Figure 4.1, it is shown that the

pattern of expansion and shrinkage of the DCPA and β-TCP compacts from 100 °C to 1200 °C are markedly different. By studying the thermal behaviour of these samples, information on the practical range of sintering temperatures can be obtained. The starting point of shrinkage corresponds to the starting of the sintering process, and the end of shrinkage corresponds to the completion of the sintering process, where densification cannot progress further.

For DCPA, an initial expansion was observed when the temperature increased from room temperature to ~ 240 °C. This expansion was considered to be the result of thermal expansion. A sharp shrinkage occurred ~ 995 °C and continued up to ~ 1070 °C. It can also be clearly distinguished in Figure 4.2 that there was a sudden and sharp increase in the rate of shrinkage at ~ 995 °C. The maximum overall shrinkage was ~ 7%. From ~ 1110 °C upwards, sample expansion was observed. This is probably because the sintering process has been completed and the material expanded due to increase in temperature. This dilatometry result indicates that densification of the DCPA particles take place at ~ 995 ° - 1070 °C, and sintering is most efficient at 1038 °C.

For β-TCP, initial thermal expansion was not obvious. The gradual shrinkage started at ~ 600 °C and the rate of shrinkage reached a second maximum at ~ 970 °C. A further sharper increase in the rate shrinkage was observed from ~ 1050 °C onwards. The overall shrinkage at 1200 °C from the starting dimension was ~ 19%, which is about 3 times more than the maximum shrinkage observed in DCPA.

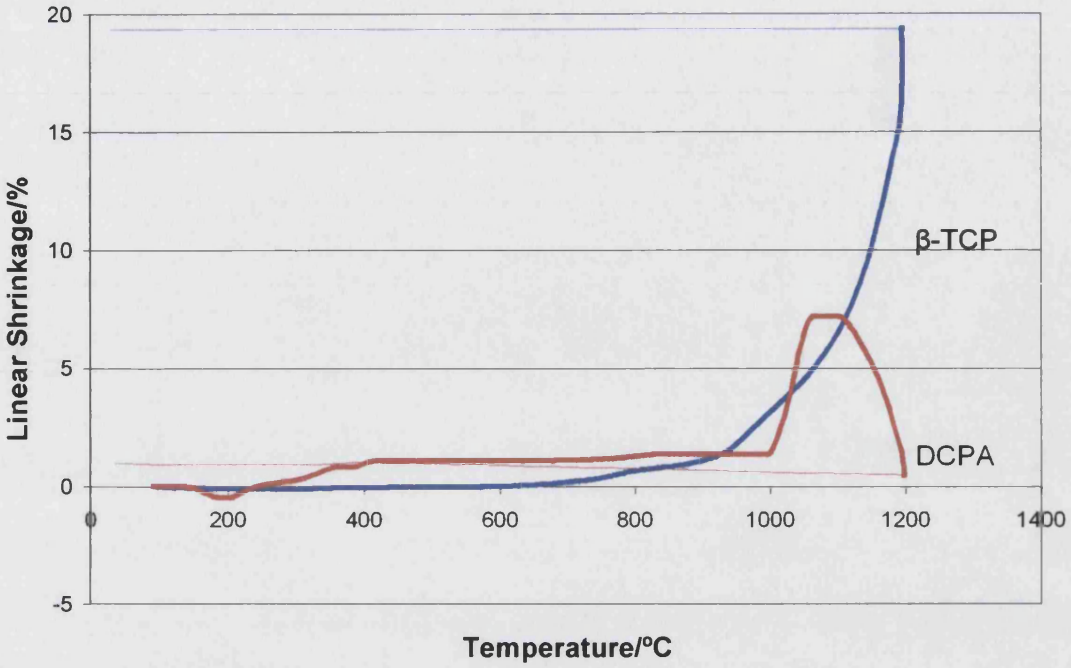

Figure 4.1 Linear shrinkage plot of DCPA and β-TCP compact heated at 3°C/min

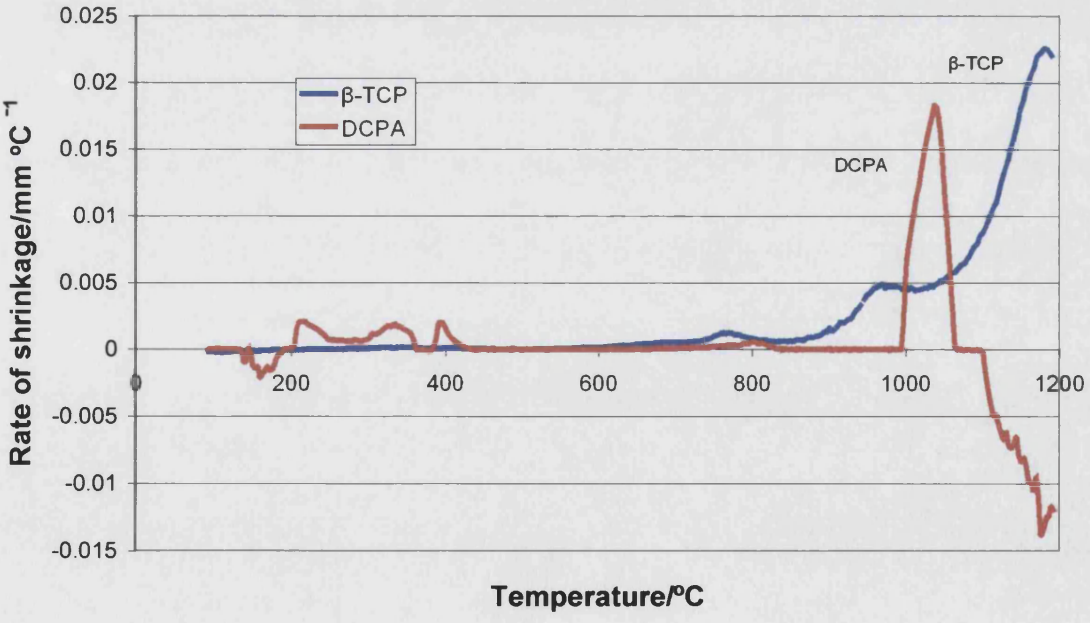

Figure 4.2 Rate of shrinkage for DCPA and β-TCP compact vs. temperature.

4.3 Sintering

In this study, a Carbolite electric chamber furnace (Type CWF 13/13, Carbolite, Sheffield, UK) was used for sintering the samples. The spray-dried microspheres were placed in a non-reactive zirconia crucible and sintered in a stagnant air atmosphere in two stages (Figure 4.3). In the first stage, the samples were heated at a rate of 100 °C/h from room temperature to 350 °C with a holding time of 1 h. Holding time refers to the period of time the sample is maintained at the same temperature. This was designed to allow the additives (binders and dispersant that were introduced during spray-drying slurry preparation) to 'burn-out' completely before the shrinkage takes place. This stage is also useful from a pharmaceutical viewpoint, because all organic additives, which are added in the slurry processing, but that are not desired in the final product, can be effectively removed to obtain a purer product. The second stage was to sinter the sample. The heating rate was increased to 300°C/h until it reached the final sintering temperature, from 900 °C – 1300 °C, with a holding time of 1 h. The sintered samples were cooled down to room temperature before characterisation.

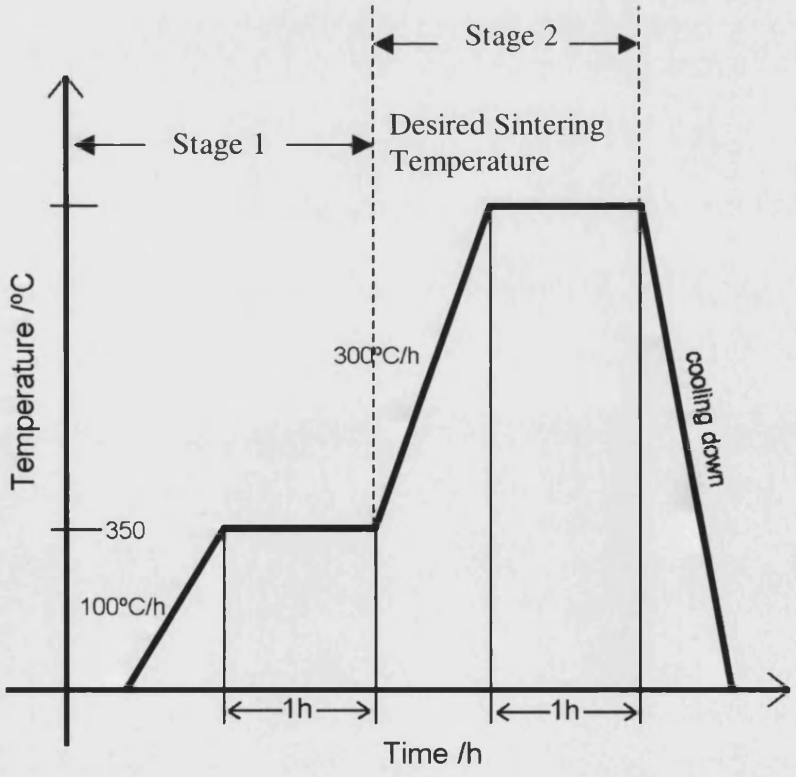

Figure 4.3 Heating stages during sintering

4.3.1 Weight Loss During Sintering

The sample and the zirconia crucible were weighed before and after sintering. The weight loss of β-TCP microspheres during sintering was calculated as follows:

$$\%\ weight\ loss = \left(\frac{B-A}{W}\right) \times 100\%$$

B = Weight of sample and crucible before sintering

A = Weight of sample and crucible after sintering

W = Weight of sample before sintering

The percentage weight loss of spray-dried β-TCP microspheres during sintering is shown in Table 4.1. The results show that there is a generally weight loss of ~ 7%. The weight loss includes the loss of adsorbed/absorbed moisture and the burnout of organic additives, binder and dispersant.

Table 4.1 Percentage weight loss of spray-dried β-TCP microspheres during sintering.

Sintering temperature	% Weight loss ± SD (n = 3)
900 °C	6.86 ± 0.13
1000°C	6.96 ± 0.23
1100 °C	7.17 ± 0.34
1150 °C	6.96 ± 0.73
1200 °C	7.43 ± 0.11

4.4 Powder Characterisation

The spray-dried β-TCP and DCPA microspheres, sintered at temperatures of 900 °C - 1300 °C, were characterised by the following methods: visual observation; SEM; tap density and true density measurements; surface area analysis; mercury intrusion porosimetry; and X-ray diffraction (XRD) analysis.

Sintered samples, especially those sintered above 1100°C were loosely bound powder blocks. These powder blocks were loosened up manually by means of a spatula, or by lightly grounding in an agate mortar with pestle, when necessary for analysis.

4.4.1 Visual Observations

The samples before and after sintering were observed visually. The shrinkage of powder beds from sintering crucible, and the easiness of breaking up the sintered sample blocks into fine powder were noted.

4.4.1.1 Results and Discussion

No colour changes after samples were sintered at all temperatures applied were noticed. Both β-TCP and DCPA microspheres were white before and after sintering.

It was observed that the powder beds shrank after sintering, and the degree of shrinkage increased with increasing sintering temperature. The initially loose powder became more and more compact powder blocks as temperature increased. At 1300 °C, the microspheres were effectively sintered ceramic blocks in the form of consolidated microspheres. It was found that the higher the sintering temperature, the more difficult it was to section the samples for internal morphology examination, due to the increased hardness of the samples.

4.4.2 Scanning Electron Microscopy (SEM)

SEM was used to examine the surface morphology and the internal morphology of microspheres sintered at various temperatures.

For surface morphology examination, all samples were pre-sputter coated with gold for 10 min. Sample preparation details are described in section 2.7.4. For internal morphology examination, samples were first embedded in epoxy resin, followed by careful manual sectioning of the sample with glass knives before they were sputter coated. Full sample preparation details are described in section 2.7.5.

Apart from topographic imaging, some samples were also analysed by backscattered imaging (section 2.7.1.) and X-ray analysis (section 2.7.2). Samples for backscattered imaging were carbon coated for 3 min in a carbon coating unit (Pirani Penning, Model

4, Edwards High Vacuum Ltd., Sussex, UK). Backscattered imaging can differentiate elements of high atomic number from elements of low atomic number. Carbon coating was used because carbon has a low atomic number of 6. Compared to gold (atomic number 79), carbon is less likely to interfere with the signal given out by calcium (atomic number 20). Therefore, areas with and without calcium phosphate can be distinguished and therefore the pores within the microspheres can be identified.

4.4.2.1 Results and Discussion

Surface morphology of DCPA microspheres, which are non-sintered, sintered at 900 °C and sintered at 1000 °C for 1 h, are shown in Figure 4.4. It can be seen that after sintering neighbouring particles fused together to form bigger grains. The particles/grain surface become smoother, and larger open pores were found.

The surface morphology of β-TCP microspheres, which are non-sintered and those sintered at selected temperatures between 900 °C and 1300 °C for 1 h, are shown in Figure 4.5. As the sintering temperature increases, marked grain growth of the β-TCP particles are observed. At 900 °C and 1000 °C, particle surface smoothing and the formation of grain boundaries started, followed by neck formation and formation of interconnected open pores. At higher temperature of 1100 °C, more energy is provided, enhancing material diffusion to occur, leading to a considerably increase in grain size. The diffusion process gradually removed smaller pores, leaving the larger pores that cannot be sintered out. Because these microspheres are highly porous, when the material moved and smaller pores disappeared, the larger interconnected pores became wider. Rounding of pores was observed at 1150 °C, followed by continuous shrinkage of open pores from 1200 °C to 1300 °C. Above 1150 °C, interconnected pores diminished gradually and the closed pores intersected grain boundaries. The open pores, which connect the external and internal structures of the microspheres, disappeared progressively as the temperature rose from 1150 °C to 1300 °C. At 1300 °C the material was effectively a fully sintered ceramic.

The sectioned open β-TCP microspheres sintered at 900°C are shown in Figure 4.6. Figure 4.6a shows the internal morphology of 12 microspheres, and Figure 4.6b is a

higher magnification micrograph of 1 of the 12 microspheres. It can be seen that hollow regions exist in the microspheres. These results show that these microspheres are highly porous. To further confirm the hollow nature of the microspheres observed, two additional techniques, X-ray analysis and backscattered imaging, as described below, were used to identify the porous regions of the microspheres. These results confirm the hollow nature of the microspheres.

1) X-Ray Analysis - Dot Map

In theory, X-ray analysis can differentiate areas with high concentration of calcium (microspheres matrix) from areas of low calcium (hollow regions). X-ray analysis using calcium as an indicator was performed and the results are presented in a dot map format (see section 2.7.2 for details) as shown in Figure 4.7. This figure shows the background noise, and compares the X-ray analysis map of the microsphere sample to its topographical image. The result illustrates that the matrix and the pores the microsphere were not distinctive in the X-ray dot map. This might be due to the spatial resolution of secondary electrons being much higher than that of X-rays. As a result, a feature large enough to be seen in the secondary electron image may not be large enough to contain the entire interactive volume from which X-rays emanate. Often, the electron beam penetrates the sample, causing X-rays to emanate from subsurface regions or surrounding regions having compositions different from that at the point of surface incidence[109]. X-rays can penetrate ~1 - 2 μm thickness into the sample, and pick up calcium signals underneath the resin. Hence, areas of calcium phosphate matrix and areas of pores cannot be clearly distinguished. The technique was not used further.

2) Backscattered Electron Imaging

Sectioned β-TCP microspheres sintered at 900 °C were examined under backscattered electron imaging (Figure 4.8). Regions containing calcium phosphate were presented as bright areas, and regions without calcium phosphate were presented as dark areas. The black and white contrast gives a clear indication of the hollowness of the microspheres.

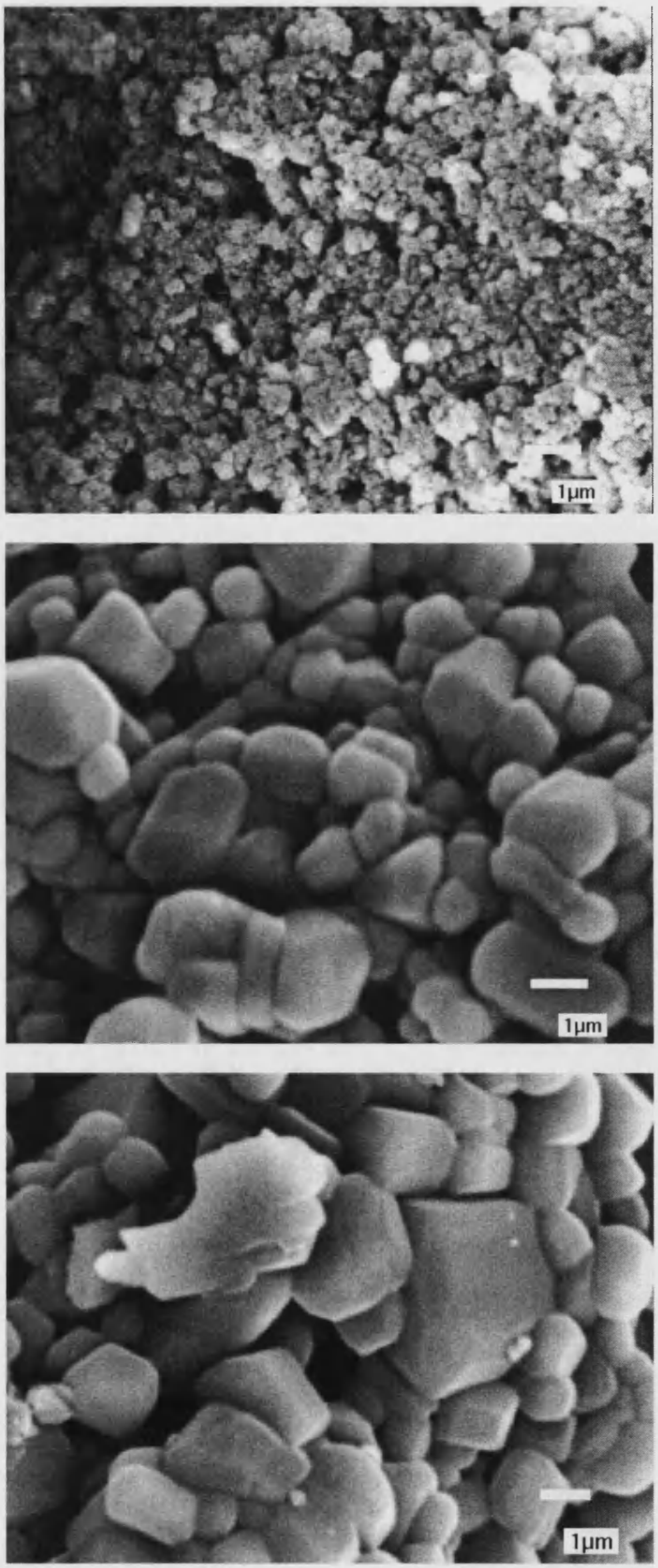

(a)Non-sintered

(b) 900 °C

(c) 1000 °C

Figure 4.4 SEM micrographs of surface morphology of DCPA microspheres (a) non-sintered, (b) sintered at 900 °C, and (c) sintered at 1000 °C.

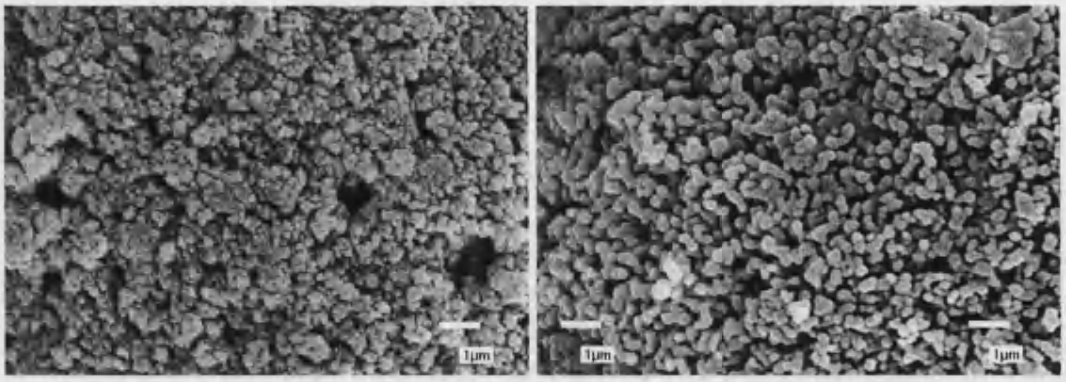

(a) non-sintered (b) sintered at 900 °C

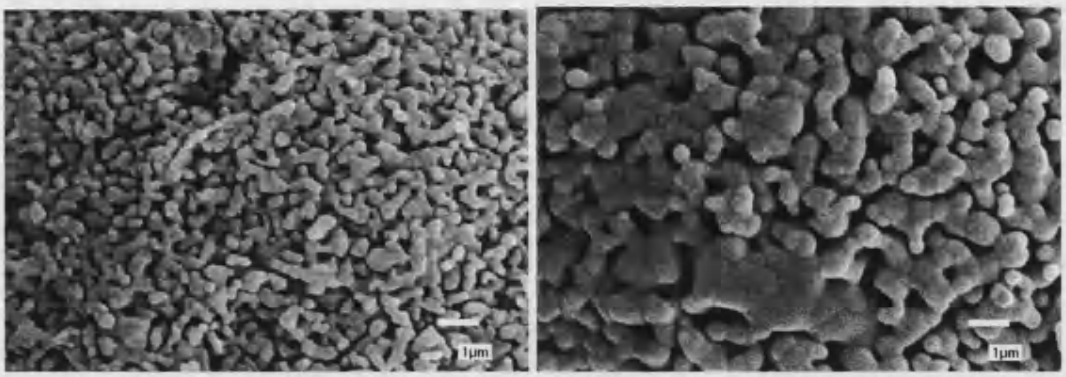

(c) sintered at 1000 °C (d) sintered at 1100 °C

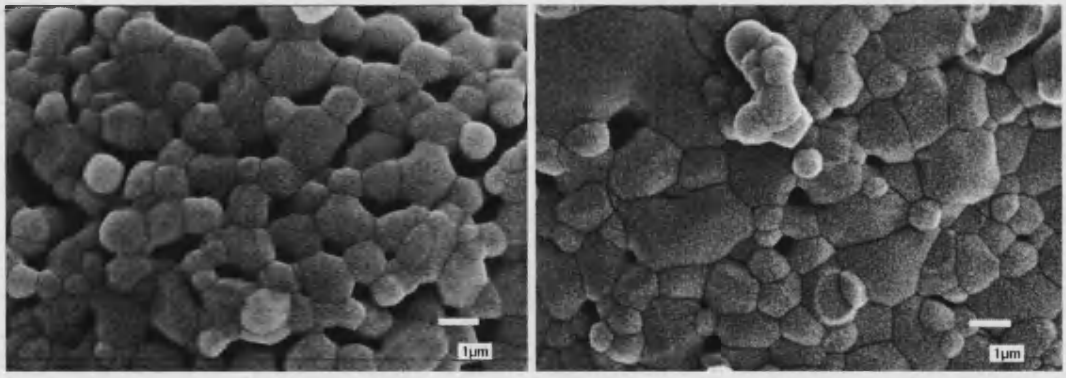

(e) sintered at 1150 °C (f) sintered at 1200 °C

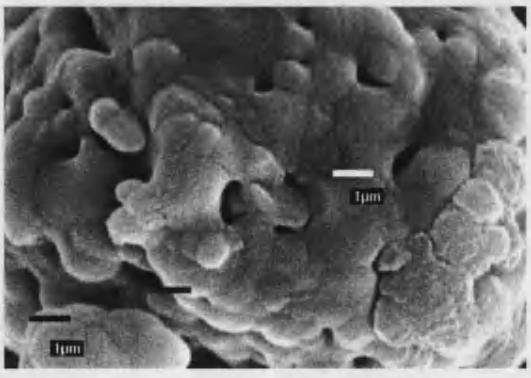

(g) sintered at 1300 °C

Figure 4.5 SEM micrographs of surface morphology of β-TCP microspheres before and after sintered at 900°C - 1300°C (constant magnification).

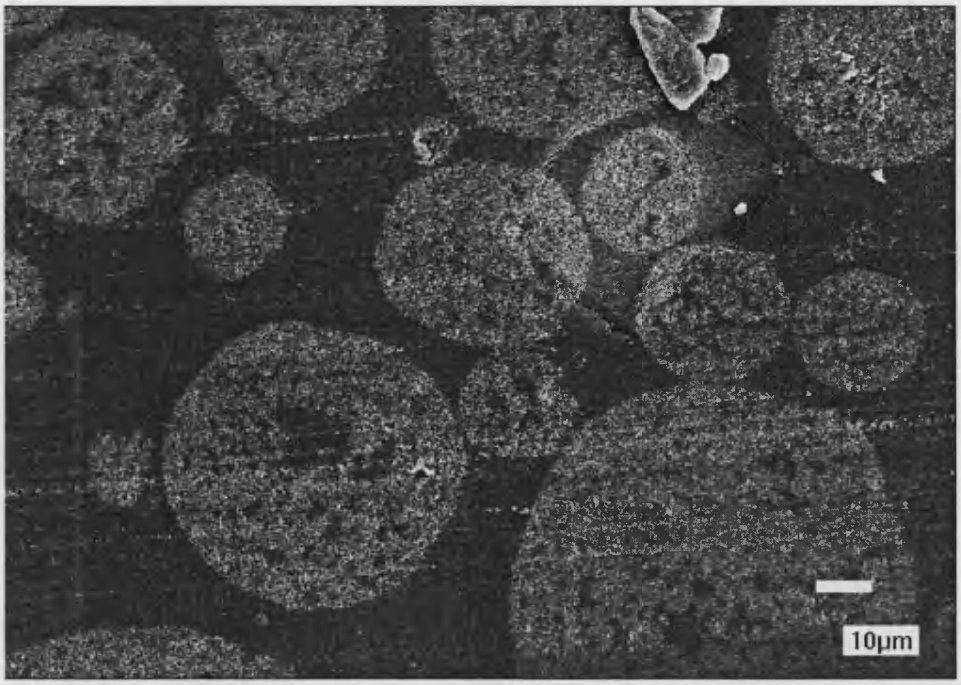

(a)

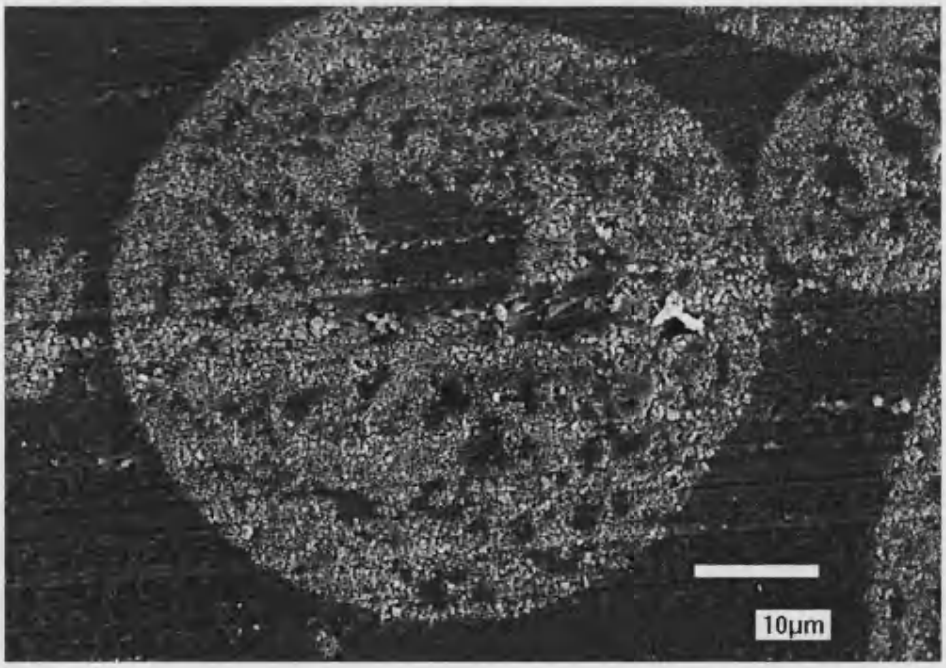

(b)

Figure 4.6 SEM micrographs of sectioned open β-TCP microspheres sintered at 900 °C (a) ×800 magnification; (b) ×1700 magnification.

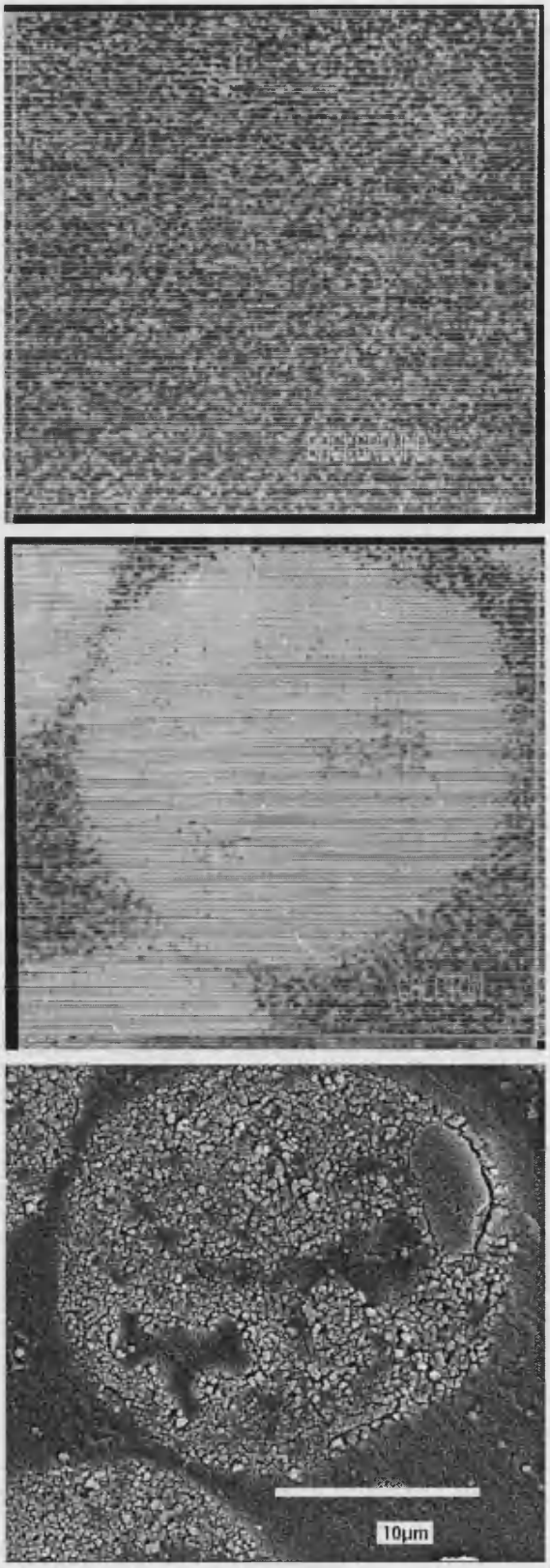

(a) Background noise

(b) Calcium x-ray dot map

(c) Topographic image

Figure 4.7 SEM micrographs comparing (a) background noise; (b) X-ray dot map; and (c) topographic image of a sectioned open β-TCP sintered (900 °C) microsphere.

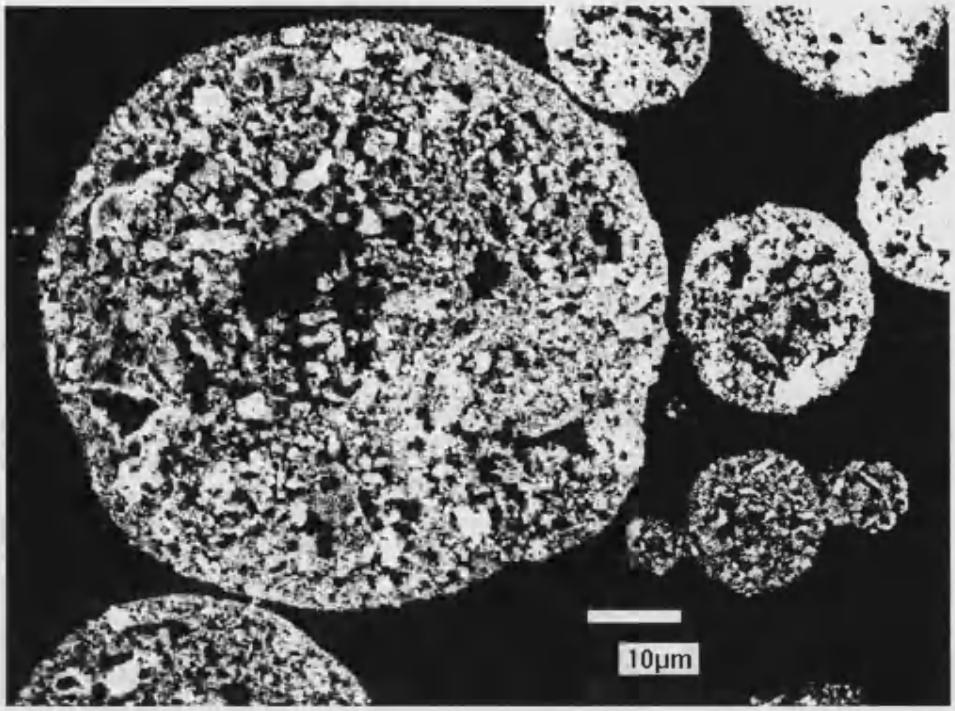

(a}

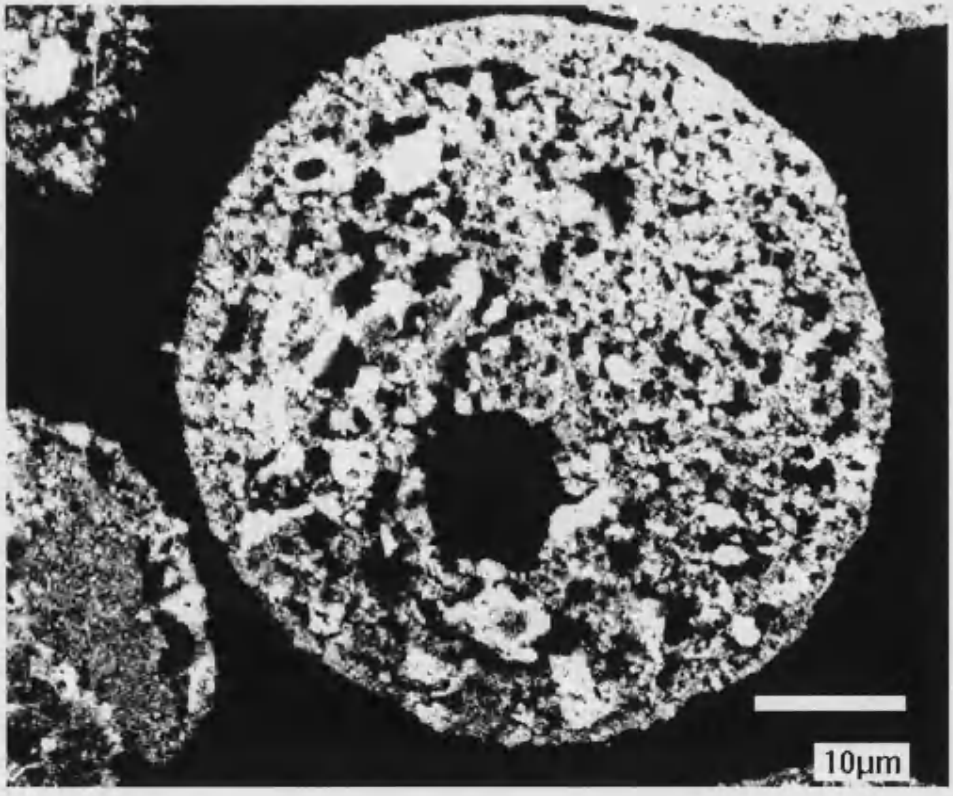

(b)

Figure 4.8 Backscattered electron SEM micrographs showing interior structure of β-TCP microspheres sintered at 900°C (a) ×1100, (b) ×1600 magnification.

4.4.3 Density Determination

4.4.3.1 Tap Density

The tap density of a powder is obtained when a predetermined amount of powder in a container of known dimensions is vibrated or tapped under predefined conditions. The tap density depends on the orientation and arrangement of the individual particles, which control their packing, and the presence, shape and size of pores between and within particles.

Tap density was measured using a tap density tester as described in section 2.4.1. Carr's compressibility index was calculated from the bulk and tap densities using the equation below[110].

$$\left(\frac{tap\ density - bulk\ density}{tap\ density}\right) \times 100 = \%\ compressibility \quad \text{Equation 4.1}$$

4.4.3.2 Results and Discussion

The measured bulk-density, tap density and the calculated Carr's compressibility index for β-TCP microspheres, before and after sintering, are presented in Table 4.2. The results show that there is a general trend of gradual increase in both bulk and tap densities as the sintering temperature increases. No sudden decrease in tap volume was observed during the tapping cycles. This indicates that there was no significant break down of microspheres due to tapping. The Carr's index is generally used to predict the powder flowability. All powder tests exhibited a Carr's compressibility index > 35. This indicates that these powders have very poor flow properties[111], which is in agreement with their poor flowability observed during the experiments.

Table 4.2 Bulk-density (n=3), tap density (n=3) and the Carr's compressibility index for spray-dried β-TCP microspheres before and after sintering.

		Bulk-density ± SD (g/cm^3)	Tap Density ± SD (g/cm^3)	Carr's Compressibility Index
	Powder as-received (Non-spray-dried)	0.259 ± 0.009	0.432 ± 0.010	40
Spray-dried β-TCP samples	Non-sintered	0.259 ± 0.011	0.436 ± 0.006	40
	Sintered at 900 °C	0.310 ± 0.015	0.537 ± 0.013	42
	Sintered at 1000 °C	0.356 ± 0.007	0.656 ± 0.012	46
	Sintered at 1100 °C	0.490 ± 0.005	0.844 ± 0.004	42
	Sintered at 1150 °C	0.532 ± 0.012	0.917 ± 0.018	42
	Sintered at 1200 °C	0.656 ± 0.011	1.124 ± 0.011	42
	Sintered at 1300 °C	0.671 ± 0.069	1.066 ± 0.010	37

4.4.3.3 True Density

True density measurements of β-TCP microspheres sintered at selected temperatures between 900 °C –1300 °C were determined using a helium pycnometer (AccuPyc 1330, V2.01, Micromeritics Instruments Co., Georgia, USA) as described in section 2.4.2. The basic principle of gas pycnometry lies within the ideal gas law: PV = nRT. For a given amount of gas, the pressure changes are directly related to the volume changes when temperature remains constant. In AccuPyc 1330, a known amount of helium gas at constant temperature flows from a calibrated reference volume into the sample tube. The volume of the sample occupied is then calculated from the pressure changes[112]. It is assumed that there is independent evidence that the gas is not absorbed, and the solid does not contain closed pores.

4.4.3.3.1 Results and Discussion

The pycnometry density measurements obtained are shown in Table 4.3. Analysis of variance using Minitab (V12.2) indicated that there are significant density differences ($F = 1389.11$, $P < 0.001$) between the mean values of the samples tested. Fisher's

pairwise comparisons at $P < 0.05$, showed that the main differences lie between the non-sintered (group 1 & 2) and the sintered samples (group 3-8) [see Appendix I (a)]. Group 1, 2 and 3 are significantly different from each other and with other groups; among groups 4 - 8 there are in general no significant differences indicating that the true density of a material does not change during sintering in most cases. The observed true density change during sintering may be due to one or a combination of the following factors:

a) The physical changes, *e.g.*, fusing of particles, result in occlusion of internal pores. This violates the assumptions that the solids do not contain enclosed pores. The measuring gas, helium, cannot reach those pores, hence, reduced density values were observed.
b) Phase changes resulting in a different crystal structure with a different true density being obtained.
c) The number of samples, n = 3, is not representative.

Table 4.3 Pycnometer true density values (n=3) for the spray-dried β-TCP microspheres before sintering and after sintering at various temperatures.

Group no.	β-TCP samples	True Density ± SD (g/cm^3)
1	Powder as-received	2.7746 ± 0.0026
2	Spray-dried, before sintering	2.8489 ± 0.0051
3	Sintered at 900 °C	3.0136 ± 0.0061
4	Sintered at 1000 °C	3.0402 ± 0.0068
5	Sintered at 1100 °C	3.0404 ± 0.0075
6	Sintered at 1150 °C	3.0276 ± 0.0030
7	Sintered at 1200 °C	3.0407 ± 0.0022
8	Sintered at 1300 °C	3.0376 ± 0.0016

4.4.4 Surface Area and Pore Structure Analysis by Gas Adsorption

Surface area analysis provides information about void spaces on the surfaces of individual particles or their aggregates. It is important in the characterisation of solid

pharmaceutical materials because factors such as chemical activity, adsorption, dissolution, and bioavailability of the drug may heavily depend on the nature and area of the surface available on the solid[113]. Generally, a powder with a larger surface area will be more reactive, have enhanced solubility, sinter at lower temperatures, have more adsorptive capacity and exhibit greater catalytic activity[114]. The flowability, which may greatly influence the handling properties of a powder, is also related to its surface area and the particle-size[111]. The BET method, developed by Brunauer, Emmett and Teller[115] is the most widely used method for surface area measurements based on gas adsorption.

The physical adsorption of gases by solids increases with decreasing temperature and with increasing pressure. This process is exothermic. The BET method is based on the monolayer adsorption of an inert gas, generally nitrogen, on the solid surface at reduced temperature. The way in which a material adsorbs a gas is referred to as an adsorption isotherm. The shape of the isotherm reflects specific conditions for adsorption, such as pore-size and heat of adsorption[114].

In this study, the surface area of sintered β-TCP microspheres was investigated by gas adsorption using two types of apparatus:

1) 5-point BET N_2 adsorption surface analyser, Gemini 2360 (Micromeritics Instruments Co., Georgia, USA).
2) Accelerated Surface Area and Porosimetry Analyser (ASAP 2010 V2.00 Micromeritics Instruments Co., Georgia, USA).

4.4.4.1 5-point BET N_2 Adsorption Analyser

The surface area of accurately weighed microsphere samples (0.5 g - 6.3 g) was determined using the 5-point BET N_2 adsorption analyser. Experimental methods are detailed in section 2.5.1. Two different batches of β-TCP powder were spray-dried and subsequently sintered at selected temperatures from 900 °C to 1200 °C. These samples were subjected to analysis and two data sets were obtained.

4.4.4.1.1 Results and Discussion

The surface area analysis results of two batches of β-TCP microspheres are shown graphically in Figure 4.9, and the detailed values are shown in Table 4.4 and Table 4.5.

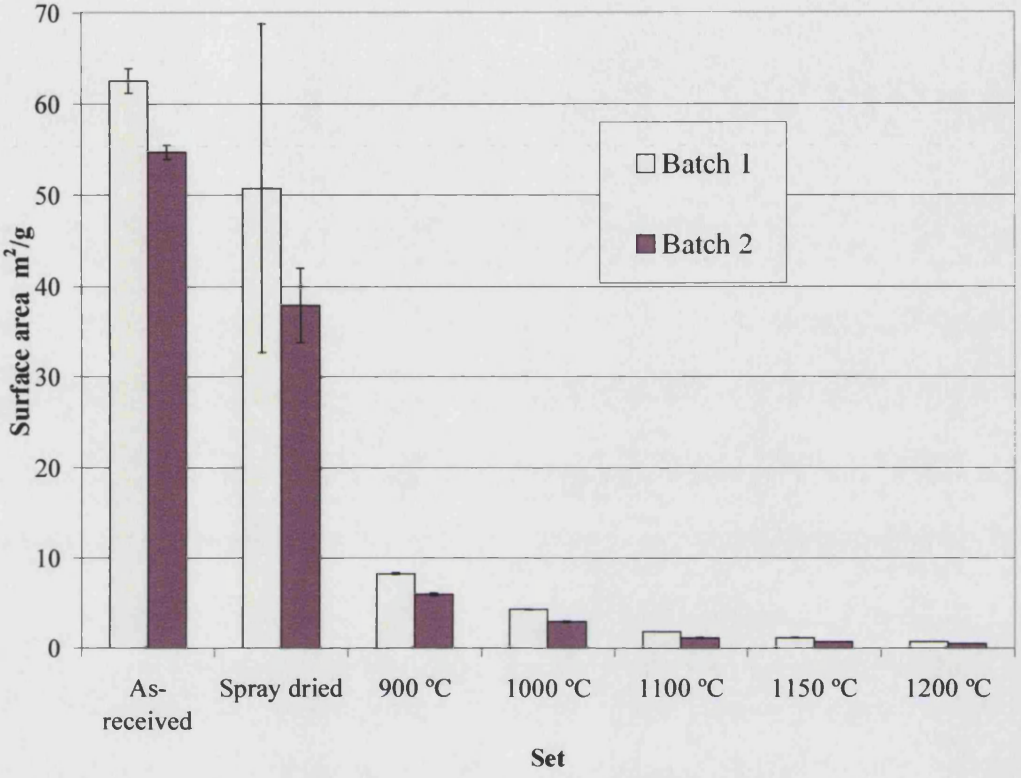

Figure 4.9 Specific surface area of β-TCP powder as received, spray-dried, and spray-dried samples which were sintered at temperatures from 900 °C to 1200 °C (n = 5).

According to Micromeritics, the Gemini 2360 apparatus is capable of measuring specific surface areas as low as 0.01 m^2/g, and total surface areas from 0.1 m^2 to 300 m^2. The microsphere surface area measurements are well within this working range. The measured values were found to be between 70 m^2/g - 0.5 m^2/g and the total surface area measured were adjusted to be within 2 m^2 - 35 m^2 by using a higher sample mass for samples with lower surface area.

Table 4.4 Surface area measurements of batch 1 β-TCP powder as received; spray-dried; and spray-dried plus subsequently sintered at various temperatures as indicated.

Batch 1 β-TCP Samples	Run	Adsorption Parameters			Specific Surface Area (m^2/g)	
		C	Intercept	Correlation Coefficient		Mean ± SD (n=5)
Powder as-received	1	183	0.0004	1.0000	61.7118	62.5490 ± 1.3350
	2	182	0.0004	1.0000	61.3497	
	3	194	0.0004	1.0000	62.6917	
	4	183	0.0004	1.0000	64.7561	
	5	181	0.0004	1.0000	62.2357	
Spray-dried but non-sintered	1	78	0.0008	0.9999	69.5886	50.7180 ± 18.0584
	2	86	0.0015	1.0000	33.3311	
	3	83	0.0008	0.9999	63.7455	
	4	95	0.0015	0.9999	29.8423	
	5	81	0.0009	0.9999	57.0824	
Sintered at 900 °C	1	170	0.0031	0.9999	8.1274	8.2629 ± 0.1047
	2	174	0.0030	1.0000	8.2974	
	3	180	0.0029	1.0000	8.3670	
	4	158	0.0033	1.0000	8.3435	
	5	160	0.0033	0.9999	8.1792	
Sintered at 1000 °C	1	137	0.0073	1.0000	4.2877	4.2874 ± 0.0328
	2	135	0.0074	1.0000	4.3230	
	3	125	0.0081	1.0000	4.2514	
	4	133	0.0072	1.0000	4.2770	
	5	134	0.0060	0.9999	4.2978	
Sintered at 1100 °C	1	116	0.0210	0.9999	1.7894	1.8264 ± 0.0274
	2	149	0.0160	0.9999	1.8199	
	3	140	0.0166	0.9999	1.8590	
	4	157	0.0150	0.9999	1.8471	
	5	86	0.0271	1.0000	1.8165	
Sintered at 1150 °C	1	171	0.0221	1.0000	1.1519	1.1808 ± 0.0366
	2	176	0.0213	1.0000	1.1598	
	3	167	0.0226	1.0000	1.1537	
	4	143	0.0247	0.9999	1.2333	
	5	138	0.0262	0.9999	1.2051	
Sintered at 1200 °C	1	188	0.0310	1.0000	0.7436	0.7429 ± 0.0162
	2	186	0.0305	1.0000	0.7636	
	3	164	0.0354	1.0000	0.7512	
	4	180	0.0322	0.9999	0.7354	
	5	157	0.0384	1.0000	0.7207	

Table 4.5 Surface area measurements of batch 2 β-TCP powder as received; spray-dried; and spray-dried plus subsequently sintered at various temperature as indicated.

Batch 2 β-TCP Samples	Run	Adsorption Parameters			Specific Surface Area (m^2/g)	
		C	Intercept	Correlation Coefficient		Mean ± SD (n=5)
Powder as-received	1	201	0.0004	0.9999	54.8920	54.7413 ± 0.7335
	2	203	0.0004	1.0000	55.2678	
	3	200	0.0004	1.0000	55.3279	
	4	180	0.0005	1.0000	53.5138	
	5	194	0.0004	1.0000	54.7051	
Spray-dried but non-sintered	1	93	0.0014	0.9999	33.1846	37.8946 ± 4.0990
	2	98	0.0010	0.9999	43.5702	
	3	87	0.0014	0.9999	36.4048	
	4	93	0.0011	1.0000	40.4430	
	5	83	0.0014	0.9999	35.8703	
Sintered at 900 °C	1	97	0.0078	0.9999	5.7328	5.9691 ± 0.1452
	2	113	0.0065	1.0000	5.9347	
	3	123	0.0059	0.9999	6.0246	
	4	136	0.0053	1.0000	6.0532	
	5	169	0.0043	0.9999	6.1000	
Sintered at 1000 °C	1	140	0.0109	0.9999	2.8550	2.9160 ± 0.0518
	2	144	0.0105	0.9999	2.8638	
	3	144	0.0102	0.9999	2.9572	
	4	167	0.0088	0.9999	2.9525	
	5	146	0.0102	0.9999	2.9514	
Sintered at 1100 °C	1	84	0.0450	0.9999	1.1545	1.1697 ± 0.0188
	2	83	0.0454	0.9998	1.1603	
	3	113	0.0325	0.9998	1.1791	
	4	85	0.0429	0.9998	1.1984	
	5	110	0.0340	0.9997	1.1560	
Sintered at 1150 °C	1	122	0.0504	1.0000	0.7058	0.7310 ± 0.0170
	2	171	0.0341	1.0000	0.7423	
	3	170	0.0347	1.0000	0.7388	
	4	174	0.0335	1.0000	0.7466	
	5	179	0.0337	0.9999	0.7217	
Sintered at 1200 °C	1	87	0.0938	0.9999	0.5318	0.5381± 0.0042
	2	104	0.0773	0.9999	0.5408	
	3	151	0.0530	1.0000	0.5427	
	4	114	0.0710	0.9999	0.5368	
	5	132	0.0614	0.9999	0.5383	

To ensure the validity of the experimental data, a few parameters were checked during data analysis. A correlation coefficient in the range of 0.999 to 1 is acceptable in most cases[114]. The constant *C* in Table 4.4 and Table 4.5 is a measure of the affinity of the adsorbate, in this case the nitrogen gas, to the material. For surface area determinations, the ideal adsorbate should exhibit *C* values sufficiently low to preclude localised adsorption of the adsorbate to specific adsorption sites, and sufficiently high that the adsorbate lateral mobility on the adsorbent surface will not disrupt any tendency for an organised structure to develop. For the majority of adsorbents the *C* value for nitrogen lies in the range 50 - 300[116].

The results show that the specific surface area of β-TCP microspheres is greatly reduced by sintering. This can be explained by the dissolution and the incorporation of smaller particles into bigger grains after sintering, as observed under the SEM (section 4.4.2.1). The high standard deviation obtained for spray-dried but non-sintered microspheres are due to the presence of other materials, *i.e.*, the binder, Eudragit L100 and the dispersant, Dispex A40.

In batch 1, the specific surface area decreased sharply from 62.5 m^2/g for non-sintered microspheres to 8.3 m^2/g for microspheres sintered at 900 °C, and further decreased to 0.74 m^2/g for microspheres sintered at 1200 °C. Batch 2 results showed a similar trend.

To investigate the effect of sintering on the samples, two-way analysis of variance (ANOVA) comparing powders as-received and powders sintered at 900 °C was carried out. The result [Appendix I(b)] indicated that there is a significant interaction between batch and the effect of sintering [$F(1,16) = 65.37$, $p < 0.001$]. There are also significant differences between batches [$F(1,16) = 218.98$, $p < 0.001$] alone, and the effect of sintering [$F(1,16) = 23000$, $p < 0.001$] alone.

To investigate the effect of sintering temperature, data obtained from samples sintered at temperatures between 900 °C and 1200 °C were analysed. Two-way ANOVA revealed a significant interaction between batch and temperature [$F(4,40) = 465.81$, $p < 0.001$]. There are also significant differences between batches alone [$F(1,40) = 3221.45$, $p < 0.001$], and sintering temperature alone [$F(4,40) = 19000$, $p < 0.001$]

[Appendix I(c)]. *Post hoc* Bonferroni-Dunn (All Means) comparisons revealed that all specific surface area values of the sintered samples were significantly different from each other ($p < 0.001$) in all cases, except the comparison of

a) Batch 1 sample sintered at 1150 °C and Batch 2 sample sintered at 1100 °C;

b) Batch 1 sample sintered at 1200 °C and Batch 2 sample sintered at 1150 °C.

Thus, it is concluded that the sintering temperature (900 °C - 1200 °C) has a significant effect on the specific surface area of β-TCP microspheres. In other words, sintering temperature has a significant effect on how far particles coalesce. Therefore, precise temperature control is crucial in the sintering process.

Two different powder batches were found to have different specific surface area after sintering. Batch 1 powder as-received has a higher specific surface area than batch 2 as-received powder. It was observed that under the same sintering conditions, batch 1 powder consistently gave higher specific surface area value than batch 2 powder.

4.4.4.2 Accelerated Surface Area and Porosimetry (ASAP) Analyser

The ASAP analyser utilises the principle of physical adsorption to obtain information about the surface area and porosity of a solid material. The ASAP 2010 analyser is capable of measuring materials with specific surface area from less than 0.01 m^2/g to 3000 m^2/g and determines pore diameter in the range of 0.35 nm - 300 nm. That is, this apparatus is capable of analysing nano-pores but not larger ones. Non-sintered microspheres, and microspheres sintered at 1000 °C and at 1100 °C from batch 1 spray-dried powder were characterised by ASAP analyser (method see section 2.5.2).

4.4.4.2.1 Results and Discussion

The adsorption and desorption isotherms obtained are shown in Figure 4.10. These are Type 2 isotherms, typical of either non-porous adsorbents or adsorbents having relatively large pores. For Type 2 isotherm, the isotherm rises comparatively rapidly at low relative pressures, rises only moderately at intermediate relative pressure, and then rises quite rapidly as the relative pressure approaches unity[114]. The initial rise in the curve is due to a single layer of adsorbing molecules, N_2, interacting with the most

energetic regions of the powder, followed by the less energetic regions. As these sites are occupied, the rising curve weakens. By midpoint of the curve, additional layers of N_2 molecules are forming as further N_2 molecules become attached to N_2 molecules already on site. The sudden rise at the end corresponds to bulk condensation of N_2 gas to a liquid. The desorption isotherms for microspheres sintered at 1000 °C and 1100 °C are nearly retraces of their absorption isotherms; these are typical isotherms for materials completely without nano-pores. The adsorption curve for non-sintered microspheres rises more rapidly in the intermediate zone and shows a hysteresis loop. This is typical behaviour of materials with mesoporous and macroporous, *i.e.* materials with pores diameter > 1.5 nm and > 100 nm, respectively. Such pores are likely to be of various sizes and shapes and they may also be interconnected.

The knee point in an isotherm indicates the monolayer coverage of N_2 and the surface area information can be extracted from the lower region of the curve. The adsorption isotherms were interpreted using the BET equation below[113]:

$$\frac{P}{V_a(P_0 - P)} = \frac{1}{V_m C} + \frac{C-1}{V_m C}\left(\frac{P}{P_0}\right) \qquad \text{Equation 4.2}$$

Where V_a = volume of gas adsorbed at pressure P

P = partial pressure of nitrogen

V_m = volume of nitrogen adsorbed in the monolayer

P_0 = saturation pressure of nitrogen gas

C = BET constant, exponentially related to the heat adsorption of the nitrogen

The surface area was determined as a product of the number of molecules in a completed monolayer and the effective cross-sectional area of nitrogen. The relevant equation is given in Equation 4.3:

$$S_t = \frac{V_m N_0 A_{CS}}{M} \qquad \text{Equation 4.3}$$

Where S_t = total surface area

N_0 = Avogadro's number, 6.022×10^{23}

A_{CS} = cross sectional area of nitrogen (0.1620 nm^2)

M = molecular weight of the nitrogen

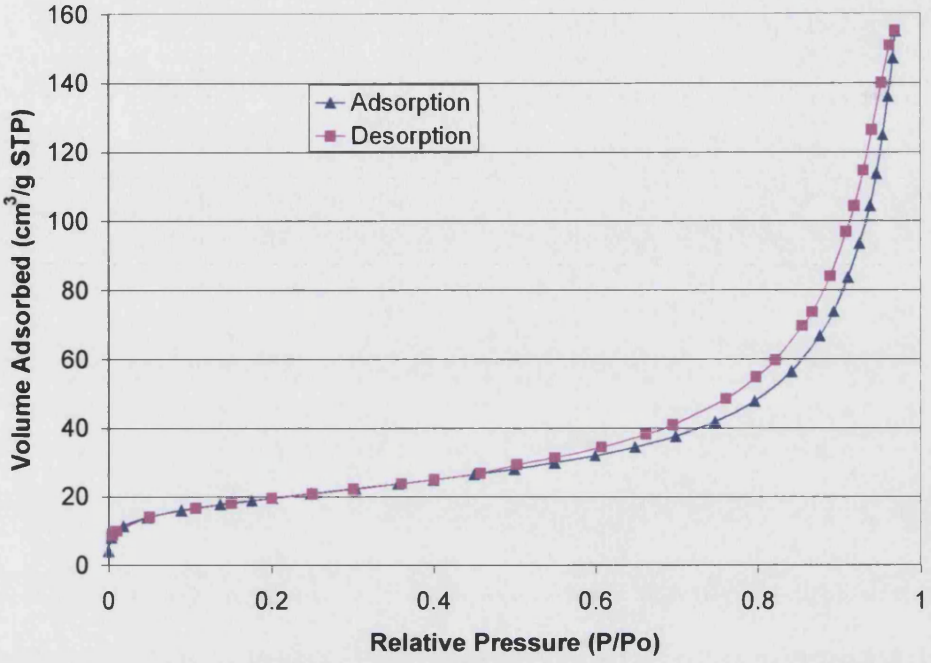

(a) Non-sintered microspheres

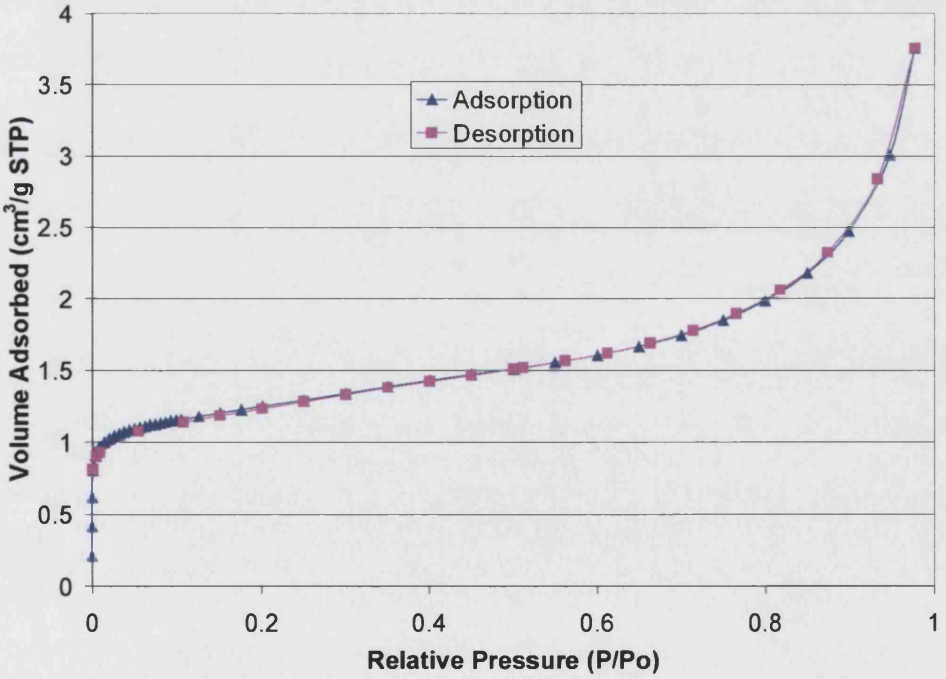

(b) Microspheres sintered at 1000°C

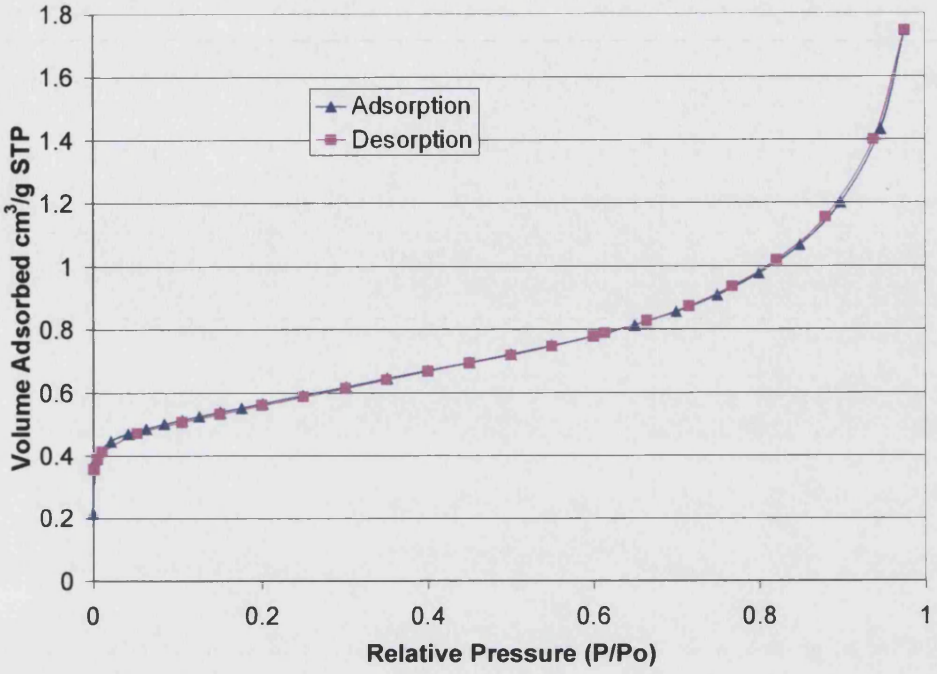

(c) Microspheres sintered at 1100°C

Figure 4.10 The adsorption and desorption isotherms of (a) non-sintered microspheres; (b) microspheres sintered at 1000°C; and (c) microspheres sintered at 1100°C.

The surface areas obtained are shown in Table 4.6. A high or a negative C value, showed for samples sintered at 1000 °C and 1100 °C, is indicative of the presence of micropores. In these cases, modification of the BET model may be needed for the analysis. However, in this study, the specific surface areas obtained using ASAP 2010 agree with the results obtained using Gemini 2360, therefore, no further calculations were performed.

Table 4.6 Results of BET surface area obtained using ASAP 2010 analyser.

β-TCP samples	Run	Adsorption Parameters			Specific Surface Area (m^2/g)
		C	Intercept	Correlation Coefficient	
Non-sintered	1	190.1	0.0003	0.9993	68.5217± 0.9635
Non-sintered	2	267.2	0.0002	0.9981	68.3928 ± 0.6293
Sintered at 1000 °C	1	-1513.7	-0.0007	0.9997	4.4199 ± 0.0220
Sintered at 1100 °C	1	7641.6	0.0003	0.9999	1.9823 ± 0.0077

4.4.5 Mercury Intrusion Porosimetry

The pore structure of a drug carrier can affect the adsorption, disintegration, dissolution and diffusion drug materials[113]. Therefore, porosity and pore-size distribution have been extensively studied in pharmaceutical powders, granules, tablets and excipients[117]. Mercury porosimetry is a well established technique for the characterisation of porous materials[118,119,120]. Apart from pharmaceutical materials, it has been used to characterise hydrogels[121] and ceramics [98;122].

Porosity is a measure of the void spaces within a material. It can be calculated using data obtained by several techniques, including density, gas adsorption, water displacement and mercury porosimetry. Among these methods, mercury porosimetry and gas adsorption can also provide information about the actual pore structure of a material, including pore radii and volume.

Lowell *et al.*[123] developed a classification system of pore-sizes as follows:

- Pores with radii > 1000 Å are termed 'macropores';
- Pores with radii from 15 Å - 1000 Å are termed 'traditional' or 'mesopores';
- Pores with radii < 15 Å are termed 'micropores'.

While gas adsorption it only useful in measuring pores micropores (< 15 Å), mercury porosimetry is capable of measuring a very wide range of pore-sizes, including macropores and mesopores[118,113].

Mercury porosimetry is based on the understanding that mercury behaves as a non-wetting liquid towards most substances and will not penetrate such a solid unless pressure is applied. For a non-wetting liquid and assuming cylindrical pores, the intrusion pressure at which the mercury enters a pore can be equated with the pore-size information required using the Washburn equation (Equation 4.4)[124]:

$$D = \frac{4\gamma \cos\theta}{P} \qquad \text{Equation 4.4}$$

Where D = pore diameter

P= applied pressure

γ = surface tension

θ= contact angle between mercury and sample

The volume of mercury, V, penetrating the pores is measured directly as a function of the applied pressure. Therefore, P-V information provides a unique characterisation of pore structure. The amount of mercury intruded in the sample is related to the pore volume of the system.

A disadvantage of this method is that it is assumed all pores are cylindrical in shape. In real life, pores are rarely cylindrical and are usually of a different shape, such as spherical or irregular. In addition, because the pressure required for mercury to enter a pore depends on the entry diameter of the pore, mercury porosimetry cannot differentiate between pore A and pore B as shown in Figure 4.11.

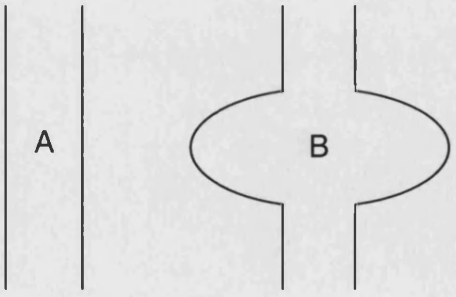

Figure 4.11 Schematic of two pore types, A and B, which cannot be differentiated by mercury porosimetry

β-TCP microspheres sintered at 900 °C - 1200 °C, were analysed by mercury porosimetry. The experimental method is detailed in section 2.6. Each sample was analysed in triplicate. Non-sintered samples were not characterised because it was perceived that the loosely agglomerated spray-dried powder probably could not withstand the high-pressure applied in mercury porosimetry.

4.4.5.1 Results and Discussion

The data obtained from mercury porosimetry can be presented in several graphic forms. Figure 4.12 shows the mercury intrusion/extrusion curves as a function of pore diameter for β-TCP microspheres sintered at various temperatures. As the pressure increases, mercury is forced into the pores and an intrusion curve is produced. When the pressure is decreased, mercury leaves the pores, resulting in a decrease in volume, and an extrusion curve is produced. The extrusion curves do not retrace the intrusion curve due to hysteresis. The extent of the hysteresis observed in Figure 4.12 indicates that some mercury was permanently trapped in the samples pores. This indicates that most pores are either interconnected or have narrow-neck openings.

Figure 4.13 shows the pore-size distribution of the microspheres sintered at various temperatures. The areas under the curves indicate pore volume. Data accumulated at very low pressures corresponding to pore diameter > 2.5 μm are not considered because these data account for the volume entering the interparticle spaces between the microspheres. SEM examination showed that pores within microspheres are unlikely to exceed 2.5 μm in diameter. The porosimetry results show that as the sintering temperature increases, the total pore volume of sample decreases. Microspheres sintered at 900 °C were found to have the biggest pore volume, and they contained a great number of small pores of 0.1 μm - 1 μm in diameter. These small pores diminished quickly as the sintering temperature increased.

The percentage porosity for the sample is extracted from the data using the Equation 4.5 and Equation 4.6.

$$Envelope\ Density = \frac{sample\ mass}{V_{Penetrometer} - V_{Mercury} - V_{Interparticle}} \qquad \text{Equation 4.5}$$

$V_{Penetrometer}$ = penetrometer volume

$V_{Mercury}$ = cumulative mercury volume

$V_{Interparticle}$ = interparticle volume

$$\% \, Porosity = 1 - \left(\frac{envelop \; density}{true \; density} \right) \times 100\% \qquad \text{Equation 4.6}$$

The interparticle volume is the sum of all the incremental mercury volume which corresponds to pores with diameter > 2.5 μm. True densities used are the density measured by the pycnometer (refer to section 4.4.3.3).

The calculated results (Table 4.7) show that there is a decrease in % porosity as the sintering temperature increases, for the same sintering duration of 1 h.

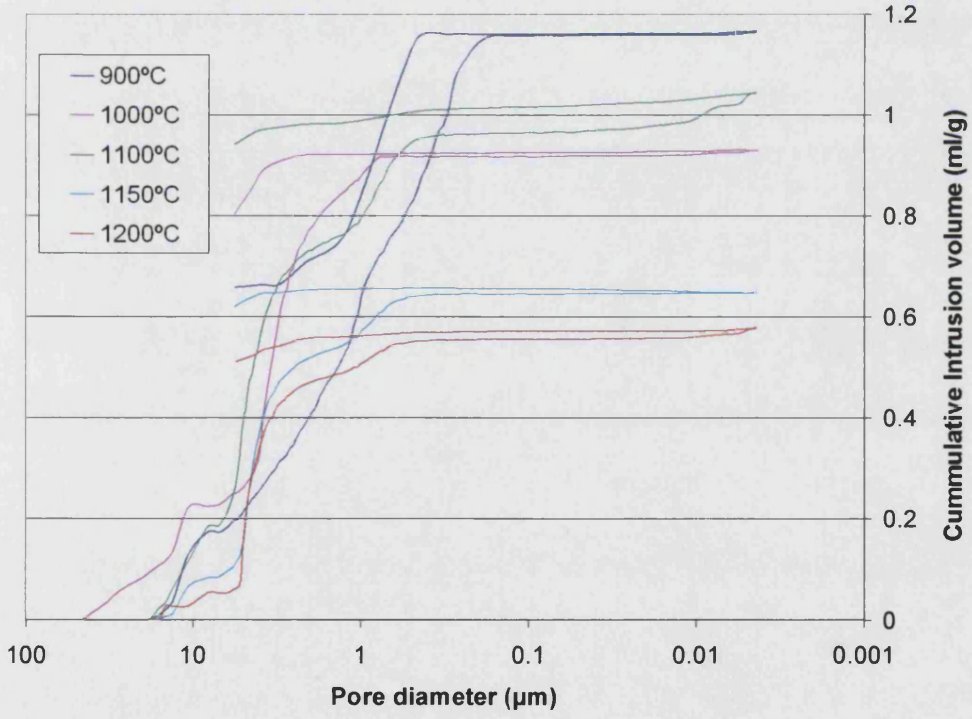

Figure 4.12 Mercury intrusion/extrusion curves as a function of pore diameter for β-TCP microspheres sintered at selected temperatures from 900 °C to 1200 °C.

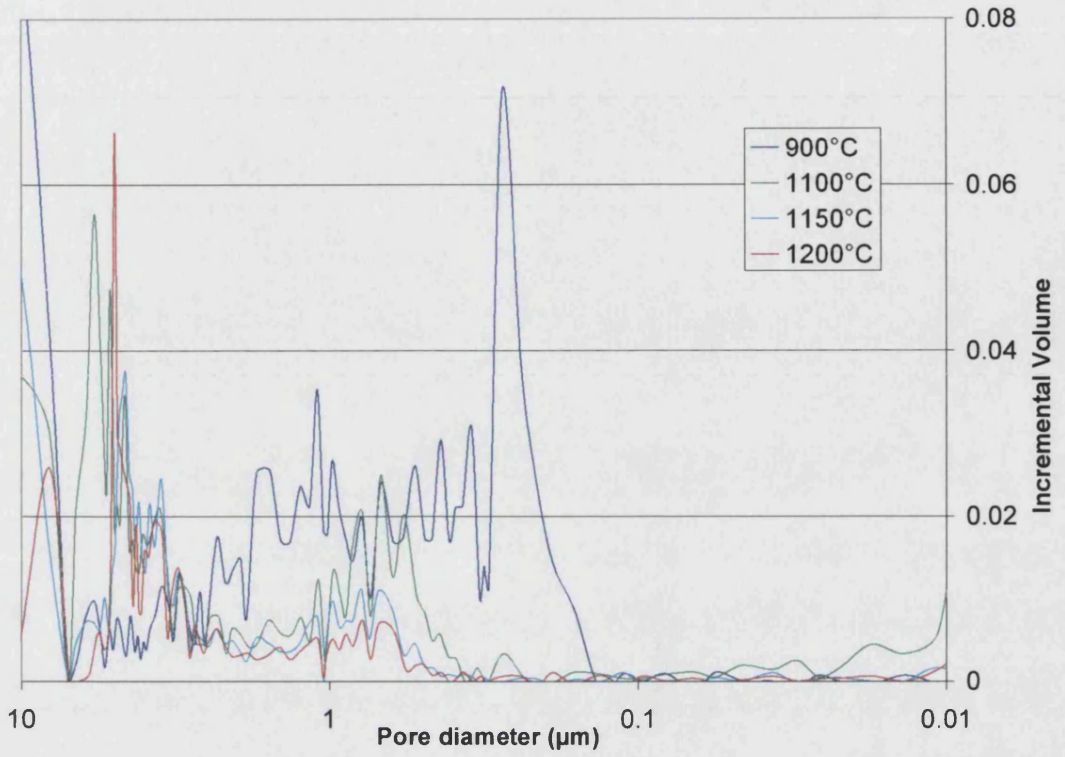

Figure 4.13 Pore diameter vs. incremental intrusion volume for β-TCP microspheres sintered at selected temperatures.

Table 4.7 % porosity of β-TCP microspheres sintered at various temperatures.

Sintering temperature	% Porosity ± SD (n =3)
900 °C	75.0 ± 0.5
1000 °C	62.3 ± 7.2
1100 °C	47.4 ± 1.8
1150 °C	37.9 ± 9.4
1200 °C	35.9 ± 12.2

4.4.6 X-ray Diffraction (XRD) Analysis

X-ray diffraction is a very useful technique in the study of ceramic materials and it can be used to:

(a) Characterise the crystalline phases present;

(b) Identify the presence of specific compounds;

(c) Provide information regarding the degree of crystallization and the orientation texture.

In this study, an X-ray diffractometer was used to characterise the phases present in the samples of DCPA as-received, β-TCP as-received, and their spray-dried microspheres sintered at various temperatures. In order to maintain the sample height constant, samples were pressed onto an aluminium sample holder for the analysis. Experimental methods are described in section 2.10.

4.4.6.1 Results and Discussion

The XRD spectra of the β-TCP powder as-received and those sintered at various temperatures from 900 °C - 1300 °C are shown in Figure 4.14. The sharpening of the characteristic peaks indicates that the crystallinity of the powder increases after sintering. The results also revealed the presence of hydroxyapatite, one of the most stable forms of calcium phosphate, in samples sintered at 1100 °C and 1300 °C. A detailed comparison of the XRD spectra for sintered β-TCP to hydroxyapatite standard and β-TCP standard is shown in Figure 4.15. The XRD spectra of β-TCP before and after sintering are shown in Figure 4.15.

The XRD spectra of DCPA before and after sintering are compared in Figure 4.17. DCPA is not stable at high temperatures[35]. The shift in peaks' positions suggests that DCPA transformed into other forms of calcium phosphate. In this study it was not possible to relate the peaks obtained with the International Centre for Diffraction Data, the database available. However, it is expected that the samples may contain calcium pyrophosphate, $Ca_2P_2O_7$, tetracalcium phosphate, $Ca_4(PO_4)_2O$, and β-TCP, as these are the more stable forms of calcium phosphate at high temperatures[35,36].

Analysis of all sintered samples of DCPA and β-TCP in this study suggests the absence of α-TCP. α-TCP might have been present if a much longer sintering holding time or a higher temperature were used as reported by Zakaria[36], who found that α-TCP was detected when hydroxyapatite was sintered at 1400 °C for 1 h, or at above 1150 °C for ≥ 10 h.

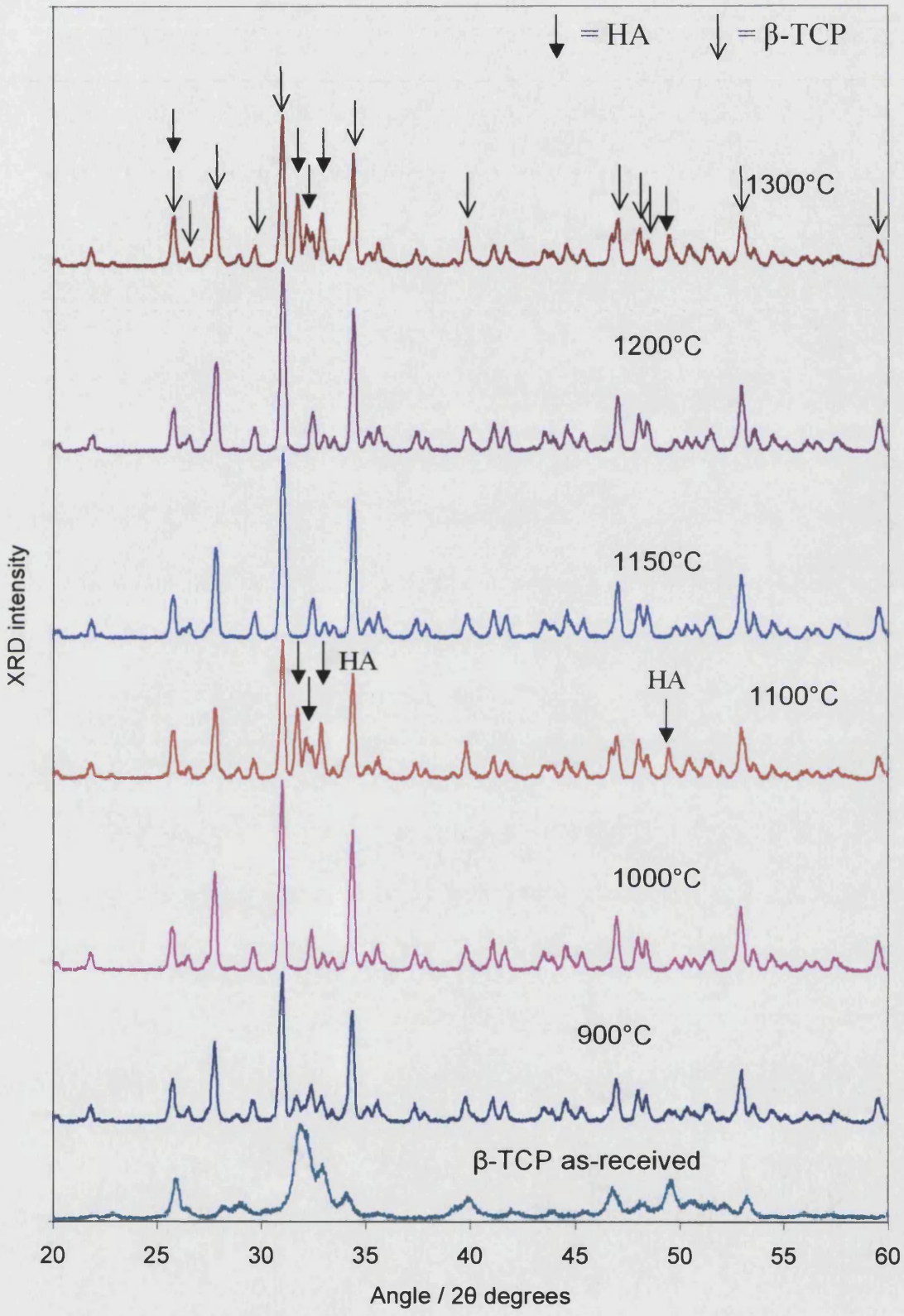

Figure 4.14 The X-ray diffraction pattern of β-TCP powder before and after sintering at temperatures ranging from 900 °C - 1300 °C.

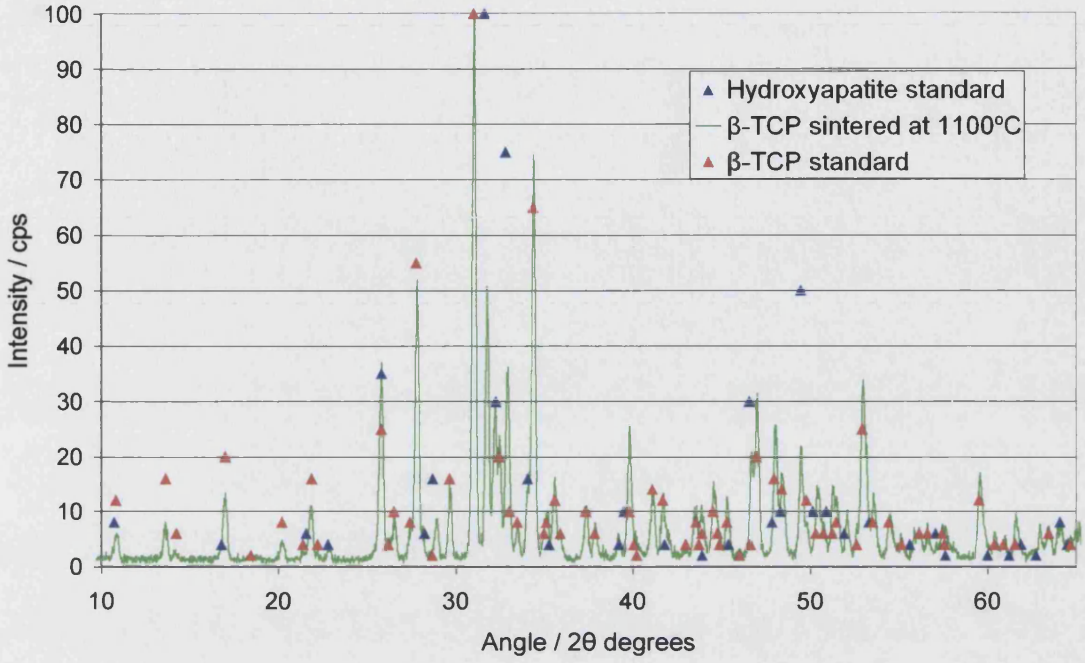

Figure 4.15 XRD spectra of β-TCP before and after sintering, and hydroxyapatite.

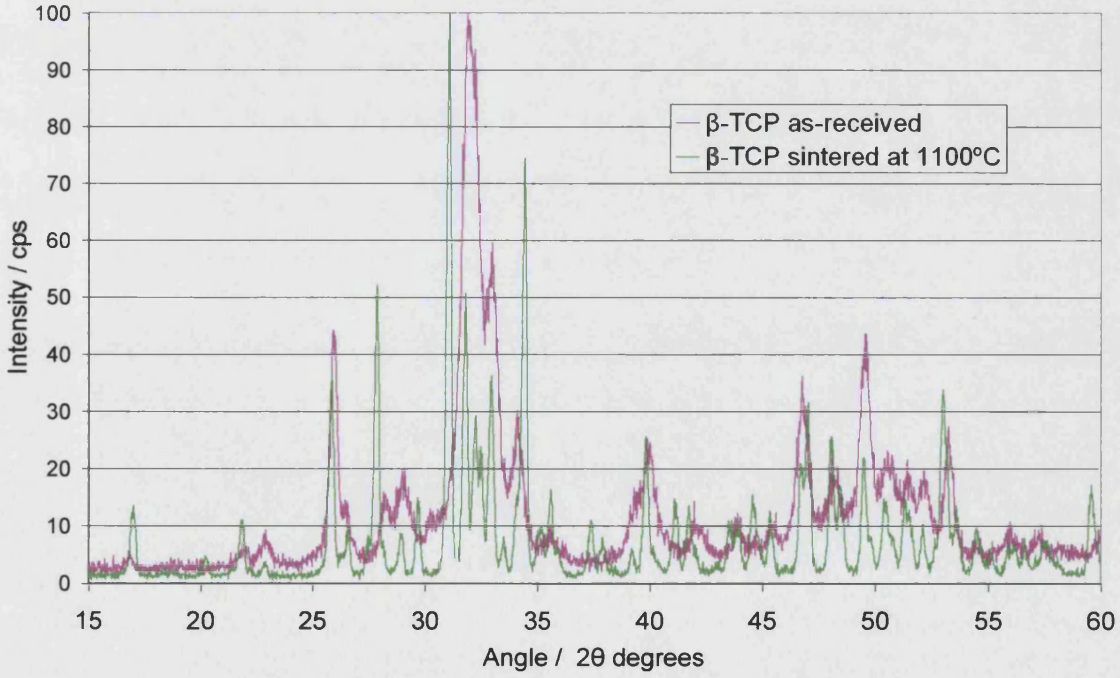

Figure 4.16 XRD spectra of β-TCP before and after sintering.

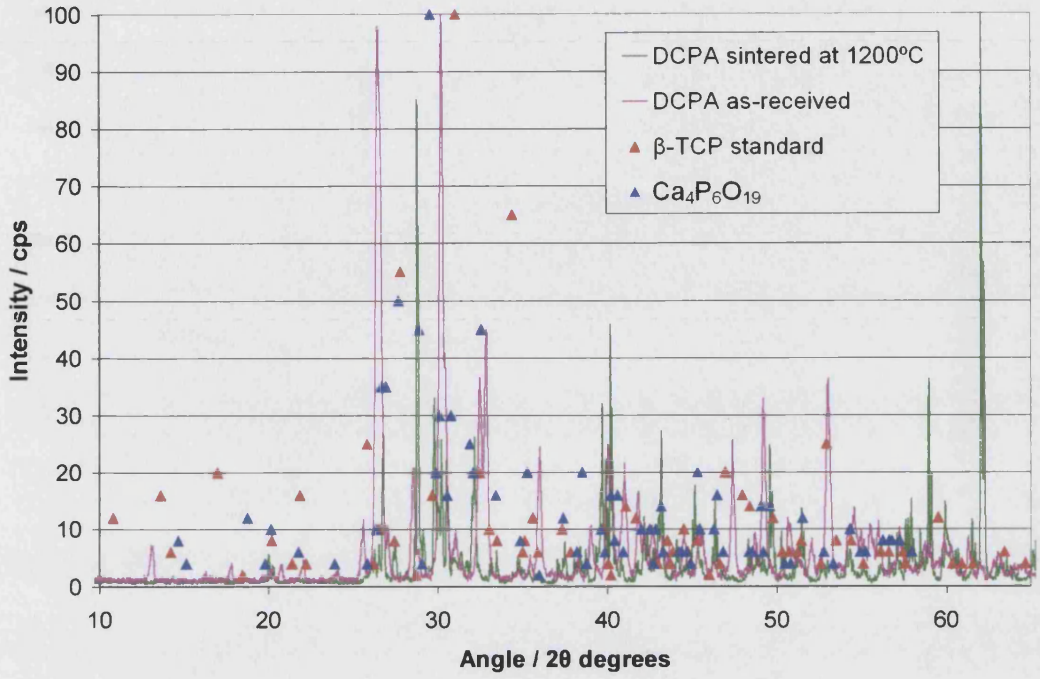

Figure 4.17 XRD spectra of DCPA before and after sintering.

4.5 General Discussion

Using controlled sintering conditions, calcium phosphate microspheres with controlled pore-size, controlled porosity, and controlled surface area were produced in this study.

It was found that DCPA and β-TCP showed different sintering patterns. DCPA is not stable at temperatures above 900 °C. The XRD results suggested transformation of DCPA into other forms of calcium phosphates after sintering. DCPA was observed to undergo sintering between 995 °C and 1070 °C.

β-TCP is a more stable form of calcium phosphate at high temperatures. Its sintering process was observed to start at ~ 600 °C, and from here, the rate of sintering gradually increased as temperature increased. Traces of hydroxyapatite were found in samples sintered at ≥ 1100°C for 1 h.

A weight loss of ~ 7% was observed during sintering of β-TCP microspheres. This weight loss is due to the loss of moisture and the burnout of organic additives, including binder and dispersant.

SEM examination of microspheres sintered at various temperatures showed the progressive stages of sintering. The process started by material diffusion that leads to particle surface smoothing and formation of grain boundaries, followed by neck formation and interconnected open pores formation. As the sintering temperature increases, marked grain growth was observed. The diffusion process gradually removed small pores, leaving larger pores that cannot be sintered out. As the sintering progresses, rounding of pores and continuous shrinkage of open pores was observed. At 1300 °C, β-TCP was effectively a fully sintered ceramic.

Under the SEM, sintered microspheres of both DCPA and β-TCP were found to be highly porous. Many of them also have a large hollow region near the centre of the microspheres. The porosity was found to decrease as the sintering temperature increases. The mercury porosimetry results suggest that the range of porosity for these microspheres is from 75% (microspheres sintered at 900 °C) to 36% (microspheres sintered at 1200 °C).

Combining the results of ASAP and mercury porosimetry suggested that these microspheres have pores of 0.1 μm - 5 μm in diameter and these pores diminished gradually during sintering. The materials hardly have any small pores in the nanometer range.

Sintered bioceramics of β-TCP were found to be physically strong and have a high density of ~ 3 g/cm^3. This dense and robust nature of the microspheres makes them a suitable candidate to be used as drug carrier in needle-free injection.

The surface area of the microsphere ceramic materials is possible by controlling the sintering time and the sintering temperature. Sintering temperature is the more important factor as it also affects the morphology of the voids/pores. The small pores sinter up and disappear. In the ceramics industry, the size of the larger voids and their

volume fraction can be controlled by pressing the green powder. In the case of spray-drying slurries, the porosity is expected to be influenced by the solids content.

The surface area of the microspheres was found to decrease significantly after sintering, and the surface area decreased further as the sintering temperature increased. Non-sintered sample was found to have a surface area of ~ 60 m^2/g, while the fully sintered sample (sintered at 1200 °C) had a surface area of only ~ 0.7 m^2/g. This study demonstrates that the surface area of the microsphere systems can be effectively controlled by controlling the sintering temperature.

Surface area characteristics of the microspheres are important for developing the microspheres into drug carrier systems because these characteristics may

1) determine the amount of drug which can be adsorbed onto the carrier;
2) influence the drug release profile of the drug;
3) provide information about the porosity of the microspheres, which in turn indicates the volume of the drug which can be carried.

Spray-dried β-TCP microspheres have a mean diameter of ~19 μm (according to Mastersizer 2000) and a density of ~ 3.0 g/ml. If the microspheres were spherical and nonporous, the expected specific surface area would be 0.10 m^2/g. However, the specific surface area obtained for microspheres sintered at 900 °C was found to be ~ 80 times higher than this value. This result confirms the porous structure of the microspheres and also suggests that these pores are mainly interconnected.

In conclusion, sintering was found to be an effective way of modifying and controlling the porosity, pore-size and surface area of the spray-dried calcium phosphate microspheres. The ability to control these parameters may allow the development of carrier systems which release drugs at various rates, *i.e.* flexible 'designer' drug carrier systems.

5 Drug Loading and *In Vitro* Release Studies

5.1 Introduction

Drugs have been incorporated into microparticles via several methods. The main methods used involve direct mixing of drugs in the carrier materials before the formation of the microspheres. These include:

- Spray-drying - Drugs were added into spray-drying slurries, and therefore incorporated into the carrier materials (usually organic polymers) during the microparticle formation process of spray-drying[15,125].
- Emulsion solvent extraction/evaporation - Drugs were added into polymer emulsions, and drug-containing microspheres were obtained as a result of solvent evaporation/extraction process[12].
- Coacervation - Oppositely charged polyions in aqueous media may spontaneously coacervate to form two liquid phases; a dense coacervate phase, which is relatively concentrated in the polyions, and a dilute equilibrium phase[126]. Coacervation has been used to encapsulate drugs by placing the drugs in a polymer solution and then changing the pH or the temperature, resulting in a layer of polymer coating formed around the drug particles[10,127]. A hardening step usually follows the formation of coacervates to obtain hard microparticles[10,126].

This chapter describes the investigation of the use of spray-dried β-TCP microspheres, in both non-sintered and sintered forms, as drug carriers. The schematic diagram of the drug loading methods used are shown in Figure 5.1:

a) Non-sintered microspheres – A model drug was added directly into the β-TCP slurry, the mixture was then spray-dried.
b) Sintered microspheres – A vacuum method was employed to incorporate model drugs into sintered microspheres.

Model drugs were not incorporated into microspheres before the microspheres were sintered because the sintering process involved high temperatures (~1000 °C), which thermally destroys the drugs.

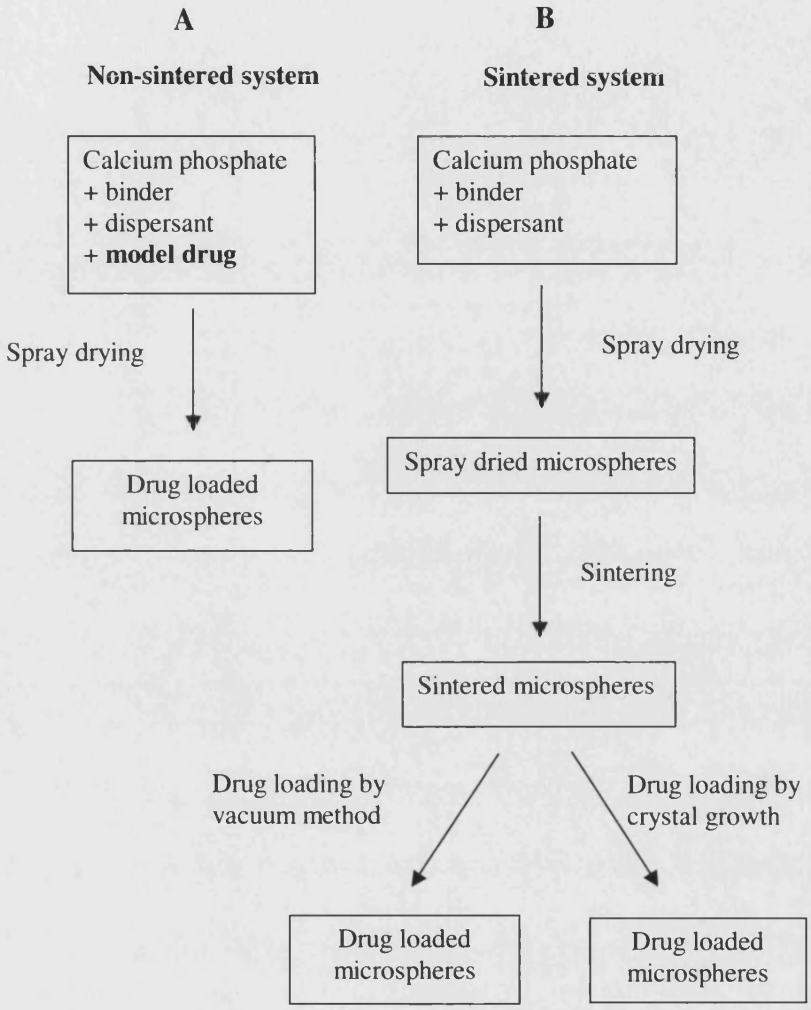

Figure 5.1 Drug-loading methods for (A) non-sintered, and (B) sintered systems.

Three model drugs - benzamide, propranolol hydrochloride (propranolol.HCl) and paracetamol - were used in this study. The drugs were chosen mainly for their solubility properties, and availability.

5.2 Background

5.2.1 Drug Loading by Spray-drying

Many researchers have studied the spray-drying of drugs with drug carrier materials, usually an organic polymer, as a way to obtain drug-containing microcarriers. In 1995, Giunchedi *et al.*[15] published a review on spray-drying as a preparation method of microparticulate drug delivery systems. Other recent examples include Billon *et al.*[86;128] that studied the spray-drying of paracetamol with microcrystalline cellulose and sodium carboxymethylcellulose; Baras *et al.*[129] studied the spray-drying of bovine serum albumin with polylactide; He *et al.*[130] studied the spray-drying of H_2-antagonists with chitosan. Depending on the type of polymers used, controlled release (*e.g.* Billion *et al.*[128] and Baras *et al.*[129]) and instant release (He *et al.*[130]) of drugs were reported.

The structure of the microparticles obtained in spray-drying depends on whether the drug is dispersed or dissolved in the feedstock prior to spray-drying. When drugs are dispersed in a polymer solution, the microcapsules obtained consist of drug crystals surrounded by a polymer coating; when the drug is dissolved in the spray-drying solution, the product obtained is composed of a matrix with drug distributed throughout[131,132].

The crystallinity of the drug in the products obtained depends on whether the drug is dissolved or dispersed before spray-drying. During spray-drying, dispersed drugs maintain their crystalline state, while dissolved drugs may become amorphous[133,134]. This is relevant because the amorphous form of a drug usually dissolves more rapidly than crystalline forms[135]. Therefore the drug dissolution profiles of the spray-dried products obtained may be affected by whether the drug is dissolved or dispersed before spray-drying.

5.2.2 Drug Loading by Vacuum Method

When a porous matrix is placed in a solution, the solution might not penetrate into the pores because these might be occupied by trapped air. If a vacuum is applied, the imposed pressure on the liquid is reduced, and the trapped air will surface and be removed. Liquid penetration into the pores can be achieved.

Itokazu *et al.*[136] investigated the loading of isepamicin sulfate, an antibiotic, into porous hydroxyapatite blocks by a vacuum method. These were 2 cm^3 cubic blocks with pore-size 2 μm - 2000 μm. The blocks were immersed in the isepamicin solution and decompressed under varying vacuum pressures. The amount of isepamicin that penetrated the block was shown to depend on the vacuum pressure, and the time the vacuum was applied.

The vacuum loading method described by Itokazu *et al.*[136] was adapted in this study to load benzamide into sintered β-TCP microspheres. To achieve higher drug loading, successive loading, and loading at elevated temperature were also studied.

To further increase the drug loading, the cultivation of drug crystals inside the pores of the microspheres was also investigated.

After loading the model drugs into the microspheres, the *in vitro* release characteristics of the drug were investigated by dissolution studies. The composition of drugs before and after loading onto microspheres were characterised by nuclear magnetic resonance (NMR) spectroscopy, mass spectroscopy (MS), and X-ray diffraction (XRD) studies.

5.3 Loading by Spray-drying

5.3.1 Model Drug – Benzamide

The first model drug used was benzamide. Its physicochemical properties are listed in Appendix II. Benzamide was chosen for this study because:

(a) It is sparingly soluble, therefore it provides a typical model of a low dose water-soluble system;

(b) It can be monitored by spectrophotometry, λ_{max} = 225 nm in phosphate buffer;

(c) It is a simple molecule, and it does not degrade easily;

(d) It is readily available.

5.3.2 Benzamide Loading by Direct Spray-drying

Benzamide was added to the β-TCP spray-drying slurry as a solute or as a suspension. The solubility of benzamide is 1 g in 74 ml of water[137]. A 100 ml of 30% w/w solids content slurry contains ~ 70 g of water. Therefore the maximum amount of benzamide that can be dissolved in the slurry is 0.95 g or 3.2 pph (parts per hundred of solids). If more then that amount of benzamide is added, not all drug will be dissolved and a drug suspension will be formed. Benzamide is more soluble in alcohol (1 g in 6 ml[137]). Therefore, to produce slurries with higher benzamide concentrations, 40% ethanol in water was used as solvent instead of water alone.

To prepare benzamide as a solution to incorporate in the slurry, benzamide powder was first dissolved in the solvent by sonication. This solution was then added to the β-TCP slurry. To prepare benzamide as a dispersion in the slurry, benzamide powder was first dry ball-milled for 10 h to reduce its particle-size (the particle-size was not measured) and then added directly into the β-TCP slurry. The β-TCP slurry contained Eudragit L100, Dispex A40 and aqueous ammonia, and was prepared as before (see section 3.7.4). Slurries as listed in Table 5.1 were spray-dried under conditions SDC Set 3 (see section 3.7.4).

Table 5.1 Spray-drying slurries containing benzamide.

	Formulation		
Ingredients	Bz1	Bz2	Bz3
*β-TCP slurry solids content	30%	30%	30%
Benzamide (pph)	2.5	15	15
Solvent	water	water	40% ethanol
Benzamide status	*dissolved*	*dispersed*	*dissolved*

*β-TCP slurry was prepared as in section 3.7.4.

Slurry Bz1 contained 2.5 pph of dissolved benzamide in water. Slurry Bz2 contained 15 pph of dispersed benzamide in water. Slurry Bz3 contained 15 pph of dissolved benzamide in ethanol. The spray-dried products were examined under the SEM. The benzamide release profiles from these microspheres were studied by dissolution tests

using phosphate buffer, pH = 6.8 as dissolution medium. The dissolution conditions and experimental details are described in section 5.4 further on.

5.3.2.1 Results and Discussion

Under the SEM, the benzamide-loaded microspheres were found to be similar to the benzamide-free microspheres. No drug crystals were observed on the surface of the microspheres.

Dissolution results showed that for microspheres produced from all three slurries, Bz1, Bz2 and Bz3, benzamide was released rapidly. More than 90% of the benzamide-loaded was released in the first 30 min. The dispersed benzamide system (Bz3) showed a slightly slower release than the dissolved system (Bz2). However, since benzamide was released rapidly in both systems, a clear difference could not be established.

According to the mechanism of droplet drying in during spray-drying, it is reasonable to expect that dissolved benzamide might deposit mainly on the outside of the microspheres. As a dissolved solute in a spray-drying slurry, benzamide diffuses together with the solvent to the surface to evaporate. After the solvent evaporates, benzamide might then crystallise, and form a layer on the outside of the dry particle. This might explain the instant release of benzamide from the drug-loaded microspheres of Bz1 and Bz3 observed during dissolution tests.

The dispersed benzamide particles in the spray-drying slurry are expected to disperse within the calcium phosphate matrix in the spray-dried product, if the particle-size of the benzamide particles are similar to, or smaller than the particle-size of the calcium phosphate. However, if the particle-size of the benzamide particles is much larger than the calcium phosphate particles, the benzamide cannot be incorporated into the microspheres, and fast dissolution profile are expected. Big benzamide particles may be the main contributing factor for the instant release of benzamide from the spray-dried products of Bz2.

5.3.3 NaCMC and Eudragit

To delay the release of benzamide from β-TCP microspheres, the addition of sodium carboxymethylcellulose (NaCMC), and the use of higher concentrations of the binder Eudragit L100, were investigated.

NaCMC is a commonly used pharmaceutical coating polymer, and it has been used as a spray-drying excipient by several researchers[86,138,139].

Eudragits have been used for developing controlled release dosage forms. For example, Eudragit L100 has been shown to sustain the release of erythromycin[140]. Many other examples can be found in the review *Acrylic polymers* by Dittgen *et al.*[21].

Slurries with compositions listed in Table 5.2 were prepared and spray-dried. Slurry Bz4 and Bz5 contained 10% and 20% w/v of NaCMC respectively. Slurry Bz6 contained in total 10 pph Eudragit L100 (8 pph now added + 2 pph already present in the initial slurry). It was found that the order of mixing was crucial for good and uniform slurry production. NaCMC had to be pre-hydrated by soaking in water for 4 to 5 h before it was mixed with other ingredients.

The benzamide release from the spray-dried products of these slurries was investigated by dissolution tests (see section 5.4).

5.3.3.1 Results and Discussion

Dissolution results (Figure 5.2) for microspheres produced from all 3 slurries (Bz4 – Bz6) showed that the release of benzamide started immediately, and more than 80% of the benzamide was released in the first 30 min. These results indicate that neither the extra Eudragit L100 nor NaCMC at the concentrations used have a marked effect on the benzamide release profiles.

Table 5.2 Spray-drying slurries containing benzamide.

	Formulation		
Ingredients	Bz4	Bz5	Bz6
*β-TCP slurry solids content/%w/w	30	30	30
Eudragit L100/pph	-	-	8
Benzamide/pph	10	10	10
NaCMC/pph	10	20	-
Solvent	40 % ethanol in water	40 % ethanol in water	40 % ethanol in water

*β-TCP slurry was prepared as in section 3.7.4.

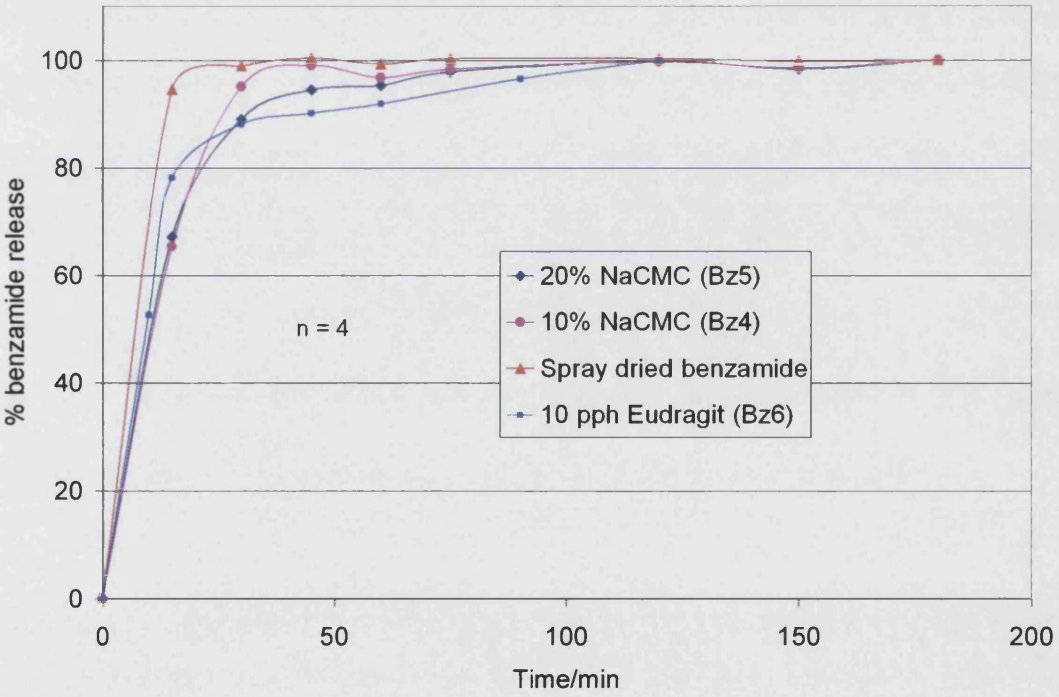

Figure 5.2 Dissolution results for spray-dried products of slurry Bz4, Bz5 and Bz6, compared to spray-dried benzamide (see section 5.4.5 for spray-dried benzamide). Standard deviations are not shown for clarity.

5.3.4 Sieving

Spray-dried microspheres had a size distribution ~ 3 μm - 50 μm (section 3.7.5.1). It is reasonable to expect that the drug release patterns from microspheres of different sizes are different. Attempts were made to separate the bigger and the smaller benzamide-loaded spray-dried microspheres by sieving. Spray-dried microspheres of slurry Bz2 and Bz5 were sieved using a 32 μm metal sieve. Particles retained by the sieve were subjected to dissolution studies as described section 5.4.

5.3.4.1 Results and Discussion

The dissolution results of the sieved and of the non-sieved products showed that almost all benzamide was released quickly in the first 30 min. The release was too fast for any differences between the benzamide release of the sieved and non-sieved products to be identified.

5.3.5 Dissolution in Acidic Media

To mimic the acidic condition in the stomach, dissolution tests using 0.1 M HCl as medium were also performed. The spray-dried products of slurry Bz2 and Bz6 were subjected to dissolution tests in acidic medium. All other dissolution conditions remained the same as described in section 5.4.

5.3.5.1 Results and Discussion

Dissolution results showed that spray-dried microspheres of slurry Bz2, including the β-TCP matrix itself, dissolved almost completely in about 15 min after dissolution. These observations confirm that β-TCP dissolved well in strong acidic conditions.

Eudragit L100 is not soluble in pH < 6[33]. Therefore, it is expected that microspheres containing high concentration of Eudragit L100 will resist acid dissolution. This is confirmed by the experimental results, which showed that capsules containing products from slurry Bz6 did not get wetted fully. Part of the collapsed capsules stayed unchanged in the dissolution medium for the whole period of the test (2 h). This observation was consistent for all 6 capsules tested. This indicates that an acid-resistant

polymer coating could be used to protect the microspheres from acid dissolution in the stomach.

5.4 Dissolution Conditions for Drug-loaded Microspheres

Dissolution studies were performed according to the British Pharmacopoeia 1998, Dissolution Test Apparatus II (paddle method). Experimental details are described in section 2.11.

5.4.1 Sampling

Sampling was carried out manually every 15 min using a 5 ml syringe withdrawing 5 ml samples from a point halfway between the surface of the dissolution medium and the top of the rotating blade. To the volume maintain constant, an equal volume (5 ml) of dissolution medium (at 37 °C ± 0.5 °C) was replaced in each dissolution vessel following each sample withdrawal. The samples were then filtered with a 1 μm PTFE membrane filter (Acrodisc® CR 25 mm syringe filter, Pall Gelman Laboratory, Portsmouth, UK), and analysed by UV spectrophotometry (Unicam 8625, ThermoSpectronic, Cambridge, UK). The filters were pre-tested to check if they absorb benzamide, by filtering solutions of known benzamide concentrations and measuring the benzamide absorbance before and after filtering. The results showed that the filters do not absorb benzamide. The quantity of drug released at each time point was calculated, allowing for the amount removed by sampling and the progressive dilution of the dissolution medium (see Appendix III for model calculation).

5.4.2 Dissolution Media Preparation

The main dissolution medium used was BP phosphate buffer, pH 6.8. It was freshly prepared using KH_2PO_4 powder, NaOH pellets and deionised water (6.81 g KH_2PO_4 + 0.95 g NaOH per litre of water). 0.1 M HCl was occasionally used as dissolution medium, and it was also freshly prepared by diluting concentrated HCl. All media were degassed by bubbling with helium gas for 1 h before use.

5.4.3 UV Spectrometry Assay and Calibrating Method

The concentration of benzamide was monitored at its λ_{max} using a Unicam spectrophotometer (Unicam Helios α, Cambridge, UK). Its λ_{max} were first determined by scanning its UV absorption in dissolution media, both phosphate buffer and acid, in the range of 200 nm - 320 nm. The λ_{max} of benzamide was found to be 225 nm in the phosphate buffer and 227 nm in the acid.

A stock solution of benzamide (0.02%) was prepared by dissolving 50 mg of benzamide in ~ 200 ml of phosphate buffer, followed by sonication (Fb200b, Decon Labs Ltd., Hove, UK) for 20 min until all particles dissolved, and then adding more phosphate buffer to made up to 250 ml volume . Aliquots of the stock solution were diluted to produce a series of solutions having target concentrations of 0.0004%, 0.0008%, 0.0012%, and 0.0016% w/v of benzamide. The absorbance of these solutions at 225 nm was determined with the Helios spectrophotometer against a pure phosphate buffer blank. The procedure was performed in triplicate, using a new stock solution each time.

The calibration data for UV absorbance of benzamide in 0.1 M HCl at 227 nm was obtained using the same method as described above.

5.4.4 Calibration Data (Benzamide)

The calibration data of benzamide in phosphate buffer, pH = 6.8, and in 0.1 M HCl are shown in Table 5.3 and Table 5.4, respectively. Calibration plots are given in Appendix IV. The calibration plots for benzamide in phosphate buffer and in acid were both found to be linear in the concentration range 0.0000% - 0.0016% w/v. Calibration plots covered a concentration range 0% - 120% of the maximum concentration achievable after full dissolution. The extra 20% coverage was to ensure that the measured results were still valid even when the measured concentration was higher than the expected value. As shown in Table 5.3 and Table 5.4, the calibration data obtained are in good agreement.

Table 5.3 Calibration data of benzamide in BP phosphate buffer, pH=6.8

Calibration Data				
Run	1	2	3	Mean
Intercept	0.0022	0.0021	0.0002	0.0015
Slope	752.00	749.25	763.50	754.92
Regression (r^2)	0.9999	1.0000	1.0000	
SD of the regression	0.0043	0.0029	0.0012	

Table 5.4 Calibration data of benzamide in 0.1M HCl

Calibration Data				
Run	1	2	3	Mean
Intercept	0.0014	0.0016	0.0014	0.0015
Slope	750.50	749.50	751.00	750.33
Regression (r^2)	1.0000	1.0000	1.0000	
SD of the regression	0.0027	0.0020	0.0019	

5.4.5 Controls and Comparisons

As discussed earlier (see section 5.2.1), spray-drying may affect the crystallinity of drugs, which in turn may affect the dissolution rate of drugs. The benzamide as-received and the spray-dried benzamide may have different dissolution rates. This was investigated by comparing the dissolution profile of benzamide release from drug-loaded spray-dried microspheres and benzamide release from spray-dried benzamide. This spray-dried benzamide was prepared by spray-drying 4.5% w/w of benzamide solution in ethanol. In all dissolution tests, a control was also run simultaneously. A control was a capsule that contained drug free microspheres with the same weight content as test capsules.

5.4.6 Determination of Drug Stability

For the dissolution tests to be valid, it is essential that the drugs remain stable. The UV absorbance of freshly prepared benzamide solutions in phosphate buffer (pH = 6.8) and

0.1 M HCl, and the same solutions kept at 37.0 ± 0.5 °C for 24 h were measured at 225 nm and 227 nm. The results showed that benzamide was stable over the dissolution period.

5.4.7 Assessment of Excipients Interference

Soluble and insoluble excipients can potentially interfere with the UV absorbance of drugs. β-TCP (non-sintered and sintered), Eudragit L100 and Dispex A40 in phosphate buffer were individually scanned in the range of λ = 200 nm to 320 nm using the Unicam spectrophotometer. The results showed that these excipients, in the concentrations used, do not interfere with the UV absorbance of the three model drugs.

5.4.8 Dosage Form

Drug-loaded β-TCP microspheres are essentially powders. To perform paddle dissolution tests on a powder, the powder has to be placed in a 'container' so that it can be put at the bottom of a dissolution vessel. Initially, benzamide-loaded microspheres were placed in size 0 hard gelatin capsules. It was found that the capsules have some absorbance at 225 nm, hence, interfering with the UV absorbance of benzamide.

The use of capsules made from other materials, starch and Hydroxypropyl Methylcellulose (HPMC), was then investigated. The starch capsules were found to dissolve readily in the phosphate buffer, and to interfere with benzamide absorbance at 225 nm. HPMC capsules were found not to interfere with absorbance at 225 nm, but it was found that HPMC capsules containing β-TCP microspheres did not dissolve adequately in either phosphate buffer at pH 6.8 or pH 5.8. In the dissolution tests, the HPMC formed a stable gel coating the microspheres. This gel was still present after 24 h for all 12 capsules tested. The agglomerate of gel plus microspheres was collected in a petri dish and examined by visual inspection. With the aid of a spatula, it was verified that the contents of the capsules were dry to the touch, indicating that there had been no contact between the microspheres and the buffer. It was then concluded that HPMC capsules were not suitable for the dissolution tests of the β-TCP matrix in a phosphate buffer.

Other forms of materials, *e.g.* heatsealable filter (Grade 117/3, Papeteries De Cascadec, Scaër, France) and precision woven nylon mesh (50 μm mesh , Lockertex, Warrington, UK) were considered to replace capsules but none of these were found to be capable of confining the fine β-TCP microspheres powder. Therefore, gelatin capsules were continued to be used in dissolution studies. A control consisting of drug free β-TCP microspheres in a gelatin capsule was performed in all dissolution experiments, and the experimental results obtained were then corrected accordingly by deducting the UV absorbance contributed by the gelatin capsules.

5.4.9 Microsphere Stability in Dissolution Medium

To investigate the stability of the microspheres in phosphate buffer dissolution medium, drug-loaded microspheres were subjected to dissolution conditions by soaking them in phosphate buffer at 37°C for 24 h. They were then filtered and dried in the oven at 50 °C overnight. The microspheres were sputter coated and examined under the SEM. The SEM results showed that the microspheres retained their structure after subjection to 24 h of dissolution test conditions. This shows that the microsphere carriers themselves are stable in phosphate buffer for that length of time.

5.5 Loading by Vacuum Method – Preliminary Studies

5.5.1 Loading of Benzamide

To incorporate the model drug, benzamide, into sintered microspheres, a vacuum loading method was investigated. β-TCP microspheres sintered at 1100 °C were used for the initial studies.

20 ml of 3.75% w/v benzamide in ethanol solution was prepared in a 100 ml beaker, and 5 g of sintered microspheres were added. The mixture was then placed in a vacuum oven (Gallenkamp, Loughborough, UK) at 87.5 kPa, at 50 °C overnight to allow for solvent evaporation. The experiment was repeated with 0.75 %w/v of benzamide in water solution. The aqueous benzamide solution has a lower benzamide concentration because benzamide is less soluble in water than in alcohol.

The drug content of the microspheres was determined by spectrophotometry (method see section 2.12). Briefly, drug-loaded samples were placed in 0.1 M HCl and the mixture was sonicated until all microspheres dissolved. The UV absorbance of drug in the final acid solution was determined spectrophotometrically and the results were compared to a calibration plot. The calibration plots for benzamide are shown in Appendix IV. It was possible to calculate the drug loading efficiency because both non-sintered and sintered β-TCP materials were found to dissolve readily in 0.1 M HCl, and their dissolution did not interfere with the chosen identification peak of benzamide in the UV spectrum.

The release of benzamide from these microspheres was studied by dissolution tests as before (method see section 5.4).

5.5.1.1 Results and Discussion

After the complete evaporation of the solvent, the dried samples were found to have a layer of benzamide crystals on the top surface. The crystal layer was removed by means of a spatula and discarded.

The results of drug loading measurements are shown in Table 5.5. Loading solution with a higher drug concentration (3.75% w/v) was found to give a higher percentage drug loading.

Table 5.5 Drug loading (%) of sintered microspheres by a vacuum loading method.

Loading solution	Drug Loading/%, n = 3
3.75 %w/v benzamide in ethanol	4.86 ± 0.62
0.75 %w/v benzamide in water	3.00 ± 0.63

Dissolution results (Figure 5.3) show an instant release of benzamide, and ~ 80% of benzamide was released in the first 15 min. The drug release profiles obtained for both loading solutions were found to be similar, indicating that the drug loading solution being aqueous or ethanolic did not affect drug loading.

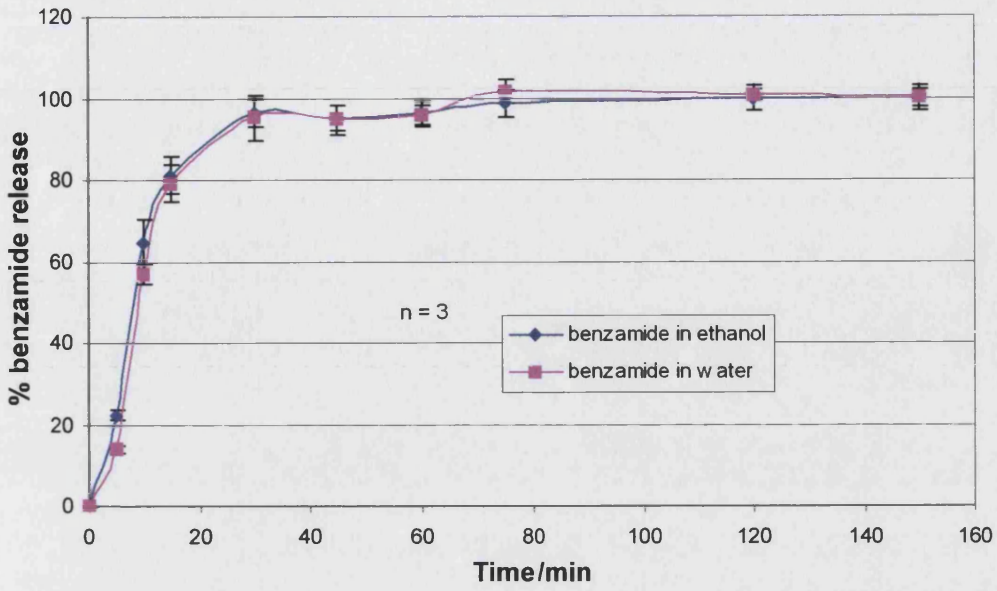

Figure 5.3 Dissolution results of vacuum loaded β-TCP sintered at 1100 °C.

The release of benzamide from the microspheres was instant. The possible reasons for this were considered as follows:

(1) A layer of benzamide was deposited on the microspheres' surfaces, hindering the loading of benzamide into the microspheres;

(2) The pores in the microsphere matrices were too big for delayed release to be achieved, as liquid can freely flow in and out of the pores;

(3) There was a physical incompatibility between β-TCP and benzamide, that interfered with the attachment of benzamide onto the microspheres matrix.

To improve the vacuum loading method, and to investigate the instant release of drug from the microspheres, the next stage of the experiments was designed as follows.

(1) To understand if the instant release of benzamide was due to the drug being only loaded on the outer surface of the microspheres, a stronger vacuum pressure should be applied. This would be to ensure the removal of trapped air inside the microspheres, and the penetration of drug loading solution to the centre of the microspheres. A washing experiment would also be carried out after the drug loading stage to aid removal of benzamide residues on the outer surface of the microspheres.

(2) Sonication would be used as an alternative for removing trapped air inside the microspheres.

(3) To determine the release profile of benzamide from microspheres from a narrow size range, the process of separating by sieving bigger microspheres from fines would be studied.

(4) To investigate the effect of pore-size and surface area on drug release, microspheres sintered at various temperatures would be used.

(5) To study the physical state of benzamide inside the microspheres, and to eliminate the possibility of incompatibilities between benzamide and β-TCP, thermal analysis would be performed.

(6) To investigate if the drug release pattern was drug specific, the release of other model drugs from the microspheres would be studied.

5.5.2 Use of a Stronger Vacuum

It was perceived that it might be advantageous to use a stronger vacuum to ensure the complete removal of trapped air, to facilitate the penetration of loading solution into the microspheres. This was achieved using an Edwards-Pearce Freeze Dryer (EPD3, BOC Edwards, Sussex, UK), with a vacuum chamber that can produce low pressures down to ~ 133 Pa (10^{-1} torr). The vacuum pressure can be manually controlled. Microspheres sintered at 1150 °C were used in this studied. 1.5 g of microspheres sample was soaked in 5 ml of 15% w/v benzamide in ethanol in a 20 ml vial. The vial was placed in the vacuum chamber of the freeze dryer and the vacuum pressure was carefully increased to such a level that air bubbles were released from the microspheres, without the liquid boiling. The vacuum was released when no more bubbles were observed (~ 5 min). The vial was then placed in a vacuum oven at 87.5 kPa at 50 °C overnight for the solvent to evaporate. Triplicate samples were run.

5.5.2.1 Results and Discussion

During vacuuming it was found that the temperature dropped dramatically due to heat loss associated with rapid solvent evaporation, and a small amount of benzamide crystallisation was observed on the surface of the solvent. The solubility of benzamide decreases as the temperature decreases (Figure 5.4). The combination of a decrease in

solvent volume and a decrease in temperature brought the drug solution to supersaturation, and therefore recrystallisation was initiated. Crystallisation is not desirable at this stage because it was perceived that rapid crystal growth would result in crystals mainly formed outside the microspheres.

During solvent evaporation in the vacuum oven, the concentration of benzamide in the solution increased further, and more benzamide crystals were formed, especially on the upper surface of the samples. After complete solvent evaporation, a layer of benzamide crystals was found on the top layer of all the samples, identical to what was observed earlier (section 5.5.1.1). The crystal layers were removed by means of a spatula and discarded. The samples were then subjected to a dissolution test. The dissolution results are shown Figure 5.5. 80% of benzamide was released in the first 50 min. The higher standard deviations observed during the first 15 min of drug release are probably due to the uneven dissolution of the gelatin capsules.

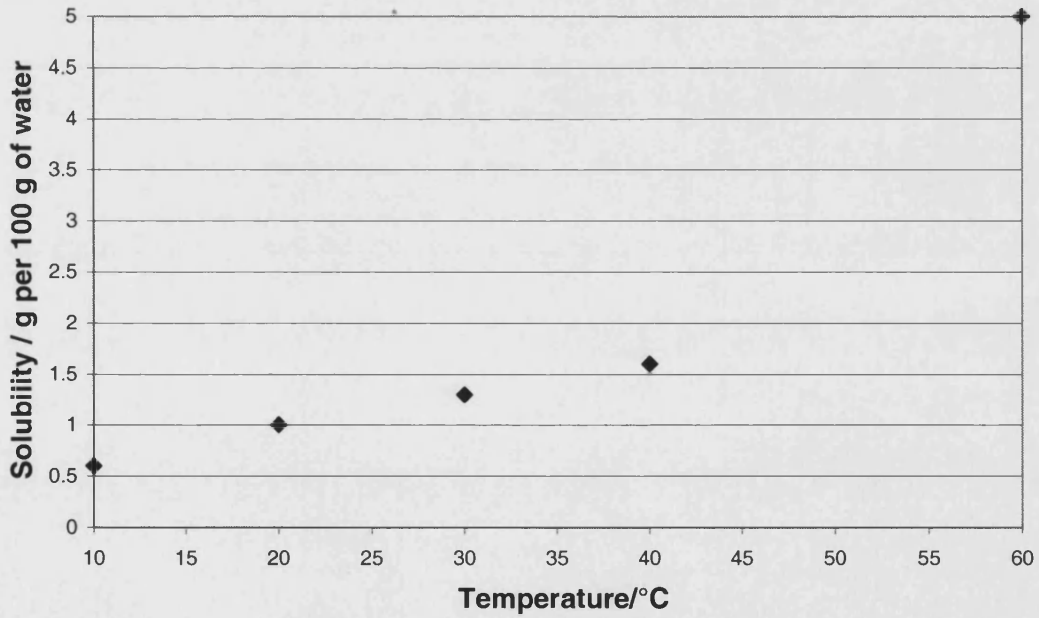

Figure 5.4 Solubility of Benzamide in water (Adapted from Mullin[141])

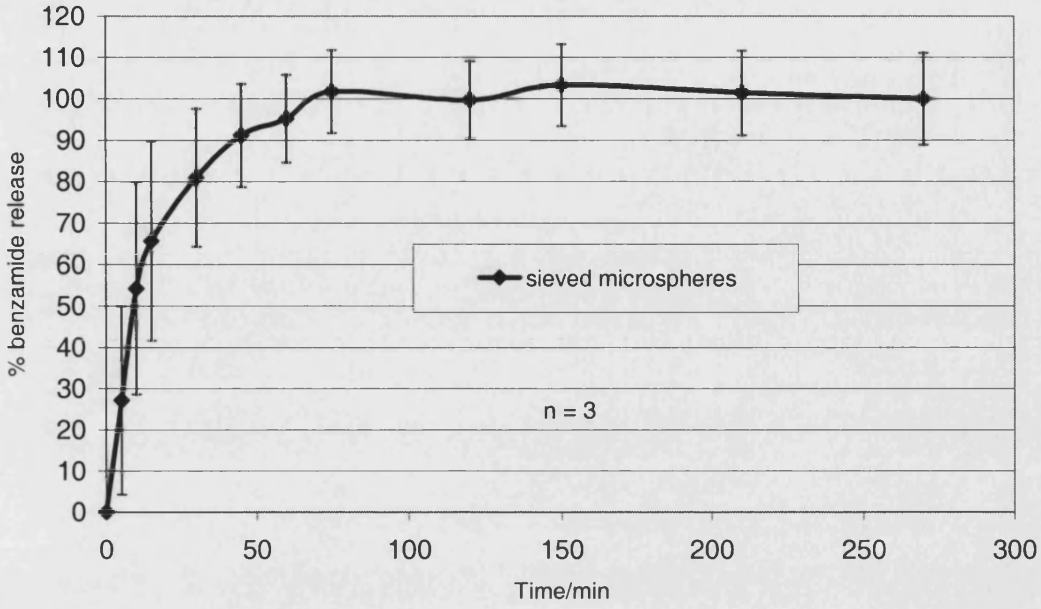

Figure 5.5 Dissolution results of vacuum loading using a freeze dryer.

5.5.3 Surface Drug Removal by Washing

The instant release profile of benzamide in dissolution tests may be because there was a substantial layer of benzamide on the microspheres surfaces. Methods to remove the drugs on the outer surface of microspheres were investigated. Leo *et al.*[142] removed surface drug from polylactic acid microspheres by washing with water, and found the method to be effective. A washing method for the removal of surface drug from β-TCP microspheres was studied.

Since benzamide is more soluble in ethanol than in water, a washing method using ethanol was developed. A batch of β-TCP microspheres sintered at 1100 °C was vacuum loaded with benzamide as before (section 5.5.2). 4 × 0.2 g of benzamide-loaded microspheres were then weighed in four 20 ml vials. 10 ml of ethanol was added to each vial. The vials were then immediately tipped upside down twice manually and left to stand for different lengths of time. The first set of vials [method (a)] was filtered immediately, and an extra 2 ml of ethanol was used in transferring the leftover solids from the vials to the filter. Other vials were left to stand for 1, 3, or 5 min [method (b), (c) and (d)]. The contents of each vial were then filtered through a 3.0

μm filter (Nuclepore®, Kent, UK) into a 250 ml conical flask connected to a tap water vacuum system. During filtering, an extra 10 ml of ethanol was used for transferring leftover solids in the vials to the filter. The filtrates were collected in an aluminium dish (43 cm, Agar Scientific, Stansted, UK) and dried in an oven (Model OV-440, Gallenkamp, Loughborough, UK) at 50 °C overnight. The whole experiment was repeated using a second batch of benzamide-loaded sample.

The amount of benzamide remaining before and after washing was determined by dissolving 0.20 g of microspheres, accurately weighed, in 50 ml of 0.1 M HCl and the drug concentration in the acid determined spectrophotometrically (see section 2.12).

5.5.3.1 Results and Discussion

The benzamide contents before and after washing are shown in Table 5.6. It was found that almost all benzamide was removed from the microspheres during washing. The results obtained for the brief washing of 10 s with 2 ml ethanol (a), are comparable to the results obtained for the longest washing of 5 min with 10 ml ethanol (d). Therefore the washing method (a) was adopted for all experiments as a quick, effective method in removing most of the benzamide from the microspheres' surface.

Table 5.6 Washing experiment results.

		Benzamide content/%	
		Sample 1	Sample 2
	Before washing	4.2	6.1
Washing method	(a) 10 s in 10 ml ethanol + 2 ml ethanol for transferring	0.09	0.08
	(b) 1 min in 10 ml ethanol + 10 ml ethanol for transferring	0.04	0.06
	(c) 3 min in10 ml ethanol + 10 ml ethanol for transferring	0.06	0.04
	(d) 5 min in 10 ml ethanol + 10 ml ethanol for transferring	0.05	0.05

5.5.4 Filtering

The process of evaporating solvent in the oven after vacuum loading was used because:

(1) It was a step for recovering the microspheres from the liquid;

(2) It was thought that evaporation would be advantageous as the drug concentration would increase and more drug would be deposited in the microspheres.

However, as discussed in sections 5.5.1.1 and 5.5.2.1, solvent evaporation results in formation of a layer of benzamide on the surface of the sample. This is undesirable. This step was therefore abandoned, and replaced with a filtration step.

A vacuum loading experiment was carried out using a freeze dryer as in section 5.5.2. The solids were then filtered immediately through a 3.0 μm filter (Nuclepore®, Kent, UK) into a 250 ml conical flask connected to a tap water vacuum system. The filtered solids were then dried in an oven overnight at 50 °C. To remove benzamide on the outer surface of the microspheres, a washing experiment [see section 5.5.3, washing method (a)] was also carried out. The drug contents of the microspheres before and after the washing experiment were determined (method see section 2.12). The experiment was repeated using microspheres sintered at 900°C, 1000 °C, 1150°C, and 1200 °C. Five replicates were produced for each sample.

5.5.4.1 Results and Discussion

Using filtration, no built up of drug crystals layers on the surface of the microspheres samples was observed. The drug content of the dried microspheres is shown in Table 5.7. It was found that the amount of drug-loaded onto the microspheres decreases with increases of the sintering temperature of the microspheres. After the washing experiment, almost all benzamide was removed from the microspheres, with microspheres sintered at 900 °C retaining the most drug.

Table 5.7 Benzamide content of microspheres, before and after washing.

	% Benzamide loading, n=5	
Microspheres sintered at	Before washing/%	After washing/%
900 °C (n = 3)	6.66 ± 0.77	0.09 ± 0.02
1100 °C (n = 5)	2.90 ± 0.61	0.03 ± 0.00
1150 °C (n = 5)	0.81 ± 0.35	0.03 ± 0.00
1200 °C (n = 2)	0.80 ± 0.13	0.02 ± 0.00

5.5.5 Sonication

It was perceived that sonication might be an alternative way of releasing trapped air in microspheres, and assisting the penetration of drug loading solution.

To investigate the feasibility of this method, firstly, the effect of sonication on microspheres itself was studied. β-TCP microspheres sintered at 1000 °C and 1100 °C were placed in water and subjected to 10 min sonication (Jenway Fb300b, Hove, UK). These microspheres, before and after sonication, were studied under the SEM.

Samples of microspheres sintered at 1100 °C were soaked in 15% w/v benzamide in ethanol and then sonicated for 30 s. The product was then filtered (3.0 μm filter, Nuclepore®, Kent, UK) and dried in the oven at 50 °C overnight. The benzamide release profile from these microspheres was then studied using dissolution tests.

5.5.5.1 Results and Discussion

Under the SEM, the sonicated microspheres appeared intact, indicating that the sintered microspheres were strong enough to maintain their structure under the sonication process. The dissolution results showed that all the benzamide was released instantly, with all drug in ~ 15 min. As sonication did not improve the drug release profiles, it was discontinued.

5.5.6 Sieving

It was perceived that microspheres with various pore-sizes might release drug in different rates. To study the drug release profile from microspheres of a narrow size range, attempts were made to separate the larger sintered microspheres from the fines by sieving. Microsphere samples sintered at 1100 °C were sieved with a 32 μm metal sieve. The sieved and retained products were then observed under the SEM.

5.5.6.1 Results and Discussion

It was found that sieving sintered microspheres was harder than sieving non-sintered samples (see section 3.7.6 for sieving of non-sintered microspheres). This is because the sintered microspheres aggregated more extensively. SEM examination showed that the sieving process was not effective in separating the bigger microspheres from the fines. Therefore, the method was discontinued.

5.5.7 Pre-Vacuuming

The loading methods described so far (section 5.5.1 and section 5.5.2) extracted the trapped air within the microspheres after they had been submerged in drug solution. It was perceived that if a vacuum is applied before the drug solution is introduced, trapped air could be better eliminated.

To enable a pre-vacuum action, the set up illustrated in Figure 5.6 was assembled. A sample of microspheres sintered at 1150 °C was placed in a quick-fit round bottom flask. A vacuum pump was run for few minutes to create a vacuum in the flask before the benzamide solution (15 %w/v in ethanol) was introduced by means of a syringe over a rubber stopper. Vacuum pumping was continued for 10 min after the addition of the benzamide solution. The sample was left overnight, and then filtered (3 μm Nucleopore® filter). The drug loading efficiency was determined (method see section 2.12) and dissolution studies (method see section 5.4) were also performed.

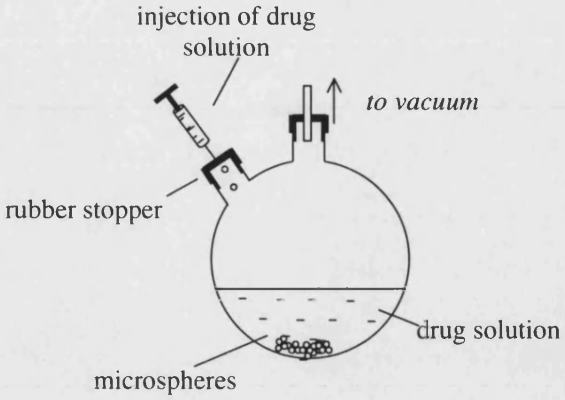

Figure 5.6 Schematic diagram of glass set up which allows pre-vacuuming.

5.5.7.1 Results and Discussion

A diamond shape benzamide crystal was found at the bottom of the round flask. The crystal was removed and the drug content determined is shown below:

Sample sintered at	Drug content/%	
	Before washing	After washing
1150 °C	3.90	0.02

The dissolution results showed that ~ 80% benzamide was released in the first 15 min.

In all the experiment conducted so far, drug contents < 7% before washing were obtained, and instant drug release in dissolution tests was observed. Almost all drugs were removed during washing, indicating that liquid penetrates into the microspheres freely.

5.5.8 Increased Temperature

To increase drug loading, it was then considered to conduct the drug loading experiments at higher temperatures. This is because a higher concentration of drug loading solution can be prepared at higher temperature, and higher drug loading solution has been shown to produce higher drug loading in microspheres (section 5.5.1.1). Furthermore, if the temperature of the loading equipment could be controlled,

by cooling the system after drug loading controlled drug crystallisation inside the pores might be encouraged.

The solubility of benzamide increases as the temperature increases, and the increase is exponential above ~ 40 °C (Figure 5.7, see also Figure 5.4 for zooming in of graph for solubility below 60°C). Therefore, by increasing the experimental temperature above 60 °C, benzamide solutions of much higher concentrations could be produced.

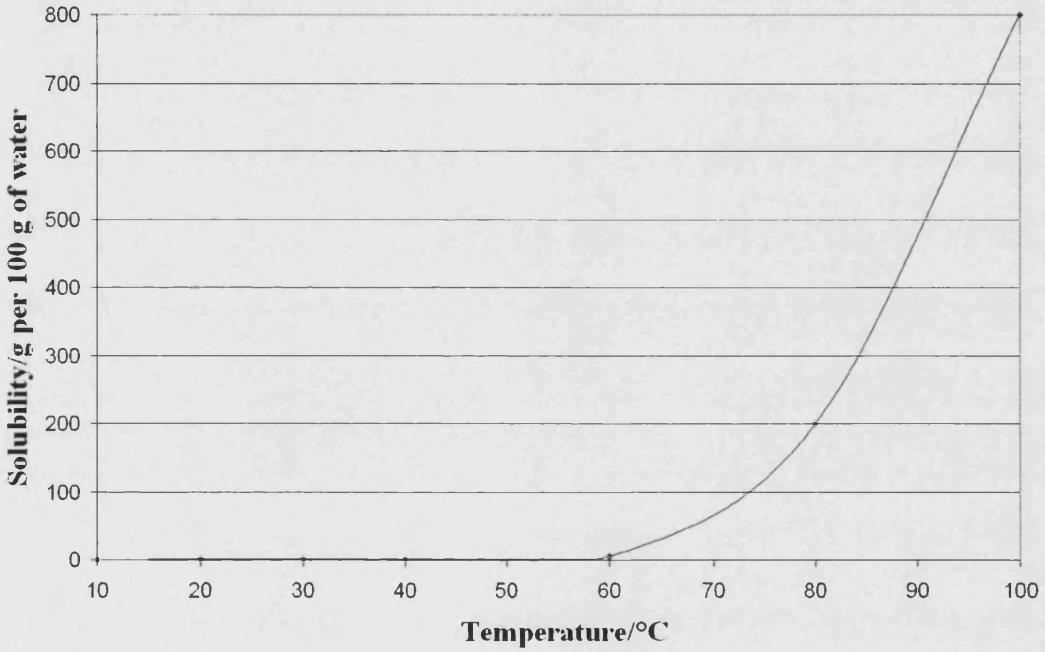

Figure 5.7 Solubility of Benzamide in water (adapted from Mullin[141]).

A set-up was assembled to allow vacuum loading experiments to be performed at controlled temperatures. The set-up is shown in Figure 5.8, and schematically represented in Figure 5.9.

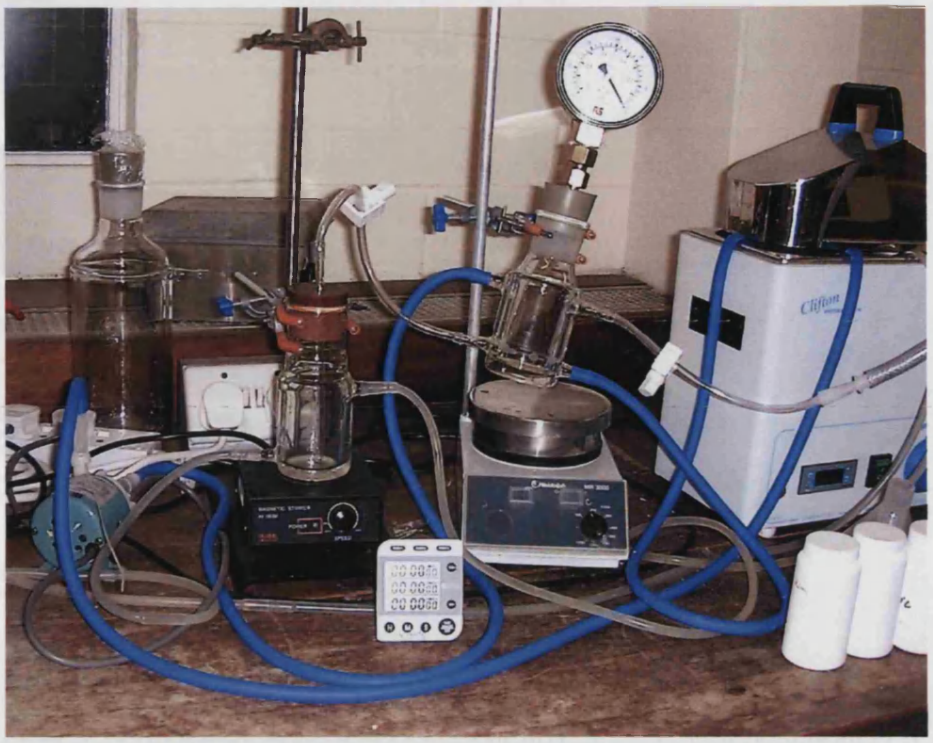

Figure 5.8 Photograph of the set-up assembled for vacuum loading experiments.

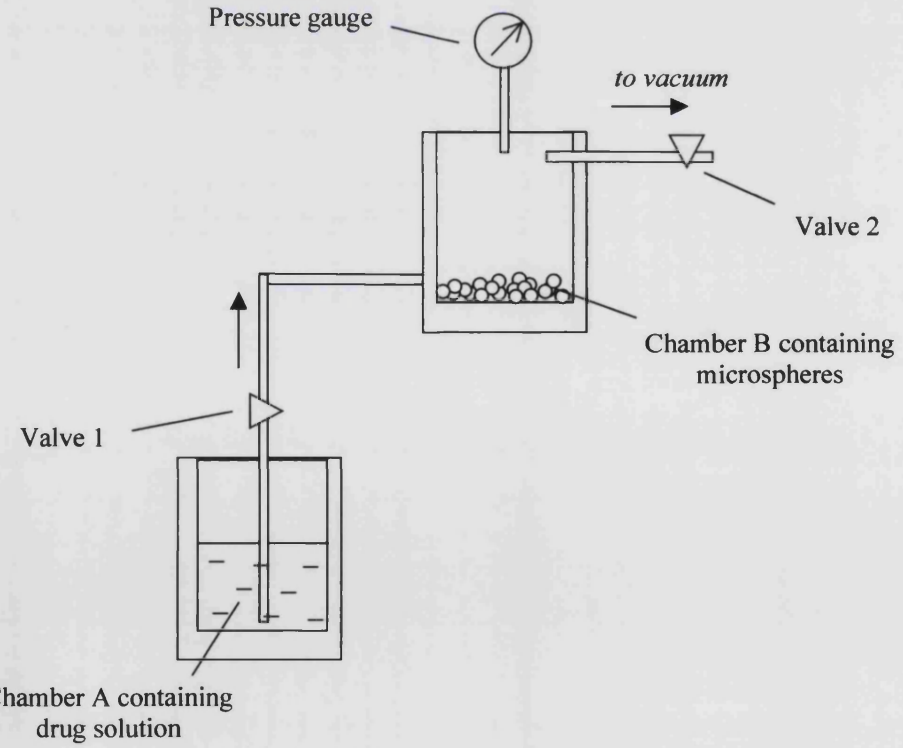

Figure 5.9 Schematic diagram of the set-up assembled for vacuum loading experiments.

The set-up consists of two chambers, A and B, which are connected via tubing with a valve (valve 1). Chamber A is the drug solution chamber; chamber B is the loading chamber where microspheres are placed. Chamber B is also connected to a vacuum pump (40 l/min) with a valve (valve 2). A pressure gauge is coupled to chamber B to monitor the loading vacuum pressure inside the chamber.

The desirable features of this set-up are:

(1) The chambers are water jacketed to allow temperature control;
(2) It has a large loading chamber (~ 200 ml volume), therefore a larger amount of sample can be loaded at any one time;
(3) It allows pre-vacuuming, *i.e.*, a vacuum can be applied to the sample before introducing the drug solution;
(2) Transparent glassware means that all the experiment process can be directly observed visually.

5.5.8.1 Loading Procedure at Increased Temperature

Before a loading experiment, the glass equipment was warmed up by circulating water at 50 °C around both chambers for ~ 15 min. The tubing connecting chamber A to valve 1 was then pre-filled with drug solution to ensure that there was no trapped air in the tubing. This was achieved as follows.

- Firstly, a drug solution was placed in chamber A;
- Secondly, low-pressure was created in chamber B by running the vacuum pump while valve 1 is closed and valve 2 is opened;
- Thirdly, valve 2 was closed, and valve 1 was carefully opened to allow the drug solution from chamber A to reach valve 1.

The temperature of circulating water in the water jackets (± 0.1°C) was controlled by a refrigerated circulator (DC5-K20, Thermo Haake, Karlsruhe, Germany).

A drug loading experiment using benzamide was performed at 50 °C. The temperature was chosen because the solubility of benzamide increase dramatically above ~ 40 °C. A drug solution of 35% w/v of benzamide in ethanol was placed in chamber A. 1.25 g of microspheres sintered at 1150 °C was placed in chamber B. While the vacuum pump was running, valve 2 was opened for ~ 5 min to create a low-pressure in the chamber

and then closed, whilst valve 1 was opened briefly for sufficient quantity of benzamide solution to enter chamber B to immerse all the microspheres. Valve 2 was then re-opened for 10 min until no bubbles could be observed rising from the sample. During this period, chamber B was gently tapped by hand to loosen trapped air. Two filtering procedures were carried out as follows:

(a) Filtering Procedure I

Half the sample was filtered with a sintered glass filter (porosity 4, BDH Laboratory Supplies, Poole, UK) into a 250 ml conical flask connected to a tap water vacuum system. The filtrate collected on the glass filter was scraped into an aluminium dish (43 cm, Agar Scientific, Stansted, UK) using an aluminium spatula and dried in an oven (Model OV-440, Gallenkamp, Loughborough, UK) at 50 °C overnight.

(b) Filtering Procedure II

The other half of the sample was poured into ~ 20 ml of water at room temperature and then immediately filtered and dried as described in Filtering Procedure I.

The experiment was performed in duplicate. Washing experiments [section 5.5.3 method (a)] and preliminary dissolution tests were also performed.

5.5.8.1.1 Results and Discussion

The % benzamide loading before and after the washing stage is shown in Table 5.8.

Table 5.8 % benzamide loading of microspheres using Filtering Procedure I and II, before and after the washing stage.

Sample 1150 °C, n = 2	Mean Drug content before washing/%	Mean drug content after washing/%
Filtering Procedure I	7.20	0.05
Filtering Procedure II	0.16	0.04

At 50 °C, a benzamide solution of high concentration (35% w/v) can be prepared, and a 7.2% drug loading (Filtering Procedure I) was obtained. This was the highest

benzamide loading achieved until then. Dissolution tests showed that the release of benzamide from these microspheres was instant, with > 90% drug release in the first 15 min.

It was observed that tiny benzamide crystals were formed, both on the surface of the microspheres and on the filter using Filtering Procedure I. It was suggested that recrystallisation happened immediately when temperature dropped during filtering. To avoid crystallisation happening during filtering, Filtering Procedure II was used. Results showed that after immersion in water, the percentage loading was dramatically reduced, from 7.20% to 0.16%.

5.5.9 DSC Analysis

DSC analysis is frequently used to investigate interactions between a drug entity and excipients during the preformulation stage. To investigate possible interactions between benzamide and sintered β-TCP surfaces and to study the physical state of benzamide inside the sintered calcium phosphate microspheres, DSC analysis was performed. The experimental methods are described in section 2.9. Benzamide as-received; sintered β-TCP microspheres (at 1100°C); physical mixture of benzamide and sintered β-TCP microspheres (20:80); and benzamide-loaded sintered microspheres were analysed. Each sample was analysed in triplicate.

5.5.9.1 Results and Discussion

The DSC thermograms obtained are shown in Figure 5.10. Under the experimental conditions, no DSC peaks were observed for the β-TCP sintered microspheres material. An endothermic sharp peak at the melting point of benzamide at ~128 °C was observed for benzamide as-received, physical mixture of benzamide and β-TCP sintered microspheres, and benzamide-loaded sintered β-TCP microspheres. This suggests that benzamide remained in a crystalline form in the physical mixture of benzamide-microspheres, and after it was loaded into microspheres. The results show that there are no physical and no chemical interactions between benzamide and the sintered β-TCP material. It was concluded that β-TCP is a compatible carrier for benzamide.

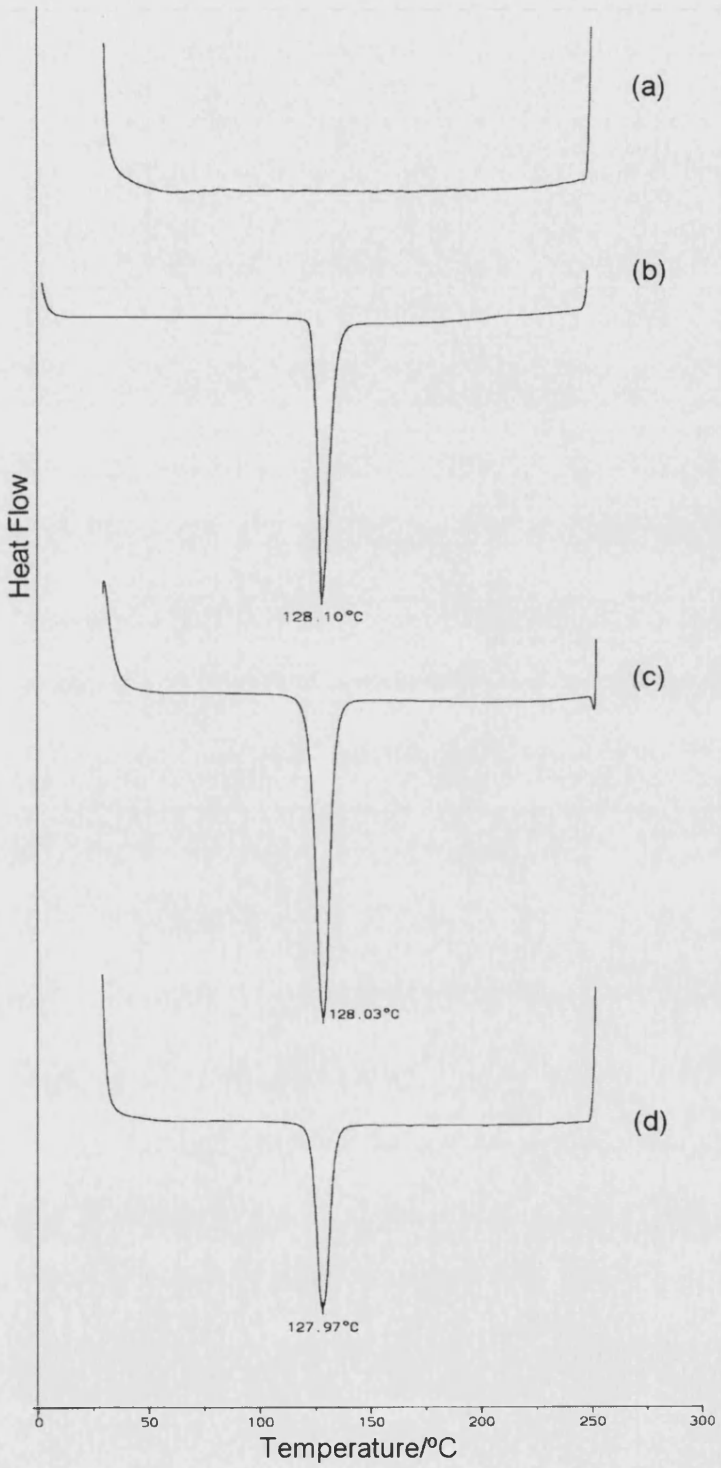

Figure 5.10 DSC thermograms obtained of (a) β-TCP microspheres sintered at 1100°C; (b) benzamide as-received; (c) physical mixture of benzamide and sintered β-TCP microspheres (20:80); and (d) benzamide-loaded β-TCP microspheres.

5.6 Loading of Propranolol

5.6.1 Model Drug - Propranolol.HCl

The incorporation of a second model drug, (RS)-propranolol hydrochloride (HCl), into the microspheres was studied. Propranolol.HCl was chosen because:

1. Propranolol.HCl is more soluble in water than benzamide (~ 4 times more soluble), therefore a higher concentration of drug solution can be prepared for loading experiments at room temperature;
2. Propranolol.HCl has a λ_{max} at 289 nm in phosphate buffer. Therefore it does not interfere with gelatin absorption as gelatin absorbs at $\lambda < 228$ nm in the UV spectrum.

Propranolol.HCl is a synthetic non-selective beta-adrenergic receptor blocking agent. It is clinically used in the management of hypertension, angina pectoris, cardiac arrhythmias and myocardiac infarction. The physicochemical properties of propranolol.HCl are listed in Appendix II.

5.6.2 Vacuum Loading

Propranolol.HCl was vacuum loaded into microspheres using the set-up described in section 5.5.8 (see Figure 5.8). A loading solution of 5% w/v propranolol.HCl. in water was placed in chamber A. About 5 g of microspheres to be loaded were placed in chamber B. The loading procedure was similar to the loading procedure of benzamide in section 5.5.8.1 but was performed at room temperature. While valve 1 was closed and valve 2 was opened, chamber B was evacuated for 5 min and the pressure gauge indicated that the vacuum pressure inside the chamber was - 95 kPa. Subsequently, valve 2 was closed and valve 1 was opened briefly to allow sufficient propranolol.HCl solution from chamber A to enter chamber B to immerse all the microspheres. Valve 2 was then re-opened for 10 min until no further bubbles could be observed rising from the sample. During this period, chamber B was then gently tapped manually, to release air trapped between the microspheres. The loaded microspheres were then poured into a glass jar and left overnight for the system to reach equilibrium.

The propranolol.HCl-loaded microspheres were then filtered using a sintered glass filter into a 250 ml conical flask connected to a tap water vacuum system. The filtrate collected on the glass filter was scraped into an aluminium dish and dried in an oven at 50 °C overnight.

The loading experiments were performed using samples of microspheres sintered at 900 °C, 1000 °C, 1100 °C, 1150 °C and 1200 °C. Experiments were performed in triplicates using three different batches of spray-dried microspheres.

Attempts were made to load drug into non-sintered microspheres in the same way. However, it was found that non-sintered samples were too frail to stand the pre-vacuum suction.

The percentage propranolol.HCl loading of the microspheres was determined (method see section 2.12). Three replicates were performed for each sample.

5.6.2.1 Results and Discussion

The results obtained (Table 5.9) show that the percentage drug loading decreases as the temperature at which the microspheres were sintered increases. This finding is consistent for all three batches of microspheres studied. With microspheres sintered at 900 °C the highest drug loading at ~ 5.6% was obtained, while with microspheres sintered at 1200 °C the lowest drug loading at ~ 1.4% was obtained. All percentage loadings are calculated in weight. If the percentage loadings were calculated in volume, these values would become ~ 3 times higher because sintered β-TCP has a high density of ~ 3 g/cm^3. It was found that these percentage loading results correlate with the specific surface area of the microspheres (see section 4.4.4.1 for surface area results). Comparisons between the percentage loadings and the surface area of the microspheres are shown in Table 5.10. A plot of specific surface area versus % drug loading is shown in Figure 5.11. The calculated regression coefficient, r^2, has a value of 0.8943, indicating a very strong correlation between surface area and percentage drug loading. These results suggest that propranolol.HCl was adsorbed on the matrix surfaces, including internal surfaces, of the microspheres. The results also confirm that the vacuum loading method has successfully introduced the drug solution into the internal

area of the porous microspheres. On close examination, the data point for samples sintered at 900 °C appears to be a rogue value in the graph. When this point is not considered, the calculated r^2 value reaches a near unity of 0.9997 (Figure 5.12). According to this regression line, the percentage drug loading for microspheres sintered at 900 °C achieved a lower value than expected. The reason for this is unknown.

Table 5.9 Results of loading percentage of propranolol.HCl into microspheres sintered at different temperatures.

	Percentage loading ± SD/ % (w/w)		
Samples sintered at	Batch 1, n = 3	Batch 2, n = 3	Batch 3, n = 3
900 °C	6.69 ± 1.63	5.37 ± 0.74	4.98 ± 0.39
1000 °C	4.60 ± 0.75	5.17 ± 0.22	4.51 ± 0.17
1100 °C	1.99 ± 0.22	2.35 ± 0.03	2.65 ± 0.23
1150 °C	1.36 ± 0.06	2.17 ± 0.06	1.73 ± 0.02
1200 °C	1.39 ± 0.30	1.43 ± 0.05	1.44 ± 0.05

Table 5.10 Comparisons between the percentage loading of propranolol.HCl and surface area of sintered microspheres.

Samples sintered at	Propranolol.HCl loading ± SD/%, n = 9	Surface Area ± SD/$m^2 g^{-1}$, n = 5
900 °C	5.67 ± 1.20	5.97 ± 0.15
1000 °C	4.76 ± 0.51	2.91 ± 0.05
1100 °C	2.32 ± 0.33	1.17 ± 0.02
1150 °C	1.75 ± 0.35	0.73 ± 0.02
1200 °C	1.42 ± 0.16	0.54 ± 0.00

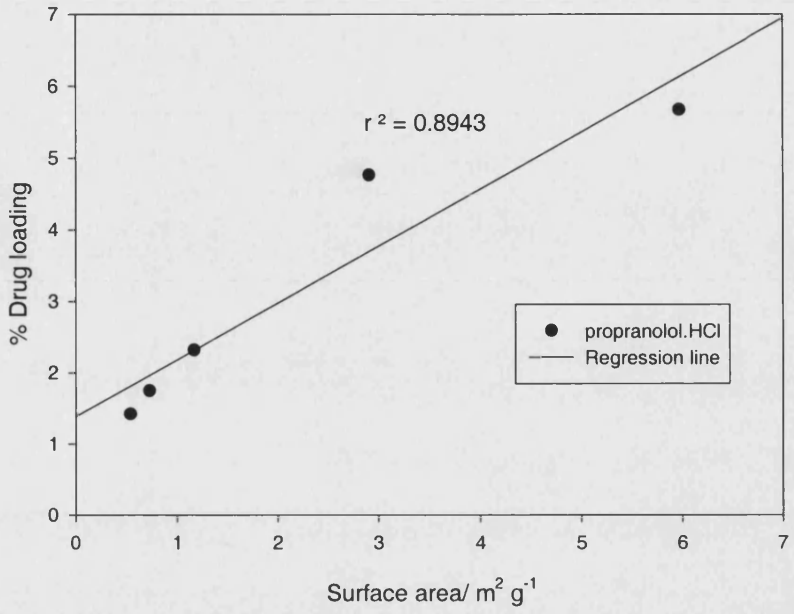

Figure 5.11 Regression line of microspheres' surface area vs. % propranolol.HCl loading.

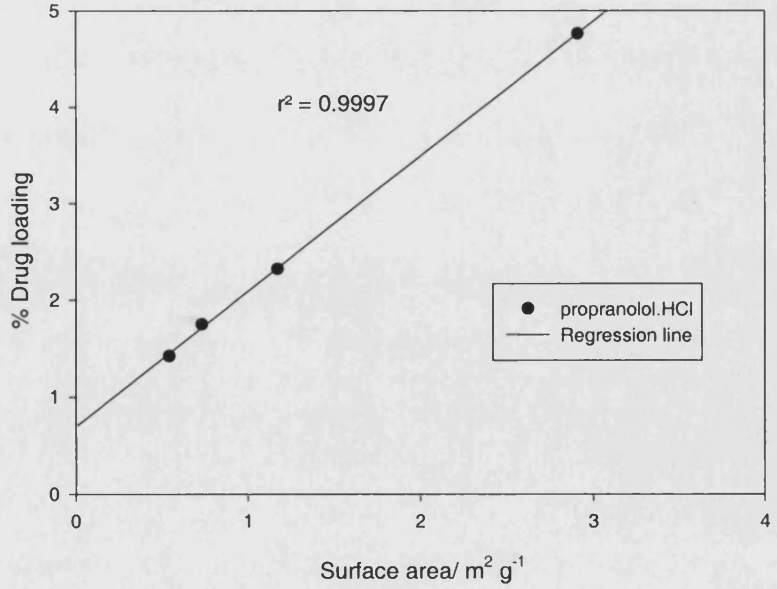

Figure 5.12 Regression line of microspheres' surface area vs. % propranolol.HCl loading, excluding the point contributed by microspheres sintered at 900 °C.

5.6.3 Modified Vacuum Loading Methods

Aiming to increase the percentage drug loading, three modified drug loading methods were investigated:

Method 1 – Successive loading

Method 2 – Increased temperature

Method 3 – Crystal growth

5.6.3.1 Method 1 - Successive Loading

It was proposed that by exposing previously drug-loaded microspheres to drug solution for a second time, a second layer of drug might be deposited in the microspheres and therefore a higher total percentage drug loading could be achieved. The propranolol.HCl-loaded microspheres (Batch 3 in section 5.6.2) were subjected to a second cycle of loading experiments. The loading method and conditions used were the same as those in section 5.6.2. Experiments were performed in duplicate for each sample. Percentage drug loading for these samples was then determined (method see section 2.12).

5.6.3.1.1 Results and Discussion

The percentage propranolol.HCl loading of the successively loaded microspheres is shown in Table 5.11. The results show that there is no consistent drug loading increment after a successive drug loading experiment. The reason for this might be that the propranolol.HCl loading solution used was not a saturated solution**. During the second loading process, the drug-loaded in the first time might have re-dissolved into the loading solution to establish equilibrium. This would explain why the total amount of drug loading did not increase after the second loading.

** The solubility of propranolol.HCl at normal laboratory temperature (~ 22 °C) was found to be 11.4 %w/v . Therefore, a 5% w/v drug loading solution was far from saturation.

Table 5.11 Percentage propranolol.HCl loading of successive loading experiments.

Samples sintered at	% Drug loading ± SD		
	After 1st loading, n=3	After 2nd loading, n=3	
	Batch 1	Successive Batch A	Successive Batch B
900 °C	4.98 ± 0.39	4.06 ± 1.01	4.28 ± 0.04
1000 °C	4.51 ± 0.17	3.23 ± 0.13	3.48 ± 0.02
1100 °C	2.65 ± 0.23	3.28 ± 0.27	2.70 ± 0.04
1150 °C	1.73 ± 0.02	1.59 ± 0.02	2.44 ± 0.09
1200 °C	1.44 ± 0.05	1.81 ± 0.14	1.96 ± 0.16

5.6.3.2 Method 2 – Increased Temperature

It has been shown in section 5.5.8 that by increasing the loading temperature, a higher concentration of benzamide loading solutions could be prepared, resulting in higher benzamide loading into the microspheres. To obtain higher drug loading for propranolol.HCl, the same concept was applied.

5.6.3.2.1 Production of a High Concentration Propranolol.HCl Solution

A high concentration propranolol.HCl solution was prepared by dissolving 170 mg propranolol.HCl in 500 ml deionised water at 60 °C, using a magnetic stirrer. The temperature of the system was then cooled down to 45 °C. No re-crystallisation was observed during the cooling process by visual observation. The solution was then filtered through a 0.02 μm filter (Nalgene MF75 with polyethersulphone filter, Nalge Nunc International Co., Rochester, NY, USA), with the aid of a hair dryer blowing hot air to prevent re-crystallisation due to temperature drops. The filtered solution was then placed in a water jacketed sealed flask and maintained at 45 °C.

The accurate concentration of the propranolol.HCl solution prepared was determined as follows. An accurately weighed amount of the propranolol.HCl solution (15 g) was left in a dark cupboard at room temperature for 5 days, until all the water evaporated, and then placed in an oven at 50 °C for 2 days. The weight of the propranolol.HCl crystals

collected was then determined. The concentration of the propranolol.HCl solution was found to be 26.65% w/w.

5.6.3.2.2 Vacuum Loading

Using the prepared high concentration propranolol.HCl solution as loading solution, drug loading experiments were performed as before (section 5.6.2) but at 45 °C. Microsphere samples sintered at 900 °C and 1150 °C were used. The percentage drug loading was then determined (method see section 2.12).

5.6.3.2.3 Results and Discussion

The results of percentage drug loading obtained are shown in Table 5.12. Compared to loading at room temperature (section 5.6.2, drug loadings of 5.67% and 1.75% were obtained for microspheres sintered at 900 °C and 1150 °C, respectively), much higher drug loadings were obtained (drug loadings of 26.7% and 12.0% were obtained for microspheres sintered at 900 °C and 1150 °C, respectively). These experimental results are in accordance with previous findings (section 5.5.8.1.1, using benzamide) that a more concentrated drug loading solution produced a higher drug loading microspheres, and microspheres sintered at a higher temperature achieved a lower drug loading.

Table 5.12 Percentage drug loading obtained using high concentration propranolol.HCl solution.

Samples sintered at	Propranolol.HCl loading (% w/w)
900 °C	26.7
1150 °C	12.0

5.6.3.3 Method 3 – Crystal Growth

As discussed earlier (section 5.6.2.1), the total surface area of the microspheres, including internal surface of the porous matrix, was found to correlate with the amount of drug-loaded into the microspheres. This shows that by using the vacuum loading method, drugs are deposited or adsorbed on the matrix of the microspheres.

It was then perceived that if the pores of the microspheres could be filled with drugs crystals, the percentage drug loading could be increased dramatically. Furthermore, such a system itself could also serve as a basis of a controlled release system - the porous area of the microspheres being the drug reservoirs. Drug near the opening of the pores would be released first, and drug deeper in the pores would be released later.

Attempts were made to grow drug crystals within the pores of the microspheres. Concepts of crystallisation, crystal growth, and the experiments carried out to grow propranolol.HCl crystals inside the microspheres are detailed in section 5.9.

5.6.4 Dissolution Studies

The drug release profiles of propranolol.HCl from propranolol.HCl-loaded microspheres using vacuum loading (section 5.6.2), and modified vacuum loading (Method 1, 2 and 3 in section 5.6.3) methods were studied by dissolution test. The conditions used were the same as those used for benzamide-loaded microspheres (section 5.4). Sampling was carried out using an automatic set-up. At programmed intervals, the solution was pumped automatically through 5 μm filters (Pharma Test, Hainburg, Germany) using a peristaltic pump (C8-midi, Watson-Marlow AliteaAB, Stockholm, Sweden) under the control of a valve machine (Ven-At, Pharma Test, Hainburg, Germany) that allows for dissolution medium to flow into a flow through cell in a spectrophotometer (Unicam 8625, Cambridge, UK). The absorbance of the medium was then measured at 289 nm. The flow rate of the pump was calibrated every week. The drug release data were calculated automatically by WinDiss 4.106 software (Pharma Test, Hainburg, Germany) based on a previously constructed referenced calibration curve (see section 5.6.4.1).

Each dissolution unit consisted of 500 mg of drug-loaded microspheres placed in a size 0 gelatin capsule, unless otherwise stated. The dissolution medium was phosphate buffer. In each dissolution run, 5 capsules of the drug-loaded samples and a control (a capsule contained drug free microspheres) were run.

The release profiles of propranolol.HCl from microspheres were compared to dissolution profiles of propranolol.HCl crystals which had been treated as follows.

Propranolol.HCl as-received was first dissolved in water. The drug crystals were then recovered by evaporating the water off in an oven at 50 °C. The dried crystals were crushed with a mortar and pestle. A control runs of these treated propranolol.HCl crystals was used as a control instead of propranolol.HCl powder as-received. This is because it was perceived that their crystallographic nature would be closer to the propranolol.HCl deposited in the microspheres, since the drug undergoes dissolution and re-crystallisation during the loading experiments. The dissolution studies of 6 capsules each containing 30 mg of the treated propranolol.HCl crystals, were performed.

5.6.4.1 Calibration Method

The λ_{max} of propranolol.HCl in phosphate buffer, pH = 6.8, and in 0.1 M HCl was found to be 289 nm and 290 nm respectively, when its absorbance was scanned from 200 nm to 320 nm (Unicam Helios α spectrophotometer, Cambridge, UK). These λ_{max} were then used to monitor the concentration of propranolol.HCl in the respective media.

A stock solution of propranolol.HCl (0.05%) was prepared by dissolving 50 mg of propranolol.HCl, accurately weighed, into ~ 80 ml of BP phosphate buffer, pH = 6.8, and then the solution was made up to 100 ml final volume. Aliquots of the stock solution were diluted to produce a series of solutions having target concentrations of 0.001%, 0.002%, 0.003%, 0.004%, and 0.005% w/v of propranolol.HCl. The absorbance of these solutions was determined at 289 nm. The procedure was performed in triplicate, using a new stock solution each time. The calibration data of propranolol.HCl in 0.1 M HCl were also obtained using the same method measuring at λ = 290 nm.

5.6.4.2 Calibration Data (Propranolol.HCl)

The calibration data of propranolol.HCl in phosphate buffer, pH = 6.8, and in 0.1 M HCl are shown in Table 5.13 and Table 5.14, respectively. Calibration plots are given in Appendix IV. The calibration plots in phosphate buffer and in acid were both found to be linear in the concentration range of 0.000% - 0.005% w/v.

Table 5.13. Calibration data of propranolol.HCl in BP phosphate buffer, pH=6.8.

Calibration Set				
	1	2	3	Mean
Intercept	0.0027	0.0022	0.0147	0.0065
Slope	192.00	192.29	190.20	191.50
Regression (r^2)	1.0000	1.0000	0.9976	
SD of the regression	0.0023	0.0025	0.0192	

Table 5.14 Calibration data of propranolol.HCl in 0.1 M HCl.

Calibration Set				
	1	2	3	Mean
Intercept	0.0018	0.0032	0.0043	0.0031
Slope	192.14	191.97	190.09	191.40
Regression (r^2)	1.0000	1.0000	1.0000	
SD of the regression	0.0015	0.0025	0.0031	

5.6.4.3 Determination of Drug Stability

The UV absorbance of freshly prepared propranolol.HCl in a phosphate buffer, before and after they were kept at 37 °C ± 0.5 °C for 10 h were measured. The results show that propranolol.HCl is stable over the dissolution period.

5.6.4.4 Dissolution Results

The dissolution results of vacuum loading at room temperature (section 5.6.2) of the three batches of microspheres sintered at various temperatures are shown in Figure 5.13, Figure 5.14 and Figure 5.15. The results show that the propranolol.HCl release from microspheres is slightly slower than the dissolution of pure propranolol.HCl. However, most of the drug was generally released quickly. ~ 50% of the drug was released in the first 20 min, and almost all drug was released in 150 min. There are no marked differences between the release profiles of the propranolol.HCl from microspheres sintered at different temperatures.

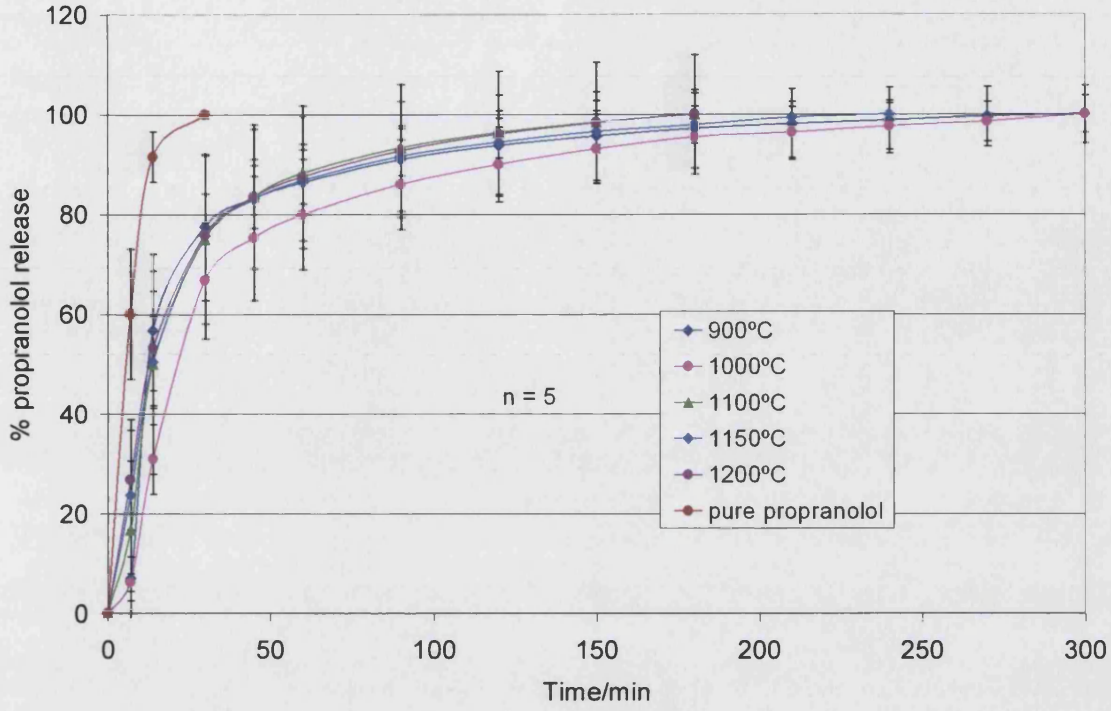

Figure 5.13 Dissolution results for Batch 1 microspheres sintered at various temperatures as indicated.

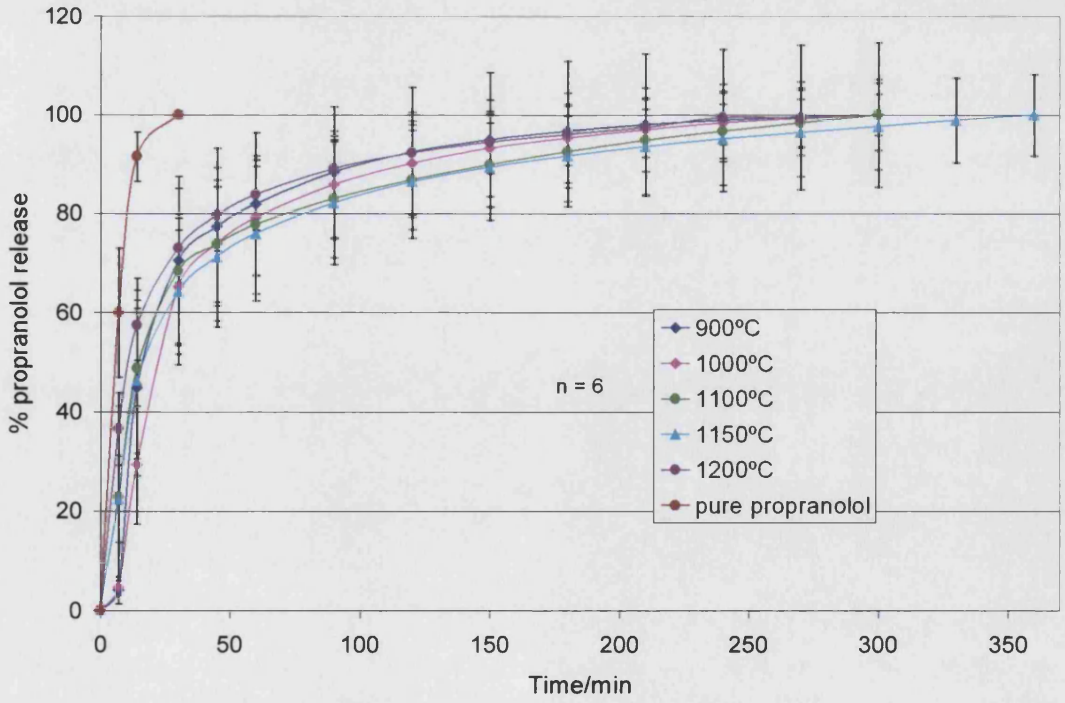

Figure 5.14 Dissolution results for Batch 2 microspheres sintered at various temperatures as indicated.

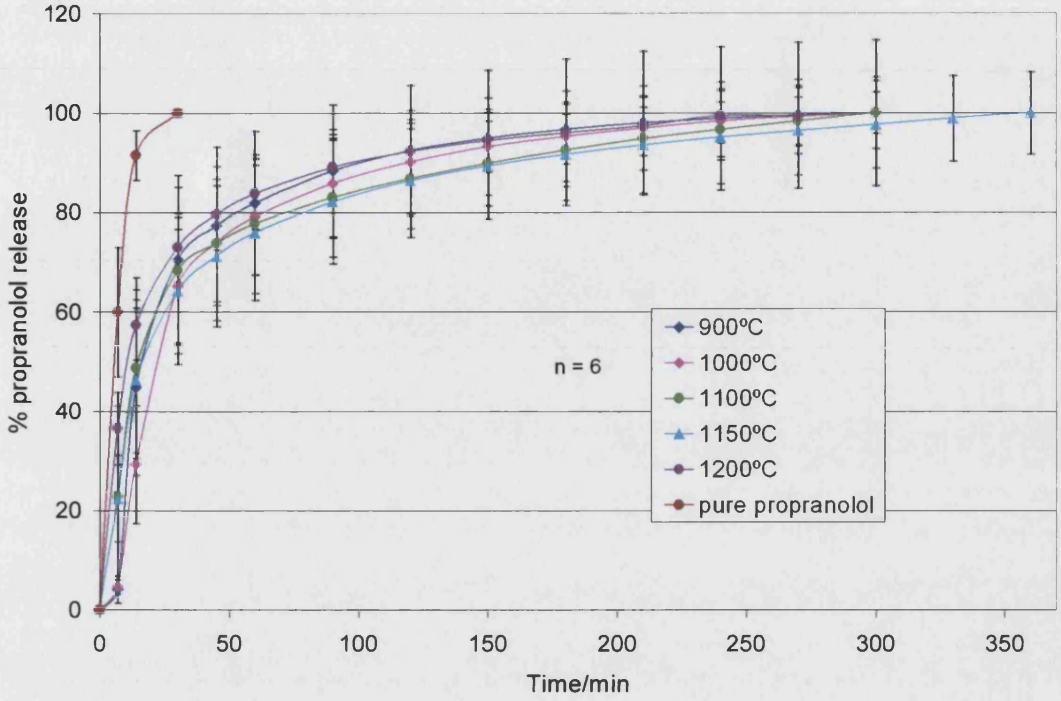

Figure 5.15 Dissolution results for Batch 3 microspheres sintered at various temperatures as indicated in the graph.

The dissolution results of microspheres loaded using Method 1 (successive loading, section 5.6.3.1) are shown in Figure 5.16. It was found that the release patterns of the propranolol.HCl were similar to that of first time loading. No marked differences were found between these results and those concerning the release patterns of microspheres sintered at different temperatures.

Loading Method 2 (increased temperature) produced high loaded microspheres (section 5.6.3.2.3). Therefore, in dissolution studies, the amount of sample in each capsule was reduced so that the final concentration in the dissolution vessel stayed within the calibration plots. Each dissolution unit was a 100 mg of microsphere sample in a size 3 gelatin capsule. Dissolution results (Figure 5.17) show that the drug release patterns are similar to those obtained using vacuum loading at room temperature and successive loading.

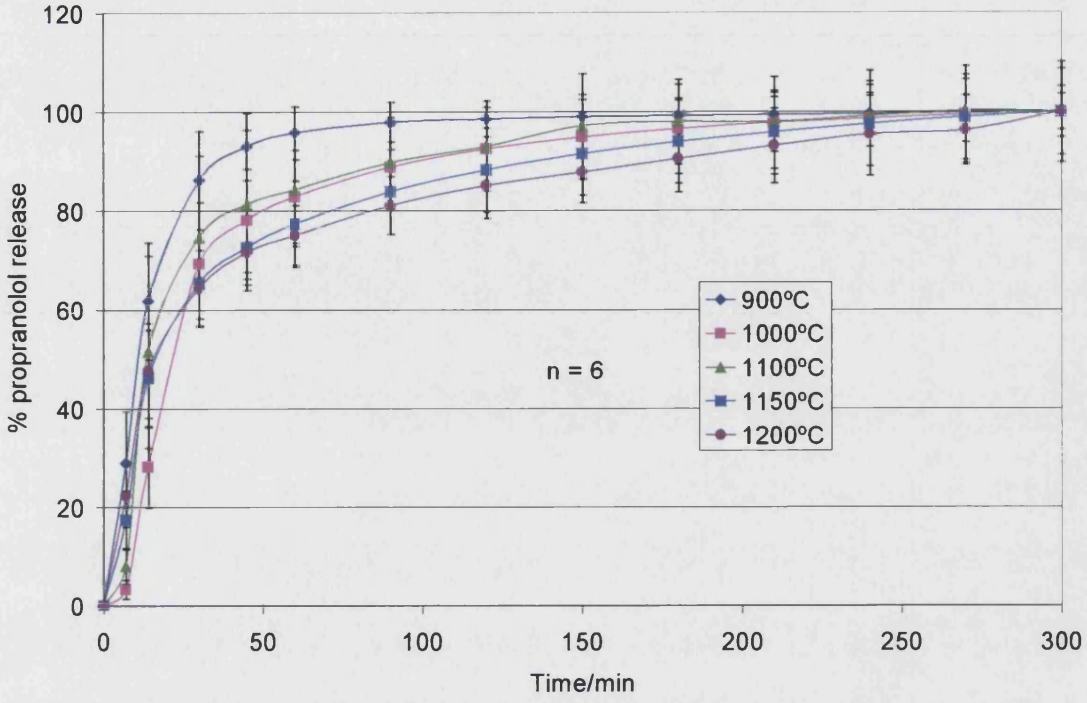

Figure 5.16 Dissolution results for successively loaded microspheres.

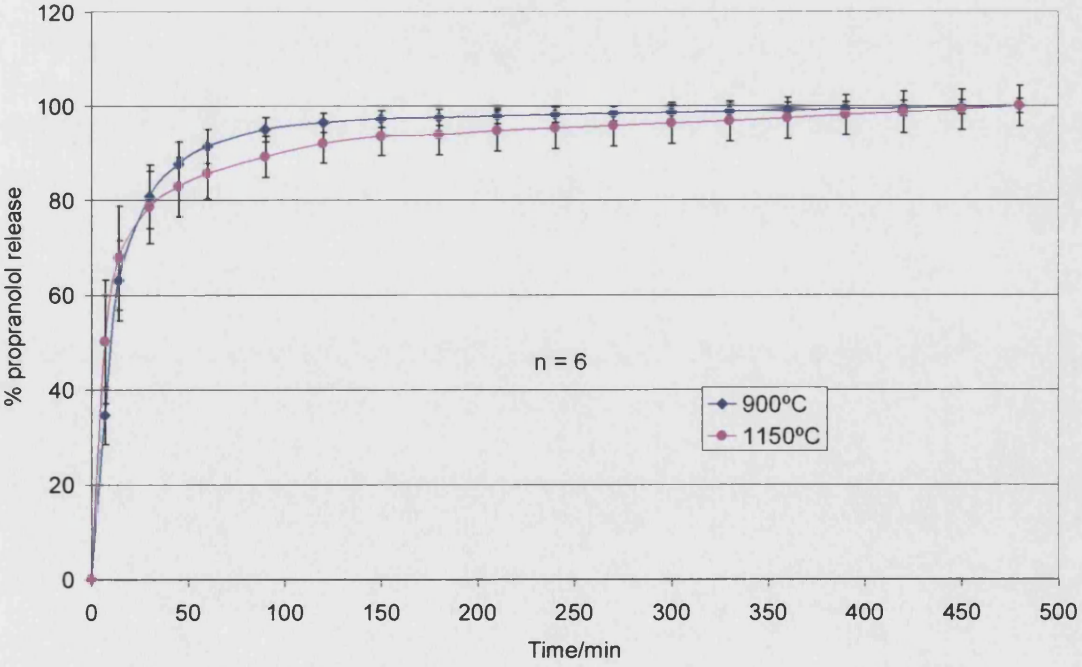

Figure 5.17 Dissolution results for microspheres loaded using Method 2.

5.6.4.5 Dissolution in Acidic Media

Dissolution of propranolol.HCl-loaded microspheres in acidic medium (0.1 M HCl) at 37 ± 0.5°C was also studied. The results showed that all microspheres dissolved in the medium after 20 min. This finding is comparable with finding of the fast dissolution of spray-dried non-sintered β-TCP in section 5.3.5. The results confirm that to be used for oral controlled release delivery the microspheres need to be enteric coated.

5.6.5 Low-Temperature Scanning Electron Microscopy (LTSEM)

To study propranolol.HCl and propranolol.HCl-loaded samples under the microscope, low-temperature SEM (LTSEM) was used. LTSEM was used because propranolol.HCl crystals were found to change shape quickly under the electron beam in a conventional SEM. This destruction may be the result of moisture sublimation from the drug crystals due to low-pressure ($<10^{-3}$ Pa), and also due to the heat generated by the electron beam. Hydrated samples are normally unstable for conventional SEM analysis.

The advantages of analysing samples at low temperatures (–100 °C to –175 °C) include[82,83]:

(a) Delicate samples can be analysed in their fully-hydrated state. Samples retain most of their associated water and display less artefacts (shrinkage or structural collapse) due to dehydration;

(b) Surface water in the specimen is stabilised, hence minimising the unwanted charging effects caused by disruption of the conducting coating.

The LTSEM sample preparation used in this study is detailed in section 2.8.1. This is a modified sample preparation procedure from Potter *et al.* [83]. The cryofixation step (to immerse sample in liquid nitrogen) used by Potter *et al.* was omitted because it was found to be unnecessary in this study.

Propranolol.HCl-loaded microspheres were studied using LTSEM combined with Energy Disperse X-Ray Analysis (EDX). EDX can be used because propranolol.HCl contains a high atomic number element, chlorine, which can be detected by the analysis. EDX elemental spot analysis was performed to confirm the identity of those structures which were identify as propranolol.HCl by visual observation under the

microscope. Both the surface morphology and internal morphology of the propranolol.HCl-loaded microspheres were studied. Sample preparations are detailed in section 2.7.4 and 2.7.5.

5.6.5.1 Results and Discussion

For microspheres that were propranolol.HCl-loaded by vacuum loading at room temperature (section 5.6.2), no structural differences were observed before and after drug loading under the LTSEM. No drug crystals could be identified. This is probably because the drug might be present as a thin layer on the surface of the microsphere matrix as suggested earlier (section 5.6.2.1).

For microspheres which were loaded by vacuum loading at 45 °C (section 5.6.3.2), well-defined propranolol.HCl crystals were observed on the surface of the microspheres, as shown in Figure 5.18. Close examination showed that some crystals were embedded in the pores of the microspheres (Figure 5.19). The crystals were confirmed to be propranolol.HCl by EDX; the analysis detected a high signal for Cl. It is suggested that drug crystals on the outer surface of the microspheres might have been formed during the filtration process. When the bulk of the drug solution was drained away, there would still be a layer of solution that covered the microspheres due to capillary force. Solvent evaporation would have started due to the low content of water in the atmosphere, therefore the concentration of drug on the microspheres' surfaces would have increased, and drug crystals were formed on the surfaces.

It was observed that some microspheres were totally covered in drug crystals (Figure 5.20). It is thought that these were the microspheres located at the base of the filter during the filtration process. These microspheres were likely to have collected drug solution seeping down from microspheres above. If the drug solution around them was not drained away sufficiently quickly, the drug crystallised rapidly due to temperature dropped, and the microspheres became coated with a layer of drug crystals. The presence of drug crystals on the surface also explains the fast release of propranolol.HCl for these high drug loading microspheres in the dissolution test.

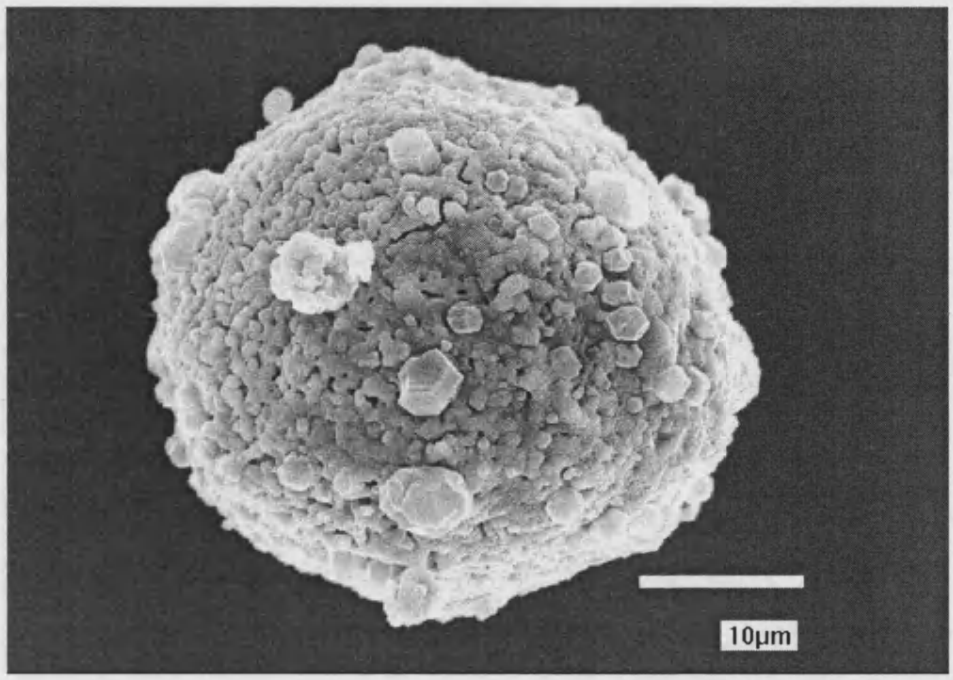

Figure 5.18 SEM micrographs showing propranolol.HCl on the surface of a microsphere.

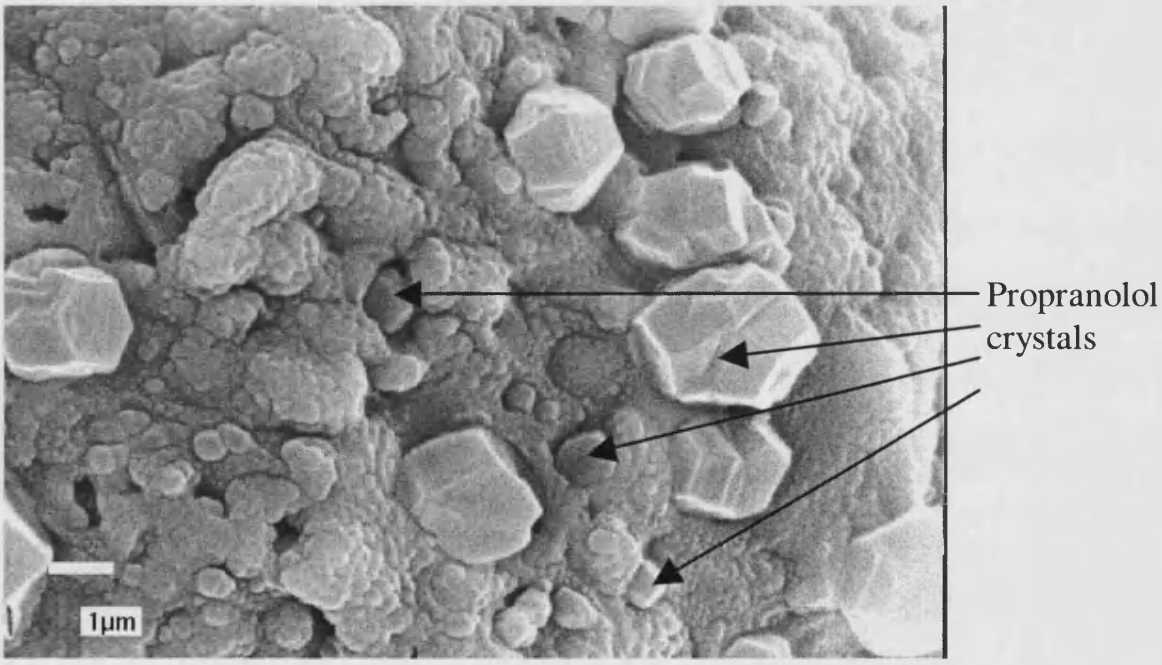

Figure 5.19 A zoom in SEM micrograph of Figure 5.18, showing how propranolol.HCl crystals attached to the microsphere surface. Some crystals were found inside pores.

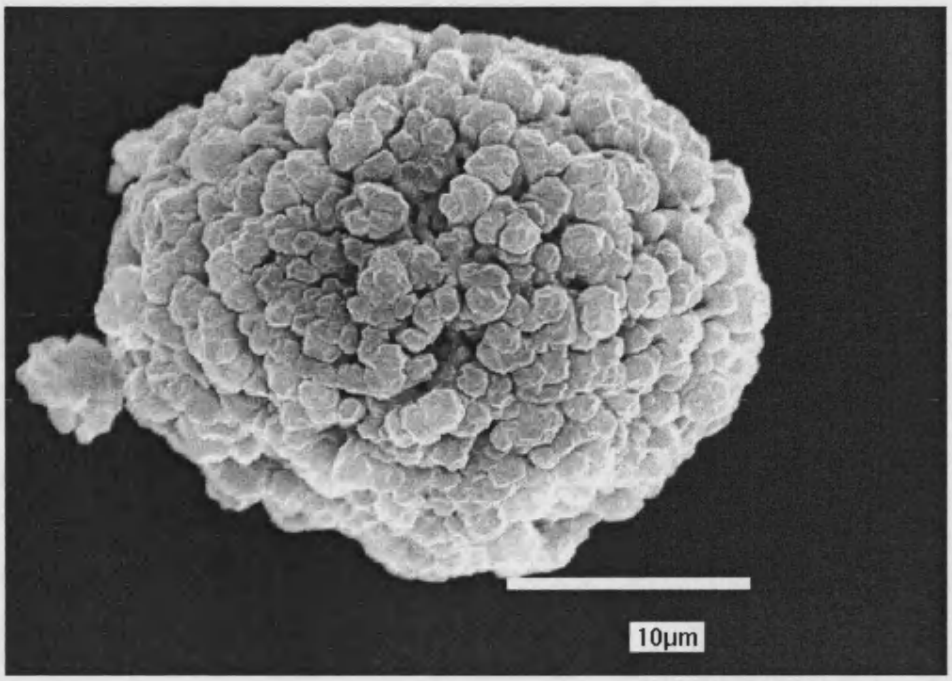

Figure 5.20 SEM micrograph of a microsphere fully covered by propranolol.HCl crystals.

These microspheres were embedded in resin and then sliced open (preparation method see section 2.7.5) for examination of the internal morphology. It was found that in the presence of resin, it was difficult to differentiate drug crystals from the microspheres' matrix. Therefore, no conclusion about the existence of drug crystals inside the microspheres can be drawn from SEM examination.

5.7 Loading of Paracetamol

5.7.1 Model Drug - Paracetamol

The loading of a third model drug, paracetamol, into β-TCP sintered microspheres was studied to ascertain that loading patterns reported are reproducible and are not drug specific. Apart from being economical, the main reasons that paracetamol was chosen was:

1. It is an active drug that is sparingly soluble in water and has a marked solubility difference in water and alcohol (it is 13 times more soluble in ethanol than in water). It was thought that the high alcohol solubility would allow a high concentration alcohol based drug loading solution to be prepared, and a low water

solubility mean a slow drug release profile in dissolution test. This would enable the release kinetics in the dissolution test to be studied more accurately.

2. It has good chromophore that can be monitored spectrophotometrically at $\lambda >$ 240 nm, therefore its absorbance will not interfere with gelatin absorbance.

The physicochemical properties of paracetamol are given in Appendix II.

5.7.2 Wavelength Determination for UV Assays

The λ_{max} of paracetamol was found to be 241 nm in both phosphate buffer, pH = 6.8, and in 0.1 M HCl, when its solutions were scanned in the range of 200 nm - 320 nm with a spectrophotometer. However, this value was not used for UV assays in this study because interference of gelatin absorption at this wavelength was found. The absorbance of gelatin capsules in buffer, paracetamol in buffer, and gelatin capsule plus paracetamol in buffer, are shown in Figure 5.21. A similar absorbance pattern was also obtained using 0.1 M HCl as media. The graph shows that at 249 nm gelatin absorbs little whilst paracetamol has a high absorbance. Therefore, 249 nm was used in all the UV assays for paracetamol in this study.

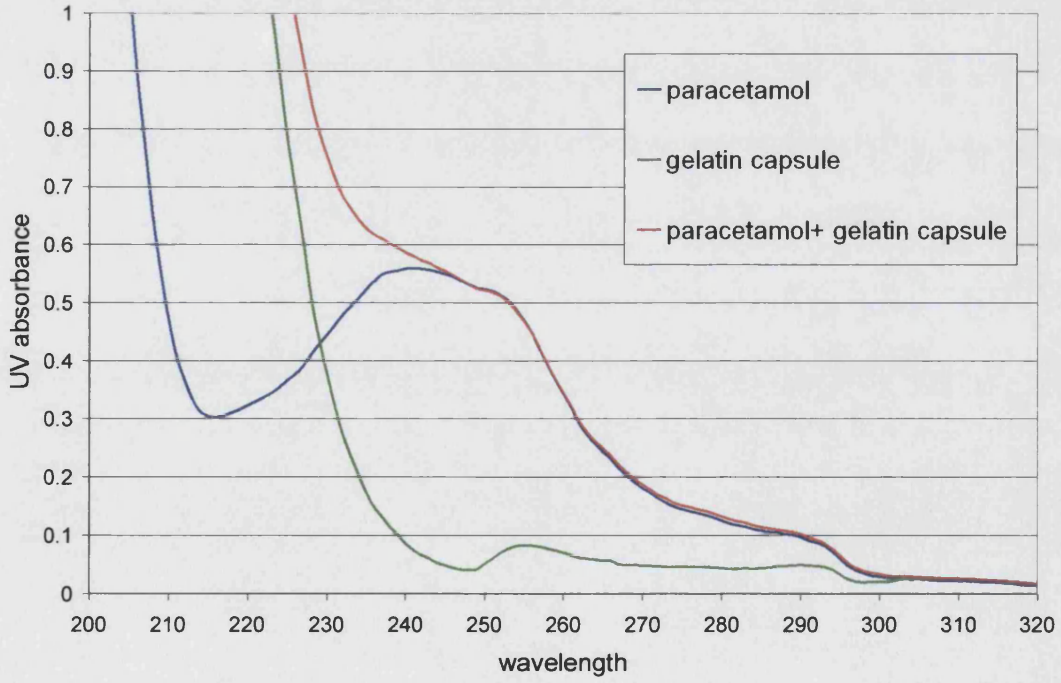

Figure 5.21 UV absorbance of paracetamol, gelatin capsule, and paracetamol plus gelatin capsule in phosphate buffer, pH = 6.8.

5.7.3 Calibration Method

A stock solution of paracetamol (0.025%) was prepared by dissolving 50 mg of the drug, accurately weighed, into 200 ml of BP phosphate buffer, pH = 6.8. Aliquots of the stock solution were diluted to produce a series of solutions having target concentrations of 0.0003%, 0.0005%, 0.0008%, 0.0010% and 0.0015% w/v of paracetamol. The absorbance of these solutions was determined at 289 nm. The procedure was performed in triplicate, using a new stock solution each time. The calibration data of paracetamol in 0.1 M HCl was also obtained using a similar method.

5.7.3.1 Calibration Data (Paracetamol)

The calibration data of paracetamol in phosphate buffer, pH = 6.8, and in 0.1 M HCl are shown in Table 5.15 and Table 5.16 respectively. Calibration plots are given in Appendix IV. The calibration plots of paracetamol in phosphate buffer and in 0.1M HCl were found to be linear in the range 0 - 0.0015% and 0 - 0.0020% w/v respectively.

Table 5.15 Calibration data of paracetamol in BP phosphate buffer, pH=6.8.

	Calibration Set			
	1	2	3	Mean
Intercept	0.0006	0.0006	0.0005	0.0006
Slope	595.64	588.79	590.74	591.72
Regression (r^2)	0.9999	0.9997	0.9998	
SD of the regression	0.0028	0.0060	0.0047	

Table 5.16 Calibration data of paracetamol in 0.1 M HCl.

	Calibration Set			
	1	2	3	Mean
Intercept	0.0032	0.0012	0.0010	0.0018
Slope	567.40	590.20	588.80	582.13
Regression (r^2)	0.9999	1.0000	1.0000	
SD of the regression	0.0046	0.0024	0.0023	

5.7.4 Determination of Drug Stability

Paracetamol in phosphate buffer (pH = 6.8) was freshly prepared and kept at 37 ± 0.5 °C for 24 h. The UV absorbance of the solution before and after the incubation was measured at 249 nm. The results show no marked difference between the absorbance, indicating that paracetamol is stable over the dissolution period.

5.7.5 Loading Experiments

Paracetamol is more soluble in alcohol than in water (see Appendix II). Therefore ethanol was chosen as solvent to allow the making of a high concentration paracetamol solution for loading experiments. The loading solution was 12.5 %w/v paracetamol in ethanol. The vacuum loading experiments were performed at room temperature using the set-up and the procedure described in section 5.6.2. The microsphere samples used were those sintered at 900 °C and at 1150 °C. Each sample was loaded in triplicate.

5.7.6 Loading Efficiency Test and Washing Experiments

The drug loading efficiency was determined as before (section 2.12, λ = 249 nm). To remove the drug adhering on the outer surface of the microspheres, a washing experiments was performed. Washing method (a) in section 5.5.3 was used, but water instead of ethanol was used as a solvent. This is because paracetamol is a lot more soluble in ethanol than in water. Complete extraction of paracetamol from the microspheres was not required.

5.7.6.1 Results and Discussion

The results of the percentage loading and washing experiments are shown in Table 5.17. More paracetamol was loaded onto microspheres with a higher surface area, *i.e.*, microspheres sintered at a lower temperature. This observation is consistent for all three model drugs tested. The ratio of drug-loaded for microspheres sintered at 900 °C and microspheres sintered at 1150 °C for propranolol.HCl and for paracetamol, were found to be similar (5.67/1.75 = 3.24 and 17.28/5.39 = 3.21 respectively). This further confirms that:

(1) the amount of drug-loaded using the vacuum loading method is related to the surface area of the microspheres;

(2) the drug was loaded as a layer on the matrix of the microspheres.

Table 5.17 Paracetamol content of microspheres, before and after washing.

	% Paracetamol loading, n=3	
Microspheres sintered at	Before washing/%	After washing/%
900 °C	17.28 ± 2.00	3.96 ± 0.88
1150 °C	5.39 ± 0.52	0.74 ± 0.04

5.7.7 Dissolution Studies

The release profile of paracetamol from the microspheres was studied (method see section 5.6.4). The drug release was compared to the dissolution of paracetamol crystals that had been dissolved in ethanol followed by drying in the oven at 50 °C. The reason for this has been explained in section 5.6.4.

5.7.7.1 Results and Discussion

The dissolution results (Figure 5.22) show that the release profile of paracetamol is similar to the release profile of propranolol.HCl and benzamide:

(1) There are no marked differences of release among microspheres sintered at different temperature;

(2) Instant release of drug was observed; ~ 80% of drug was released in 30 min.

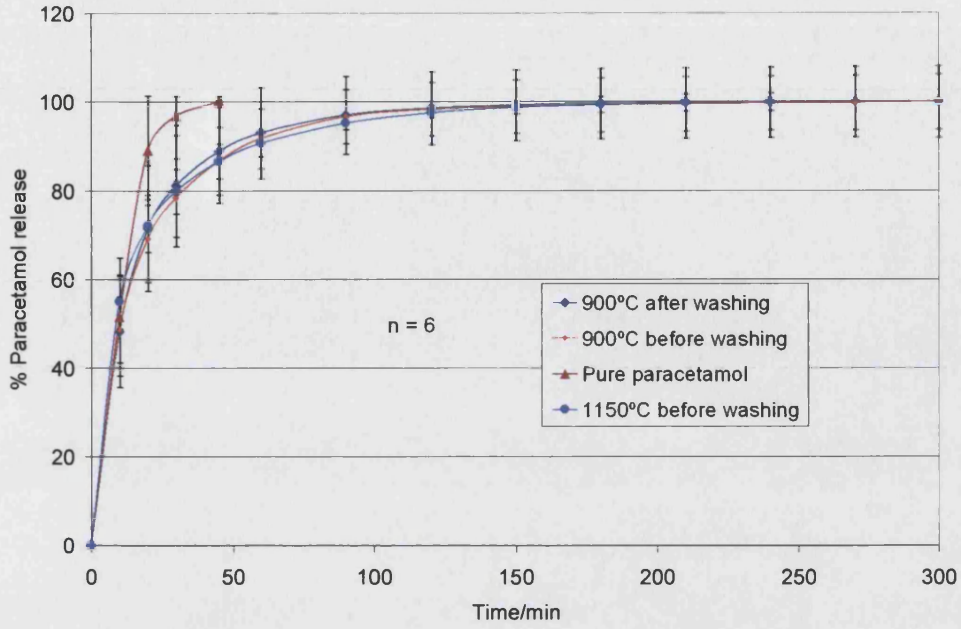

Figure 5.22 Dissolution results of paracetamol release.

5.8 Drug Composition Studies Before and After Loading Experiments

β-TCP has a surface that is acidic in nature. In order to ensure that model drugs did not degrade when they came into contact with this acidic surface, possible changes to the drugs after loading into the sintered β-TCP surfaces were investigated. Furthermore, for all the loading calculations and dissolution results to be valid, the model drugs before and after loading experiments should remain the same.

All three model drugs were also subjected to analysis, as-received and after loading into β-TCP microspheres sintered at 900 °C. The analytical tests carried out were nuclear magnetic resonance (NMR) spectroscopy, mass spectroscopy (MS), and X-ray diffraction (XRD) studies.

5.8.1 Nuclear Magnetic Resonance (NMR) Spectroscopy

NMR spectroscopy is a most valuable analytical technique used to determine the structure of an organic molecule. It is based on energy transitions of spinning nuclei in

an applied magnetic field. It is used to identify the carbon-hydrogen structural framework in molecules.

As-received drug (benzamide, propranolol.HCl and paracetamol) were compared to drugs loaded into the β-TCP microspheres with ^{1}H-NMR and ^{13}C-NMR spectrometry.

^{1}H-NMR spectroscopy is used to determine the number of different types of environment experienced by *hydrogen* atoms in a molecule, and where these hydrogen atoms are located along a carbon skeleton. The structure of a chemical is determined by analysing four characteristics of the spectrum:

1. The number of signals,
2. The position of a signal – chemical shift,
3. The area under the signal – integral,
4. The splitting of a signal into several lines – coupling and multiplicity.

^{13}C-NMR spectroscopy is used to determine the number of different types of environment experienced by *carbon* atoms in the molecules. It gives information about the electronic environment of the different types of carbon and the number of 'neighbours' a carbon atom has.

DMSO, $(CD_3)_2SO$, was chosen as the solvent used for analysis because all three sample drugs dissolve well in it. Samples containing drugs as-received were prepared by dissolving ~ 30 mg of model drugs in DMSO. Drugs in microsphere samples were prepared by mixing microspheres that contained ~ 30 mg of drugs in DMSO. The mixtures were allowed to settle and the supernatants were used in the NMR studies. Samples were analysed by the University of Bath NMR Service, Department of Pharmacy and Pharmacology using a Jeol JNM-XGX270 FT NMR spectrometer.

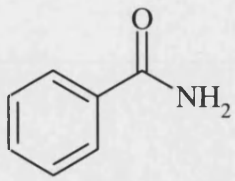

benzamide

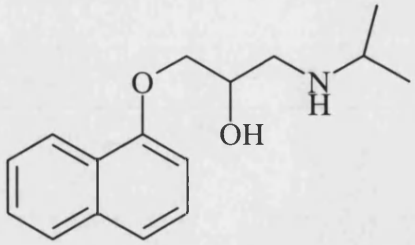

(*RS*-)propranolol

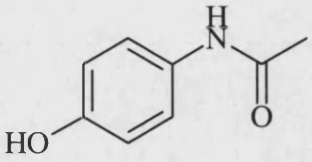

paracetamol

5.8.1.1 Results and Discussion

The following NMR spectra were obtained:

Benzamide as-received

δ_H(400 MHz; DMSO) 8.0 (1H, bs, NH), 7.90-7.42 (5H, m, Ar), 7.40 (1H, bs, NH).

δ_C(100 MHz, DMSO) 167.7 (C=O), 134.1, 131.0, 128.0, 127.3 (Ar).

Benzamide in microspheres

δ_H(400 MHz; DMSO) 8.0 (1H, bs, NH), 7.85-7.42 (5H, m, Ar), 7.33 (1H, bs, NH).

δ_C(100 MHz, DMSO) 167.6 (C=O), 134.0, 131.0, 128.0, 127.3 (Ar).

Propranolol.HCl as-received

δ_H(400 MHz; DMSO) 8.24-6.92 (7H, m, Ar), 6.07 (1H, bs, OH exchangeable with D_2O), 4.37-4.31 (1H, sextet, C*H*OH), 4.14-4.12 (2H, d, OCH_2), 3.45 (1H, bs, NH exchangeable by D_2O), 3.39-3.31 (1H, heptet, NC*H*CH_3), 3.24-3.07 (2H, m, CH_2N), 1.27-1.24 (6H, t, 2×CH_3).

δ_C(100 MHz, DMSO) 153.5, 133.8, 127.2, 126.3, 125.9, 125.0, 124.7, 121.6, 120.0, 105.1 (Ar), 69.9, 65.2 (2×C–O), 49.8, 47.0 (2×C–N), 18.6, 18.3 (2×CH_3).

Propranolol.HCl in microspheres

δ_H(400 MHz; DMSO) 8.24-6.94 (7H, m, Ar), 6.05 (1H, bs, OH exchangeable with D_2O), 4.31-4.28 (1H, sextet, C*H*OH), 4.14-4.12 (2H, d, OCH_2), 3.45 (1H, bs, NH exchangeable by D_2O), 3.40-3.32 (1H, heptet, NC*H*CH_3), 3.24-3.07 (2H, m, CH_2N), 1.26-1.23 (6H, t, 2×CH_3).

δ_C(100 MHz, DMSO) 153.5, 133.8, 127.3, 126.4, 126.0, 125.1, 124.7, 121.6, 120.1, 105.1 (Ar), 69.9, 65.3 (2×C–O), 49.9, 46.9 (2×C–N), 18.8, 18.3 (2×CH_3).

Paracetamol as-received

δ_H(400 MHz; DMSO) 10.18 (1H, CONH exchangeable with D_2O), 9.68 (1H, s, OH exchangeable by D_2O), 7.88-7.84 (4H, m, Ar), 2.50 (3H, s, CH_3).

δ_C(100 MHz, DMSO) 167.4 (C=O), 153.0, 130.9, 120.8, 114.9 (Ar), 23.8(CH_3).

Paracetamol in microspheres

δ_H(400 MHz; DMSO) 9.66 (1H, s, CONH exchangeable with D_2O), 9.17 (1H, s, OH exchangeable by D_2O), 7.34-6.64 (4H, m, Ar), 1.97 (3H, s, CH_3).

δ_C(100 MHz, DMSO) 167.4 (C=O), 152.9, 130.9, 120.7, 114.9 (Ar), 23.8 (CH_3).

In the ^{1}H-NMR spectra for benzamide, the exchange between CONH and D_2O was not obvious as the proton exchange can be slow in amides. Also, two separate peaks were shown for the two H atoms in the $CONH_2$ functional group. This is because the oxygen atom affects their local magnetic environment to different extents. Propranolol has one chiral centre, racemic propranolol.HCl was used in this study.

Comparisons of ^{1}H-NMR and ^{13}C-NMR spectra, between the same drugs before and after they had been loaded into the microspheres, consistently show similar spectra. This suggests that the molecular structure of these compounds is similar. It was concluded that the loading experiment and the adsorption of drugs into β-TCP microspheres did not alter the drugs chemically. Nevertheless, one should bear in mind that this technique may not be sensitive enough to detect very small amounts of decomposition of the sample, should it have occurred.

5.8.2 Mass Spectroscopy (MS)

In MS, a vaporised substance is bombarded with atoms (or a high energy electron beam for electron impact) to produce detectable ions as a function of their mass-to-charge ratio (*m/z*). Ions having lower mass will be deflected more while high momentum ions will be deflected less by the applied magnetic field. By varying the strength of this field, a range of *m/z* particles can be bent to follow the path of the analyser, and is detected and recorded.

Samples of model drugs as-received and drugs after loading into microspheres were analysed by the Mass Spectrometry Service, University of Bath, using a VG AutoSpec (Fisons Instruments, Manchester, UK). Positive and negative ion modes were used.

5.8.2.1 Results and Discussion

The output of the mass spectrometer shows a plot of relative intensity *vs.* mass-to-charge ratio (*m/z*). The results are:

Benzamide, C_7H_7NO, MW = 121 Da

As-received: *m/z* (FAB+*ve*) 122 (100%, $[M+H]^+$)

m/z (FAB -*ve*) 120 (100%, $[M-H]^-$)

In microspheres: *m/z* (FAB -*ve*) 120 (50%, $[M-H]^-$)

Propranolol.HCl is a salt and the HCl salt is lost in MS. The working mass is that of the free base, $C_{16}H_{21}NO_2$, MW = 259 Da.

As-received: *m/z* (FAB+*ve*) 260 (100%, $[M+H]^+$)

In microspheres: *m/z* (FAB+*ve*) 260 (100%, $[M+H]^+$)

Paracetamol, $C_8H_9NO_2$, MW = 151 Da

As received: *m/z* (FAB+*ve*) 152 (100%, $[M+H]^+$)

In microspheres: *m/z* (FAB+ve) 152 (100%, $[M+H]^+$)

When a molecule picks up a proton, it carries a unit positive charge, the value *m/z* is equivalent to the molecular weight of the molecule plus 1, $[M+H]^+$. When a molecule loses a proton, the value *m/z* is equivalent to the molecular weight of the molecule minus 1, $[M-H]^-$. Small peaks (not shown here) are also observed one and two units above the calculated molecular weight due to the natural isotopic abundance of ^{13}C and ^{2}H. These results show that all three model drugs remained the same after being loaded into the microspheres.

5.8.3 X-Ray Diffraction (XRD) Studies

X-ray diffraction is useful in the study of solid materials. In contrast to spectrochemical methods, it identifies the crystallography of the compounds rather than just the elements. It can also differentiate between polymorphs, isomers and different hydrate forms. This is because each of these forms has a different crystallographic structure which gives rise to a different X-ray diffraction pattern. Model drug samples before and after loading into β-TCP microspheres sintered at 900 °C were analysed by XRD.

5.8.3.1 Results and Discussion

Comparisons of XRD analysis for benzamide, propranolol.HCl, and paracetamol as-received, and after loading into microspheres are shown in Figure 5.23, Figure 5.24 and Figure 5.25, respectively. XRD peaks of drugs that correspond to drugs loaded into microspheres have a lower intensity because the percentages of drugs were low compared to the β-TCP matrix. Nevertheless, the results showed that the XRD peaks of drug-loaded microspheres were a combination of pure drug and sintered β-TCP microspheres. No new peaks were identified. It is concluded that all three model drugs maintain their crystallographic structures after being loaded into the microspheres.

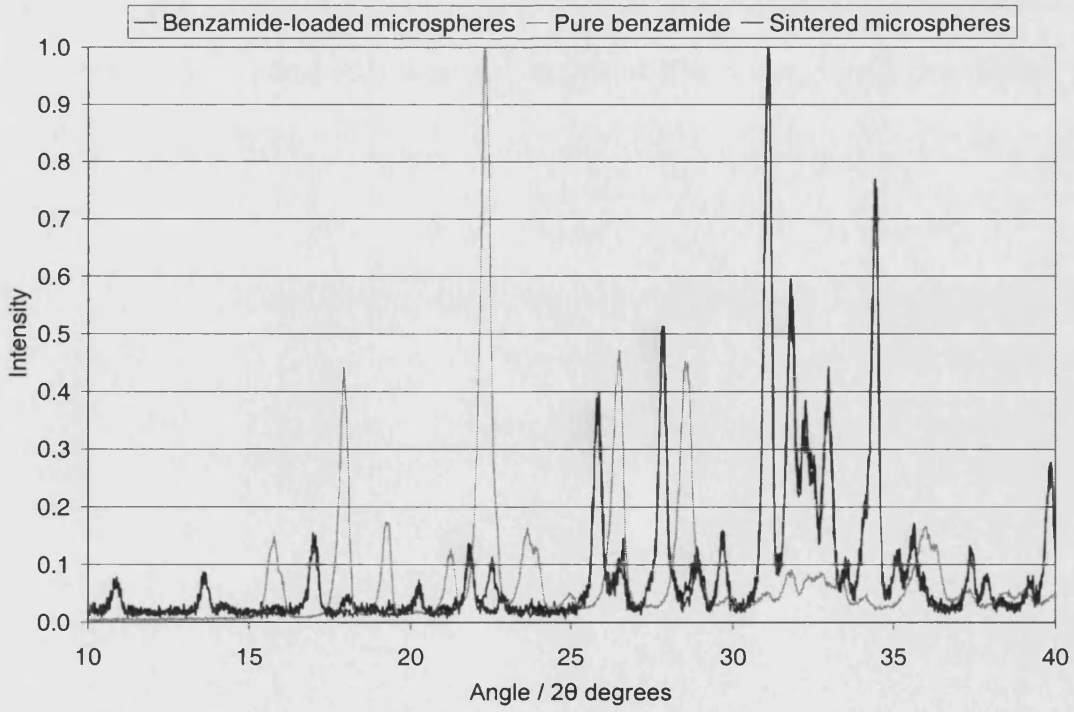

Figure 5.23 XRD results for benzamide and benzamide-loaded microspheres.

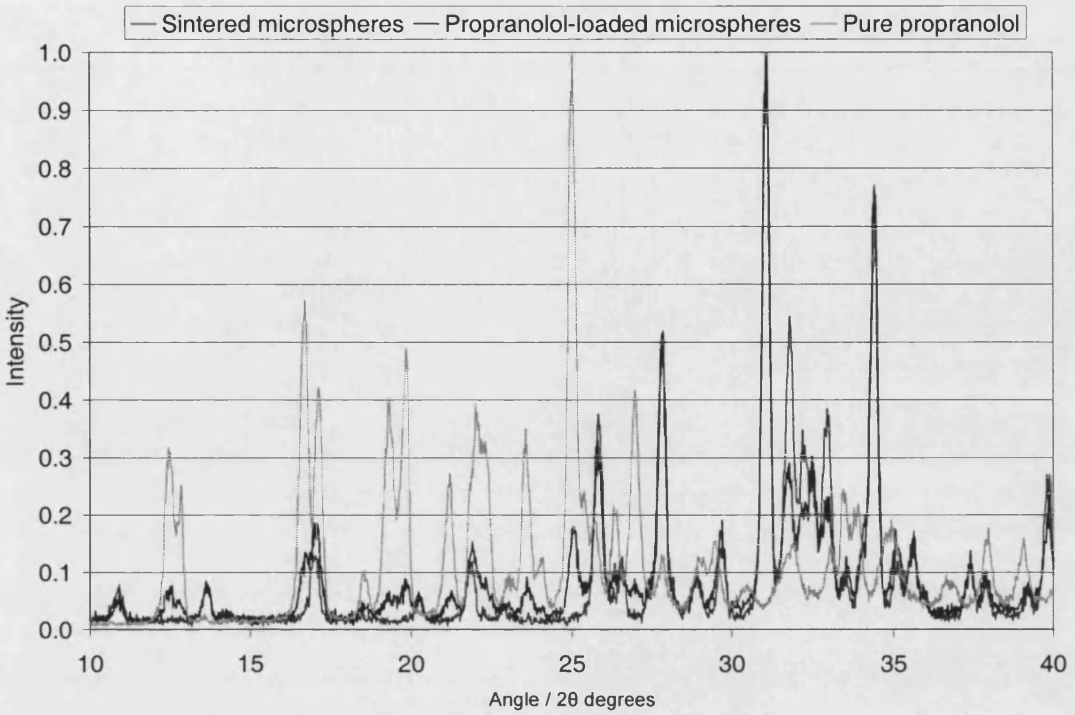

Figure 5.24 XRD for propranolol.HCl and propranolol.HCl-loaded microspheres.

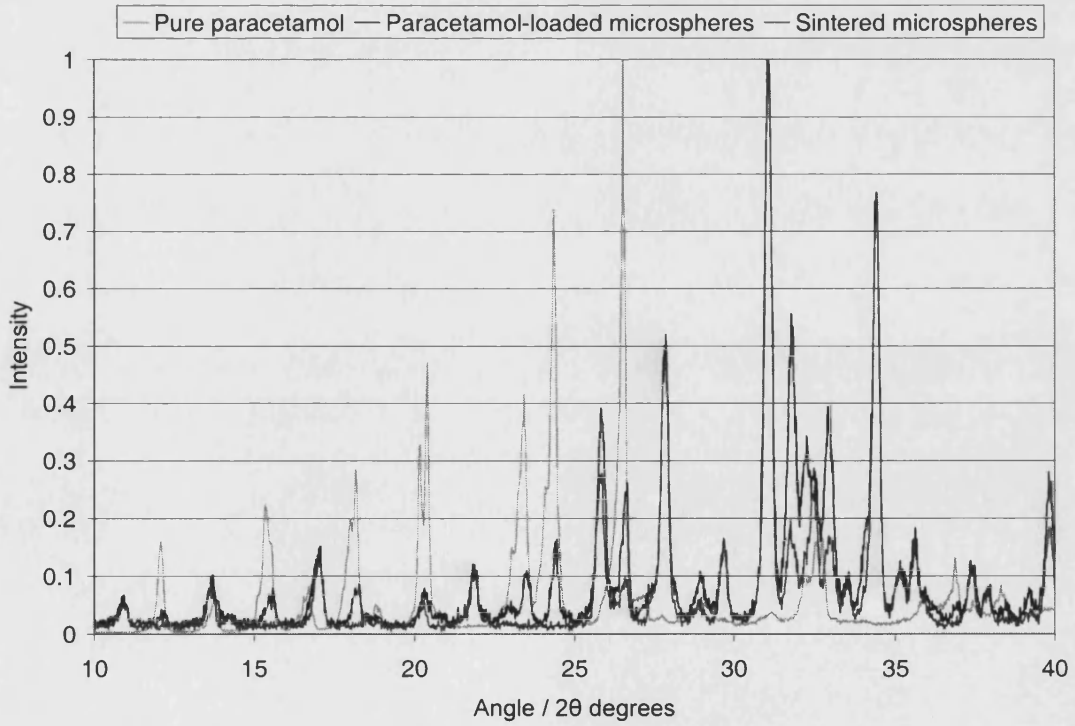

Figure 5.25 XRD for paracetamol and paracetamol-loaded microspheres.

5.9 Crystallisation

5.9.1 Background

At a given temperature, there is a maximum amount of solute that can dissolve in a given amount of solvent to form a solution. When this maximum amount is reached, the solution is said to be saturated. The amount of solute required to make a saturated solution at a given condition is called solubility. Solubility provides the concentration at which the solid solute and the liquid solution are in equilibrium. A supersaturated solution is a solution in which the solute concentration exceeds the equilibrium solute concentration at a given temperature (saturation). Supersaturated solutions are not in equilibrium; in order to relieve the supersaturation and move towards equilibrium, the solution crystallises, and separation occurs.

Atoms in crystals are arranged in a periodic repeating pattern that extends in three dimensions. Crystallisation is a separation and purification technique commonly employed in the pharmaceutical industry. It may be defined as a phase change in which a crystalline is obtained from a solution. It can be thought as a two-step process:

1) Nucleation – phase separation, or formation of new crystals.
2) Crystal growth – growth of present crystals into larger ones.

A supersaturated solution is essential for crystallisation to occur. There are four main methods to generate a supersaturated solution[143]:

1) Temperature change;
2) Evaporation of solvent;
3) Chemical reaction;
4) Changing the solvent composition.

Most solutes exhibit increasing solubility with increasing temperature. In reference to a hypothetical solubility diagram shown in Figure 5.26, a solution at Z is a stable system; the solute is dissolved in the solvent. If the solution is then cooled down to A, the solute and the solvent are in equilibrium, *i.e.*, the solution is now saturated. If the solution is further cooled down to B, the solution is now supersaturated and it becomes a metastable system. Metastable means that even though the solubility of the solute has

exceeded its solubility, crystals do not form readily. The metastability of a solution decreases as the supersaturation increases. If we further cool the solution down to C, the solution crystallises rapidly and no longer stable.

Supersaturated solutions exhibit a metastable zone and a labile zone. Nucleation is not spontaneous in the metastable zone. This is because at these concentrations the molecules start to associate and form aggregates, but these aggregates are unstable and will dissolve. The region where nucleation occurs spontaneously is called the labile zone. In this zone, the formed aggregates grow spontaneously and new crystals are created.

If a seed crystal is placed in a supersaturated solution, solute molecules in the solution will adsorb onto the crystal surface and therefore the size of the crystal grows. Crystals are thought to grow in a layer-by-layer sequential fashion[144]. The rate of crystal growth is proportional to the degree of supersaturation, and the degree of supersaturation can be controlled by precise temperature management. The difference between supersaturation and saturation (*e.g.*, the difference between point B and point F in Figure 5.26) is the amount of solute that will crystallise out.

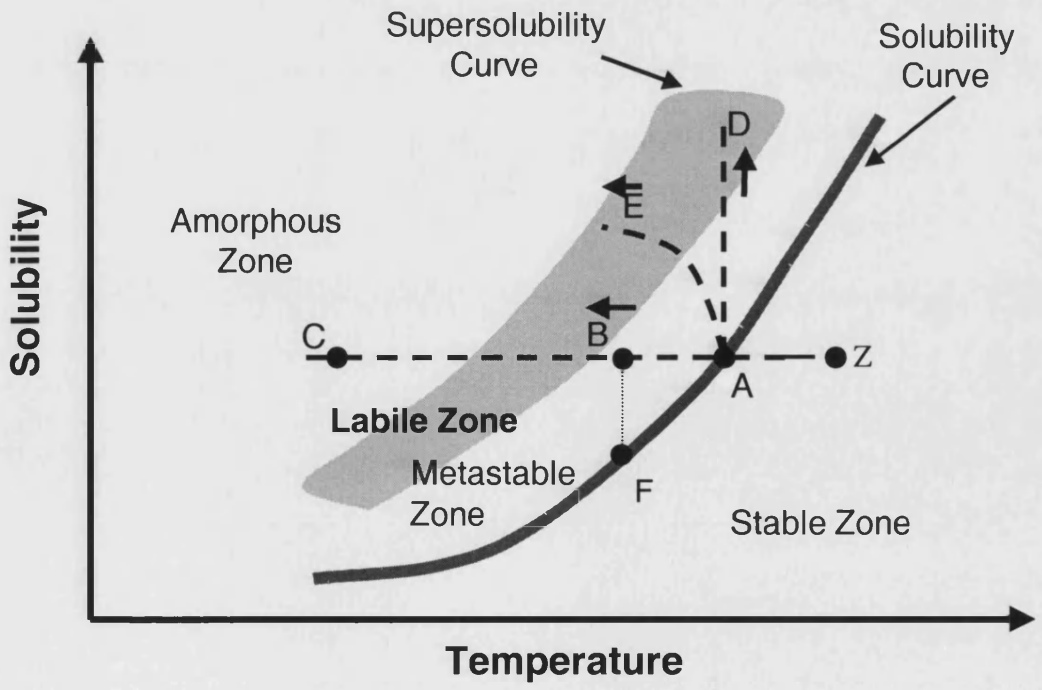

Figure 5.26. Solubility and supersolubility curves (adapted from Price[145])

Supersaturation can be expressed in terms of degree. This refers to the difference between the temperature of the solution and the saturated temperature of the solution at the existing concentration. For example, when the temperature of a saturated solution at temperature A is lowered to temperature B, a solution with a degree of supersaturation = (A - B) is formed.

It is the relationship between the extent of nucleation to the extent of crystal growth that controls the product crystal size and size distribution.

The aim of this study was to fill the pores of the microspheres with drug crystals. The experiment was performed in two stages: 1) nucleation; and 2) crystal growth. In stage 1, a vacuum loading experiment was performed to implant drug crystal seeds in the microspheres. In stage 2, the drug-seeded microspheres were placed in a supersaturated solution to allow the crystals to grow in the pores of the microspheres. The supersaturated solution was prepared by lowering the temperature of a saturated solution. Propranolol.HCl was used as a model drug.

5.9.2 Experimental Methods

Small amounts of impurities can have dramatic effects on nucleation and crystal morphology[144]. To avoid any contamination, all glassware used in this work was thoroughly cleaned (by soaking in Decon 90 solution overnight), and only deionised water was used in the experiments and for washing up.

Stage 1 - Nucleation

Microspheres sintered at 900 °C and 1150 °C were vacuum loaded at 45 °C as described in section 5.6.3.2.

Stage 2 - Crystal Growth

A saturated propranolol.HCl solution was prepared by dissolving an excess (~ 32 g) of propranolol.HCl in 50 ml of deionised water at 35 °C. The solution was stirred overnight to allow the system to reach equilibrium. The solution was then filtered

(Nalgene MF75 with 0.02 μm polyethersulphone filter, Nalge Nunc International Co., Rochester, NY, USA) and kept at 35 °C until used.

A set-up as shown in Figure 5.27 was used for the experiment. Test tubes were placed in a water bath maintained at 35 ± 0.1 °C (refrigerated circulator DC5-K20, Thermo Haake, Karlsruhe, Germany). ~ 0.6 g of microspheres was placed in each test tube, and the test tubes were then sealed with rubber stoppers. Through a needle, a rotary vacuum pump was used to produce a low pressure in the test tubes. 2 ml of the prepared saturated solution was injected into each test tube with a needle while the vacuum pump was still running. Both needles were then removed, and the temperature of the water bath was immediately dropped (δT) by either 5 °C, or 15 °C. The test tubes were then incubated for either 6 h or 24 h. The variables tested in the experiments are shown in Table 5.18. After the incubation period, the powders were filtered (porosity 4 sintered filter, BDH Laboratory Supplies, Poole, UK) and dried in an oven at 50 °C.

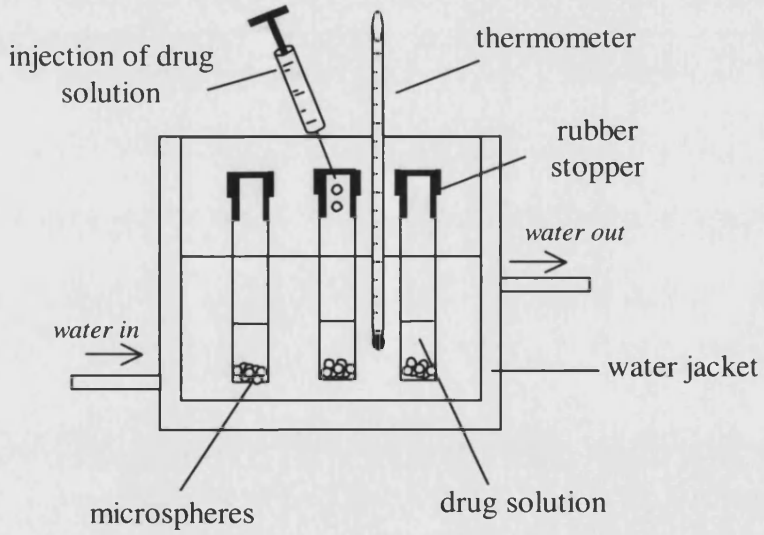

Figure 5.27 Set-up used for crystal growth experiments.

Table 5.18 Variables used in crystal growth experiments.

Experiment Set	Microspheres sintered at/°C	Temperature drops/°C	Incubation time/h
1	900	15	6
2	900	15	24
3	1150	15	6
4	1150	15	24
5	900	5	6
6	900	5	24
7	1150	5	6
8	1150	5	24

The microspheres were then examined using LTSEM. Some microspheres were mounted in epoxy resin and sliced open for study of the internal structure. These samples were then gold coated for 6 x 0.5 min in the sputter coater and observed using conventional SEM.

Attempts were also made to open microspheres to examine drug crystals inside the microspheres without the interference of resin. Microspheres were first sieved with 50 μm nylon cloth, and then a few of the larger microspheres were carefully hand picked with a thin wire under the optical microscope. Tempfix resin (Neubauer, Munster, Germany. Supplied by Agar Scientific, Stansted UK) was melted at 120 °C onto an aluminium surface then cooled to room temperature to harden it. The aluminium substrate and resin were then heated to 40 °C at which temperature the resin becomes 'sticky' and microspheres were sprinkled on to the resin surface. Tempfix resin is a thermoplastic adhesive containing no solvents and is stable in a high vacuum. It has a smooth featureless surface when viewed in the SEM which becomes adhesive at 40 °C allowing small particles to be mounted in it without being submerged. A metal weight was placed on top of the samples and briefly impacted with a hammer to break open the microspheres. Loose portions of microspheres were removed with a jet of compressed air. The samples were then prepared for LTSEM as before (see section 2.8.1).

5.9.3 Results and Discussion

During LTSEM examination, it was found that ice crystals were formed on the sample's surface due to the sub-zero temperatures used. Ice crystals can be differentiated from propranolol.HCl crystals by EDX elemental spot analysis looking for chlorine (Cl). The signals were collected over a period of 100 seconds. A definite and strong chlorine peak confirmed the identity of drug crystals.

The SEM micrographs of crystal growth experiments are shown in Figure 5.28 and Figure 5.29. These micrographs show that larger temperature drops (δT) allowed cultivation of larger size crystals. At δT = 15 °C, large crystals of propranolol.HCl were formed. Some of these crystals are bigger than the microspheres themselves. The results also show that the amount of crystal growth is related to length of the incubation time. 6 h incubation produced smaller size crystals than 24 h incubation.

The results show that δT = 15 °C was too large a temperature drop for the amount of crystal growth desired. The crystals produced were too big to fit in the pores of the microspheres. δT = 5 °C is more suitable as smaller crystals were produced. To study how crystals were attached on the β-TCP matrix, samples were examined under higher magnifications and the results are shown in Figure 5.30 and Figure 5.31. Figure 5.30 shows how propranolol.HCl crystals attached on the microspheres sintered at 900 °C. The matrix of these microspheres is made from very small grains, and propranolol.HCl crystals inserted themselves between these grains. Figure 5.31 shows how propranolol.HCl crystals attached on the microspheres sintered at 1150 °C. These microspheres consisted of bigger grains, and propranolol.HCl crystals 'fused' themselves with these grains. It can be seen that some crystals were grown inside out from the pores of the microspheres.

To examine the growth of drug crystals inside the microspheres, microspheres were resin-embedded and sliced open. While examining these samples, it was found that the recognition of drug crystals was difficult in the presence of resin. To locate the drug crystals, the dissected microspheres were analysed by EDX analysis looking for Cl. The results (Figure 5.32) show that Cl was found in all areas of the microspheres, but higher peaks of chlorine compared to peaks of Ca were recorded nearer to the edge of

the microspheres. This may indicate that more drug crystals were found in the peripheral areas of the microsphere. It was considered that EDX analysis might not be an accurate method of quantifying or locating drug crystals because incident electrons can penetrate into a deeper layer (up to 2 μm) of the microsphere, and the EDX detector can pick up the Cl signals from adjacent areas. However, with the consistent trend that a more intense Cl signal was detected near the periphery of the microspheres, it was concluded that more propranolol.HCl was found in the peripheral areas.

To avoid the interference of resin, it was attempted to crack open of the microspheres by force. However, the results show that microspheres were not cracked open as expected, but became flattened under the applied force. A flattened microsphere is shown in Figure 5.33. Some drug crystals on the surface of the microsphere can still be clearly identified.

These initial experiments indicate that crystallisation can be used to load drug into the microspheres. It is envisaged that by careful manipulation of the degree of supersaturation, incubation time, and the filtering process, β-TCP microspheres filled with drug crystals in their pores can be produced.

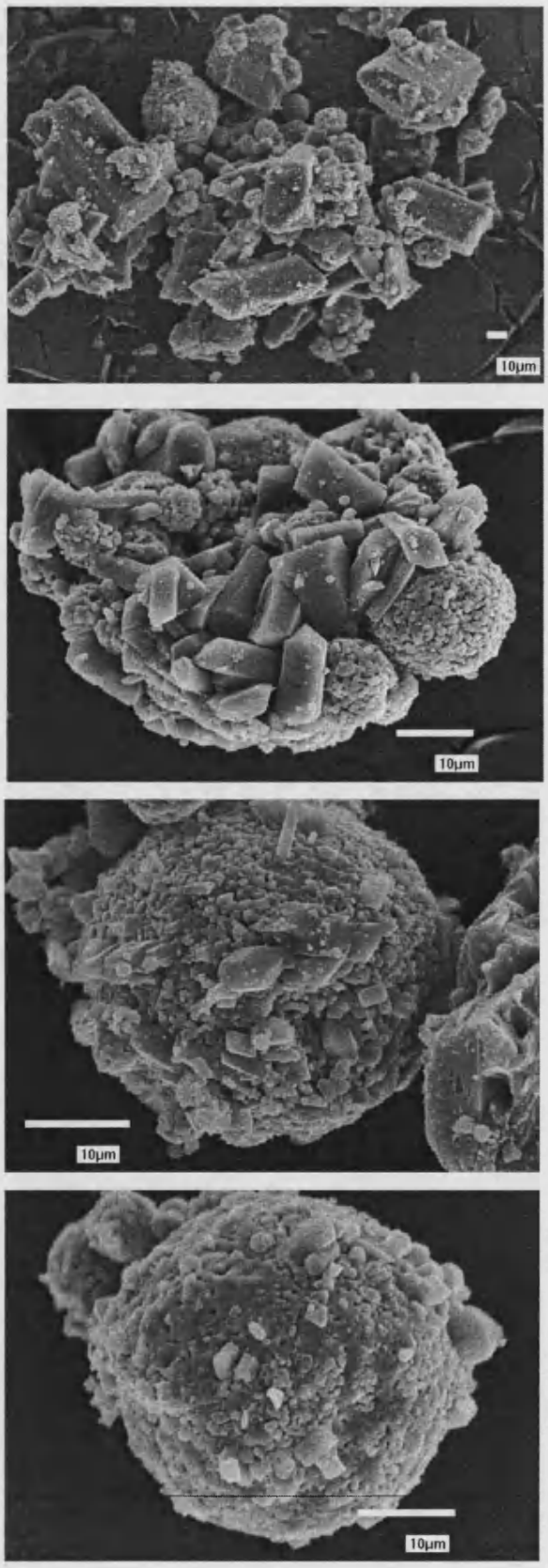

(a)
δT = 15 °C
time = 24 h

(b)
δT = 15 °C
time = 6 h

(c)
δT = 5 °C
time = 24 h

(d)
δT = 5 °C
time = 6 h

Figure 5.28 Results of crystal growth experiments using microspheres sintered at 1150 °C, under conditions as indicated.

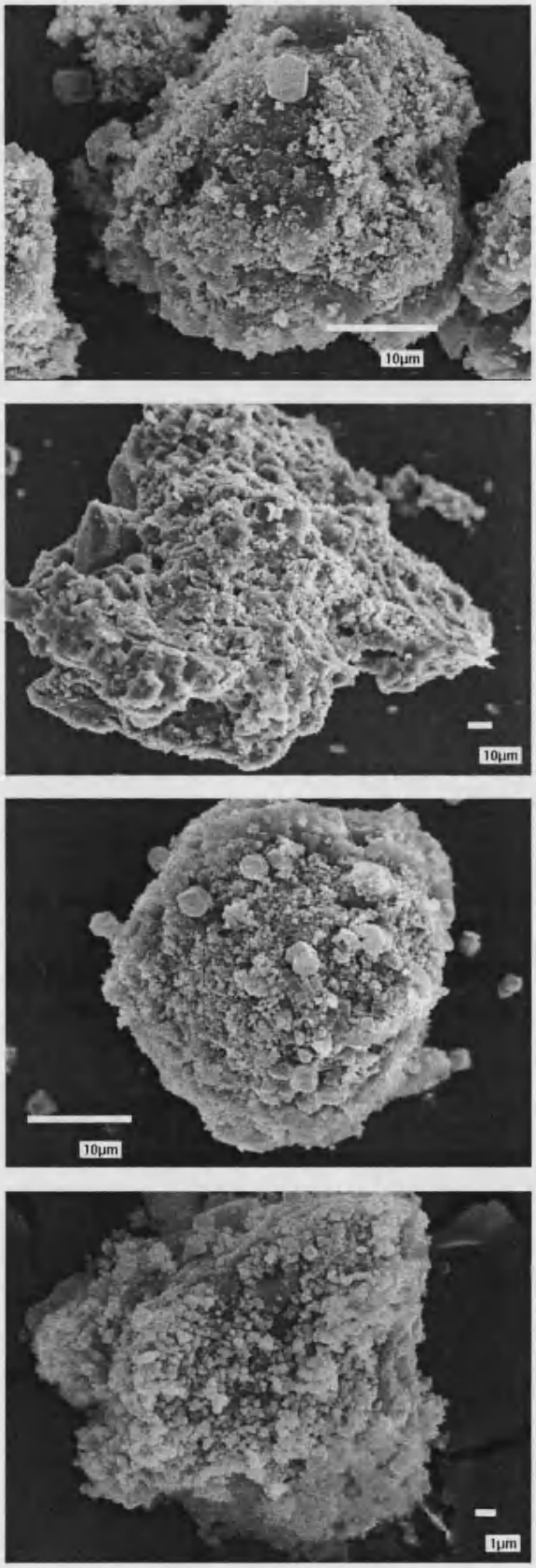

(a)
δT = 15 °C
time = 24 h

(b)
δT = 15 °C
time = 6 h

(c)
δT = 5 °C
time = 24 h

(d)
δT = 5 °C
time = 6 h

Figure 5.29 Results of crystal growth experiments using microspheres sintered at 900 °C, under conditions as indicated.

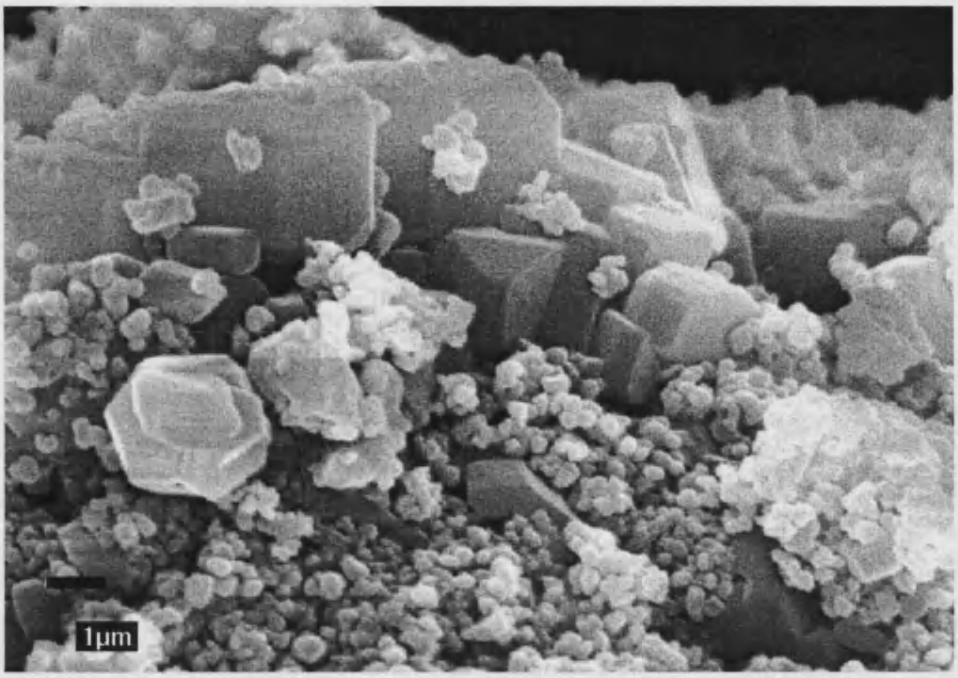

(a)

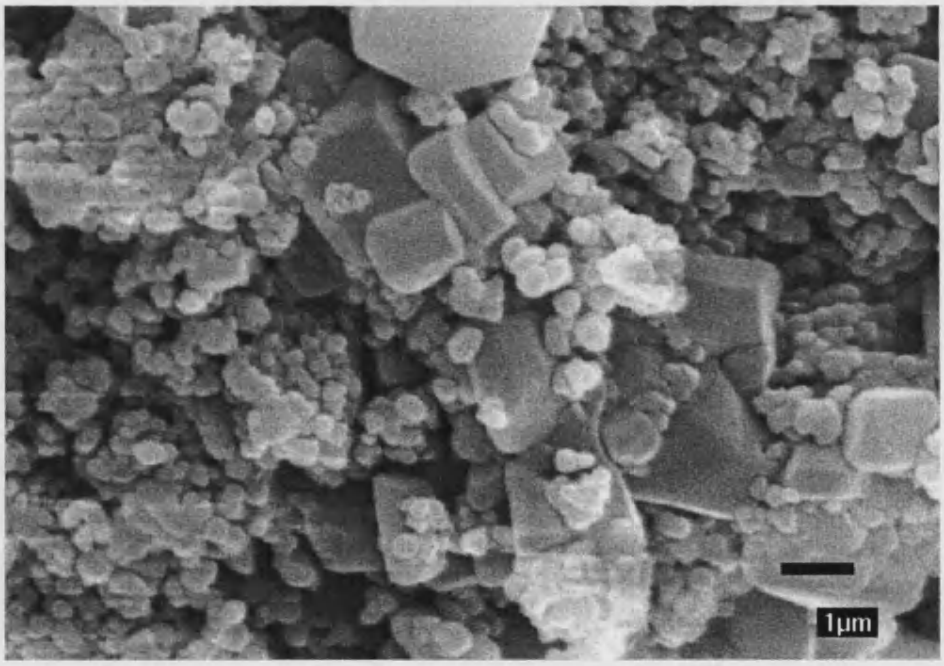

(b)

Figure 5.30 Two SEM micrographs showing propranolol.HCl crystals on the surface of a microsphere sintered at 900 °C (δT = 5 °C, time = 24 h)

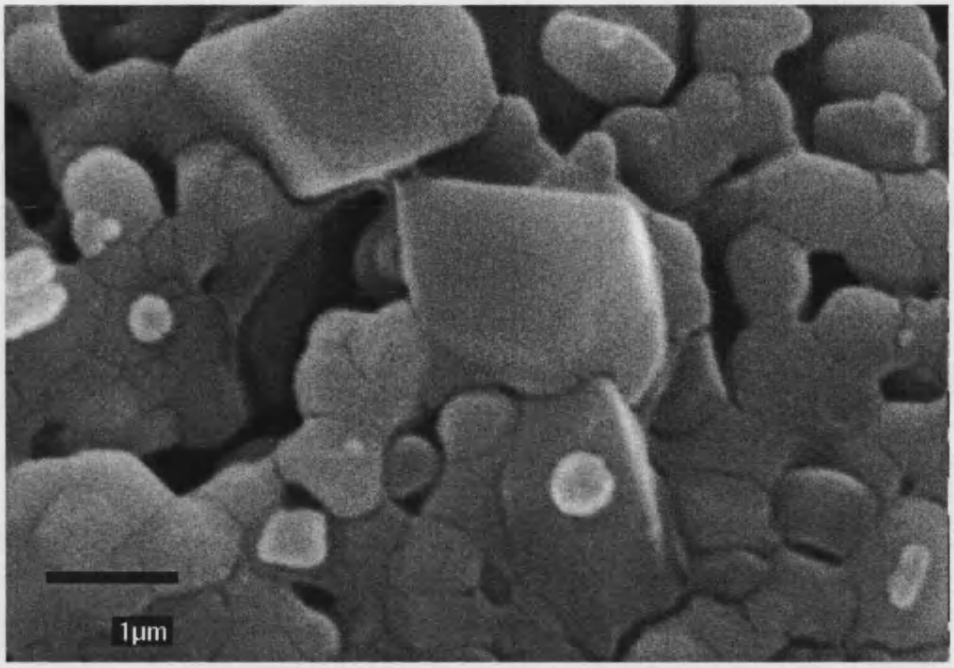

(b)Conditions: δ = 15 °C, time = 6 h.

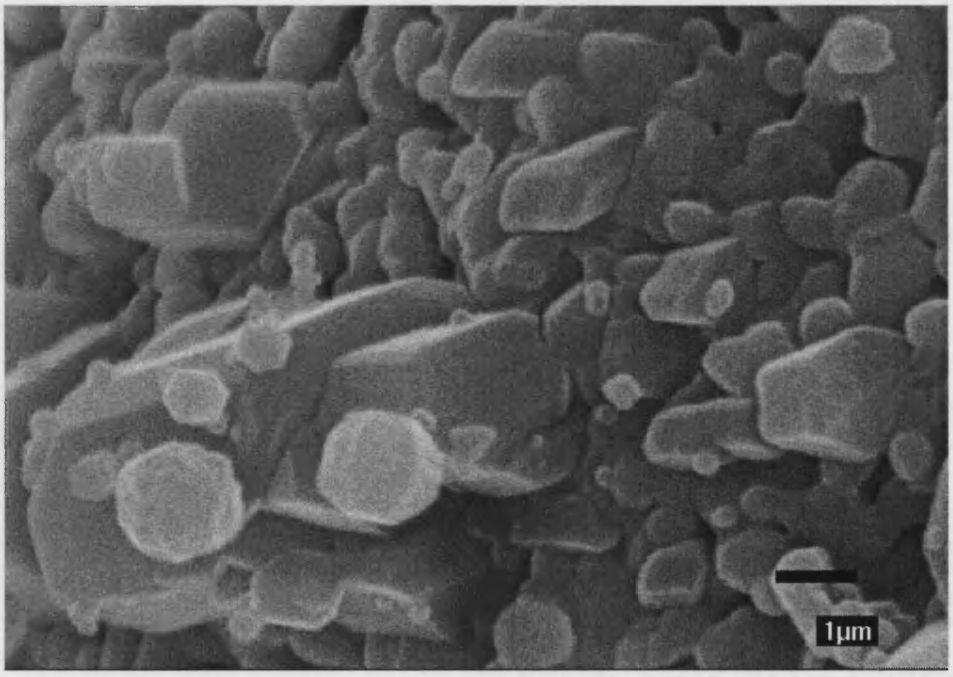

(b) Conditions: δ = 5 °C, time = 24 h

Figure 5.31. SEM micrographs of propranolol.HCl crystals grown on the surface of the microspheres.

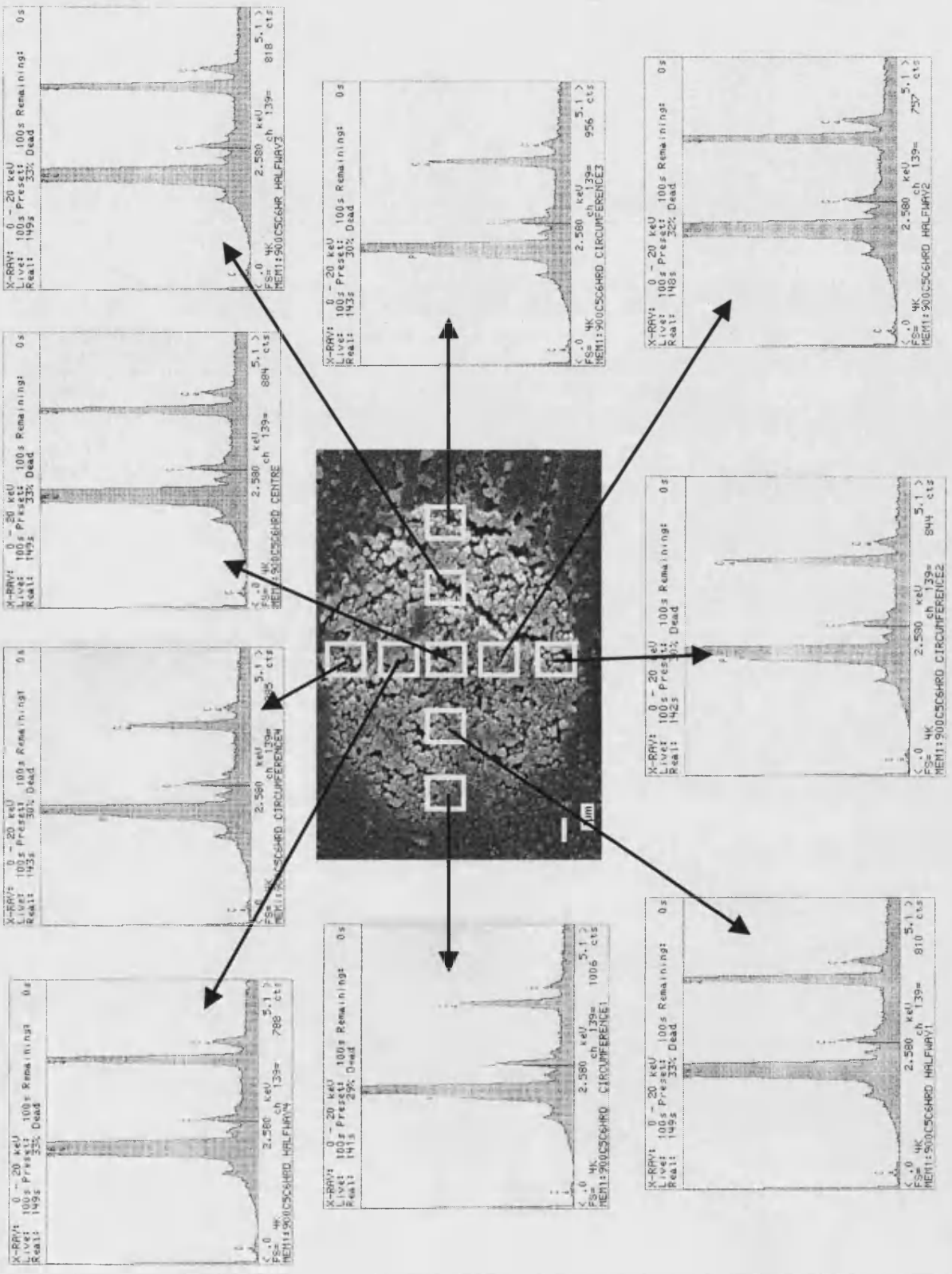

Figure 5.32 The results of EDX analysis of areas of a dissected microspheres.

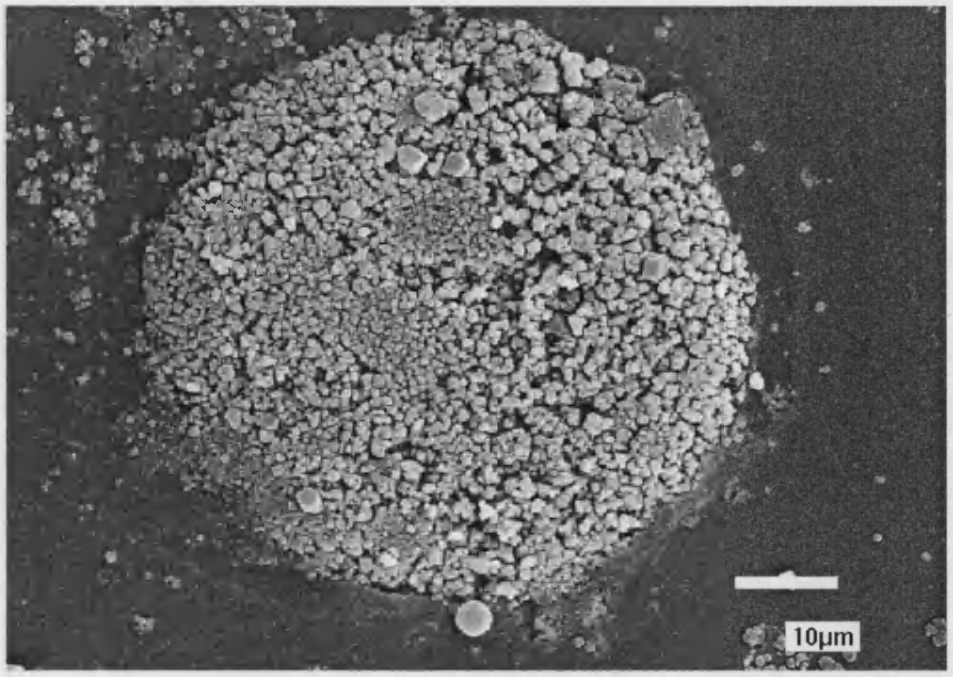

Figure 5.33 A flattened microsphere.

5.10 General Discussion

In this study, methods for loading model drugs into β-TCP microspheres, both non-sintered and sintered, were investigated. For non-sintered systems, benzamide was added directly to the β-TCP spray-drying slurry as a solute or as a suspension. The drug was then spray-dried together with the β-TCP. The benzamide-loaded and benzamide-free microspheres were found to be similar under the SEM. No drug crystals were observed. *In vitro* dissolution results show instant release of benzamide from the microspheres.

Based on the mechanism of how droplets dry in the spray-drying process, it is reasonable to expect that dissolved benzamide will stay mainly deposited on the outside of the microspheres and therefore quick release of benzamide resulted. Fine dispersed benzamide particles are expected to disperse evenly within the β-TCP matrix. However, the particle-size of the benzamide particles used may be too large for incorporation into the microspheres.

The loading of model drugs into sintered microspheres was achieved by a vacuum method, followed by a filtration technique. It was found that using a higher concentration of drug loading solution, a higher percentage drug loading into the microspheres was achieved. This is consistent for all three model drugs tested. Therefore it is concluded that if a high drug loading is intended, a higher concentration of drug loading solution should be used. The methods to obtained high concentration drug solution include using an alternative solvent or using an increased temperature.

Drugs covering the outer surface of the microspheres were effectively removed by a brief washing method. However, the washing might have also extracted some of the drugs that were inside the microspheres.

It was found that the percentage drug loading is closely related to the surface area of the microspheres. Microspheres sintered at higher temperature had a lower total surface area and were found to achieve lower drug loading. For microspheres which were sintered at 900 °C, 1000 °C, 1100 °C and 1150°C, a correlation of $r^2 = 0.9997$ was obtained for their specific surface area and percentage drug loading. These results suggest that drugs were adsorbed as a thin layer on the matrix surfaces, including internal surfaces, of the porous microspheres. No drug crystals could be observed under the SEM.

When a concentrated drug solution (prepared at an increased temperature) was used in loading, drug crystals were observed on the surface of the microspheres in the SEM. It is proposed that these surface crystals were mainly formed during the filtration process due to sudden temperature drops and rapid solvent evaporation.

Dissolution results for all drug-loaded microspheres show that drugs were released quickly with ~ 50% being released in the first 20 min in most cases. There were no marked differences between the drug release profiles from microspheres sintered at different temperatures. It is proposed that the reason for this observation is because the pores in these microspheres are too big to constrain the water entrance into the microspheres; water enters and leaves the microspheres freely. It is therefore concluded that these systems would be ideal for fast release drug delivery systems. It is also

envisaged that delayed release could be achieved by coating the microspheres with a rate controlling polymer.

Analytical techniques including DSC, NMR, MS, and XRD suggested that the model drugs maintain their physical properties, chemical properties, and crystallographic structure after loaded into the microspheres.

To achieve very high drug loading, the cultivation of drug crystals inside the microspheres were studied. It was found that the size and the amount of the propranolol.HCl crystals produced are dependent on the degree of supersaturation and the incubation time. Some propranolol.HCl crystals were found inserted between the grains of the microspheres. It was also observed that some crystals were grown inside out from the pores of the microspheres. Based on these results, it is believed that with further work microspheres filled with drug crystals in all their pores, with no or limited crystals on their outer surface could be harvested. The future work could include growing drug crystals slowly by careful control of the degree of supersaturation, incubation time, and using an improved filtration technique. Filtration was found to be a crucial step in harvesting drug-loaded microspheres since concentrated solutions crystallise readily during filtration.

Both non-sintered and sintered β-TCP microspheres were found to dissolve readily in acidic media. They were found to dissolve completely in ~ 15 to 20 min using 0.1 M HCl under the standard BP dissolution test conditions. These observations reveal that if the microspheres are to be used orally and the drug is not targeted to the stomach, they have to be enteric coated to protect them from the stomach acid. This study also found that by adding 10 pph of an acid-resistance polymer, Eudragit L100, to the slurry, acid-resistant microspheres were produced.

6 Conclusions and Further Work

Organic microspheres for drug delivery have been extensively studied; however, the use of inorganic microspheres for such applications has barely been explored.

This project was therefore organised and undertaken to develop inorganic microspheres and to investigate the use of these microspheres for drug delivery. The materials chosen as the ceramic carrier were pharmaceutical grade calcium phosphates on the basis that they are mechanically strong, chemically stable and biocompatible.

In this study, inorganic bioceramic microspheres consisting of two types of calcium phosphates, DCPA and β-TCP, were produced by spray-drying. These were highly porous microspheres. The production was achieved by spraying a high solids content aqueous-based ceramic slurry, which also contained a binder (Eudragit L100) and a dispersant (Dispex A40), at ~ 200 °C. A binder was found to be necessary because it acted as the 'glue' that acted to bind the ceramic powder together to form microspheres. In this work, Eudragit L100 was found to be a suitable binder. The high solids content produced a high viscosity slurry that assists in forming a stable suspension of the particles in the liquid. A dispersant was required to reduce the viscosity of the slurry and to produce a stable and homogeneous ceramic slurry.

The freshly spray-dried microspheres consisted of loosely bound, highly porous soft agglomerates with an average particle-size of ~ 10 μm - 20 μm and a high surface area of ~ 45 m^2/g. The high porosity and high surface area of the microspheres are desirable characteristics for the system to be used as drug carriers because it means the carriers have a big capacity for drugs, *i.e.*, there is available both a large-volume for drug containment, and a large surface area for drug adsorption.

It was observed that the characteristics of the sprayed products, including surface morphology, porosity, moisture content, and particle-size could be modified by changing the slurry compositions (solids content; binder type and binder concentration; dispersant concentration; ceramic powder type; and powder particle-size) and spray-drying operation conditions (temperature; jet size). This has important implications in

that it means that a wide variety of calcium phosphate microspheres drug carriers with various characteristics could be produced.

In the ceramics industry, both traditional and advanced, the size of the voids and their volume fraction in a finished piece are controlled by the pressing regime on the green body. In the case of spray-dried products, the voids and porosity can be controlled by the solids content of the slurry used in the spray-drying and the control systems on the spray drier. In this study, it was found that the spraying temperature also affects the 'hollowness' of the microspheres produced. At 180 °C - 220 °C, hollow centred microspheres were obtained; while at 245 °C, solid centred microspheres were obtained. This is probably because the rate of water evaporation is very fast at high temperature and the outer layer of a microsphere formed a crust immediately. This crust restricts the microsphere from expanding in size. The centre of the microsphere never reaches the boiling temperature of the water. Water at the centre of the microsphere diffuses to the surface through capillary action for evaporation. The heat flow in the system would also be expected to have a significant influence on the product.

A model drug, benzamide, was loaded into the microspheres by co-spray-drying benzamide with the ceramic powder. The dissolution test results show that the benzamide was released quickly from the systems. The reasons proposed for this observation are:

1) Dissolved benzamide travels with the solvent to the microspheres surface during solvent evaporation in the spray-drying process. The drug therefore finally deposits near the outer surface of the microspheres.
2) The microspheres are themselves highly porous and have pores that allow water to enter and leave freely.

It is therefore suggested that the basic microsphere system can be suitable for instant release applications.

The β-TCP microspheres were sintered over a temperature range of 900 °C to 1300 °C. It was found that after sintering, the microspheres became mechanically strong and hard. This study also found that the sintering treatment significantly alters the grain

size, porosity, density, mechanical strength, surface area, and pore-size of the microspheres. These changes are the consequences of material diffusion at high temperatures. The particles fused together to reduce the surface area, which in turn reduced the energy state of the system. In the process, a desirable structure and morphology was developed.

The porosity, pore-size, and surface area are important characteristics of a drug carrier because:

1) They determine the quantity of drug that can be adsorbed onto the carrier;
2) They determine the volume of drug that can be contained in the carrier;
3) They influence the drug release profile because the drug being adsorbed on the carrier surface and the drug being contained in the carrier may be released at a different rate;
4) Different pore-sizes may release drugs at different rates.

In this study, principally, the effect of sintering temperature was investigated, simply because temperature is considered to be the most important factor in sintering as it affects the morphology of the voids/pores. However, it is also well established that the length of time and the atmosphere within which the sintering is carried out also affects the extent and the results of sintering. With further work, these variables could be used to extend the range of controls for optimising the properties of the microspheres.

It is envisaged that by controlling the spray-drying processes and the sintering conditions, a porous microsphere drug delivery systems with a wide range of controlled characteristics and manufacturing flexibility can be produced. In other words, with further work, these microspheres could eventually be developed into 'designer' carrier systems for different applications.

Sintering changes the physical form of the microspheres but it does not modify their biocompatibility. It is believed that as a bone implant, calcium phosphate bioceramic microspheres, either sintered or non-sintered, would be a superior drug carrier to organic materials. This is because apart from being biocompatible and resorbable, the carrier material is bioactive. This means that after drug delivery the calcium phosphate can act as a bone precursor, supplying raw material for osteogenesis and be

incorporated into the new bone. This removes the painful and costly procedure of surgically removing the drug carrier materials after drug delivery, which at the present is the standard procedure for treating patients with osteomyelitis. Calcium phosphate bioceramics will also have a greater mechanical strength and stability that organic materials cannot match.

The sintered bioceramic microspheres have also been found to have the characteristics desired for transdermal needle-free powder injection, namely biocompatibility, physical hardness, high density, chemical stability and the correct particle-size. It was found that the sintered β-TCP microspheres have a density of ~ 3 g/cm^3 and are physically robust. The high density allows them to achieve a high momentum, to penetrate deeper into the skin and the physical robustness allows the particle to survive the process of travelling at sonic speeds and the subsequent impact on the skin. The carriers currently used for powder injection are organic polymers and gold particles. Calcium phosphate microspheres are mechanically stronger and denser than organic materials, and they do not have the toxicity and cost associated with gold.

The depth of particle penetration in needle-free injection is dependent on particle momentum, which in turn is related to the velocity, size and density of the particles. Various particle penetration depths could be achieved by using microspheres of different sizes and densities. This study shows that sintered calcium phosphate microspheres of various controlled sizes can be obtained by altering the spray-drying process and sintering conditions. With further work, the particle-size distributions can be further strictly controlled by sieving. A narrow particle-size range can improve ability to target a specific depth of delivery.

The depth of penetration is directly proportional to particle density. Based on the calculation that sintered β-TCP microspheres have a density of 3 g/cm^3, if a particle of x μm in diameter can achieve a particle penetration of y μm, then, by using a bigger size particle of $2x$ μm, a particle penetration of $2y$ μm can be achieved. It has been shown that particles up to 100 μm are suitable for needle-free injection without excessively damaging the skin. Organic particles (density < 1 g/cm^3) of 20 μm – 70 μm have been used to achieve extracellular particle delivery, and dense gold particles (density ~

19.5 g/cm^3) of ≤ 3 μm have achieved intracellular delivery. In this experimental work, bioceramic particles in range of 10 μm – 20 μm were made. By varying the spray-drying process, particles of up to 100 μm could be produced by spray-drying with the present system. Using larger commercial equipment, spray-dried particles of three times this size can be made. Thus there is a good range of particle-sizes available for achieving controlled depth delivery.

The main challenges of the needle-free powder delivery technology today are:

1) Limited payload - The current system has a restricted skin treatment area of up to 2 cm^2, therefore, doses are generally limited in the low milligram range;
2) Lack of carriers with sustained release properties;
3) Organic carriers do have limited chemical and physical shelf stability;
4) The production should be high yield and a scalable process.

It is envisaged that calcium phosphate bioceramic microspheres could meet these challenges because:

1) They are highly porous; therefore a high payload can be achieved.
2) They are inert materials which will have unlimited chemical and physical stability giving an extended shelf life. Being inert also infers that they do not react with drugs.
3) Their production (spray-drying and sintering) is a high yield, scalable, economic process capable of being fully automated.
4) By controlling the pore-size of the microspheres, they could be themselves developed into controlled release carriers. Furthermore, they could also be coated with a rate-controlling polymer to achieve other levels of controlled release.

Calcium phosphate microspheres could also be used for oral delivery because the compound is orally acceptable. Calcium phosphate microspheres may be used as carriers for drug or food to mask the bitter taste. This study found that the β-TCP microspheres are stable in alkaline conditions, but dissolved completely in strong acidic conditions in ~ 20 min. Therefore they can be used as instant release formulations for drug release in the stomach. These microspheres can also be further modified into oral controlled release systems by coating them with an acid-resistance polymer or rate-

controlling polymers to achieve enteric coated formulations and controlled release formulations. They could also function as a scaffold for subsequent coatings of control release systems, giving greater flexibility to the design of control systems.

Model drugs were loaded into sintered microspheres by a vacuum method. It was found that using non-concentrated drug loading solutions, drugs were adsorbed as a layer on the surface of the porous matrix. This study also demonstrates that it is possible to grow crystals inside the pores of the microspheres. This would be a way to pack a larger quantity of drugs inside the microspheres. It was found that the size and the quantity of crystals growth could be controlled by the degree of supersaturation of the drug solution and the incubation time. Therefore, with the correct conditions, it is possible to generate microspheres filled with drug crystals in all their pores (Figure 6.1). The implication is that the depth (length to diameter) of the pores could be an important control mechanism for controlled release whilst at the same time a high drug loading could also be obtained.

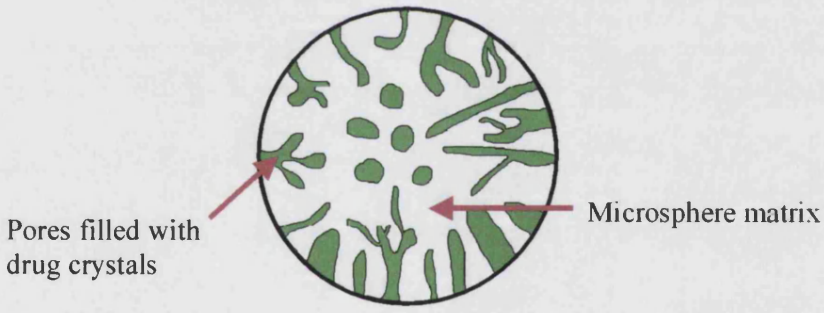

Figure 6.1 Schematic diagram of a microsphere filled with drug crystals in pores.

Filtration was found to be a crucial step in harvesting microspheres containing drug crystals since supersaturated solutions crystallise readily during filtration. It is proposed that instant crystallisation could be avoided by surrounding the microspheres with a liquid in which the drug is not soluble after the crystal growth, before the filtration takes place. Alternatively, a washing experiment that will remove all the surface crystals that form during filtration could also be used.

Therefore, with further investigation into the effects of a wider range of degree of supersaturation and incubation time, and with an improved filtering technique, it is believed that a microsphere densely packed with drug crystals could be achieved.

Dissolution test results show that the flexible delayed release of drugs was not achieved solely in the sintered microsphere systems. Model drugs were released quickly (in most cases, ~ 50% was released in the first 20 min) and no marked differences were observed for microspheres with varying pore-sizes. It is believed that this is because the pores in the microspheres are too big to constrain the water movement in and out of the microspheres. However, controlled release or targeted release could be achieved by coating the microspheres with polymers of various characteristics (*e.g.*, rate-controlled and environment sensitive). Furthermore, a standard 900 ml dissolution medium was used for the *in vitro* release in this study. The conditions will be different if the microspheres were used as an implant or by transdermal powder delivery. In such environments, there is a limited supply of fluid; hence, the microspheres' reservoirs might be expected to release their contents more slowly over an extended period of time.

An investigation into the use of the microsphere systems in a commercial needle-free injectable delivery device, such as the Powderject® device, should be performed to explore and assess its practical pharmaceutical value.

In conclusion, in this study it was found that:

1) Microspheres of two calcium phosphates, DCPA and β-TCP, were produced by spray-drying high solids content slurries which contained a binder and a dispersant.

2) The spray-dried microspheres are affected by the slurry composition (solids content; binder type and binder concentration; dispersant concentration; ceramic powder type; and powder particle-size) and spray-drying operation conditions (temperature; jet size).

3) The production of β-TCP microspheres is easier and quicker than DCPA microspheres because there are less process steps and therefore more suitable for larger scale production.

4) Sintering changes the mechanical hardness, porosity, pore-size, and surface area of the DCPA and β-TCP microspheres. The soft agglomerates of spray-dried microspheres became mechanically hard and strong after sintering.

5) Sintered microspheres have pores of ~ 0.1 μm - 5 μm in diameter with hardly any small pores in the nanometer range.

6) The porosity and the specific surface area of the microspheres decrease as the sintering temperature increases.

7) Drugs can be loaded into non-sintered microspheres by direct addition of the drug into the spray-drying slurry, and then co-spray-drying with the ceramic powder. Drugs can be loaded into sintered microspheres by a vacuum method.

8) Using a vacuum method for drug loading, the percentage drug loading is closely related to the surface area of the microspheres. Microspheres with a lower total surface area were found to achieve lower drug loading and *vice versa.*

9) BP standard dissolution test results showed that drugs were released quickly from both non-sintered and sintered drug-loaded microspheres. No marked differences were observed among the drug release profiles from microspheres sintered at different temperatures.

10) Drug crystals could be grown inside the pores of the microspheres. The size and the quantity of the crystals produced were dependent on the degree of supersaturation of the drug solution and the incubation time.

Reference List

In the Style of British Medical Journal

1. Sastry SV, Nyshadham JR, Fix JA. Recent technological advances in oral drug delivery - a review. *Pharmaceutical Science & Technology Today* 2000;**3**:138-45.

2. Tranter D. Pharmaceutical science and technology today: evolving to reflect the modern industrial life-science environment. *Pharmaceutical Science & Technology Today* 2000;**3**:399-400.

3. Czaban, JN. Attorney review. *Drug Delivery Technology* 2001;**1**:24-6.

4. Yokoyama M. Gene delivery using temperature-responsive polymeric carriers. *Drug Discovery Today* 2002;**7**:426-32.

5. Chien YW. Rate-control drug delivery systems - controlled release vs sustained-release. *Medical Progress Through Technology* 1989;**15**:21-46.

6. Chien YW, Cabana BE, Mares SE. Controlled-release drug administration: Logic. In: *Novel drug delivery systems: fundamentals, developmental concepts, biomedical assessments.* New York: Marcel Dekker, 1982:1-11.

7. Lee PI, Good WR. Overview of Controlled-Release Drug Delivery. In Lee PI, Good WR, eds. *Controlled Release Technology - Pharmaceutical Application.* Washington DC: American Chemical Society. 1987:1-13.

8. Supersaxo A, Kou JH, Teitelbaum P, Maskiewicz R. Preformed porous microspheres for controlled and pulsed release of macromolecules. *Journal of Controlled Release* 1993;**23**:157-64.

9. Langer R. Polymer-controlled drug-delivery systems. *Accounts of Chemical Research* 1993;**26**:537-42.

10. Conti B, Giunchedi P, Conte U. Cellulose microparticles in drug delivery. *STP Pharma Sciences* 1997;**7**:331-42.

11. Woo BH, Jiang G, Jo YW, Deluca PP. Preparation and characterization of a composite PLGA and poly(acryloyl hydroxyethyl starch) microsphere system for protein delivery. *Pharmaceutical Research* 2001;**18**:1600-6.

12. Sato T, Kanke M, Schroeder HG, Deluca PP. Porous biodegradable microspheres for controlled drug delivery .1. assessment of processing conditions and solvent removal techniques. *Pharmaceutical Research* 1988;**5**:21-30.

13. Mi FL, Tan YC, Liang HF, Sung HW. In vivo biocompatibility and degradability of a novel injectable-chitosan-based implant. *Biomaterials* 2002;**23**:181-91.

14. Sakagami M, Sakon K, Kinoshita W, Makino Y. Enhanced pulmonary absorption following aerosol administration of mucoadhesive powder microspheres. *Journal of Controlled Release* 2001;**77**:117-29.

15. Giunchedi P, Conte U. Spray-drying as a preparation method of microparticulate drug- delivery systems - an overview. *STP Pharma Sciences* 1995;**5**:276-90.

16. Vasheghani-Farahani E, Khorram M. Hydrophilic drug release from bioerodible polyanhydride microspheres. *Journal of Applied Polymer Science* 2002;**83**:1457-64.

17. van der Lubben IM, Verhoef JC, Borchard G, Junginger HE. Chitosan for mucosal vaccination. *Advanced Drug Delivery Reviews* 2001;**52**:139-44.

18. Lestini BJ, Sagnella SM, Xu Z, Shive MS, Richter NJ, Jayaseharan J, Case AJ, Kottke-Marchant K, Anderson JM, Marchant RE. Surface modification of liposomes for selective cell targeting in cardiovascular drug delivery. *Journal of Controlled Release* 2002;**78**:235-47.

19. Hong MS, Lim SJ, Oh YK, Kim CK. pH-sensitive, serum-stable and long-circulating liposomes as a new drug delivery system. *Journal of Pharmacy and Pharmacology* 2002;**54**:51-8.

20. Cortesi R, Esposito E, Osti M, Squarzoni G, Menegatti E, Davis SS, Nastruzzi C. Dextran cross-linked gelatin microspheres as a drug delivery system. *European Journal of Pharmaceutics and Biopharmaceutics* 1999;**47**:153-60.

21. Dittgen M, Durrani M, Lehmann K. Acrylic polymers - a review of pharmaceutical applications. *STP Pharma Sciences* 1997;**7**:403-37.

22. Hino T, Shimabayashi S, Nakai A. Silk microspheres prepared by spray-drying of an aqueous system. *Pharmacy & Pharmacology Communications* 2000;**6**:335-9.

23. Li XH, Zhou SB, Wu XR, Yuan ML, Liu L, Jia WX, Deng XM, Huang ZT. Poly-DL-lactide-poly (ethylene glycol) microspheres as oral and parenteral delivery systems for hepatitis B surface antigen. *Journal of Applied Polymer Science* 2002;**83**:850-6.

24. Herrero-Vanrell R, Refojo MF. Biodegradable microspheres for vitreoretinal drug delivery. *Advanced Drug Delivery Reviews* 2001;**52**:5-16.

25. Cantor AS, Choi HO, Delgado J, Ko CU, Tran TV. Adhesive microsphere drug delivery composition. PCT/US99/06577 (WO 99/56782). 11-11-1999.

26. Sakakibara Y, Jikuya T, Mitsui T. Application of lipid microspheres containing prostaglandin E-1 ointment to peripheral ischemic ulcers. *Dermatology* 1997;**195**:253-7.

27. Illum L, Jabbal-Gill I, Hinchcliffe M, Fisher AN, Davis SS. Chitosan as a novel nasal delivery system for vaccines. *Advanced Drug Delivery Reviews* 2001;**51**:81-96.

28. Soppimath KS, Kulkarni AR, Rudzinski WE, Aminabhavi TM. Microspheres as floating drug-delivery systems to increase gastric retention of drugs. *Drug Metabolism Reviews* 2001;**33**:149-60.

29. Kortesuo P, Ahola M, Kangas M, Kangasniemi I, Yli-Urpo A, Kiesvaara J. In vitro evaluation of sol-gel processed spray-dried silica gel microspheres as carrier in controlled drug delivery. *International Journal of Pharmaceutics* 2000;**200**:223-9.

30. Nicoll SB, Radin S, Santos EM, Tuan RS, Ducheyne P. In vitro release kinetics of biologically active transforming growth factor-β1 from a novel porous glass carrier. *Biomaterials* 1997;**18**:853-9.

31. Frayssinet P, Braye F, Weber G. Analysis of sections of implanted macroporous calcium phosphate bone substitutes by proton-induced x-emission method and energy-dispersive spectrometry. *Scanning* 1997;**19**:253-7.

32. Pautard FGE. Calcium-phosphate microspheres in biology. *Progress in Crystal Growth and Characterization of Materials* 1981;**4**:89-98.

33. Wade A, Weller PJ. Handbook of Pharmaceutical Excipients. 2nd ed. London: The Pharmaceutical Press, 1994.

34. Lin SY, Cheng CL, Lin PC. Preparation and evaluation of sodium diclofenac controlled-release tablets .2. Dibasic calcium phosphate as a retardent in mixtures for direct compression. *Pharmacy World & Science* 1995;**17**:42-7.

35. De Groot K, Klein CPAT, Wolke JGC, Blieck-Hogervorst JMA. Chemistry of Calcium Phosphate Bioceramics. In: Yamamuro T, Hench LL, Wilson J, eds. *CRC Handbook of Bioactive Ceramics Vol II: Calcium Phosphate and Hydroxyapatite Ceramics.* Boca Raton: CRC Press Inc, 1990:3-16.

36. Zakaria, FA. Sintering and microstructure property relationships of porous hydroxyapatite. Bath:University of Bath, 2000 (PhD Thesis).

37. Uchida A, Nade SML, Mccartney ER, Ching W. The use of ceramics for bone-replacement - a comparative - study of 3 different porous ceramics. *Journal of Bone and Joint Surgery-British Volume* 1984;**66**:269-75.

38. Shinto Y, Uchida A, Korkusuz F, Araki N, Ono K. Calcium hydroxyapatite ceramic used as a delivery system for antibiotics. *Journal of Bone and Joint Surgery-British Volume* 1992;**74-B**:600-4.

39. Uchida A, Shinto Y, Araki N, Ono K. Slow release of anticancer drugs from porous calcium hydroxyapatite ceramic. *Journal of Orthopaedic Research* 1992;**10**:440-5.

40. Lasserre A, Bajpai PK. Ceramic drug-delivery devices. *Critical Reviews in Therapeutic Drug Carrier Systems* 1998;**15**:1-56.

41. Itokazu M, Matsunaga T, Kumazawa S, Oka M. Treatment of osteomyelitis by antibiotic-impregnated porous hydroxyapatite block. *Clinical Materials* 1994;**17**:173-9.

42. Martins VCA, Goissis G, Ribeiro AC, Marcantonio E, Bet MR. The controlled release of antibiotic by hydroxyapatite: Anionic collagen composites. *Artificial Organs* 1998;**22**:215-21.

43. Itokazu M, Sugiyama T, Ohno T, Wada E, Katagiri Y. Development of porous apatite ceramic for local delivery of chemotherapeutic agents. *Journal of Biomedical Materials Research* 1998;**39**:536-8.

44. Otsuka M, Matsuda Y, Suwa Y, Fox JL, Higuchi WI. A novel skeletal drug-delivery system using self-setting calcium- phosphate cement. 2. Physicochemical properties and drug-release rate of the cement-containing indomethacin. *Journal of Pharmaceutical Sciences* 1994;**83**:611-5.

45. Otsuka M, Matsuda Y, Suwa Y, Fox JL, Higuchi WI. A novel skeletal drug-delivery system using self-setting calcium- phosphate cement. 4. Effects of the mixing solution volume on the drug-release rate of heterogeneous aspirin-loaded cement. *Journal of Pharmaceutical Sciences* 1994;**83**:259-63.

46. Otsuka M, Nakahigashi Y, Matsuda Y, Fox JL, Higuchi WI, Sugiyama Y. A novel skeletal drug delivery system using self-setting calcium phosphate cement VIII: The relationship between in vitro and in vivo drug release from indomethacin-containing cement. *Journal of Controlled Release* 1997;**43**:115-22.

47. Otsuka M, Matsuda Y, Wang Z, Fox JL, Higuchi WI. Effect of sodium bicarbonate amount on in vitro indomethacin release from self-setting carbonated-apatite cement. *Pharmaceutical Research* 1997;**14**:444-9.

48. Otsuka M, Nakahigashi Y, Matsuda Y, Fox JL, Higuchi WI, Sugiyama Y. Effect of geometrical cement size on in vitro and in vivo indomethacin release from self-setting apatite cement. *Journal of Controlled Release* 1998;**52**:281-9.

49. Masters K. Introduction. *Spray-drying Handbook*. London: George Godwin, 1985:1-18.

50. Broadhead J, Rouan SKE, Rhodes CT. The spray-drying of pharmaceuticals. *Drug Development and Industrial Pharmacy* 1992;**18**:1169-206.

51. Masters K. Spray-dryer components. *Spray-drying Handbook*. London:George Godwin, 1985:111-37.

52. Shaw FV. Spray-drying - a traditional process for advanced applications. *American Ceramic Society Bulletin* 1990;**69**:1484-9.

53. Luo P, Nieh TG. Preparing hydroxyapatite powders with controlled morphology. *Biomaterials* 1996;**17**:1959-64.

54. Lukasiewicz SJ. Spray-drying ceramic powders. *Journal of the American Ceramic Society* 1989;**72**:617-24.

55. Walker WJ, Reed JS, Verma SK. Influence of slurry parameters on the characteristics of spray-dried granules. *Journal of the American Ceramic Society* 1999;**82**:1711-9.

56. Niven RW. Delivery of biotherapeutics by inhalation aerosol. *Critical Reviews in Therapeutic Drug Carrier Systems* 1995;**12**:151-231.

57. Masters K. Applying spray-drying to ceramics. *American Ceramic Society Bulletin* 1994;**73**:63.

58. Zhang Y, Tang XX, Uchida N, Uematsu K. Binder surface segregation during spray-drying of ceramic slurry. *Journal of Materials Research* 1998;**13**:1881-7.

59. Takami K, Machimura H, Takado K, Inagaki M, Kawashima Y. Novel preparation of free flowing spherically granulated dibasic calcium phosphate anhydrous for direct tabletting. *Chemical & Pharmaceutical Bulletin* 1996;**44**:868-70.

60. Ring TA. Sintering. *Fundamentals of Ceramic Powder Processing and Synthesis*. London: Academic Press Ltd., 1996:781-874.

61. Cutler IB. Active powders. In Onoda GY, Jr., Hench LL, eds. *Ceramic Processing Before Firing*. New York: John Wiley & Sons, 1978:21-9.

62. Shanefield DJ. Ceramic processing fundamentals. *Organic Additives and Ceramic Processing, with Applications in Powder Metallurgy, Ink, and Paint*. London: Kluwer Academic Publishers, 1996:91-114.

63. Shanefield DJ. Binders. *Organic Additives and Ceramic Processing, with Applications in Powder Metallurgy, Ink, and Paint*. London: Kluwer Academic Publishers, 1996:255-79.

64. Ichinose N, Komeya K, Ogino N, Tsuge A, Yokomizo Y. Fundamentals of ceramics: questions and answers. In: Ichinose N, ed. *Introduction to Fine Ceramics - Applications in Engineering.* Chichester: John Wiley & Son Ltd., 1987:1-41.

65. http://www.medmedia.com/o16/27.htm (17-2-2002). Addition of antibiotics to cement.

66. Petty WMD. The effect of methylmethacrylate on bacterial phagocytosis and killing by human polymorphonuclear leukocytes. *The Journal of Bone and Joint Surgery* 1978;**60-A**:752-7.

67. Hickey PL. Powder injection - a novel mode of drug delivery opening the way for new modes of therapy. *Drug Delivery Systems and Science* 2001;**1**:25-9.

68. Gardner MA, Stout R, Segarra V, Redmond M, Milne L. North Carolina clinical survey: implementation of the Bioject needle-free injection management system™ into North Carolina's state public health system. 5-3-1997. Bioject Inc., Portland, Or. USA.

69. Mckenzie R. Clinical-applications of jet injection. *New Zealand Medical Journal* 1982;**95**:815-7.

70. Bellhouse BJ, Sarphie DF, Greenford JC. Needleless syringe using supersonic gas flow for particle delivery. 94912038.0 (EP0693119B1) 1997.

71. http://www.powderject.com/vaccines_fs.htm (14-4-2002). PowderJect Pharmaceuticals plc research and development update.

72. http://www.powderject.com/powderinjection_fs.htm (14-4-2002). Vaccines in development.

73. Johnson M-J, Longridge DJ, Hickey PL. Development of an insulin dermal Powderject particle-delivery system to achieve high bioavailability in the rat. *Journal of Pharmacy and Pharmacology* 2000;**52** (Suppl):48.

74. http://www.powderject.com/powderinjection_fs.htm (2-3-2002). Powderject vaccines.

75. Burkoth TL, Bellhouse BJ, Hewson G, Longridge DJ, Muddle AG, Sarphie DF. Transdermal and transmucosal powdered drug delivery. *Critical Reviews in Therapeutic Drug Carrier Systems* 1999;**16**:331-84.

76. Roy MJ, Wu MS, Barr LJ, Fuller JT, Tussey LG, Speller S, Culp J, Burkholder JK, Swain WF, Dixon RM, Widera G, Vessey R, King A, Ogg G, Gallimore A, Haynes JR, Fuller DH. Induction of antigen-specific CD8+T cells, T helper cells, and protective levels of antibody in humans by particle-mediated administration of a hepatitis B virus DNA vaccine. *Vaccine* 2000;**19**:764-78.

77. http://www.powderject.com/vaccines_fs.htm (4-3-2002). PowderJect systems for particle delivery.

78. http://www.powderject.com/mains/vaccines.htm (15-3-2000). Vaccines.

79. Staniforth JN. Particle size analysis. In: Aulton ME, ed. *Pharmaceutics: The Science of Dosage Form Design*. London: Churchill Livingstone, 1988:564-80.

80. Malvern Instruments brochure: Mastersizer 2000 – a unified system for particle sizing. Hungerford: C. Force Communications Limited, 2001.

81. Pathak YV, Labhashetwar VD. Evaluation of drug delivery systems by electron-microscopy techniques. *Cells and Materials* 1993;**3**:51-66.

82. Read ND, Jeffree CE. Low-temperature scanning electron-microscopy in biology. *Journal of Microscopy-Oxford* 1991;**161**:59-72.

83. Potter UJ, Love G. Scanning electron microscopy. *Microscopy* 1999;1397-406.

84. http://www.xraydiffrac.com/xrd.htm (27-1-2002). Technology of materials - X-ray diffraction studies.

85. Nath S, Satpathy GR. A systematic approach for investigation of spray-drying processes. *Drying Technology* 1998;**16**:1173-93.

86. Billon A, Bataille B, Cassanas G, Jacob M. Development of spray-dried acetaminophen microparticles using experimental designs. *International Journal of Pharmaceutics* 2000;**203**:159-68.

87. Withop A, Malinowski W. Organic sources of voids in ceramics. *American Ceramic Society Bulletin* 1978;**57**:523-4.

88. Carbone TJ, Reed JS. Dependence of sintering response with a constant rate of heating on processing-related pore distribution. *American Ceramic Society Bulletin* 1978;**57**:749-50.

89. Lefebvre AH. Atomization and sprays. London: Hemisphere Publishing Corporation, 1989.

90. Masters K. Control systems. *Spray-drying Handbook*. London: George Godwin, 1985:355-72.

91. Wu XK, Whitman DW, Kaufell WL, Finch WC, Cumbers DI. Acrylic binders for dry pressing ceramics. *American Ceramic Society Bulletin* 1997;**76**:49-52.

92. Shanefield DJ. Dispersants. *Organic Additives and Ceramic Processing, with Applications in Powder Metallurgy, Ink, and Paint*, pp 211-54. London: Kluwer Academic Publishers, 1996.

93. Lefebvre AH. Drop-size distribution from pneumatic atomizers. *Atomization and Sprays*, pp 74-80. London: Hemisphere Publishing Corporation, 1989.

94. Lin SY, Kao YH. Effect of eudragit resins and dibasic calcium-phosphate on the compaction and dissolution behavior of directly compressible controlled-release theophylline tablet. *Drug Development and Industrial Pharmacy* 1990;**16**:855-74.

95. Masters K. Atomization. *Spray-drying Handbook*. London: George Godwin, 1985:171-262.

96. Hollinger M. Fineparticle Research Group, Department of Physics, Laurentian University, Canada, 2002 (Personal communication).

97. Kaye BH. Sieve fractionation of powders. *Direct Characterization of Fineparticles*. New York: John Wiley & Sons, 1981:55-95.

98. Takahashi H, Shinohara N, Okumiya M, Uematsu K, Junichiro T, Iwamoto Y, Kamiya H. Influence of slurry flocculation on the character and compaction of spray-dried silicon-nitride granules. *Journal of the American Ceramic Society* 1995;**78**:903-8.

99. Greenwood R, Bergstrom L. Electroacoustic and rheological properties of aqueous Ce-ZrO2 (Ce-TZP) suspensions. *Journal of the European Ceramic Society* 1997;**17**:537-48.

100. Shanefield DJ. Colloid science - as applied to ceramics. *Organic Additives and Ceramic Processing, with Applications in Powder Metallurgy, Ink, and Paint*. London: Kluwer Academic Publishers, 1996:131-70.

101. Kayes JB. Disperse systems. In: Aulton ME, ed. *Pharmaceutics: The Science of Dosage Form Design*. London: Churchill Livingstone, 1988:81-118.

102. Vogel EM. Dispersants for ferrite slurries. *American Ceramic Society Bulletin* 1979;**58**:453-8.

103. Jarnstrom L, Stenius P. Adsorption of polyacrylate and carboxy methyl cellulose on kaolinite - salt effects and competitive adsorption. *Colloids and Surfaces* 1990;**50**:47-73.

104. Okuyama M, Garvey GJ, Ring TA, Haggerty JS. Dispersion of silicon-carbide powders in nonaqueous solvents. *Journal of the American Ceramic Society* 1989;**72**:1918-24.

105. Abel JS, Stangle GC, Schilling CH, Aksay IA. Sedimentation in flocculating colloidal suspensions. *Journal of Materials Research* 1994;**9**:451-61.

106. Karas A, Kumagai T, Cannon WR. Casting behavior and tensile-strength of cast $BaTiO_3$ tape. *Advanced Ceramic Materials* 1988;**3**:374-7.

107. Mistler RE, Shanefield DJ, Runk RB. Tape Casting of Ceramics. In: Onoda GY, Jr., Hench LL, eds. *Ceramic Processing Before Firing*. New York: John Wiley & Sons, 1978:411-48.

108. Tas AC. Combustion synthesis of calcium phosphate bioceramic powders. *Journal of the European Ceramic Society* 2000;**20**:2389-94.

109. Vaughan D. Energy-dispersive X-ray microanalysis - An introduction, pp 31-48. Foster City: Kevex Corporation, 1983.

110. Carr RL Jr. Evaluating flow properties of solids. Chemical Engineering. 1965:163-168.

111. Staniforth JN. Powder flow. In: Aulton ME, ed. *Pharmaceutics: The Science of Dosage Form Design*. London: Churchill Livingstone, 1988:600-15.

112. Micromeritics AccuPyc 1330 Operational Manual V2.01, Appendix B, 1995:B1-B3.

113. Newman AW. Micromeritics. In: Brittain H.G., ed. *Physical Characterization of Pharmaceutical Solids*. New York: Marcel Dekker, 1995:253-80.

114. Webb PA, Orr C. Analytical methods in fine particle technology. Micromeritics Instrument Corporation, Norcross, USA, 1997.

115. Brunauer S, Emmett PH, Teller E. Adsorption of gases in multimolecular layers. *Journal of American Chemical Society* 1938;**60**:309-19.

116. Lowell S, Shields JE. Adsorbate cross-sectional areas. *Powder Surface Area and Porosity*, pp 36-43. London: Chapman and Hall Ltd, 1984.

117. Westermarck S, Juppo AM, Koiranen K, Yliruusi J. Mercury porosimetry of pharmaceutical powders and granules. *Journal of Porous Materials* 1998;**5**:77-86.

118. Leon CALY. New perspectives in mercury porosimetry. *Advances in Colloid and Interface Science* 1998;**77**:341-72.

119. Lowell S, Shields JE. Powder surface area and porosity. London: Chapman and Hall Ltd., 1984.

120. Webb PA, Orr C. Pore structure by mercury intrusion porosimetry. *Analytical Methods in Fine Particle Technology*. Norcross: Micromeritics Instrument Corporation, 1997:155-92.

121. Kim SH, Chu CC. Pore structure analysis of swollen dextran-methacrylate hydrogels by SEM and mercury intrusion porosimetry. *Journal of Biomedical Materials Research* 2000;**53**:258-66.

122. Juppo AM. Change in porosity parameters of lactose, glucose and mannitol granules caused by low compression force. *International Journal of Pharmaceutics* 1996;**130**:149-57.

123. Lowell S, Shields JE. Microporosity. *Powder Surface Area and Porosity*, pp 75-86. London: Chapman and Hall Ltd., 1984.

124. Washburn EW. Note on a method of determining the distribution of pore sizes in a porous material. *Proceedings of the National Academy of Sciences* 1921;**7**:115-6.

125. Bain DF, Munday DL, Smith A. Modulation of rifampicin release from spray-dried microspheres using combinations of poly-(DL-lactide). *Journal of Microencapsulation* 1999;**16**:369-85.

126. Burgess DJ, Carless JE. Manufacture of gelatin/gelatin coacervate microcapsules. *International Journal of Pharmaceutics* 1985;**27**:61-70.

127. Lim ST, Martin GP, Berry DJ, Brown MB. Preparation and evaluation of the in vitro drug release properties and mucoadhesion of novel microspheres of hyaluronic acid and chitosan. *Journal of Controlled Release* 2000;**66**:281-92.

128. Billon A, Petit M, Doko MB, Bataille B, Jacob M. Effects of cellulose derivatives and additives in the spray-drying preparation of acetaminophen delivery systems. *Drug Development and Industrial Pharmacy* 1999;**25**:1149-56.

129. Baras B, Benoit MA, Gillard J. Parameters influencing the antigen release from spray-dried poly(DL-lactide) microparticles. *International Journal of Pharmaceutics* 2000;**200**:133-45.

130. He P, Davis SS, Illum L. Chitosan microspheres prepared by spray-drying. *International Journal of Pharmaceutics* 1999;**187**:53-65.

131. Voellmy C, Speiser P, Soliva M. Microencapsulation of Phenobarbital by Spray Polycondensation. *Journal of Pharmaceutical Sciences* 1977;**66**:631-4.

132. Forni F, Coppi G, Vandelli MA, Cameroni R. Drug release from spray-dried and spray-embedded microparticles of diltiazem hydrochloride. *Chemical & Pharmaceutical Bulletin* 1991; **39**:2091-5.

133. Kristmundsdottir T, Gudmundsson OS, Ingvarsdottir K. Release of diltiazem from Eudragit microparticles prepared by spray- drying. *International Journal of Pharmaceutics* 1996;**137**:159-65.

134. Giunchedi P, Genta I, Conti B, Muzzarelli RAA, Conte U. Preparation and characterization of ampicillin loaded methylpyrrolidinone chitosan and chitosan microspheres. *Biomaterials* 1998;**19**:157-61.

135. Proudfoot SG. Factors influencing bioavailability. In: Aulton ME, ed. *Pharmaceutics: The Science of Dosage Form Design*. London: Churchill Livingstone, 1988:135-73.

136. Itokazu M, Yang WY, Aoki T, Ohara A, Kato N. Synthesis of antibiotic-loaded interporous hydroxyapatite blocks by vacuum method and in vitro drug release testing. *Biomaterials* 1998;**19**:817-9.

137. The Merck index. An encyclopedia of chemicals, drugs, and biologicals. 11th ed. New Jersey: Merck & Co., Inc., 1989.

138. Wan LSC, Heng PWS, Chia CGH. Action of plasticizers on sodium carboxymethylcellulose as a coating polymer for spray-dried products. *STP Pharma Sciences* 1994;**4**:114-21.

139. Bernkop-Schnurch A, Scholler S, Biebel RG. Development of controlled drug release systems based on thiolated polymers. *Journal of Controlled Release* 2000;**66**:39-48.

140. Morishita I, Morishita M, Machida Y, Nagai T. Controlled release microspheres based on Eudragit L100 for the oral administration of erythromycin. *Drug Design & Delivery* 1991;**7**:309-19.

141. Mullin JW. Crystallization. 3rd ed. Oxford: Butterworth-Heinemann, 1993:442-3

142. Leo E, Forni F, Bernabei MT. Surface drug removal from ibuprofen-loaded PLA microspheres. *International Journal of Pharmaceutics* 2000;**196**:1-9.

143. Myerson AS. Solutions and solution properties. In: Myerson AS, ed. *Handbook of Industrial Crystallization*. London: Butterworth-Heinemann, 1993:1-31.

144. Myerson AS, Ginde R. Crystals, crystal growth, and nucleation. In: Myerson AS, ed. *Handbook of Industrial Crystallization*. London: Butterworth-Heinemann, 1993:33-63.

145. Price, R. Pharmaceutical Technology Research Group, Department of Pharmacy and Pharmacology, University of Bath, UK, 2002 (Personal communication).

Appendix I Statistical Analysis

(a)True Density

One-way Analysis of Variance

```
Analysis of Variance for stacked
Source     DF        SS        MS        F        P
subscrip    7 0.2310133 0.0330019  1389.11    0.000
Error      16 0.0003801 0.0000238
Total      23 0.2313934

                                  Individual 95% CIs For Mean
                                  Based on Pooled StDev
Level       N      Mean     StDev ----+---------+---------+---------+--
1           3   2.77461   0.00255 (*)
2           3   2.84893   0.00512          (*)
3           3   3.01365   0.00610                           (*
4           3   3.04019   0.00685                              (*)
5           3   3.04044   0.00755                              (*)
6           3   3.02757   0.00295                             *)
7           3   3.04072   0.00221                              (*)
8           3   3.03757   0.00159                              (*
                                  ----+---------+---------+---------+--
Pooled StDev =  0.00487             2.800     2.880     2.960     3.040

Fisher's pairwise comparisons

    Family error rate = 0.443
Individual error rate = 0.0500

Critical value = 2.120

Intervals for (column level mean) - (row level mean)

                1           2           3           4           5           6

       2    -0.08275
            -0.06588

       3    -0.24747    -0.17316
            -0.23060    -0.15628

       4    -0.27401    -0.19970    -0.03498
            -0.25714    -0.18282    -0.01810

       5    -0.27427    -0.19995    -0.03523    -0.00869
            -0.25740    -0.18308    -0.01836     0.00818

       6    -0.26140    -0.18708    -0.02236     0.00418     0.00444
            -0.24452    -0.17021    -0.00549     0.02105     0.02131

       7    -0.27455    -0.20023    -0.03551    -0.00897    -0.00872    -0.02159
            -0.25768    -0.18336    -0.01864     0.00790     0.00816    -0.00472

       8    -0.27140    -0.19708    -0.03236    -0.00582    -0.00556    -0.01844
            -0.25452    -0.18021    -0.01549     0.01105     0.01131    -0.00156


                7

       8    -0.00528
             0.01159
```

(b) Sintering Temperature and Surface Area
Two-way Analysis of Variance
(comparisons for samples which were non-sintered and were sintered at 900°C)

```
Source        DF        SS        MS        F        P
temperature    1  13273.19  13273.19  2.3E+04    0.000
batch          1    127.85    127.85   218.98    0.000
Interaction    1     38.17     38.17    65.37    0.000
Error         16      9.34      0.58
Total         19  13448.55

                        Individual 95% CI
temperature     Mean    ------+---------+---------+---------+-----
1              58.64                                        *
3               7.12    (*
                        ------+---------+---------+---------+-----
                          15.00     30.00     45.00     60.00

                        Individual 95% CI
batch           Mean    --+---------+---------+---------+---------
1              35.41                                     (--*--)
2              30.35     (--*---)
                        --+---------+---------+---------+---------
                      30.00     31.50     33.00     34.50
```

(c) Sintering Temperature and Surface Area
Two-way Analysis of Variance
(comparisons for samples which were sintered between 900 °C and 1200 °C)

```
Analysis of Variance for 2nova,
Source        DF        SS        MS        F        P
ra0w fac       4  290.2265   72.5566  1.9E+04    0.000
column f       1   12.3828   12.3828  3221.45    0.000
Interaction    4    7.1620    1.7905   465.81    0.000
Error         40    0.1538    0.0038
Total         49  309.9251

                        Individual 95% CI
ra0w fac        Mean    -------+---------+---------+---------+----
3              7.116                                            *)
4              3.602                        (*
5              1.498           *)
6              0.956       *
7              0.640     *
                        -------+---------+---------+---------+----
                           1.600     3.200     4.800     6.400

                        Individual 95% CI
column f        Mean    -+---------+---------+---------+---------+
1              3.260                                          (*)
2              2.265     (*)
                        -+---------+---------+---------+---------+
                     2.250     2.500     2.750     3.000     3.250
```

Appendix II Physicochemical Properties of Model Drugs

Benzamide[i,ii,iii]

Molecular formula: $C_6H_5CONH_2$
Molecular weight: 121.14
Appearance: off-white crystals or powder
Melting point: 127 °C
Boiling point: 288 °C
Density: 1.34 g cm^{-3}
Solubility: 1 g in 74 ml water; 1 g in 6 ml alcohol

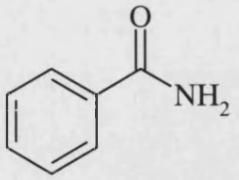

Propranolol hydrochloride[iv,v,vi]

Molecular formula: $C_{16}H_{21}NO_2.HCl$
Molecular Weight: 295.81
Appearance: white crystalline powder
pKa = 9.3
Bulk-density: 0.42 g cm^{-3}
0.55 g cm^{-3} after 20 tappings
Melting point: 163-164 °C
Solubility: 1 g in 20 ml water and alcohol
Solutions are most stable at pH = 3
and decompose rapidly in alkali.

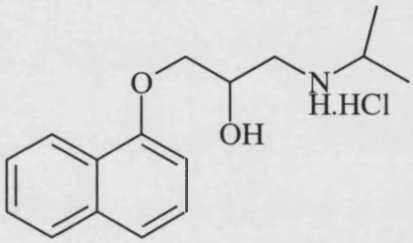

Paracetamol[iv,vii]

Molecular formula: $C_8H_9NO_2$
Molecular Weight: 151.17
Appearance: White crystalline powder.
Melting point: 169-172 °C
pKa = 9.5
Solubility: 1 g in 67 ml water, 1 g in 5 ml ethanol[viii]
Density: 1.29 g cm^{-3}

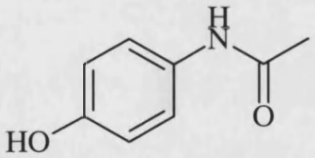

---

[i] The Merck index - an encyclopedia of chemicals, drugs, and biologicals, Merck & Co., Inc., Rahway, N.J., USA, 1986.

[ii] http://physchem.ox.ac.uk/MSDS/BE/benzamide.html (15/12/2001), The Physical and Theoretical Chemistry Laboratory, Oxford University, Chemical and Other Safety Information for benzamide.

[iii] http://www.jtbaker.com/msds/b0720.htm (15/12/2001), Material Safety Data Sheet, Mallinckrodt Baker, Inc., Phillipsburg, NJ, USA.

[iv] Martindale - The Extra Pharmacopoeia, 30th Edition, Pharmaceutical Press, London, UK, 1993.

[v] Clarke's isolation and identification of drugs: in pharmaceuticals, body fluids and post-mortem material, Pharmaceutical Press, London, UK, 1986.

[vi] http://www.chemicals-india.com/propranolol.html (21-4-2002), Propranolol hydrochloride B.P/U.S.P.

[vii] http://www.chemicalland21.com/arokorhi/lifescience/phar/PARACETAMOL.htm (20/12/2002)

[viii] Solubility obtained from experiments in our laboratory.

Appendix III Model Calculation for % Drug Release

Calculation model for % drug release taking into account the removal of 5 ml sample during each sampling and replace with 5 ml of fresh medium.

E.g. If Y = absorbance, X = drug concentration, and Y = 0.0015 + 754.92X

Time /min	Absorbance	Drug concentration /% w/v	Drug concentration /μg ml^{-1}	Amount of drug in 5 ml volume /μg	Cumulative drug concentration /μg ml^{-1}	Total amount of drug in 900 ml dissolution medium/μg	Cumulative amount of drug release /μg	% drug release
	Y_1	$X_1 = (Y_1-0.0015)/754.92$	$10000X_1 = a_1$	$5 \times a_1$	0	$900 \times a_1 = c_1$	$c_1 + 0 = d_1$	$(d_1$/total drug release)×100
	Y_2	$X_2 = (Y_2-0.0015)/754.92$	$10000X_2 = a_2$	$5 \times a_2$	$(5 \times a_1) + 0 = b_2$	$900 \times a_2 = c_2$	$b_2 + c_2 = d_2$	$(d_2$/total drug release)×100
	Y_3	$X_3 = (Y_3-0.0015)/754.92$	$10000X_3 = a_3$	$5 \times a_3$	$(5 \times a_2) + b_2 = b_3$	$900 \times a_3 = c_3$	$b_3 + c_3 = d_3$	$(d_3$/total drug release)×100
	Y_4	$X_4 = (Y_4-0.0015)/754.92$	$10000X_3 = a_4$	$5 \times a_4$	$(5 \times a_3) + b_3 = b_4$	$900 \times a_4 = c_4$	$b_4 + c_4 = d_4$	$(d_4$/total drug release)×100

Appendix IV Calibration Plots

benzamide in buffer, lamda = 225 nm

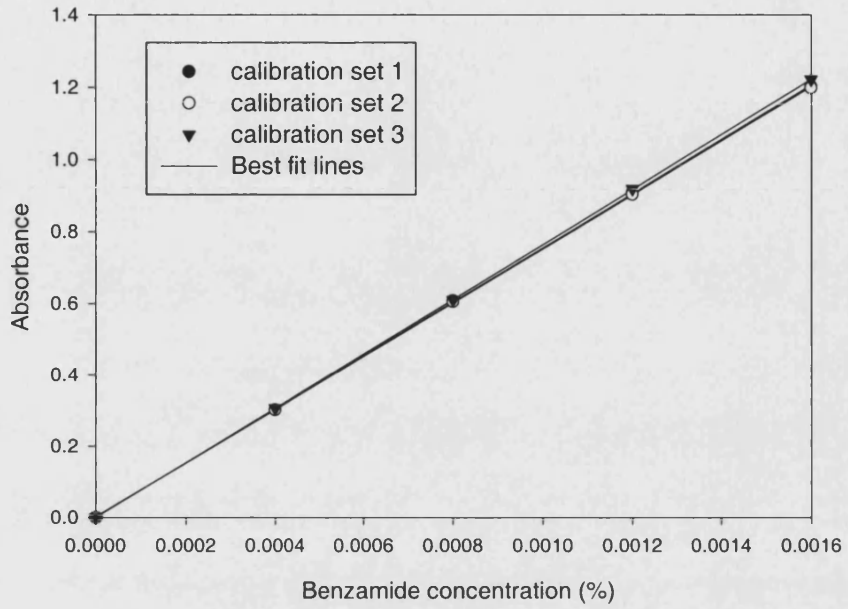

benzamide in acid, lamda = 227 nm

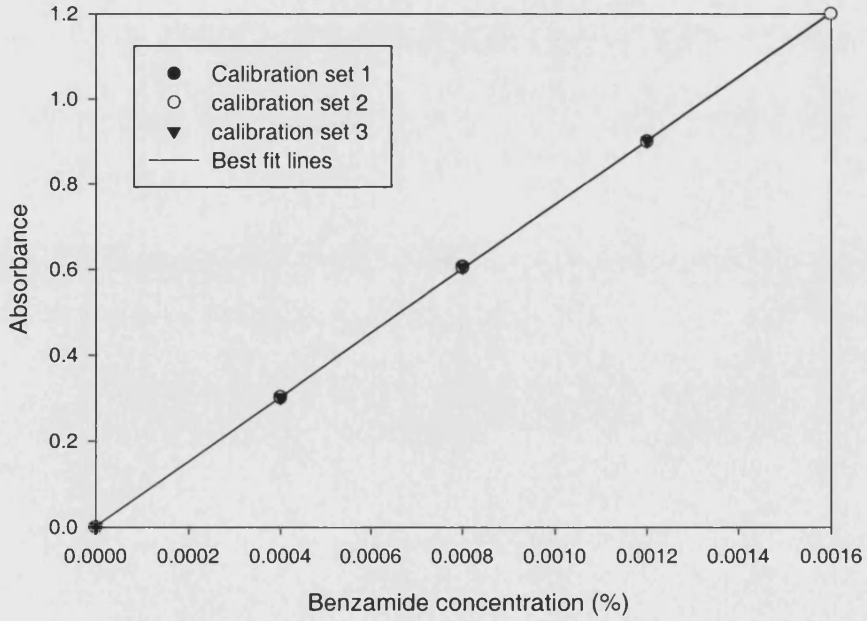

Propranolol in phosphate buffer, lamda = 289 nm

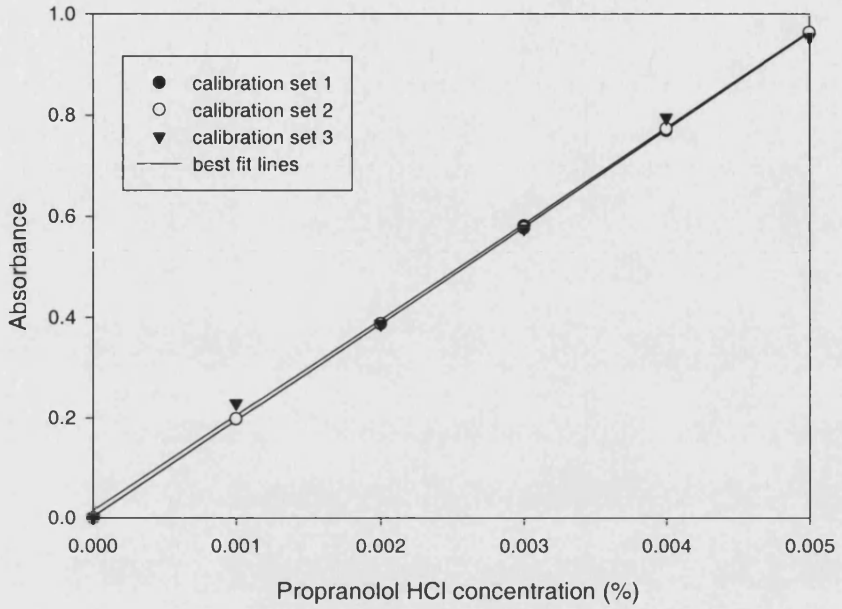

Propranolol in acid, lamda = 290 nm

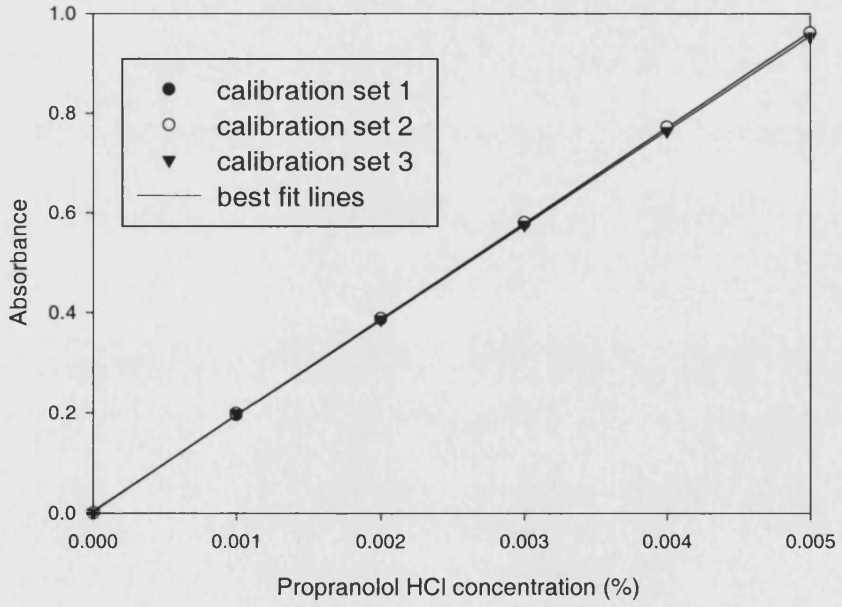

Paracetamol in phosphate buffer, lamda = 249 nm

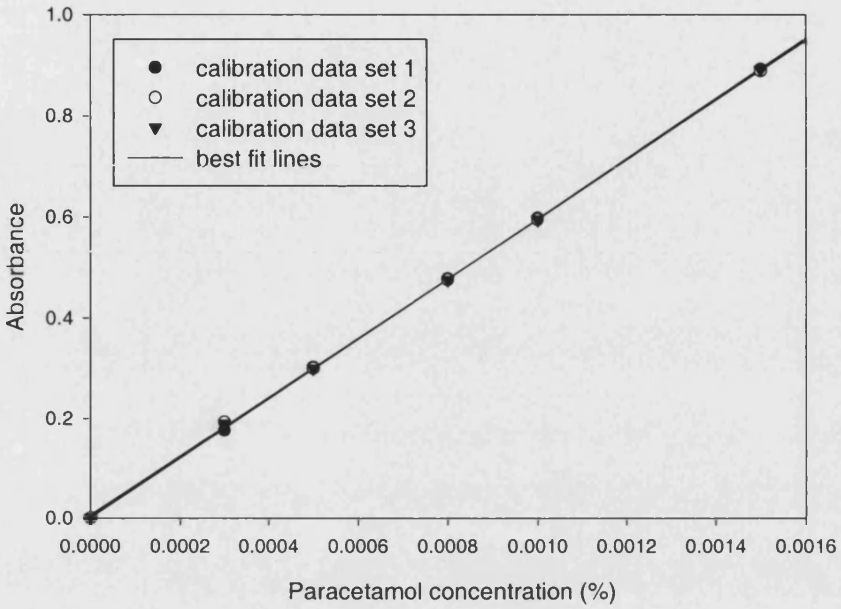

Paracetamol in acid, lamda = 249 nm

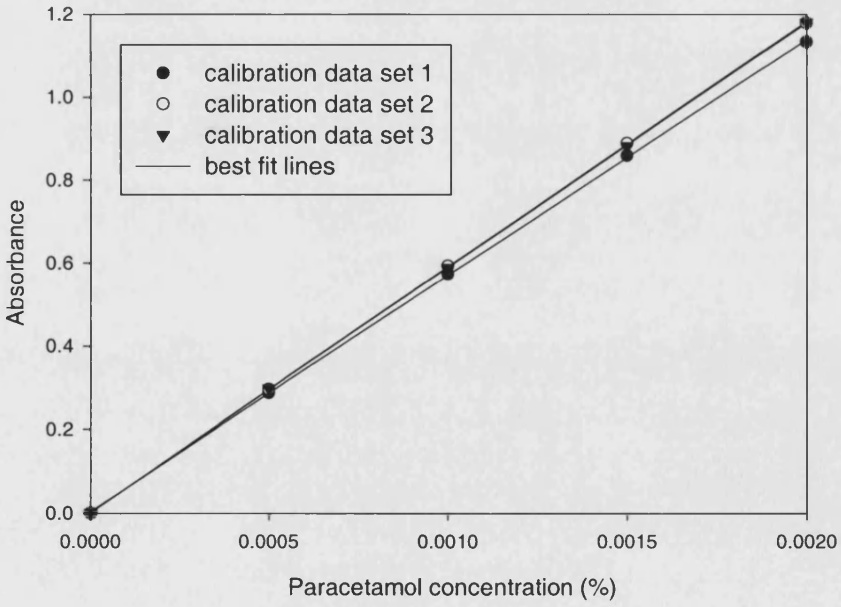

Appendix V AAPS 2000 Poster Abstract

Poster presentation at AAPS Annual Meeting and Exposition 2000 at Indianapolis, Indiana, USA on 30th Oct 2000.
in AAPS PharmSci Supplement, Volume 2, Number 4.

THE PRODUCTION OF INORGANIC POROUS MICROSPHERES AS CARRIERS FOR CONTROLLED RELEASE

Ching Kim Tye[1], Michael J. Tobyn[1], Ronald Stevens[2]

[1]Pharmaceutical Technology Research Group, Department of Pharmacy and Pharmacology, University of Bath, Bath BA2 7AY, UK.

[2]Department of Engineering and Applied Science, University of Bath, Bath BA2 7AY, UK.

Purpose. To produce inert porous microspheres for use as controlled release carriers. To tailor the characteristics (sizes and porosity) of the calcium phosphate systems by spray-drying and sintering. **Methods.** Aqueous mixtures of tri-calcium phosphate (10, 20, 30, 40%w/w), binder (Eudragit L100) and dispersant (Dispex A40) were spray-dried at various temperatures (160°C-245°C). The products were then sieved to retain the bigger microspheres. These microspheres were then sintered at high temperatures (900°C-1200°C) to produce carriers having different pore sizes. **Results.** Spray-drying tri-calcium phosphate mixtures produced porous microspheres ranging from 5μm to 30μm (microscopic observation). The mean microsphere size increases with increased solid concentrations (10-30%w/w). Solid loading lower than 10%w/w and higher than 30%w/w were not suitable to be spray-dried. Systems prepared at 245°C produced microspheres with solid centres while those at 160°C-200°C produced hollow microspheres. Sintering produced microspheres with different porosity. It also reduced the total surface area (and also pore density) of the microspheres from $50m^2/g$ (before sintering) to $1m^2/g$ (after sintering at 1200°). **Conclusion.** By combining spray-drying and sintering techniques, tri-calcium phosphate microspheres with various degrees of controlled porosity can be produced. These inert microspheres have a potential use as controlled release carriers.

Acknowledgements. We thank University of Bath and Overseas Research Students Award for funding this studentship (CKT).

Appendix VI AAPS 2001 Poster Abstract

Poster presentation at AAPS Annual Meeting and Exposition 2001 at Denver, Colorado, USA on 23rd Oct 2001.
in AAPS PharmSci Supplement, Volume 3, Number 3.

THE EFFECT OF SINTERING TEMPERATURE ON A PHARMACEUTICAL GRADE CALCIUM PHOSPHATE

Ching Kim Tye[1], Michael J. Tobyn[1], Ronald Stevens[2]

[1]Pharmaceutical Technology Research Group, Department of Pharmacy and Pharmacology, University of Bath, Bath BA2 7AY, UK.

[2]Department of Engineering and Applied Science, University of Bath, Bath BA2 7AY, UK.

Purpose. To study the effect of sintering temperatures on a pharmaceutical grade tri-calcium phosphate (Merck, Darmstadt, Germany). **Methods.** Spray-dried tri-calcium phosphate systems were sintered at 900°C, 1000°C, 1100°C, 1150°C and 1200°C respectively for one hour. Their morphologies were examined by scanning electron microscopy (SEM). The internal structure of these systems was examined by first mounting them in resin, then cross-sectioned through with a diamond knife before SEM analysis. The change of porosity was measured by mercury intrusion porosimetry. Their total surface area was determined by 5-point BET N_2 adsorption. The true density was measured by helium pycnometry and tap density was also determined. To determine the effect of gastrointestinal conditions on these systems, they were suspended in phosphate buffer (pH=6.8) and 0.1 M hydrochloric acid respectively. **Results.** SEM showed a distinct change in tri-calcium phosphate morphology (grain size grew) with increasing sintering temperatures. Mercury intrusion porosimetry analysis indicated a decrease in total porosity as the temperature increased. The total surface area decreased from 8.3 m^2/g to 1.8 m^2/g when temperature increased from 900°C to 1200°C. Density measurements illustrated that true density and tap density increased with increasing temperature. All sintered tri-calcium phosphate systems were found to retain their structure (SEM examination) after suspension in phosphate buffer overnight but totally dissolved in diluted acid. **Conclusion.** Sintering temperature has a marked effect on the morphology, porosity, surface area and density of the spray-dried tri-calcium phosphate microspheres.

Acknowledgements. We thank University of Bath and Overseas Research Students Award for funding this studentship (CKT).